EPFL

Exploiting Marginal Stability in Slow-Fast Quasilinear Dynamical Systems

Alessia FERRARO

■ École
polytechnique
fédérale
de Lausanne

2022

Gutta cavat lapidem, non vi sed saepe cadendo.

Lucrezio
(*De rerum natura, I 313 et IV 1286-1287*)

To my parents.
For everything, for ever.

Abstract

The accurate investigation of many geophysical phenomena via direct numerical simulations is computationally not possible nowadays due to the huge range of spatial and temporal scales to be resolved. Therefore advances in this field rely on the development of new theoretical tools and numerical algorithms.

In this work we investigate a new mathematical formalism that exploits the property of quasi-linear systems to self-tune towards marginally stable states. The inspiration for this study comes from the asymptotic analysis of strongly stratified flows, performed by Chini *et al.*. The application of multi-scale analysis to this problem, mathematically justified by the presence of scale separation, yields to a simplified quasi-linear model. In this reduced description small-scale instabilities evolve linearly about a large-scale hydrostatic field (whose evolution is fully non-linear) and modify it via a feedback term. From the only assumption of scale separation, physically caused by the presence of a strong stable stratification, two extremely interesting features of this model arise. First the presence of the coupling term between the two dynamics and second the quasi-linearity of the dynamics. The first aspect, generally not present in the hydrostatic approximation, can capture the non-local energy transfer between the small scales and the large ones, which is key for the quantification of the mixing efficiency in the deep ocean. The second aspect, namely the quasi-linearity, together with the multi-scale nature of the model is suggestive of the self-organisation of the dynamics about marginally-stable states, as it is observed for many other quasi-linear systems. This results in a coupled evolution where the supposedly fast dynamics adapts, or better is slaved, to the mean field, maintaining the marginal stability of the latter. The low-dimensional evolution that arises, enables the integration of the reduced system on temporal scales comparable to the characteristic time scale of the slow dynamics. These ingredients collectively make this novel approach highly suited to the investigation of the stratified flow problem.

Building upon the results obtained by Chini *et al.* in the present work we extend this methodology addressing three different aspects of the reduced model.

As a first case we investigate the twofold nature of the fluctuation feedback, which is not sign-definite and might lead to intense bursting events where the fluctuations exhibit positive growth rates on a fast time scale. In this scenario the scale separation is temporarily lost

Abstract

and the two dynamics have to be co-evolved until a new marginally stable manifold can be approached. Here we propose three different co-evolution techniques and test their efficacy on a carefully constructed one-dimensional model problem.

The second aspect we address is the presence of a finite, yet large, scale separation between the two dynamics. In these case we develop an algorithm that carefully identifies the validity regions of the quasi-linear reduction and determines the relevance of the fluctuation feedback with respect to the characteristic time scale of the slow dynamics and the growth rate of the fluctuations.

As a third case we derive an efficient extension of the original methodology to two-dimensional model problems. The introduction of the additional spatial dimension now requires the marginally stable condition to be satisfied not only in time but also by the fastest growing mode. Moreover, due to the time variability of the wavenumber associated to this mode, its identification has to be carried out at each time step. In this regard we derive an evolution equation for the wavenumber of the fastest growing mode in both stable and marginally-stable conditions.

Eventually the methodologies derived in the context of the two model problems are applied and discussed for the strongly stratified flow problem.

Sommario

Lo studio di una gran parte dei fenomeni geofisici tramite simulazioni numeriche dirette (DNS), rappresenta ad oggi una delle piú grandi sfide della fluidodinamica computazionale, a causa dell'enorme range di scale spaziotemporali caratterizzanti questa categoria di fenomeni. Pertanto, i progressi in questo campo, dallo studio della turbolenza in oceano e atmosfera alla modellistica climatologica, sono necessariamente legati allo sviluppo di nuovi strumenti teorici e algoritmi numerici. Il presente lavoro si propone di analizzare e presentare un nuovo formalismo matematico per lo studio di questa classe di problemi, basato sulla proprietà dei sistemi quasi-lineari di evolvere spontaneamente verso stati marginalmente stabili. Tale metodologia, inizialmente proposta da Chini *et al.* nel contesto di flussi fortemente stratificati in oceano, consiste nello sfruttare la natura multi-scala del fenomeno fisico in esame al fine di derivare un modello ridotto computazionalmente capace di simulare i regimi fisici di interesse per la turbolenza in oceano e atmosfera. Nel caso di flussi fortemente stratificati, l'analisi asintotica delle equazioni primitive rivela l'evoluzione del sistema su diverse scale spaziotemporali dando origine ad un sistema accoppiato di equazioni differenziali (PDE) classificabile come quasi-lineare. In tale sistema ridotto le instabilità di piccola scala evolvono linearmente rispetto ad un flusso medio idrostatico (la cui evoluzione al contrario è non-lineare) e interagiscono con esso attraverso un meccanismo di retroazione e avvezione.

Come conseguenza della sola assunzione di separazione di scale, fisicamente imposta dalla presenza di una forte stratificazione stabile, il sistema risultante presenta due caratteristiche di notevole interesse: l'accoppiamento tra le due dinamiche di piccola e grande scala, e la natura quasi-lineare del sistema congiunto. Il primo aspetto, normalmente non presente nei modelli idrostatici adoperati per la modellizzazione climatica, è di fondamentale importanza nel catturare i trasferimenti energetici (non locali) tra le due scale spaziotemporali e conseguentemente, nel caratterizzare i fenomeni di *mixing* in sistemi come oceano e atmosfera, ad oggi non ancora pienamente compresi. Il secondo aspetto, ossia la quasi-linearità, insieme alla natura multi-scala del modello, suggerisce invece un'auto-organizzazione della dinamica verso stati marginalmente stabili, come si osserva per molti altri sistemi quasi-lineari. L'evoluzione risultante del sistema complessivo mostra un adattamento della dinamica (presumibilmente veloce) delle fluttuazioni al campo medio (lento), al fine di mantenere la stabilità marginale di

Sommario

quest'ultimo. La ridotta dimensionalità della dinamica che ne deriva consente l'integrazione di tale modello su scale temporali paragonabili a quella sulla quale il campo medio evolve. L'insieme delle suddette caratteristiche, dall'accoppiamento delle dinamiche di piccola e grande scala alla ridotta dimensionalità del modello asintotico, rende questo nuovo approccio particolarmente adatto allo studio di flussi stratificati in oceano.

Con il fine ultimo di ottenere una struttura algoritmica capace di catturare i fenomeni fisici rilevanti in turbolenza oceanica, l'intento di questo lavoro è di ampliare la metodologia proposta da Chini *et al.* focalizzando l'attenzione su tre aspetti fondamentali.

In primo luogo, verrà analizzata la duplice natura del meccanismo di retrazione tra le due dinamiche. Tale accoppiamento, responsabile per l'adattamento della dinamica delle fluttuazioni alla dinamica del flusso medio in condizioni di stabilità marginale, può altresì spingere il sistema verso condizioni instabili qualora le fluttuazioni esibissero *growth rates* positivi. Il verificarsi di una crescita esponenziale delle fluttuazioni porterebbe ad una risposta del flusso medio su tempi scala veloci, invalidando temporaneamente la separazione di scale alla base della metodologia proposta, e richiedendo la coevoluzione del sistema fino al ristabilimento della stabilità marginale. A tal riguardo, due metodologie di coevoluzione, alternative alle equazioni primitive, verranno proposte e la loro efficacia testata su un modello unidimensionale attentamente costruito.

In secondo luogo, verrà affrontata la presenza di una separazione di scale finita (sebbene ampia) tra le due dinamiche. In tal caso l'algoritmo verrà modificato al fine di identificare le regioni di validità del modello quasi-lineare e determinare la rilevanza della retroazione sulla base della scala temporale caratteristica del flusso medio e del tasso di crescita delle fluttuazioni.

Successivamente, la metodologia proposta verrà estesa allo studio di sistemi bidimensionali. L'aggiunta di un'ulteriore dimensione spaziale richiederà in tal caso che la condizione di stabilità marginale sia non solo preservata nel tempo, ma che questo si verifichi per il modo avente il *growth rate* più elevato. A causa della variabilità temporale della relazione di dispersione, l'identificazione del modo a crescita più rapida deve essere in principio effettuato ad ogni iterazione temporale. A tal proposito verranno presentati diversi approcci per derivare un'equazione di evoluzione per il numero d'onda associato al modo con crescita più rapida, sia in condizioni di stabilità, sia in condizioni di stabilità marginale.

In ultimo le metodologie sopra elencate, e sviluppate in un contesto semplificato con l'aiuto di diversi *toy models* verranno applicate e discusse nel caso d'interesse di turbolenza stratificata.

Résumé

L'investigation détaillée d'une grande partie des phénomènes géophysiques par le biais de simulations numériques directes (DNS) reste hors de portée de la puissance de calcul actuelle, dû à l'éventail immense d'échelles spatiales et temporelles qui doivent être adéquatement résolues. C'est pourquoi les progrès dans ce domaine dépendent à la fois du développement de nouveaux outils théoriques, ainsi que d'algorithmes numériques spécialisés. Au cours de cette thèse, nous investiguons un nouveau formalisme mathématique qui exploite la propriété des systèmes quasi-linéaires de s'auto-ajuster vers un état marginalement stable. Cette étude a été inspirée de l'analyse asymptotique des écoulements fortement stratifiés, effectuée par Chini *et al.*. L'application de l'analyse multiscalaire à ce problème, mathématiquement justifiée par la présence d'une séparation des échelles, résulte en un modèle quasi-linéaire simplifié. Dans cette description réduite, les instabilités de petite échelle évoluent linéairement autour d'un champ hydrostatique de grande échelle (dont l´évolution est entièrement non linéaire) tout en le modifiant au travers d'un terme de rétroaction.Simplement par cette hypothèse d'une séparation des échelles, physiquement due à la présence d'une forte stratification stable, deux caractéristiques extrêmement intéressante de ce modèle émergent, à savoir la présence d'un terme de couplage entre les deux dynamiques (rapides et lentes) ainsi que la quasi-linéarité de la dynamique.

La première caractéristique, généralement absente dans l'approximation hydrostatique, peut rendre compte du transfert non-local d'énergie des petites aux grandes échelles, qui est fondamental pour la quantification de l'efficacité de mélange dans l'océan profond. Le second aspect, à savoir la quasi-linéarité, ajouté à la nature multiscalaire du modèle suggère une auto-organisation de la dynamique autour d'états marginalement stables, comme cela est observé dans beaucoup d'autres systèmes quasi-linéaires. Cela résulte en une évolution couplée au cours de laquelle la dynamique supposément rapide s'adapte, voire se plie au champ moyen, maintenant ainsi la stabilité marginale de ce dernier. L'évolution dimensionnellement petite qui en découle permet d'intégrer le système réduit sur des échelles temporelles comparables à l'échelle de temps caractéristique de la dynamique lente. Tous ces ingrédients font de cette nouvelle approche un outil hautement approprié à l'analyse des problèmes d'écoulements stratifiés.

Résumé

En se basant sur les résultats obtenus par Chini *et al.* et les poursuivant, nous étendons dans cet ouvrage la méthodologie en considérant trois différents aspects du modèle réduit. Comme premier aspect, nous investiguons la nature duale de la rétroaction des fluctuations, qui n'est pas de signe définie et peut résulter en une flambée intense au cours de laquelle les fluctuations présentent un taux de croissance positif sur une échelle de temps rapide. Dans ce scénario, la séparation des échelles est temporairement perdue et les deux dynamiques doivent alors être coévoluées jusqu´à ce qu'une nouvelle variété marginalement stable puisse être approchée. Ici, nous proposons trois différentes techniques de coévolution et testons leur efficacité à l'aide d'un modèle unidimensionnel soigneusement construit.

Le deuxième aspect sur lequel nous nous penchons est la présence d'une séparation des échelles entre les deux dynamiques, aussi grande soit-elle, mais finie. Dans ce cas nous développons un algorithme capable d'identifier avec soin les régions de validité de la réduction quasi-linéaire et de déterminer la pertinence de la rétroaction des fluctuations vis à vis de l'échelle de temps caractéristique de la dynamique lente ainsi que du taux de croissance des fluctuations. Enfin, pour le troisième aspect nous dérivons une extension efficiente de la méthodologie originale pour les modèles de problèmes bidimensionnels. L'ajout d'une dimension spatiale supplémentaire requiert que la condition de stabilité marginale ne soit pas uniquement satisfaite par rapport au temps, mais également par le mode croissant le plus rapidement. De plus, du fait de la variabilité temporelle du nombre d'onde associé à ce mode, son identification doit être effectuée à chaque stade temporel lors de l'intégration. À cet égard, nous dérivons une équation d'évolution pour le nombre d'onde du mode croissant le plus rapidement dans le cas de conditions stables, ainsi que dans le cas de conditions marginalement stables.

Finalement, les méthodologies dérivées dans le contexte des deux modèles sont appliquées et débattues dans le cas des écoulements fortement stratifiés.

Contents

Contents

Contents

1 Introduction

Most of the processes surrounding us fall under the category of *complex systems*. No precise and unique definition of this categorization exits though. In its broadest meaning this terminology refers to systems consisting of many different (deceptively) simple elements that are highly interconnected to each other [Newman (2011)]. The behaviour of the single parts, or agents, is often describable by classical models (not complex), but the collective, resulting from the many-body interaction is not, and can not be inferred from the evolution of the single elements. This feature is referred to as *emergent behaviour*. Moreover, different emergent behaviours can characterise the same system at different scales, or levels of interaction, resulting in the presence of critical thresholds. Therefore the modeling of these systems represents a huge challenge and is often as complex as the system itself. From a mathematical point of view, models that attempt to capture the whole dynamics of a complex system are highly non-linear, due to the high degree of interaction, sensitive to the initial conditions, as a consequence of the non-linearity, and often heterogeneous or multi-scale as a consequence of the different levels of interaction. Countless are the systems that require these types of modeling, from neural interactions, to protein folding, to biological ecosystems, to the stock market, to condensed matter and many many others. However one of the most important, at least in the context of this work, is without any doubt the turbulent motion of fluids. The largest fluid systems on the Earth are represented by the ocean and the atmosphere, both complex on its own and mutually interacting. The coupling of these two dynamics, together with the Earth's rotation, gives rise, among many other phenomena, to the *global overturning circulation* which consists in the downwelling and upwelling of fluid masses in the ocean's basins. This phenomenon, of crucial importance for the distribution of heat, nutrients and carbon over the planet, is still poorly understood. While it is clear that wind-driven currents are responsible for the transport of warm surface water from the equatorial latitudes to the poles, where the downwelling of these masses occurs, the mechanisms that causes the upwelling of deep cold water is still not fully identified [Wunsch and Ferrari (2004), Ferrari (2014)].

Turbulence in geophysical flows is characterised by the presence of two important effects: the Earth's rotation and the stratification, due to density variations in the fluid. The first one intro-

duces in the fluid motion the *Coriolis* force, while the second one buoyancy forces due to the effect of gravity. In the ocean, as well as in the atmosphere, the relative importance of one or the other effect results in very different types of turbulent motion. At large spatial scales (above $10\,km$) the combined effect of rotation and strong stable stratification stirs the flow mainly on quasi-horizontal planes, while at the so-called microscale, $O(1-100)\,m$, three-dimensional turbulence is observed. The latter scenario occurs when the shear forces among large layers of fluid, characterised by different density, provide enough kinetic energy to overcome the energetic barrier imposed by gravity. This triggers shear instabilities that cause an overturning of the fluid and therefore mixing events. Mixing events in turn increase the potential energy of the flow and generate vertical velocity gradients, whose cumulative effect might play a key role in closing the global circulation. The scale at which these instabilities develop is considerably smaller then the characteristic horizontal length scale of the structures that generate them and on which they feed back. The multi-scale nature of this system, caused by the non-local interaction in space of the small isotropic disturbances with the large anisotropic flow, makes the modelling of this dynamics particularly challenging. More quantitatively, the spatial scales relevant for this phenomenon span from scales L that are small enough not to be affected by the Coriolis force to the Ozmidov scale $L_O = (\epsilon_h/N^3)^{1/2}$, the largest horizontal flow scale *not* to be influenced by stratification [Riley and Lindborg (2008)]. Here ϵ_h is the turbulent energy dissipation rate ($\epsilon_h \sim U^3/L$), U is the characteristic horizontal velocity, and N is the buoyancy frequency from which a measure of the stratification can be defined via the inverse of the Froude number $Fr = U/NL$. Then the range of spatial scales to be resolved, expressed as the ratio $L/L_O = O(Fr^{-3/2})$, would require a numerical resolution of about 10^6 grid points just in the vertical direction, when $Fr < 10^{-3}$ (a typical value in the strongly stratified oceanic regime)[Bartello and Tobias (2013)]. Such a computational cost is far beyond today's super-computers.

Due to the impossibility of employing direct numerical simulations of the governing equations, the collective effect of the described small-scale processes has been estimated and introduced in general large-scale circulation models in the form of a mixing coefficient, resulting from specific parametrisation choices. Among the oldest, yet still used currently, is the approximation of a constant value of the mixing efficiency $\Gamma \sim 0.2$ of Osborn and Cox [Osborn and Cox (1972), Osborn (1980)]. Although based on reasonable physical assumptions, this quantification of mixing has been proven to be considerably inaccurate in many circumstances, both numerically and experimentally [Barry et al. (2001), Shih et al. (2005), Davis and Monismith (2011)].

Since fully-resolved DNS capturing all dynamical scales is impossible, and parametrisations of small-scale effects are uncontrollable and inaccurate, many different intermediate-complexity modelling approaches have been developed in the past years. Julien and Knobloch [Julien and Knobloch (2007)] show how the emergence of scale separation in many fluid flows is related to presence of strong constraint, such as strong rotation or intense magnetic fields. Moreover their work shows how this scale separation, which represents an insurmountable obstacle for

DNS, can actually be exploited to derive reduced models via asymptotic techniques. In the same spirit, the application of multi-scale analysis yielded, for example, a simplified model for spatially-extended Langmuir circulation [Malecha et al. (2014)], and very recently to an asymptotic reduction of the strongly stratified flow system [Chini et al. (2022)]. In the latter work, Chini *et al.* show how multi-scale analysis of the governing equations, in the limit of small Froude number and large Reynolds number, reveals two disparate spatiotemporal scales and yields a set of coupled equations for the large anisotropic dynamics and the small-scale disturbances. The reduced coupled equations are reported below for illustration purposes only, and will be fully derived and analysed in § 5. These two different spatiotemporal scales are indicated in equations (1.1)-(1.8) below by T, x for the slow dynamics and by $\tau = T/\varepsilon$, $\chi = x/\varepsilon$ for the fast dynamics, where $\varepsilon = \sqrt{Fr}$ is the small parameter in the multi-scale expansion. Denoting by **u**, w, b, the horizontal velocity vector, the vertical velocity and the buoyancy deviation from a linear background profile, respectively, (1.1)-(1.4) show that in this specific limit the slowly varying fields (denoted by the overbar) obey the hydrostatic primitive equations and their dynamics is modified by the cumulative effect of the small-scale fluctuations (denoted by the prime) via the eddy momentum and the buoyancy fluxes highlighted in red. The evolution of the fast dynamical modes ((1.5)-(1.8)) instead, is described by a linear and homogeneous system coupled to the slow dynamics via the mean-field coefficients highlighted in blue. An interesting feature of this reduced system is the two-way coupling between the slow and the fast dynamics: the feedback produced by the fluctuations on the mean variable is not sign-definite meaning that its effect may be stabilizing or destabilizing in nature.

$$\frac{\partial \overline{\boldsymbol{u}}}{\partial T} + (\overline{\boldsymbol{u}} \cdot \nabla_{\boldsymbol{x}})\overline{\boldsymbol{u}} + \overline{w}\frac{\partial \overline{\boldsymbol{u}}}{\partial z} = -\nabla_{\boldsymbol{x}}\overline{p} - \frac{\partial(\overline{w'\boldsymbol{u}'})}{\partial z} + \frac{1}{Re_b}\frac{\partial^2 \overline{\boldsymbol{u}}}{\partial z^2} + \overline{f} \tag{1.1}$$

$$0 = -\frac{\partial \overline{p}}{\partial z} + \overline{b} \tag{1.2}$$

$$\frac{\partial \overline{b}}{\partial T} + (\overline{\boldsymbol{u}} \cdot \nabla_{\boldsymbol{x}})\overline{b} + \overline{w}\frac{\partial \overline{b}}{\partial z} = -\overline{w} - \frac{\partial(\overline{w'b'})}{\partial z} + \frac{1}{PrRe_b}\frac{\partial^2 \overline{b}}{\partial z^2} \tag{1.3}$$

$$\nabla_{\boldsymbol{x}} \cdot \overline{\boldsymbol{u}} + \frac{\partial \overline{w}}{\partial z} = 0 \tag{1.4}$$

$$\frac{\partial \boldsymbol{u}'}{\partial \tau} + (\overline{\boldsymbol{u}} \cdot \nabla_{\chi})\boldsymbol{u}' + w'\frac{\partial \overline{\boldsymbol{u}}}{\partial z} = -\nabla_{\chi}p' + \frac{Fr}{Re_b}\left(\nabla^2_{\chi}\boldsymbol{u}' + \frac{\partial^2 \boldsymbol{u}'}{\partial z^2}\right) \tag{1.5}$$

$$\frac{\partial w'}{\partial \tau} + (\overline{\boldsymbol{u}} \cdot \nabla_{\chi})w' = -\frac{\partial p'}{\partial z} + b' + \frac{Fr}{Re_b}\left(\nabla^2_{\chi}w' + \frac{\partial^2 w'}{\partial z^2}\right) \tag{1.6}$$

$$\frac{\partial b'}{\partial \tau} + (\overline{\boldsymbol{u}} \cdot \nabla_{\chi})b' + w'\frac{\partial \overline{b}}{\partial z} = -w'\frac{Fr}{PrRe_b}\left(\nabla^2_{\chi}b' + \frac{\partial^2 b'}{\partial z^2}\right) \tag{1.7}$$

$$\nabla_{\boldsymbol{x}} \cdot \boldsymbol{u}' + \frac{\partial w'}{\partial z} = 0 \tag{1.8}$$

The reduced set of equations, obtained by Chini *et al.*, falls under the category of *generalised quasi-linear models* (GQL), characterised by a linear evolution of the fast variable about a slowly spatially-varying mean field which conversely evolves fully non-linearly due to the presence of the fluctuation-fluctuation non-linearity. The remarkable aspect of this result is that the quasi-linearity is not enforced as an approximation but naturally arises from the multi-scale nature of the dynamics.

The evolution of the two fields on different temporal and spatial scales, together with the linearity of the fast dynamics, poses the question in the first place on the choice of an appropriate integration method that can stably, accurately and efficiently evolve the coupled dynamics. Possible choices, widely used in similar cases, are represented by the co-evolution of the reduced system via the re-introduction of the scale separation parameter, or by the application of heterogeneous multi-scale algorithms [E et al. (2007), Abdulle and E (2003)]. However none of the two classes of integration methodologies simultaneously satisfies the requirements of accuracy and efficiency required by the stratified flow problem (as it will be discussed in § 2).

Based on the observation that many slow-fast QL systems have the tendency of self-organize around marginally stable states, Michel and Chini [Michel and Chini (2019)] have recently proposed a new integration strategy that exploits a marginal stability constraint. Intuitively, the linear evolution of the fast dynamics can be described by modal solutions that exponentially grow or decay over the fast temporal scale, on which the mean dynamics is considered as steady. While a decay of the fluctuations would produce a zero feedback on the mean dynamics, their growth would compromise the convergence of this coupling term, causing the response of the "mean" variable over fast temporal scales. The first case results in a non-coupled system where the mean field evolves without any effect from the fluctuations (under the hydrostatic approximation in the case of the stratified flow problem). The second invalidates the entire quasi-linear approximation, nullifying the scale separation between the two dynamics. It follows that the coupling between the fluctuation an the mean field is only possible in condition on marginal stability. The key idea at the basis of this approach can be quickly summarised as the slaving of the fluctuation dynamics to the mean field such that marginally-stable conditions (and therefore the coupling) can be maintained in time.

The promising results obtained on simple model problems [Michel and Chini (2019)] and the later successful application to the two-dimensional stratified flow problem [Chini et al. (2022)], makes this novel methodology highly promising for the investigation of many complex geophysical flows. However, as pointed out by the authors, further development of this formalism is needed before simulations of the extreme parameter regimes that characterise real stratified turbulence in the ocean are possible.

The aim of this work is to proceed in that direction, extending the framework of the original QL methodology to enable the investigation of a wider range of physical phenomenon characterising the stratified flow problem.

Specifically we will focus on the following three topics:

- **Occurrence of bursting events**
  The collective effect of the fast fluctuations on the mean dynamics has been shown have a twofold nature. Namely the sign of the "Reynolds-like" stresses and buoyancy flux terms (highlighted in red in (1.1)-(1.4)) is not *a priori* defined, allowing for scenarios in which the fluctuations drive the marginally stable mean fields towards unstable states. This results in a bursting event in which scale separation is transiently lost, requiring some sort of co-evolution of the two dynamics until a new neutrally-stable state can be approached. These events, observed in the simulations of Chini *et al.* [Chini et al. (2022)], might be representative of strong mixing events and are therefore of fundamental importance in the stratified flow dynamics.

- **Presence of a finite scale separation**
  In this case we will account for more realistic values of the scale separation parameter ε, which are normally finite yet small. With the aim of developing a robust methodology, we will explicitly re-define the validity ranges of the QL reduction, based on the characteristic temporal scale of the two dynamics and the stability condition of the system. We will then relax the strict constraint of marginal stability for exactly zero growth rates by including physically understandable (therefore controllable) tolerances on the fluctuation evolution near this region. This will result in a compounded algorithmic structure which coherently connects different approximations valid in different stability/parameter conditions.

- **Identification of the marginally stable mode in two-dimensional problems**
  The spatial variability of the coupled dynamics (1.1)-(1.8) upon two spatial coordinates (a vertical one z and an horizontal one x) translates, in terms of marginal stability constraint, into the presence of a time-varying dispersion relation and therefore in a time-varying spatial variability (or wavenumber variability) of the fast mode that first become marginally stable. Leaving the details to Chapter § 4, in this scenario, the QL algorithm essentially requires the additional (costly) step of identifying the marginally stable mode that then will be slaved to the mean dynamics. In this regard we will overcome the problem by deriving an additional evolution equation for the identification of the neutral mode (precisely of its wavenumber) based on differential geometry considerations.

The first two scenarios will be investigated and tested in chapter 3 making use of a one-dimensional model problem. The third one will be first presented in chapter 4 in the context of a two dimensional model problem and then applied to the stratified flow problem in chapter 5.

2 Analytical and Numerical Tools for Slow-Fast QL Systems

Contents

Chapter summary

In this chapter we introduce the general concept of quasi-linear systems, providing a brief overview of their features and common techniques to handle them. We will mainly focus on the scenarios in which this systems result from more a complex dynamics in presence of scale separation, manifesting a multi-scale nature. In this regard we will remark the technical issues that need to be faced to numerically integrate them and we will introduce the core idea of the new integration methodology proposed by Michel and Chini [Michel and Chini (2019)] at the basis of this work. These ideas and concepts will be the common thread of the next chapters where they will find a specific applications to different problems. After outlining the general analytical framework in which we will operate, we introduce the numerical tools that will be used to handle the investigation of QL systems, providing a brief synopsis of the *Dedalus* software [Burns et al. (2020)].

2.1 Introduction to QL systems and their integration

We start by considering a non-linear dynamical system defined by the temporal evolution of the state-space vector $\boldsymbol{q} \in \mathscr{H}$, with $\mathscr{H}$ an infinite-dimensional function space,

$$\partial_t \boldsymbol{q} = \mathscr{F}(\boldsymbol{q}) = \mathscr{L}(\boldsymbol{q}) + \mathscr{N}(\boldsymbol{q}) \tag{2.1}$$

where $\mathscr{F}$ is an evolution function consisting of a linear part $\mathscr{L}$ and a non-linear one $\mathscr{N}$.

The *quasi-linear* (QL) formulation of the evolution equation (2.1) can be obtained by decomposing the state-space vector into a suitable (to be defined) mean component and fluctuations with respect to the mean

$$\boldsymbol{q} = \overline{\boldsymbol{q}} + \boldsymbol{q}' \quad \text{with} \quad \overline{\overline{\boldsymbol{q}}} = \overline{\boldsymbol{q}} \quad \text{and} \quad \overline{\boldsymbol{q}'} = \overline{0} \tag{2.2}$$

and then neglecting the fluctuation-fluctuation non-linearities except when they feed back on the mean variable

$$\partial_t \boldsymbol{q} = \begin{pmatrix} \partial_t \overline{\boldsymbol{q}} \\ \partial_t \boldsymbol{q}' \end{pmatrix} = \begin{pmatrix} f^{QL}(\overline{\boldsymbol{q}}, \boldsymbol{q}') \\ g^{QL}(\overline{\boldsymbol{q}}, \boldsymbol{q}') \end{pmatrix} = \begin{pmatrix} \mathscr{L}(\overline{\boldsymbol{q}}) + \overline{\mathscr{N}(\boldsymbol{q}')} \\ \mathscr{L}(\boldsymbol{q}') + \mathscr{N}'(\boldsymbol{q}', \overline{\boldsymbol{q}}) \end{pmatrix}. \tag{2.3}$$

A generalisation of (2.3), falls under the name of *generalised quasi-linear* formulation (GQL) [Marston et al. (2016)] and differs from the QL model by the presence of the mean-mean non-linearities $\overline{\mathscr{N}(\overline{\boldsymbol{q}})}$ and consequently by the linearisation of the fast dynamics around a spatially modulated mean.

The resulting reduced systems of equations, often used as an *ad hoc* approximation for simplification, naturally arise in many physical systems in the presence of scale separation. Considering a scenario where scale separation is present in time, different temporal scales can be formally introduced. Denoting with $\widetilde{T_s}$ the dimensional temporal scale over which slow processes occur (e.g. measured in years) and with $\widetilde{T_f}$ the dimensional characteristic time for the fast processes (e.g. measured in seconds), such that $\widetilde{t} = \tau \widetilde{T_f} = T \widetilde{T_s}$, the scale separation between the two dynamics yields the small non-dimensional parameter ε

$$\varepsilon = \frac{\widetilde{T_f}}{\widetilde{T_s}} = \frac{T}{\tau} \tag{2.4}$$

which can be exploited to derive reduced equations via asymptotic techniques.

When this is the case, re-interpreting the averaging procedure as an average over the fast coordinate ($\overline{\boldsymbol{q}}$ is frozen in fast time), the multi-scale analysis automatically leads to a QL

formulation (or GQL depending on the specific evolution function),

$$\partial_t \boldsymbol{q} = \begin{pmatrix} \partial_t \overline{\boldsymbol{q}} \\ \varepsilon \partial_t \boldsymbol{q}' \end{pmatrix} = \begin{pmatrix} f^{QL}(\overline{\boldsymbol{q}}, \boldsymbol{q}') \\ g^{QL}(\overline{\boldsymbol{q}}, \boldsymbol{q}') \end{pmatrix} = \begin{pmatrix} \mathcal{L}(\overline{\boldsymbol{q}}) + \overline{\mathcal{N}}(\boldsymbol{q}') \\ \mathcal{L}(\boldsymbol{q}') + \mathcal{L}_{\overline{\boldsymbol{q}}}(\boldsymbol{q}') \end{pmatrix} . \tag{2.5}$$

The evolution of the fluctuation is order $O(\varepsilon^{-1})$ faster then the one of the mean variable, is linear and homogeneous in the fluctuations and is coupled to the mean dynamics via two mechanisms: first the parametric dependence on the mean dynamics $\overline{\boldsymbol{q}}$ (e.g. an advection term) and second the feedback that in turn the fluctuations exert on the mean field via $\overline{\mathcal{N}(\boldsymbol{q}')}$. Because of the multi-scale nature of the problem, a key issue to be addressed concerns the choice of a numerical integration method. The commonly used techniques are

- The *single-scale* (or *single-time*) integration method [Marston et al. (2016),Malecha et al. (2014)] which re-introduces the small parameter ε into the equations (2.5), discards the fast-time average, and integrates both dynamics on the same temporal scale.

- Multi-scale integration methods, like the *heterogeneous multi-scale method* [E et al. (2007), Abdulle and E (2003)], *super-parametrisation* [Grabowski (2004), Gear et al. (2003)], and various adaptations of them [Malecha et al. (2014)]. In this case the fast dynamics is integrated on a fast time scale with a constant mean field, until a steady state is reached (if this happens), and the collective effect of the fluctuations is then computed to update the slow variable with a larger time step.

Both methodologies come with advantages and disadvantages. The first approach does not take advantage of the multi-scale nature of the reduced system, still requiring a time-step small enough to resolve the fast dynamics (about εdT) and it is normally stiff due to the presence of the scale-separation parameter. In some cases the single-time QL might results even stiffer than the fully non-linear original dynamics depending on the form of the non-linearity that has been suppressed during the QL approximation. However it is normally accurate (within the approximation) and has an advantage over the full dynamics in the fact that implicit numerical schemes can be used to integrate the fluctuation dynamics (linear in the reduced model). Conversely, the second approach is normally more efficient but at the expense of the loss of accuracy. After any update of the coarse-grained dynamics the fluctuations dynamics needs to be re-initialised and integrated for a certain amount of time until a steady state is approached, but neither of these steps is well defined. More importantly, the steady state might even not exist if the fast fluctuations blow up while the mean field is frozen, requiring in this case again the co-evolution of the two dynamics on the same temporal scale.

A third option that has the accuracy of the single-scale integration method and leverages, at the same time, the multi-scale nature of the system is however possible. This approach is the central topic of investigation of this work. A new methodology for the integration of slow-fast quasi-linear systems has been recently proposed by Michel and Chini [Michel and

Chini (2019)], based on the observation that most of the dynamics that asymptotically reduce to QL-type systems have the tendency to self-tune towards marginally stable states.

Owing to the linearity and homogeneity of the fast dynamics, its solutions can be expressed as a superposition of modal solutions

$$\boldsymbol{q}'(\tau, T) = \sum_i A_i(T)\hat{\boldsymbol{q}}_i(T)e^{\sigma_i \tau} \tag{2.6}$$

with $A(T)$ an amplitude to be determined, $\hat{\boldsymbol{q}}$ a structure function and $\text{Re}\{\sigma\}$ a growth rate.

Substituting this ansatz into (2.5) yields an initial value problem for the mean dynamics and an eigenvalue problem for the evolution of the fluctuations

$$\partial_t \boldsymbol{q} = \begin{pmatrix} \partial_t \overline{\boldsymbol{q}} \\ \varepsilon \partial_t \boldsymbol{q}' \end{pmatrix} = \begin{pmatrix} \partial_t \overline{\boldsymbol{q}} \\ \sigma \hat{\boldsymbol{q}} \end{pmatrix} = \begin{pmatrix} \mathscr{L}(\overline{\boldsymbol{q}}) + |A|^n |\hat{\boldsymbol{q}}|^n \overline{e^{n\sigma\tau}} \\ \mathscr{L}(\hat{\boldsymbol{q}}) + \mathscr{L}_{\overline{\boldsymbol{q}}}(\hat{\boldsymbol{q}}) \end{pmatrix}. \tag{2.7}$$

with n, the degree of the non-linearity.

By inspection of (2.7) it is immediate that for the feedback term not to diverge the growth rate has to be non-positive. When $\text{Re}\{\sigma\} < 0$, $\overline{\mathscr{N}(\boldsymbol{q}')}$ converges to zero and the mean dynamics evolves without any effect from the fluctuations. When $\text{Re}\{\sigma\} = 0$, the feedback $\overline{\mathscr{N}(\boldsymbol{q}')}$ becomes finite, and the two dynamics are coupled via the fluctuation amplitude

$$\overline{\mathscr{N}(\boldsymbol{q}')} = |A(T)|^n |\hat{\boldsymbol{q}}|^n \tag{2.8}$$

The key idea at the core of the novel integration methodology is to determine the, *a priori* unknown, amplitude A such that the marginal stability of the mean variable can be maintained in time. In other words once zero growth rates are realised, the amplitude A plays the role of a "control knob" that can be turned to ensure the evolution of the two dynamics on the marginally stable manifold. The details of this new methodology, together with its validity conditions and extensions will be subject of the next chapters, where applications to different specific problems of increasing complexity will be discussed.

2.2 The Dedalus software – A sparse τ-method

The integration methodology introduced in the previous section requires to solve the coupled system of equations (2.7) consisting of an initial value problem for the slow dynamics and an eigenvalue problem for the fast fluctuations. Further extensions of this method, presented in the next chapters, will additionally require the solution of boundary value problems, and more specifically of singular boundary value problems due to the marginal stability constraint at the basis of this approach.

To handle all of this tasks we will make use of the open-source software *Dedalus* [Burns et al. (2020)], designed to solve a wide range of PDEs, written in python with an object-oriented and high performance design.

The advantageous feature of this software is to provide a sparse representation of spectrally discretised differential operators from a symbolic input. These discretised operators can then be used to solve initial, eigenvalue and boundary value problems. The sparseness of the representation is achieved via a first-order formulation of the problems together with the implementation of a modified spectral τ-method.

When considering a generic problem with boundary conditions

$$
\begin{aligned}
Lu(x) &= f(x) \, x \in A \subset \mathbb{R}^d \\
Bu(\tilde{x}) &= 0 \, \tilde{x} \in \partial A
\end{aligned}
\tag{2.9}
$$

with L and B first-order differential operators, u the solution to be found and f a right hand side, spectral methods generally expand u and f in terms of a complete orthogonal basis ϕ, named *trial functions*, with a truncation at the order $N-1$

$$
u = \sum_{n=0}^{N-1} \hat{u}_n \phi_n(x)
\tag{2.10}
$$

leading to a set of equations for the spectral coefficients $\hat{u}_n$. Due to the impossibility of finding an exact solution satisfying simultaneously the PDE and its boundary conditions when considering a finite-dimensional sub-space of the trial functions (truncation at order $N-1$), spectral methods in general seek for an approximate solution u^* that minimizes the residual $R = Lu^* - f$ with respect to the inner product against a specified *test function* ψ (hence a weighted residual)

$$
\sum_{n=0}^{N-1} \hat{u}_n \left\langle \psi_j \middle| L\phi_n \right\rangle - \sum_{n=0}^{N-1} \hat{f}_n \left\langle \psi_j \middle| \phi_n \right\rangle = 0
\tag{2.11}
$$

with $j = 0, 1, 2, \dots N-1$.

The choice of the trial function discriminates the different spectral methods. For instance in the case of the *collocation method* ψ is chosen to be a Dirac delta at the collocation points, and in the *Galerkin method* a smooth function satisfying the boundary conditions chosen identical to the trial functions. An improvement of this method is represented by the τ-*method* , which modifies the problem (2.9) such that the truncated solution is an exact solution of the modified problem. That is to say, a truncation in the expansion of the solution produces a perturbation in the original problem, and vice versa for any perturbation of the initial problem we can find an exact solution within a finite dimensional subspace. The original problem (2.9)

is then replaced by

$$Lu(x) + \tau P(x) = f(x) \quad x \in A \subset \mathbb{R}^d \tag{2.12}$$

where τ is a parameter to satisfy the boundary conditions and $P(x)$ a specified polynomial. When using the same basis for both the test and the trial functions, $\psi = \phi$, and setting the polynomial $P(x) = \phi_{N-1}$, the last row of (2.12) (for $j = N-1$), known as the τ-*equation* ensures that $\hat{u}_n = 0$ for $n > N-1$. Because the expansion is already truncated at order $N-1$ by construction, this equation does not carry extra information and can be conveniently replaced by the boundary conditions.

The same choice for test and trial functions, however, is not ideal when using non-trigonometric functions to discretise a problem that involves differential operators. For problems with wall bounded domains a common choice for the expansion basis is normally the Chebyshev polynomials of the *first kind* $T_n(x) = \cos(n\cos^{-1}(x))$. Although their relation with the cosine-transform allows for the usage of the Fast Fourier Transform, these polynomials produce dense differentiation matrices when projected against the same basis, due to the recursive relation

$$T'_n(x) = n\left(2T_{n-1} + \frac{T'_{n-2}}{(n-2)}\right) = \sum_{i=0}^{N-1} = T_i \frac{2n[(n-i)mod2]}{1+\delta_{i,0}} \ . \tag{2.13}$$

The solution to this problem is achieved in the *Dedalus* software by expanding the differential operator of the first kind Chebyshev polynomials T'_n, with respect to the *second kind* Chebyshev polynomials

$$U_n = \frac{\sin[(n-1)\cos^{-1}(x)]}{\sin(\cos^{-1}(x))} \tag{2.14}$$

making use of the relation between the two basis

$$T_n(x) = \frac{1}{2}[U_n(x) - U_{n-2}(x)] \quad \text{and} \quad T'_n(x) = nU_{n-1}(x) \ . \tag{2.15}$$

This results in a diagonal representation of the differential operator

$$\sum_{n=0}^{N-1} \hat{u}_n \underbrace{\langle U_j|\partial_x T_n\rangle}_{n\delta_{j,n-1}} + \tau \underbrace{\langle U_j|T_{N-1}\rangle}_{P^L_{j,N-1}} = \sum_{n=0}^{N-1} \hat{f}_n \underbrace{\langle U_j|T_n\rangle}_{P^L_{j,n}} \tag{2.16}$$

where $P_{i,j} = \langle U_i|T_j\rangle$ is the T-to-U operator, referred in *Dedalus* as a left preconditioning P^L.

However with this choice of trial and test functions the boundary conditions remain dense. Once again this issue is overcome in *Dedalus* exploiting relations and re-combinations of

the Chebyshev polynomials. Noticing that with a first order formulation all the boundary conditions reduce to Dirichlet-type, and that $T_n(\pm 1) = \pm 1$, the following choice for the trial function

$$D_n^T(x) = \begin{cases} T_n(x) & n = 0,1 \\ T_n(x) - T_{n-2}(x) & n \geq 2 \end{cases} \quad \rightarrow \quad D_n^T(\pm 1) = \begin{cases} \pm 1 & n = 0,1 \\ 0 & n \geq 2 \end{cases} \tag{2.17}$$

together with its projection on the basis T_j, allows to condense the boundary condition row to only two modes, given that $\langle T_i | D_j \rangle = \delta_{i,j} - \delta_{i,j-2}$. *Dedalus* refers to this projection as right preconditioning P^R, and combined with the left preconditioning P^L leads to the following sparse representation of the original problem

$$\underbrace{P^L L P^R}_{\mathscr{L}} (P^R)^{-1} u = \underbrace{P^L f}_{\mathscr{M}} . \tag{2.18}$$

Figure 2.1 summarises the main steps taken in the *Dedalus* software to construct the operators $\mathscr{L}$ and $\mathscr{M}$ in the case of an eigenvalue problem resulting from the one dimensional diffusion equation with Neumann boundary conditions, expressed in the first-order formulation as

$$\partial_x^2 u = \sigma u \quad \rightarrow \quad \begin{cases} \partial_x u_x = \sigma u & u_x|_0 = 0 \\ \partial_x u - u_x = 0 & u_x|_L = 0 \end{cases} . \tag{2.19}$$
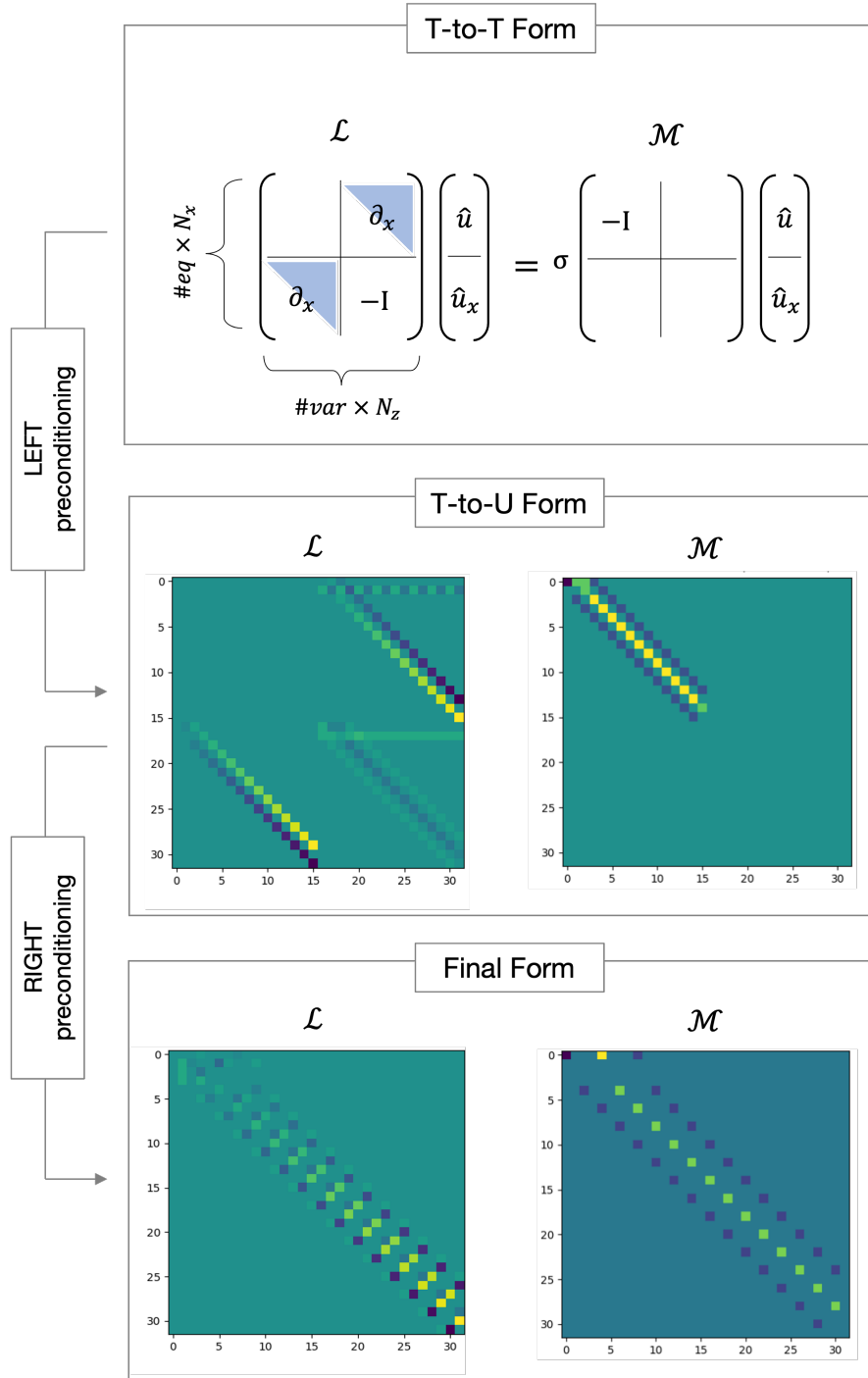
Figure 2.1 – Construction of the sparse representation of the spectrally discretised operators in the *Dedalus* software, for the one dimensional eigenvalue problem (2.19), with Neumann boundary conditions. From a symbolic entry of the equations (expressed with a first-order formulation), a generalised τ-method with appropriate transformations between Chebyshev polynomial basis (of the first and second kind) is used to obtain the final sparse form of the operators describing the problem.

3 1D Model Problem
Approaching, Leaving and Evolving on
the Marginally-Stable Manifold

Contents

Chapter summary

In this chapter we present and extend the quasi-linear reduction proposed in Michel and Chini [Michel and Chini (2019)] for systems that evolve on different spatiotemporal scales and self-adjust to marginally stable states. This type of reduction is characterised by the coupling between a non-linear slow dynamics and a linear fast dynamics (hence the quasi-linear

categorisation) via a feedback produced by the fast field on the slow one and the advection of the fast field by the slow one. The nature of the fluctuation-induced feedback on the mean dynamics is, however, for many systems twofold: it is responsible for the marginally-stable evolution of the coupled system in certain cases and conversely for the realisation of unstable scenarios in others. The latter case being represented by bursting events where the formally slow and fast dynamics respond on the same temporal scale. Owning to the occurrence of these events in many physically relevant systems, including the stratified flow problem, here we discuss an extension of the QL methodology to capture and deal with the departure of the dynamics from the marginally-stable condition, proposing different possible techniques. Finally we present a modification of the original algorithm developed to account for finite scale separation.

3.1   Introduction

Systems characterized by an evolution that occurs over a large range of spatial and temporal scales are commonplace in the study of complex systems. Their fully-resolved simulation would normally require computational resources at the limit of the existing technology, or beyond. Many emblematic instances of such a type of systems can be found in geophysical and astrophysical flows where scale separation is the often the result of the interaction between different phenomena (e.g. Quasi-biennial oscillations [Lindzen and Holton (1968)]) and/or the presence of strong dominant effects, like rotation or stratification [Julien and Knobloch (2007)]. Strongly stratified flows in oceanic turbulence, for example, are characterized by Reynolds numbers around 10^8 and Froude numbers of the order of 10^{-3} (where the Reynolds number is the ratio between the inertial forces and the viscous ones, and the Froude number an inverse measurement of the stratification). In such a regime the strong stratification is responsible for the spontaneous emergency of large horizontal flow-structures whose relative motion triggers shear instabilities with a considerably smaller characteristic size [Fincham et al. (1996), Herring and Métais (1989), Métais and Herring (1989), Riley et al. (1981)]. Owing the impossibility of fully numerically resolving all the dynamically relevant scales for the real oceanographic phenomena [Brethouwer et al. (2007), Bartello and Tobias (2013)], much progress has been made in the past years in developing simplified models and reductions [Fitzgerald and Farrell (2014), Fitzgerald and Farrell (2018), Constantinou et al. (2014), Tobias et al. (2011), Tobias and Marston (2013), Srinivasan and Young (2012), Farrell et al. (2016)]. In the specific case of the strongly stratified flow problem, scale separation can be exploited to obtain reduced models by means of asymptotic techniques [Chini et al. (2022)]. Accounting for different temporal and spatial scales, the multi-scale analysis of this system automatically yields a quasilinear (QL) coupled system of PDEs for a slowly varying mean field and the fast varying small-scale instabilities. The (now) linear evolution of the fast field remains coupled to the slow dynamics (fully non-linear) feeding back on it and being advected by it. Due to the linearity of the fast dynamics, the numerical integration of this type of systems requires a carefully constructed procedure to avoid an exponential growth of the instabilities, while the

mean field is frozen. In this regard Michel and Chini [Michel and Chini (2019)] have recently proposed a new algorithmic procedure that leverages the tendency of many QL system, as well as of stratified flows, to evolve towards marginally-stable states. Heuristically, the condition of marginal stability, once realized, is maintained by the slaving of the fast dynamics to the mean field which produces a stabilizing effect on the latter. The successful application of this algorithm to the two-dimensional strongly stratified flow problem [Chini et al. (2022)] has been however limited to cases where $Re_b = ReFr^2 < 10$ (with a $Fr = 0.01$) due to the stability loss of the marginal state. In these scenarios, describable as a bursting event, the fast fluctuations becomes linearly unstable and their growth induces a response of the "slow" dynamics on the fast time scale, invalidating the scale separation at the basis of the QL reduction.

The aim of this chapter is to illustrate an algorithmic extension to the QL methodology proposed by Michel and Chini [Michel and Chini (2019), Chini et al. (2022)], able to efficiently cope with this type of bursting phenomena in which marginal-stability is transiently lost and the two dynamics have to be integrated on the same temporal scale. For this purpose we make use of a deceptively simple one-dimensional model problem, proposed in [Michel and Chini (2019)], to limit the complexity of the investigation of the unstable events. Moreover we propose a modification of the algorithm to account for finite (yet large) scale separations, as is normally the case in real systems, which also has the advantage of providing a more systematic and precise control on the numerical approximations.

3.2 Governing equations and multi-scale analysis

In this first example, from [Michel and Chini (2019)], the slow field $U(z, t)$ and the fast fluctuations $\eta(z, t)$ evolve according to

$$\frac{\partial U}{\partial t} = F - \nu U - \eta^2 e^{-U^2} \tag{3.1}$$

$$\varepsilon \frac{\partial \eta}{\partial t} = U \eta e^{-U^2} + \frac{\partial^2 \eta}{\partial z^2} - \epsilon \eta^3 \, , \tag{3.2}$$

where $F(z, t)$ is a space and time dependent forcing and νU is a linear damping. As in the stratified flow problem the slow variable feels the effect of the fluctuations via a quadratic feedback, here multiplied by the exponential term in (3.1), $\eta^2 e^{-U^2}$; and the fluctuations in turn are "advected" by the mean flow via the term $U \eta e^{-U^2}$. The scale separation is set by the small parameter ε in (3.2) (analogous of the Fr number in the reduced Boussinesq equations (1.5)-(1.7).

Explicitly taking into account the temporal scale separation by introducing two time scales $t \to (T, \tau)$, with $T = t$ and $\tau = T/\varepsilon$ and positing the following asymptotic expansions for U and η

$$U = U_0 + \varepsilon U_1 + \varepsilon^2 U_2 + O(\varepsilon^3) \tag{3.3}$$

$$\eta = \eta_0 + \varepsilon \eta_1 + \varepsilon^2 \eta_2 + O(\varepsilon^3) \tag{3.4}$$

a two-scale reduced system governing the leading-order dynamics ($O(1)$ for the mean variable and $O(1/\varepsilon)$ for the fluctuations) can be obtained [Michel and Chini (2019)]:

$$\frac{\partial U_0}{\partial T} = F - \nu U_0 - \overline{\eta_0^2} e^{-U_0^2} \tag{3.5}$$

$$\frac{\partial \eta_0}{\partial \tau} = U_0 e^{-U_0^2} \eta_0 + \frac{\partial^2}{\partial z^2} \eta_0 \tag{3.6}$$

where $U_0 = U_0(z, T)$ depends on slow time only. The overbar $\overline{(\cdot)}$ indicates an average over the fast time τ, that for a generic function ψ reads

$$\overline{\psi(z, \tau)} = \tilde{\psi}(z) = \lim_{\tau_f \to \infty} \frac{1}{\tau_f} \int_0^{\tau_f} \psi(z, \tau) d\tau \tag{3.7}$$

and τ_f represents the limiting process time scale, considerable fast compared to T but slow

compared to τ, over which the function ψ evolves.

Because the evolution equation for the fluctuations is linear and homogeneous in the fluctuation field and autonomous in the fast time τ, it is not restrictive to assume modal solutions of the form $\eta_0 = A(T)\hat{\eta}_0(z, T)e^{\sigma(T)\tau}$ where $A(T)$ is a slowly varying amplitude; $\hat{\eta}_0(z, T)$ is a vertical structure function; and $\mathrm{Re}\{\sigma(T)\}$ is a growth rate. Substituting this ansatz into (3.5)-(3.6), it is immediately clear that for the feedback term to be physically meaningful the fast-time average of the fluctuations

$$\overline{\eta_0^2} = |A|^2|\hat{\eta}_0|^2 \lim_{\tau_f \to \infty} \frac{1}{\tau_f} \int_0^{\tau_f} e^{\sigma\tau}\, d\tau \tag{3.8}$$

has to converge, excluding then the possibility for positive growth rates if $A(T) \neq 0$. In the limit of infinite scale separation $\varepsilon \to 0$ ($\tau \to \infty$), if $\mathrm{Re}\{\sigma\} < 0$ there is an exponential decay of the fluctuations on the fast time scale and, hence, a zero feedback on the slow dynamics, leading to the simplified dynamics

$$\frac{\partial U_0}{\partial T} = F - \nu U_0. \tag{3.9}$$

If $\mathrm{Re}\{\sigma\} > 0$, however, the fluctuation field could grow without bound while the mean field U_0 remains "frozen", invalidating the asymptotic scaling. This observation suggests that the system naturally selects a zero growth rate by self-adjusting to a marginally stable state. Correspondingly the asymptotic analysis must attempt to enforce the condition $\mathrm{Re}\{\sigma\} \leq 0$.

Therefore, the simplified equations for the leading-order dynamics can be reduced to an initial-value problem for the evolution of U_0 and to an eigenvalue problem for the fluctuations $\hat{\eta}_0$ being the vertical eigenfunction associated with the zero real parts of the eigenvalue σ:

$$\frac{\partial U_0}{\partial T} = F - \nu U_0 - |A|^2|\hat{\eta}_0|^2 e^{-U_0^2}, \tag{3.10}$$

$$\sigma\hat{\eta}_0 = \left(U_0 e^{-U_0^2} + \frac{\partial^2}{\partial z^2}\right)\hat{\eta}_0, \tag{3.11}$$

where the linear operator is given by

$$L = U_0 e^{-U_0^2} + \frac{\partial^2}{\partial z^2}\,. \tag{3.12}$$

Although the eigenvalue problem (3.11) is well defined for any eigenvalue σ, the reduced dynamics (3.10)-(3.11) is valid only when zero growth-rates are attained, making the operator L a singular operator. Moreover defining the L^2 inner product for two generic functions ψ_1 and ψ_2 as

$$\left\langle \psi_1(z) \middle| \psi_2(z) \right\rangle = \int_0^L \psi_1(z)^* \psi_2(z)\, dz\,, \tag{3.13}$$

we can notice that for this specific problem the linear operator is also self-adjoint; consequently the spectrum will be real ($\mathrm{Re}\{\sigma\} = \sigma$) and so will the eigenfunction $\hat{\eta}_0$.

3.3 QL algorithm and slaving of the fast dynamics

The fast and slow dynamics are now coupled by the presence of an unknown amplitude for which an evolution equation has to be derived. As shown in Michel and Chini [Michel and Chini (2019)], the standard procedure of imposing a solvability condition on the higher-order terms in the expansion of η does not yield a closed set of equations, and an alternative constraint has to be found. The key idea of this new approach is to exploit the natural tendency of the slow dynamics to evolve near to a state of marginal stability, as noted above, in order to prescribe the fluctuation amplitude required to maintain that state. Consequently the slow time derivative of the growth rate has to be zero whenever the growth rate $\sigma = 0$. To derive the necessary condition, we use perturbation analysis at the first order. By expanding in series the eigenvalue problem (3.11) around a point M (and dropping the subscript 0 for both $\hat{\eta}_0$ and U_0)

$$\sigma(T_M + \Delta T) \sim \sigma_M + \left.\frac{\partial \sigma}{\partial T}\right|_M \Delta T \tag{3.14}$$

$$L(T_M + \Delta T) \sim L_M + \left.\frac{\partial L}{\partial T}\right|_M \Delta T \tag{3.15}$$

$$\hat{\eta}(T_M + \Delta T) \sim \hat{\eta}_M + \left.\frac{\partial \hat{\eta}}{\partial T}\right|_M \Delta T \tag{3.16}$$

we obtain at order $O(\Delta T)$ the following boundary value problem for the first order correction of the eigenfunction

$$L_M \left.\frac{\partial \hat{\eta}}{\partial T}\right|_M = -\left.\frac{\partial L}{\partial T}\right|_M \hat{\eta}_M + \left.\frac{d\sigma}{dT}\right|_M \hat{\eta}_M \tag{3.17}$$

and setting the marginal stability condition $\sigma_M = 0$.

Due to the singular nature of the operator L in condition of marginal stability, the boundary

value problem (3.17) requires a solvability condition. Considering a general operator $\mathscr{L}$ with adjoint $\mathscr{L}^\dagger$ with respect to the inner product (3.13) and a generic boundary value problem $\mathscr{L}u = f$, only one of the following affirmations is true:

1. the inhomogeneous problem $\mathscr{L}u = f$ has a unique solution

2. the homogeneous adjoint problem $\mathscr{L}^\dagger \psi^\dagger = 0$ has a non-trivial solution

While the first case is verified when the adjoint operator is not singular, the second one implies that the direct problem, $\mathscr{L}u = f$, has either no solutions or infinitly many. Whenever the nullspace of the adjoint operator $\mathscr{L}^\dagger$, $ker(\mathscr{L}^\dagger)$, has a non-zero dimension, the Fredholm Alternative theorem determines the solvability of the direct problem depending on the projection of the right-hand-side f onto the onto the nullspace of $\mathscr{L}^\dagger$. Denoting with $\psi^\dagger$ the eigenfunctions of $\mathscr{L}^\dagger$ associated to the zero eigenvalue, if $\langle f | \psi^\dagger \rangle = 0$ the problem $\mathscr{L}u = f$ has infinite many solutions, and it is not solvable otherwise.

Imposing the solvability condition to the problem (3.17), and recalling that the operator L is in this specific case self-adjoint, we obtain

$$\left\langle -\left.\frac{\partial L}{\partial T}\right|_M \hat{\eta}_M + \left.\frac{d\sigma}{dT}\right|_M \hat{\eta}_M \middle| \hat{\eta}_M \right\rangle = 0 \,, \tag{3.18}$$

which results in an expression for the derivative of the growth rate, after using the normalization condition $\int_{L_z} |\hat{\eta}|^2 dz = 1$:

$$\begin{aligned}
\left.\frac{d\sigma}{dT}\right|_M &= \int_0^{Lz} \left.\frac{\partial L}{\partial T}\right|_M |\hat{\eta}_M|^2 dz \\
&= \int_0^{Lz} (1 - 2U^2)(F - \nu U)e^{-U^2}|\hat{\eta}_M|^2 dz - |A|^2 \int_0^{Lz} (1 - 2U^2)e^{-2U^2}|\hat{\eta}_M|^4 dz
\end{aligned} \tag{3.19}$$

Renaming the two integrals in (3.19) as

$$\alpha = \int_0^{L_z} (1 - 2U_0^2)(F - \nu U_0)e^{-U_0^2}|\hat{\eta}_0|^2 dz, \qquad \beta = \int_0^{L_z} (1 - 2U_0^2)e^{-2U_0^2}|\hat{\eta}_0|^4 dz \tag{3.20}$$

yields

$$\frac{d\sigma}{dT} = \alpha - |A|^2 \beta. \tag{3.21}$$

Imposing the marginal stability condition $d_T\sigma = 0$ when $\sigma(T) = 0$, yields an expression for the

amplitude that ensures the slow dynamics remains tangent to the marginally stable manifold

$$A = \sqrt{\alpha/\beta} \tag{3.22}$$

provided that the ratio α/β is non-negative.

3.4 Approaching and leaving the marginally-stable manifold

The reduced dynamics in condition of marginal stability (3.10)-(3.11) as well as the simplified one for negative growth rates (3.9), are derived based on the central assumption of infinite scale separation between the evolution of the mean field and the fluctuations. In this section we aim at analysing the two different scenarios in which this assumption is not strictly satisfied: first the case in which the posited scaling is temporarily lost during the evolution of the system due to intermittent bursting events, and second the case in which a finite scale separation, yet large, is set from the beginning.

3.4.1 Destabilizing effect of the fluctuations – Bursting events

It is straightforward to notice that the amplitude expression (3.22) is only defined for positive ratios of α and β. In this example, as in the stratified flow problem, however neither α nor β is sign-definite disallowing for the determination of A whenever $\alpha\beta < 0$. In this case, while negative values of α increase the stability of the system, eventually leading to a zero amplitude for the fluctuations (as is clear from (3.21)), negative values of β necessarily drive the system away from the marginally stable condition. In the latter scenario, the marginally stable manifold ceases to exist and the fluctuations quickly attain an asymptotically large magnitude due to the linear instability mechanism. This inevitably causes the slow variable U to respond on the fast time scale, resulting in a bursting dynamics, that eliminates the scale separation at the basis of the multi-scale analysis. In order to accommodate turbulent events associated to positive growth rates the two fields must be co-evolved on the fast time scale until the marginal-stability condition is satisfied again, i.e. until $\sigma = 0$. From a dynamical system point of view, these bursting events can be considered as "homoclinic" or "heteroclinic" connections between marginally stable manifolds.

As pointed out in [Michel and Chini (2019)], the integration of the initial finite-ε set of equations (3.1)-(3.2) is not the only co-evolution strategy that is appropriate for this fast dynamical regime. Instead, by positing the modified asymptotic expansions

$$U = U_0 + \varepsilon U_1 + \varepsilon^2 U_2 + O(\varepsilon^3),$$

$$\eta = \frac{1}{\sqrt{\varepsilon}}\eta_0 + \sqrt{\varepsilon}\eta_1 + \varepsilon\sqrt{\varepsilon}\eta_2 + O(\varepsilon^2\sqrt{\varepsilon}), \tag{3.23}$$

which incorporate the asymptotic amplification of η, the following modified reduced system is obtained:

$$\frac{\partial U_0}{\partial \tau} = -\eta_0^2 e^{-U_0^2} \tag{3.24}$$

$$\frac{\partial \eta_0}{\partial \tau} = U_0\eta_0 e^{-U_0^2} + \frac{\partial^2 \eta_0}{\partial z^2} - \eta_0^3 \tag{3.25}$$

Equation (3.25) retains the cubic non-linearity present in the original set of equations, mechanism responsible for the saturation of the exponentially growing instabilities, and thus (3.24)-(3.25) is not of QL form. Nevertheless, the system (3.24)-(3.25) has the great computational advantage of not including the small parameter ε (being the asymptotic expansion valid for $\varepsilon \to 0$) and the forcing term $F(z, t)$ in the slow dynamics. The first aspect in principle allows for a larger numerical t-step, and the second one reduces the time needed to restore the marginally-stable manifold.

We refer to this co-evolution strategy as ε-free DNS. A further option to integrate the reduced system (3.10)-(3.11) when bursting events occur and no fluctuation amplitude can be determined, is inspired by gradient descent techniques. Because of the fast and abrupt growth of the fluctuations in this regime it is reasonable to assume they dominate the evolution equation of the mean variable U, making the forcing F and the damping νU negligible (as also confirmed by the asymptotic analysis above). Then, although $A(T)$ is unknown, the mean variable U can be updated in the direction that minimizes $d_T\sigma$ making use of the eigenfunction $\hat{\eta}$ resulting from the linear eigenvalue problem (3.11):

$$\frac{\partial U}{\partial T} = C|\hat{\eta}|^2 e^{-U^2} \tag{3.26}$$

where C is an arbitrary constant.

Although these two co-evolution techniques might be computationally advantageous they might not lead to the same statistically-averaged representation of the long term dynamics. Because of the chaotic nature of the system any approximation (including the QL model) will produce a different trajectory in the state-space. Imagining a single realisation as a walk in the state-space around the building blocks of the dynamics (invariant solutions and more general

manifolds) biased by the stability of these blocks, the long term dynamics is then defined by the time spent by the trajectory in proximity of each structure. The alteration of this structures landscape, or of their stability features, might preclude some states from being reached and therefore from being represented in the final statistical ensemble/temporal average. The proof of this statement is in general not trivial, and not a topic of investigation in this work, but rather a warning for feature implementations and further developments of co-evolution techniques.

3.4.2 Beyond spherical cows – QL algorithm for finite scale separation

After having discussed the validity of the reduced dynamics when positive growth rates are realized, in this section we want to analyze the validity of the two QL filtered dynamics (3.10)-(3.9) defined for $\sigma \leq 0$, in presence of finite scale separation and how to smoothly connect them. By inspection of the feedback term (3.8), rewritten here for convenience,

$$\overline{\eta_0^2} = |A|^2 |\hat{\eta}_0|^2 \lim_{\tau_f \to \infty} \frac{1}{\tau_f} \int_0^{\tau_f} e^{2\sigma\tau} d\tau \tag{3.27}$$

the cumulative effect of the fluctuations has been set to zero for any negative growth rate and a finite amplitude has been allowed only in the case of exactly zero growth rates, leading to the two dynamics (3.9) and (3.10) respectively. However this is no longer true when considering finite τ_f (namely finite scale separation). Expressing the fast variable τ using a characteristic time-scale for the evolution of the slow dynamics $\tau_f = T_f/\varepsilon$, expression (3.27) provides the boundaries of applicability for the QL reduction when ε is finite for the given (fixed) T_f. The fluctuation effects on the slow dynamics are negligible when the growth rate is such that the exponential decay occurs in a time comparable or smaller than the characteristic time scale of the slow evolution, namely

$$\left| \frac{\varepsilon}{T_f} \int_0^{T_f/\varepsilon} e^{2\sigma\tau} d\tau \right| \simeq 0 \tag{3.28}$$

and analogously, the fluctuation dynamics is slaved to mean field when

$$\left| \frac{\varepsilon}{T_f} \int_0^{T_f/\varepsilon} e^{2\sigma\tau} d\tau - 1 \right| \simeq 0. \tag{3.29}$$

Analytically solving the integral and re-writing (3.28) as

$$\left| \frac{\varepsilon}{2 T_f \sigma} \left(e^{2\sigma T_f/\varepsilon} - 1 \right) \right| \simeq 0 \tag{3.30}$$

we can notice that the zero is only approached asymptotically for σ going to infinitely negative

values,in principle invalidating the simplified dynamics (3.9) whenever the scale separation is not infinite. However, from the practical point of view, where the root of a function can be computationally determined only up to machine precision (in the best case), this problem can be solved by introducing a finite tolerance δ and finding the values of σ for which the following inequalities are satisfied

$$
\left| \frac{\varepsilon}{2T_f\sigma} \left(e^{\sigma 2 T_f/\varepsilon} - 1 \right) \right| < \delta \qquad \rightarrow \begin{cases} \dfrac{\varepsilon}{2T_f\sigma} \left(e^{2\sigma T_f/\varepsilon} - 1 \right) < \delta & \forall \sigma < \sigma_1 \\[2mm] \dfrac{\varepsilon}{2T_f\sigma} \left(e^{2\sigma T_f/\varepsilon} - 1 \right) > -\delta & \forall \sigma \in \mathbb{R} \end{cases} \tag{3.31}
$$

$$
\left| \frac{\varepsilon}{2T_f\sigma} \left(e^{2\sigma T_f/\varepsilon} - 1 \right) - 1 \right| < \delta \qquad \rightarrow \begin{cases} \dfrac{\varepsilon}{2T_f\sigma} \left(e^{2\sigma T_f/\varepsilon} - 1 \right) - 1 < \delta & \forall \sigma < \sigma_2 \\[2mm] \dfrac{\varepsilon}{2T_f\sigma} \left(e^{2\sigma T_f/\varepsilon} - 1 \right) - 1 > -\delta & \forall \sigma > \sigma_3. \end{cases} \tag{3.32}
$$

where $\sigma_1 < \sigma_2 < 0$ and $\sigma_3 > 0$.

When growth rates smaller than σ_1 are realized the mean field evolves only under the effect of the damping and the external forcing F, and the fluctuation feedback is restored when $\sigma_2 < \sigma < \sigma_3$. Moreover, the introduction of a non-zero tolerance δ, while necessary for solving (3.28), weakens the exact constraint $\sigma = 0$, allowing for a marginal growth/decay of the fluctuations close to marginal stability. The behaviour of the integral $f = \dfrac{1}{\tau_f} \int_0^{\tau_f} e^{2\sigma\tau} d\tau$ as a function of σ is shown in figure 3.1 for both the infinite and finite scale separation case (assuming T_f fixed), highlighting in the latter case the two validity regions of the QL reductions in grey.
Moreover the presence of an extended σ-range close to marginal stability, in which the fluctuation dynamics is slaved to the mean field, might in principle allow for the presence of multiple "marginally-stable" modes (i.e. modes with a growth rate $\sigma_2 < \sigma < \sigma_3$). This case, not treated in the present work, would require the computation of multiple amplitudes, as many as the modes close to marginal stability each of them contributing to the fluctuation feedback in the mean field evolution.

It directly follows from solving (3.28) and (3.29) that none of the two reduced systems is suited to describe the real dynamics when the growth rate falls in the range $\sigma_1 < \sigma < \sigma_2$ or is beyond σ_3, in which cases the two fields need to be co-evolved on the same time scale. The latter case is only verified in the context of bursting events as previously discussed, while the first one is necessarily encountered when approaching the marginally stable manifold from a stable initial condition, or when leaving it due to α switching sign in (3.21).
We remark here that the two co-evolution regions, although serving the same purpose of bringing the system to a marginally stable state (from above or below the marginally-stable region), have a structurally different nature and find their justification in different arguments.

The co-evolution caused by a bursting event aims at stabilizing a dynamics otherwise tending towards unstable states, and its existence is independent of the value of ε. The finite scale separation assumption only shifts the σ-threshold above which it is triggered from $\sigma = 0$ (for $\varepsilon \to 0$) to $\sigma = \sigma_3$ (for $\varepsilon > 0$). On the contrary the co-evolution region identified by $\sigma_1 < \sigma < \sigma_2$, independently of whether it is approached from more stable states (σ growing from negative values smaller than σ_1) or from marginally stable states due to $\alpha < 0$ (whenever the feedback produces over-stabilizing effects) is meant to "destabilise" the dynamics (remember that $\sigma_2 < 0$) and it only exists in the case of finite scale separation. Tending τ_f to infinity in the infinite scale separation scenario, the convergence of the integral expression in (3.27) is indeed guaranteed for any negative growth rate regardless its magnitude, extending the validity region of the QL dynamics with zero fluctuation feedback (3.9) up to the marginally stable region (in this case represented by a single value $\sigma = 0$).

In § 3.4.1 three different co-evolution techniques have been presented to cope with the realization of positive growth rates, the first one being the fully non-linear dynamics (3.1)-(3.2), the second one the ε-free non-linear dynamics (3.24)-(3.25) and the third one the gradient descent-inspired evolution (3.26). Although computationally more advantageous due to absence of the small parameter ε (which allows for the implementation of a larger time-step), the last two do not include the external forcing term F, whose role might be relevant in destabilising the dynamics whenever the co-evolution is performed in the region $\sigma_1 < \sigma < \sigma_2$. For this reason, while the ε-free DNS is preferable to co-evolve the mean and the fluctuation dynamics when positive growth rates are realized, the fully non-linear ε-finite DNS must be employed for the co-evolution in stable conditions.

3.4.3 On the (non-)smoothness of the algorithm

In the limit of infinite scale separation the definition of the fluctuations feedback via the average over fast time scales (3.27) makes the QL algorithm evidently non-smooth: the feedback is finite in condition of marginal stability (provided that the integrals α and β have positive values), and it is set to zero otherwise. In contrast, the procedure developed in the previous section by taking into account a finite scale separation, allows in principle for a smooth connection among the different algorithms implemented for different stability conditions, although not ensuring it for any system.

Imagining a scenario where the system is initially placed in stable conditions, with a corresponding growth rate $\sigma < \sigma_1$, the mean dynamics evolves without any effect from the fast modes due to their exponentially fast decay, accordingly to (3.9). Because of the external forcing the slow field U progressively loses stability and the growth rate approaches the first co-evolution region between $\sigma_1 < \sigma < \sigma_2$. Here, by evolving the system via the fully non linear equations (3.1)-(3.2), the fast fluctuations slowly start playing a role that becomes more relevant the closer the system gets to the marginally-stable region. At the entrance of this region the fast dynamics resulting from the co-evolution is in principle close to the QL approximation
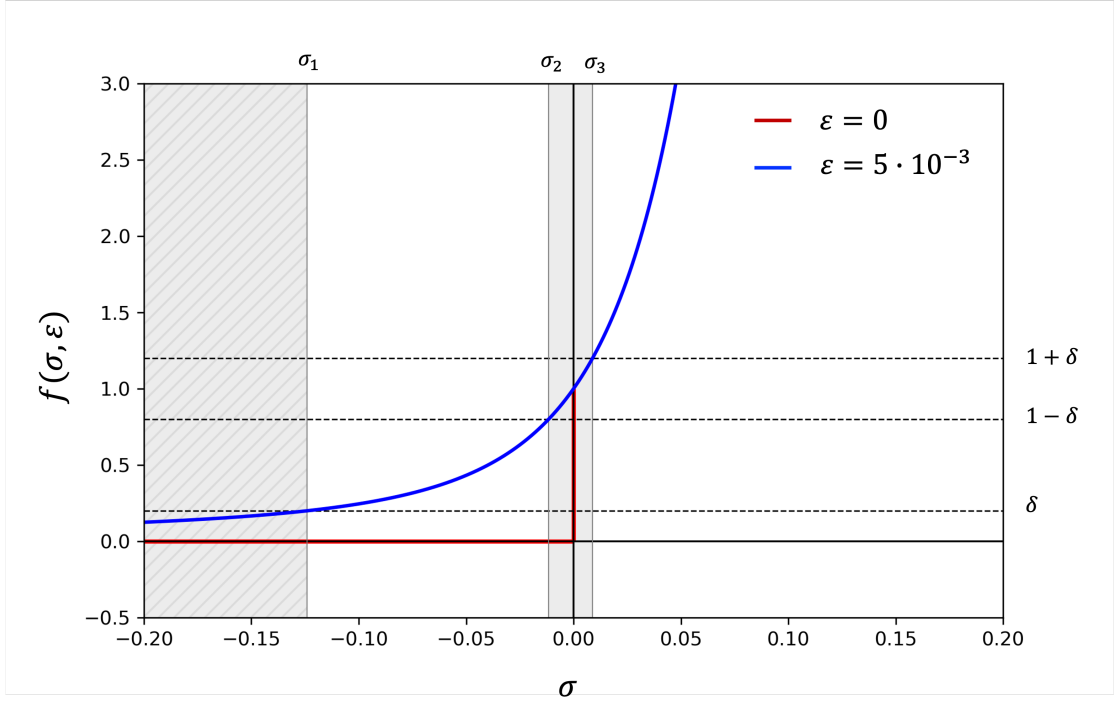
Figure 3.1 – Schematic for the finite scale separation QL methodology, as a function of the fluctuations growth rate σ, for two different values of ε and fixed $T_f = 0.1$. For values of σ smaller than σ_1 the mean field U evolves without fluctuation feedback as a consequence of the exponentially fast damping of the fast modes. The fluctuation feedback is restored close to marginal stability in the region $\sigma_2 < \sigma < \sigma_1$. The co-evolution of the two dynamics is otherwise required: either in the case of positive growth rates ($\sigma > \sigma_3$ or $\beta < 0$) or in the case of negative ones between σ_1 and σ_2 (namely when the marginally-stable manifold is approached from below or when is left due to negative values of α.

(3.10)-(3.11) (namely $\eta \sim A\hat{\eta}e^{\sigma T_f/\varepsilon}$ with $\sigma \sim \sigma_2$) and the slaving procedure of the amplitude can eventually start without any abrupt jump in magnitude of the fluctuations (characteristic of the infinite scale separation case where the fluctuation amplitude is either zero or finite). However, remarking that this procedure has been derived just by inspection of the feedback term (3.27), identical for any system, it does not take into account the peculiar features of the fully non-linear dynamics.

As is the case for many other QL reductions, the problem analysed in this chapter is characterized by an non-linear evolution equation of the fast field (3.2) that is homogeneous in the fluctuation field and autonomous in time, allowing for a zero solution that is linearly stable for negative growth rates. Therefore when initializing the system with a stable initial condition (i.e. with $U(t = 0)$ which leads to negative fluctuation growth rates $\sigma < \sigma_2$), fluctuations will generally approach zero during the co-evolution prior marginal stability (if not already zero when starting from $\sigma < \sigma_1$, in which case the fluctuations will also not grow

during the co-evolution) and they will instantaneously be finite after the marginally stable region is approached. Moreover, by examination of the non-linear dynamics in this specific problem (3.1)-(3.2) and its QL formulation for negative growth-rates (3.9), it is possible to notice that the two dynamics are identical in the case of zero fluctuations. This observation allows for the implementation of the QL reduction without feedback (in principle valid for $\sigma < \sigma_1$) even in the region $\sigma_1 < \sigma < \sigma_2$, with the computational advantage of a larger time step. However, this is in general no longer possible whenever the non-linear evolution of the slow field differs from the QL reduction, in which case even in the absence of the fluctuations the full DNS has to be performed. Differently a smooth scenario would be expected in the case of a non-homogeneous evolution of the fluctuations, where the fast non-linear dynamics would include, for example, an external forcing at order $O(\varepsilon)$ such that the zero solution would not be present, while leaving the QL reduction unchanged. However, independently of its smoothness properties, the methodology developed in the case of finite scale separations remains formally valid, legitimizing the co-evolution regions, although non-smooth, as the only possible evolution when the QL formalism is mathematically not justifiable.

3.4.4 Tertium non datur – A conjecture on the computation of the amplitude

The slaving of the fast dynamics to the mean field represents the core of the QL methodology discussed in this work. This is pursued setting the fluctuation amplitude via (3.22) such that, once the marginal stability condition is satisfied it is maintained in time. It is straightforward to notice that the computation of A is not only conditioned on the realisation of a zero growth rate, but also on positive ratios of the integral quantities α and β. Although the real-valued amplitude is mathematically well defined when both α and β are either positive or negative, we hypothesise that only the first case yields a stable evolution of the system. This insight comes from the investigation of the intermediate-time processes, whose behaviour might compromise the convergence of the fluctuation-induced feedback in (3.10). When performing the multi-scale analysis of the original system for infinite scale separations (3.1)-(3.2) introducing three time scales, T, $\psi = T/\sqrt{\varepsilon}$ and $\tau = \psi/\sqrt{\varepsilon}$ (slow,intermediate and fast time respectively), asymptotics leads to an evolution equation for the amplitude on the intermediate time-scale ψ which allows for unstable solutions when both α and β are negative. The mathematical confirmation of this postulation has not been achieved (yet) in the context of this specific model problem due to the non-linearity in U of the feedback term in (3.10) and of the advection term in (3.11), but it can be proved for a slightly modified model problem, specifically the one investigated by Michel and Chini [Michel and Chini (2019)]. The calculation for this case is presented for the sake of completeness in appendix A.

Moreover we conjecture that when considering a finite scale separation between the two dynamics the effect of the intermediate-time processes might be twofold in the marginally stable range: they explode when the scenario $\alpha < 0$ and $\beta < 0$ occurs for "marginally-stable" yet positive growth rates (namely $0 < \sigma < \sigma_3$) and they decay when the same scenario $\alpha < 0$ and $\beta < 0$ is realised for negative ones ($\sigma_2 < \sigma < 0$). The first case would drive the system towards more unstable states while the second one towards more stable conditions, requiring

either ways the co-evolution of the two fields on the same temporal scale. In view of the above, we conclude that the only possible scenario for the computation of an amplitude requires the simultaneous realisation of marginal growth rates and positive values of the integrals α and β, while any other case would lead to the co-evolution of the two dynamics.

In figure 3.2 we provide a schematic summarizing all the possible scenarios discussed in this chapter for the different validity regions of the QL reduction, and the values of α and β, including the speculation regarding the case $\alpha < 0$, $\beta < 0$, discussed above. We remark once more that the latter case remains a conjecture due to the lack of a formal prof and of a numerical evidence at this stage of the investigation.
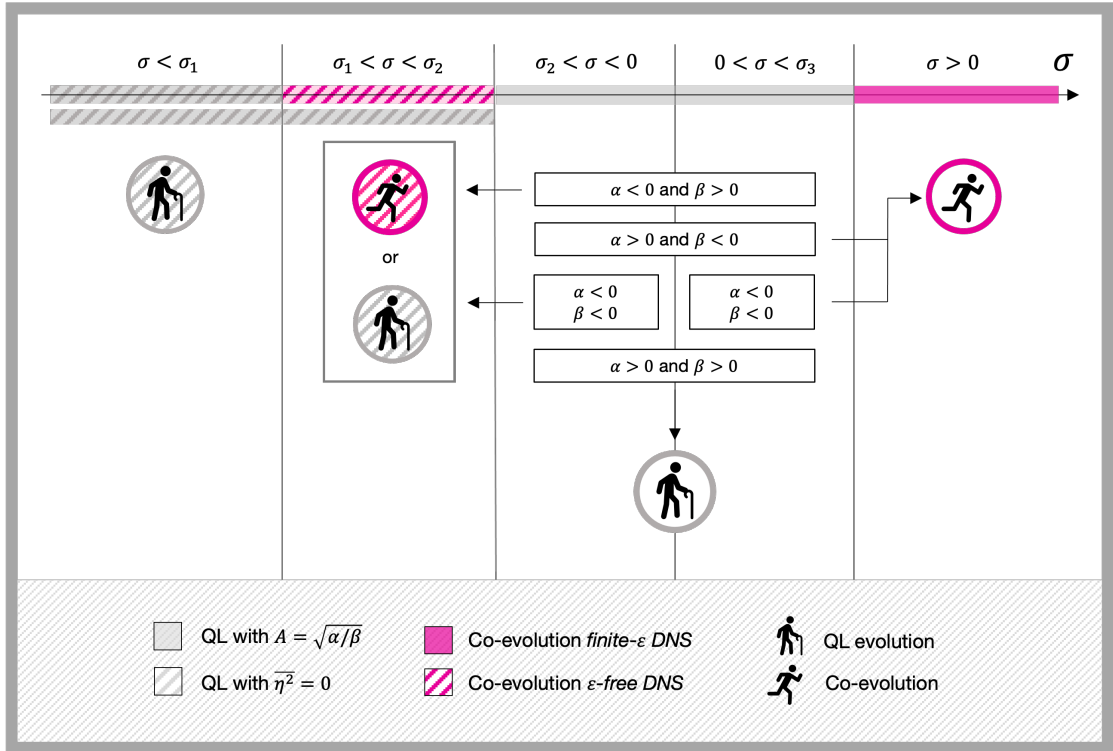
Figure 3.2 – Schematic for the finite scale separation QL methodology, conditional to the fluctuations growth rate σ and the the values of α and β. For values of σ smaller than σ_1 the mean field U evolves without fluctuation feedback as a consequence of the exponentially fast damping of the fast modes. In systems with an homogeneous and autonomous evolution of the fast modes this region can be extended up to $\sigma = \sigma_2$ due to the presence of a stable zero solution. The fluctuation feedback is restored closed to marginal stability in the region $\sigma_2 < \sigma < \sigma_3$ provided that α and β are positive and the co-evolution of the two dynamics is otherwise required. When positive growth rates are realised [in one of these cases: a)$\sigma > \sigma_3$; b) $(\sigma_2 < \sigma < \sigma_3) \wedge (\beta < 0 \wedge \alpha > 0)$; c)$(0 < \sigma < \sigma_3) \wedge (\beta < 0 \wedge \alpha < 0)$] the co-evolution is performed via the ε-free DNS (3.24)-(3.25) and conversely the finite-ε DNS is used when negative growth rates are realised [cases: d)$\sigma_1 < \sigma < \sigma_2$; e)$(\sigma_2 < \sigma < \sigma_3) \wedge (\alpha < 0 \wedge \beta > 0)$; f)$(\sigma_2 < \sigma < 0) \wedge (\beta < 0 \wedge \alpha < 0)$].

3.5   Numerical implementation and results

In this section we test the accuracy of the reduced QL algorithm presented above when a finite scale separation is taken into account and when bursting events, associated with positive growth rate of the fluctuations are realized, where in the letter case two co-evolution techniques, the finite-ε and the ε-free DNS, are compared. The results obtained from the reduced QL model are compared to the results obtained from the simulations of the fully non-linear dynamics (3.1)-(3.2).

3.5.1   Numerical set-up

For the simulations of the three different algorithms presented in this section, the QL algorithm, the finite ε DNS and the ε-free DNS, a Python code was written in-house and implemented within the open-source framework Dedalus [Burns et al. (2020)]. The original set of equations (3.1)-(3.2) and the corresponding reduced model (3.10)-(3.11) are solved in a periodic domain with $L_z = 2\pi$ using a Fourier and Chebyshev discretisation scheme respectively, with 64 grid points in each case. The use of a Chebyshev spectral method, although not optimal for problems with periodic boundary conditions, is dictated by the necessity of solving the eigenvalue problem with non-constant coefficients (3.11) within the Dedalus framework, which is presently only possible using Chebyshev polynomials.

For all the simulations the damping coefficient is set to $\nu = 1$, the scale separation parameter to $\varepsilon = 10^{-2}$ and a second-order Runge Kutta time-stepping scheme has been used. We remark that while the original QL reduction is derived in the case $\varepsilon \to 0$, its modification in the case of finite scale separation depends on ε for the determination of the regions where different algorithms are implemented (namely $\sigma_1, \sigma_2, \sigma_3$). Fixing the time-step for the slow dynamics U in the QL algorithm to $dt = 10^{-2}$ and owing the scale separation ε, resolving the fast dynamics in the finite-ε DNS requires a time step that is at least $dt = 10^{-4}$ (in order to keep $dt/\varepsilon = 10^{-2}$)

$$\frac{\partial U}{\partial t} = \frac{U^{n+1} - U^n}{dt} \qquad \varepsilon\frac{\partial \eta}{\partial t} = \varepsilon\frac{\eta^{n+1} - \eta^n}{dt} = \frac{\eta^{n+1} - \eta^n}{dt/\varepsilon} \ . \tag{3.33}$$

Such a small time-step is no longer necessary for the simulation of the ε-free dynamics (3.24)-(3.25), where both fields evolve on the fast time scale τ, and therefore the time-step can be set identical to the one for the QL dynamics $dt = 10^{-2}$.

All the numerical parameters are summarised in table 3.1

Finally, in all of the cases presented here (both for QL simulations and the finite ε-DNS), the external forcing term F is represented by the *Chini* force

$$F = 1 + 0.5\cos(t)\cos(x) + 0.5\sin(0.6t)\cos(2x) \tag{3.34}$$

whose time-dependency makes the system non-autonomous.

	L_z	N_z	dT	dt	ε
DNS	2π	64	-	10^{-4}	10^{-2}
QL	2π	64	10^{-2}	10^{-4}	10^{-2}

Table 3.1 – Numerical parameters used in this study. L_z is the domain size, N_z the number of collocation points, dT the "slow" time-step for the QL dynamics and the ε-free co-evolution, dt the time-step for the DNS and the ε-finite co-evolution, and ε the scale separation.

The algorithmic procedure developed in § 3.4, requires the communication between the QL algorithm and the non-linear dynamics whenever a co-evolution is needed. Indicating with T^* the moment at which the co-evolution is triggered, the QL solver passes the mean field $U_{QL}(T^*)$ and the fluctuation field η_{QL} to the DNS solver, in the form of $\eta_{QL} = A\hat{\eta}(T^*) + c.c.$ when an amplitude is available and initialized with Gaussian noise otherwise, and once the co-evolution is over (after a time ΔT) it receives back the updated mean field $U_{DNS}(T^* + \Delta T)$ and the fluctuation feedback $\eta_{DNS}^2 e^{-U_{DNS}^2}(T^* + \Delta T)$. The global times T^* and $T^* + \Delta T$ are also exchanged between the solvers to properly initialise the external forcing.

3.5.2 QL dynamics with finite scale separation

We start presenting the investigation of the QL dynamics in a scenario where a finite scale separation is considered but no bursting events are observed. Fixing $\varepsilon = 0.01$ and $T_f = 10 \cdot dT$, we choose here two values for the tolerance $\delta = 10^{-1}$ and $\delta = 2 \cdot 10^{-1}$ to compare the differences in the QL procedure when allowing for a larger/smaller variations of the fluctuations near marginal stability. Solving the inequalities (3.28)-(3.29) yields the following values of σ_1, σ_2 and σ_3

$$
\begin{aligned}
\delta_1 = 10^{-1} \quad &\rightarrow \quad \sigma_{1,1} = -0.4999, \quad \sigma_{1,2} = -0.0107, \quad \sigma_{1,3} = 0.0094 \\
\delta_2 = 2 \cdot 10^{-1} \quad &\rightarrow \quad \sigma_{2,1} = -0.2482, \quad \sigma_{2,2} = -0.0232, \quad \sigma_{2,3} = 0.0177
\end{aligned}
\tag{3.35}
$$

representing the validity boundaries of the QL dynamics (3.10)-(3.11) and (3.9) in the two different cases as shown in figure 3.3. An increase in the tolerance, for fixed ε, widens the validity regions of both the two reduced dynamics (grey regions), and a decrease in ε, for fixed tolerances, while increasing the σ-range for the QL dynamics (3.9) (grey textured regions) it constricts the slaving of the fluctuation dynamics (3.10)-(3.11) in a narrower region close to $\sigma = 0$ (plane grey regions).

The initialisation of the QL dynamics with a uniform mean field $U(z, t = 0) = -1$, yields a fluctuations growth rate $\sigma(t = 0) = -0.3678$, which immediately triggers a co-evolution in the simulation with a smaller tolerance ($\sigma_{1,1} < \sigma(t = 0) < \sigma_{1,2}$) and the QL evolution with zero feedback in the one with a larger tolerance ($\sigma(t = 0) < \sigma_{2,1}$). The evolution of the growth rate is shown for both simulations in figure 3.4, over slow time T and over fast time τ (top) and over
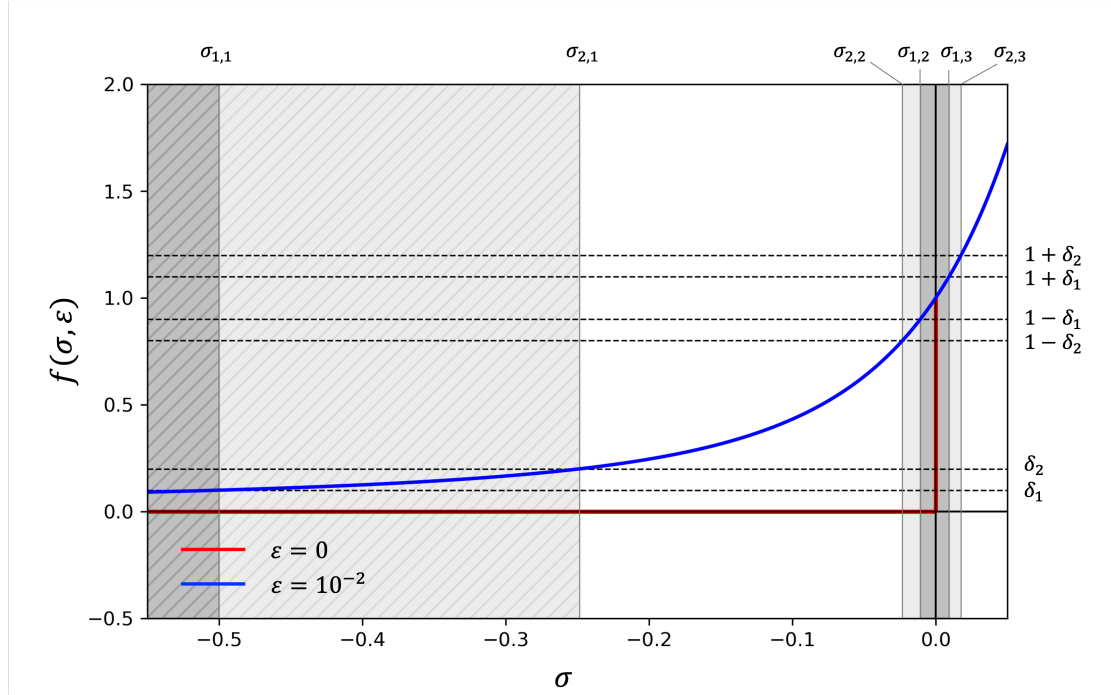
Figure 3.3 – Behaviour of the integral expression f, defining the fast average over τ of the fluctuations feedback, as a function of the growth rate σ and the scale separation parameter ε (red line for an infinite scale separation and blue one for $\varepsilon = 0.01$). Fixing T_f to 0.1 and the two different values for the tolerance δ used to solve the inequalities (here δ_1 and δ_2), the intersection of the horizontal dashed lines with the blue curve provides the graphic solutions of the equations associated with the inequalities (3.28)-(3.29) σ_{ij}, marked by the vertical lines. The regions between this solutions σ_{ij} (where the first subscript indicates the tolerance they refer to) represent the validity of the different algorithms in the QL methodology: grey textured regions ($\sigma < \sigma_{1,1}$ and $\sigma < \sigma_{2,1}$) for the the QL dynamics with $\overline{\eta^2}$ (3.9), plane grey regions ($\sigma_{1,2} < \sigma < \sigma_{1,3}$ and $\sigma_{2,2} < \sigma < \sigma_{2,3}$) for the QL algorithm near marginal stability (3.10-3.11) and white regions for the co-evolution algorithms. the different shades of grey refer to the different tolerances δ_1 (dark grey) and δ_2 (light grey).

global time $t = T + \tau/\varepsilon$ (bottom). Solid lines represent the evolution of the growth rate over slow time in the QL system (obtained from solving (3.11)), and the dashed lines the evolution of the growth rate when the co-evolution of the two dynamics is required, corresponding to the evolution of the eigenvalue of the linearised form of the full dynamics. Namely, during a co-evolution event, performed in both test cases via (3.1)-(3.2), the two fields evolve fully non-linearly and additionally the mean field U is used to solve the linear eigenvalue problem (3.11) in order to capture the moment at which the linearised system becomes marginally stable, and the QL procedure can be employed.

In the first scenario, associated to $\delta = 10^{-1}$, the condition of marginal stability is satisfied at time $t = 0.67$ with a growth rate $\sigma = -0.0008$, while in the second one ($\delta = 2 \cdot 10^{-1}$) it occurs earlier, due to the narrower co-evolution region (red dashed line) with $\sigma = -0.0132$. In both realizations the slaving of the fluctuations dynamics via the determination of the amplitude

(3.22) maintains the evolution of the system constrained to the marginally stable manifold until the end of the simulation time.
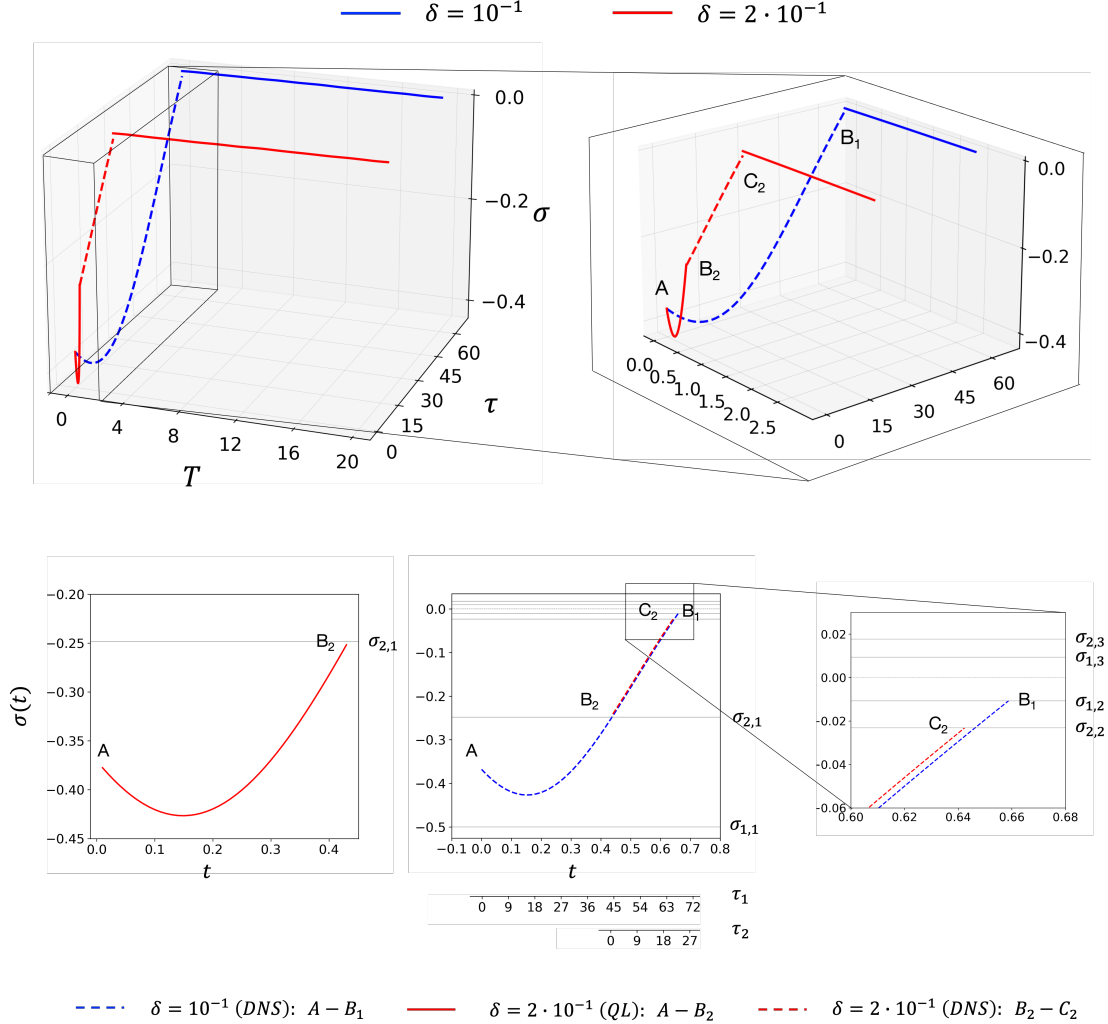
Figure 3.4 – (Top) Evolution of the growth rate σ over slow time T (solid lines) and fast time τ (dashed lines) and (Bottom) over global time $t = T + \tau/\varepsilon$ from the QL simulations with tolerances $\delta = 10^{-1}$ (blue lines) and $\delta = 2 \cdot 10^{-1}$ (red lines). For both simulations the finite scale separation is set to $\varepsilon = 0.01$ and $T_f = 0.1$. Capital letters marks the connections between the different algorithms in the two different simulations: the test case with $\delta = 1e^{-1}$ performs a co-evolution from A to B_1 at which a zero growth rate is realised, while the test case with $\delta = 2 \cdot 10^{-1}$, first performs a QL evolution with zero feedback, from A to B_2, and then a co-evolution to approach the marginally stable manifold from B_2 to C_2.

The results obtained from the QL model for $\delta = 2 \cdot 10^{-1}$ are compared to those obtained from the simulation of the fully non-linear dynamics (3.1)-(3.2) (where fluctuations have been initialised with $\eta = \cos(x)$) in figures 3.5 and 3.6, where the time-evolution of the energy and the space-time diagrams of the slow variable $U(z, t)$ and of the fluctuations $\eta(z, t)$, respectively, are presented. As is clearly evident, the reduced model not only qualitatively captures the long

term dynamics of the full system but also the detailed quantitative features of the structures underlying it, from the wavelength to the amplitude and the phase, are reproduced. This agreement between the QL model and the DNS is remarkable given the finite value of ε chosen to set the scale separation in the full system, and the non-exactly zero growth rate realized by the QL system due to the finite tolerance δ_2. The only significant observable difference in the two dynamics relates to the initial transient, as shown in figure 3.5. After an initial decay of the fluctuations field in both dynamics (as a result of the linear stability of the zero solution) the full system (continuous lines, red for the fluctuations and blue for the mean field) exhibits fast bursting events before relaxing onto the marginally stable manifold, while it occurs instantaneously in the reduced system (dashed lines) because of the slaving of the amplitude.

Although in the finite scale separation case the marginal stability condition is identified by the QL algorithm for slightly negative growth rates (given that $\sigma_2 < 0$) and therefore earlier in time if compared to the DNS, a similar shift in time would persists even with the original QL formulation for $\varepsilon \rightarrow 0$, due to the necessity for the DNS to realise positive growth rates in order to grow the almost zero fluctuations. However, owing to the chaotic nature of the full system, we remark that the QL reduction, as any approximation, can not aim at reproducing point-wise in time the original dynamics but should rather aim at capturing its long term structural features in a statistical sense.

Moreover, from the algorithmic point of view, the decay of the fluctuations for negative growth rates (and hence a zero feedback on the mean dynamics) in the full systems leads to an evolution equation for the mean field that is, for this specific problem, identical to its QL reduction (3.9), valid for $\sigma < \sigma_1$. This consideration practically allows for the extension of the region delimited by σ_1 to growth rates up to σ_2, avoiding the necessity for a co-evolution to approach marginal stability in the QL simulations.
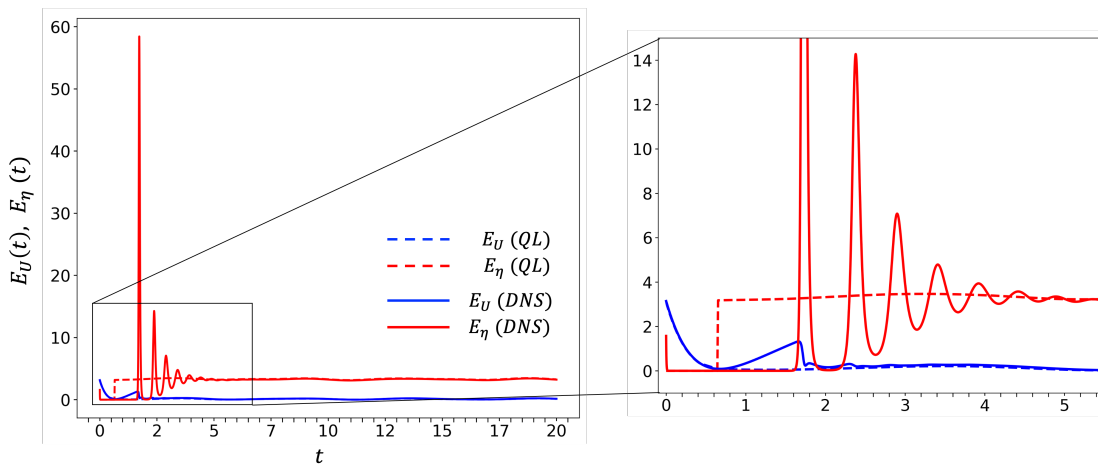
Figure 3.5 – Temporal evolution of the mean field energy (blue lines) and fluctuation energy (red lines) from the DNS (solid lines) and the QL simulation with tolerance $\delta = 2 \cdot 10^{-1}$ and finite scale separation parameter $\varepsilon = 0.01$ (dashed lines).
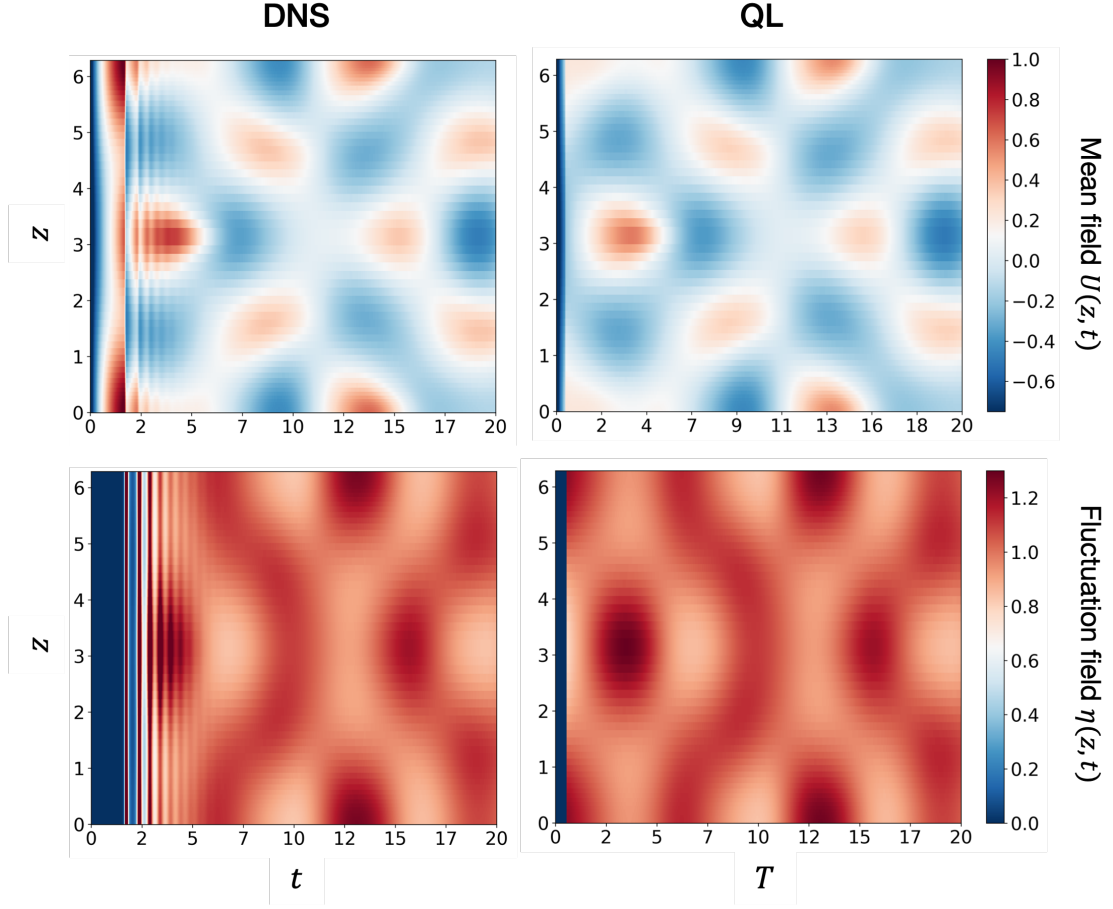
Figure 3.6 – Space-time evolution of the mean field U (top row) and of the fluctuations η (bottom row) from the DNS (left column) and from the QL simulation with tolerance $\delta = 2\cdot10^{-1}$, $T_f = 0.1$ and finite scale separation parameter $\varepsilon = 0.01$ (right column) .

3.5.3 QL dynamics with bursting events - connecting marginally-stable manifolds

To assess the efficacy of the strategies presented in section 3.4.1, for coping with fluctuation events associated either with an initial positive growth rate or with subsequent occurrences of positive feedback (i.e. $\beta < 0$) for $\sigma = 0$, the second test case has been initialized with the initial condition $U_0(z, 0) = 1.3 \tanh(8\cos(z))$, corresponding to a stable state within the range $\sigma_1 < \sigma < \sigma_2$. After a short evolution of the mean field without effects from the fluctuations feedback (QL algorithm (3.9)), the marginally-stable condition is satisfied and the fast dynamics adjusted to maintain it. Unlike the scenario previously discussed, where a zero growth rate was persisting in time, in this case it is quickly lost due to a bursting event detected by the QL algorithm as a change in sign of the integral quantity β in (3.21) which precludes the computation of an amplitude, driving the system towards unstable states. That is, the fluctuation-induced feedback has a destabilizing effect on the mean field and the co-evolution of the two fields is necessary until a neutral growth rate is re-established. The evolution of the

35

growth rate over time is shown in this case in figure 3.7: blue dashed line for the QL dynamics without fluctuation feedback, blue solid line for the QL dynamics in condition of marginal stability and red curve for the co-evolution ($\beta < 0$) event.

Figure 3.7 – Evolution of the growth rate σ over slow time T (blue lines) and fast time τ (red lines) from the QL simulations with tolerance $\delta = 2 \cdot 10^{-1}$ in t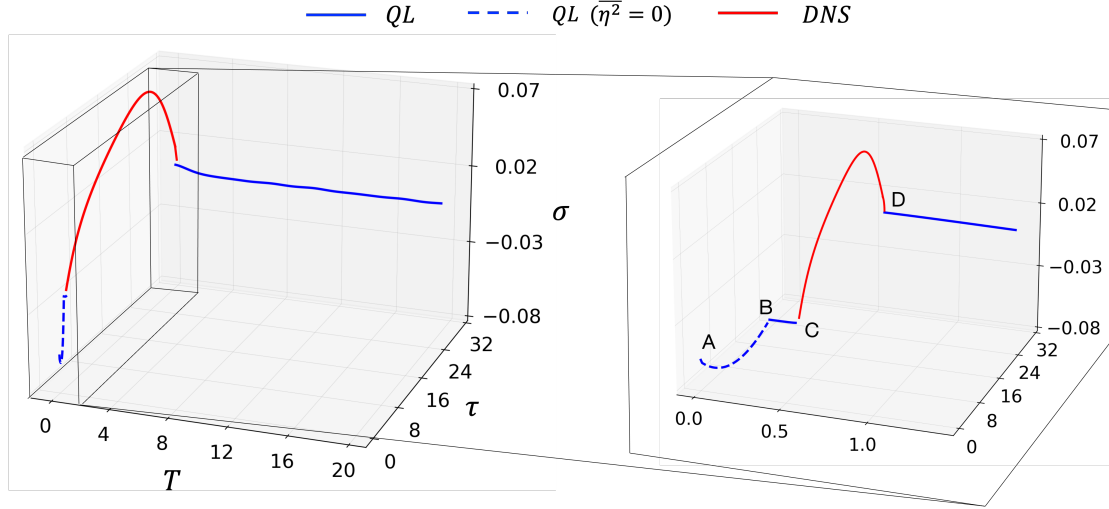he case of finite scale separation ($\varepsilon = 0.01$, and $T_f = 0.1$). Capital letters mark the connections between the different algorithms: the QL algorithm with zero fluctuation feedback (3.9) is performed from A to B for growth rates $\sigma < \sigma_2$ (blue dashed line); the QL algorithm in condition of marginal stability (3.10)-(3.11) is executed when $\sigma_2 < \sigma < \sigma_3$ in $B - C$ and in D (solid blue lines); the finite-ε DNS (3.1)-(3.2) is simulated from C to D in the region $\sigma_2 < \sigma < \sigma_3$ with $\beta < 0$ (solid red line).

As visible in figure 3.8, showing the evolution of the energy of both the fast and the slow dynamics, the cessation of the marginally-stable manifold in the QL dynamics corresponds to a bursting event in the full dynamics where the fluctuation field exponentially grows causing a response on the fast time scale of the mean dynamics. Although seemingly similar to the bursting event observed in the initial transient of the previous test case (fig. 3.5), here the mean field from the non-linear dynamics (blue solid curve) is clearly approaching a neutrally-stable state, even if for short time, prior to the fluctuations exponential growth. The inset region of figure (fig. 3.5), where the energy of both fields is shown during the co-evolution event (black dashed curve for the fluctuation energy and black solid line for the mean field energy), clearly shows the saturation of the instability due to the restoring effect of the cubic non linearity and the re-establishment of the marginally stable condition in the QL dynamics. In this specific scenario the bursting event is responsible for bringing the system from the initial marginally-stable state, ($B - C$) in fig. 3.7, to a new one, (D) in fig. 3.7, with different features, serving as "heteroclinic connection" between distinct marginally-stable manifolds. Already visible from the evolution of the energy (fig. 3.5)), this transition between marginally-stable manifolds is directly noticeable in the evolution of the vertical profile of the mean field $U(z)$ through the co-evolution event, shown in figure 3.9. Once again, we point out that the occurrence of the bursting event (as for the detection of the marginally-stable manifold) at a different

time in the QL dynamics, compared to the DNS, is a consequence of the chaotic behavior of the original dynamics, by definition sensitive to small variations in the initial conditions and in the governing equations. Moreover, because the system is non-autonomous due to the presence of the time-dependent force $F(z, t)$, a time difference in the occurrence of these events will necessarily drive the systems to different states on the short term dynamics, making a point-wise comparison of the two dynamics useless. The remarkable feature of the reduced dynamics, in this case, is rather its capability of capturing the transition between the two marginally stable manifolds, an event that clearly takes place in the full dynamics even if at a different time and therefore through different "states".
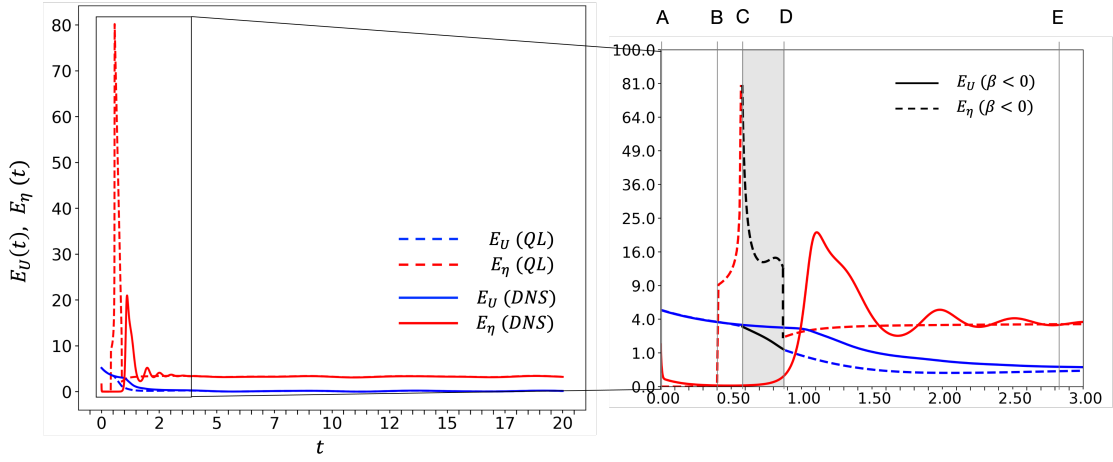
Figure 3.8 – Temporal evolution of the mean field energy (blue lines) and fluctuations energy (red lines) from the DNS (solid lines) and the QL simulation with tolerance $\delta = 2 \cdot 10^{-1}$, $T_f = 0.1$, and finite scale separation parameter $\varepsilon = 0.01$ (dashed lines). Black lines in the zoomed inset region represent the energy of the fluctuations (dashed line) and of the mean field (solid line) during the co-evolution event (performed with the finite-ε full dynamics (3.1)-(3.2) and highlighted in grey) triggered by the occurrence of $\beta < 0$ in the QL dynamics.

Differently from the co-evolution used to approach marginal stability (discussed in the previous section and not implemented for this test case) whose aim was to smoothly connect the QL dynamics valid $\sigma < \sigma_1$ and the one in marginally-stable condition, the co-evolution triggered by the termination of the marginally-stable manifold (specifically due to $\beta < 0$) is meant to re-stabilize the dynamics otherwise exploding in the quasi-linear reduction. For this reason the destabilising effect of the external force $F(z, t)$ (useful to reach marginally-stable growth rates from stable conditions) can be ruled out, performing the co-evolution via the re-scaled equations (3.24)-(3.25), as discussed in § 3.4. In addition to the absence of the external forcing, these equation have the great advantage of evolving the two dynamics on the same temporal scale, allowing for the implementation of a time-step that is two orders of magnitude larger then the one used in presence of the small parameter ε. This represents a key feature for systems (like the stratified flow problem) where the full DNS has extremely high computational costs.

Figure 3.10 shows the evolution of the growth rate over global time, $t = T + \tau / \varepsilon$, (top figure) and

the evolution of the corresponding quantities α and β for two QL simulations (with $\delta = 2 \cdot 10^{-1}$ and $\varepsilon = 0.01$) where the bursting event is treated using the different co-evolution dynamics: finite-ε DNS (3.1)-(3.2) (blue dashed curve for σ, grey solid curve for β and grey dashed curve for α) and ε-free DNS (3.24)-(3.25) (red dashed curve for σ, black solid curve for β and black dashed curve for α). In this specific case, the usage of the re-scaled non-linear dynamics yields a much longer co-evolution event, due to the persistence of a negative value of the integral β together with a negative value of α. While negative values of β reflect an increase of the growth rate, delaying the moment at which the grow rate reaches again the marginally-stable region (the system starts gaining stability after β crosses again zero and becomes positive), negative values of α impede the co-evolution from ceasing when the marginally-stable region is again approached (point F in fig. 3.10), due to the impossibility of computing an amplitude. Therefore the co-evolution is prolonged until the growth rate reaches σ_2 (point G) where the QL approximation without fluctuations feedback is used (therefore independently of the sign of α and β) to reach again the marginally stable manifold (point H). The seemingly more cumbersome scenario obtained when using the ε-free DNS to cope with positive growth rate, it is not related to any structural feature of the re-scaled dynamics but it is just a specific trajectory in its state space, realised for the given initial condition (at point C) and numerical parameters. Figure 3.11 shows the different evolution of σ obtained applying the same co-evolution technique on a slightly different QL system where the tolerance has been lowered to $\delta = 10^{-1}$ (red line). As evident, the resulting behaviour in this case is qualitatively much closer to one obtained from the finite-ε co-evolution technique (blue curve).

Moreover, although the duration (in global time units) of the bursting events is longer when co-evolving the two fields with the re-scaled non-linear dynamics (for both scenarios with $\delta = 2 \cdot 10^{-1}$ and $\delta = 10^{-1}$), this technique is computationally far more efficient than the full DNS, as visible in figure 3.12. The zero growth rate is reached, with the $\varepsilon-$free DNS, in about 20 solver iterations in the test-case with $\delta = 10^{-1}$, and after 150 iterations in the case with $(\delta = 2 \cdot 10^{-1})$, respectively 2 orders of magnitude fewer when compared to the full DNS in the first case (QL with $\delta = 10^{-1}$) and one order of magnitude fewer in the second one (QL with $\delta = 2 \cdot 10^{-1}$). Regardless of the different paths followed by the three numerical simulations (DNS and QL dynamics with different co-evolution techniques) to transition between the two marginally-stable manifolds, the same long term dynamics is eventually approached in the three cases. This is clearly visible in figure 3.13 and 3.14, where the space-time evolution of the mean field U and the fluctuations η are visualized, and in figure 3.15, showing the vertical profiles of the two fields at time $t = 18$ (far from the initial transient) for the same three test cases (top row) and for a QL scenario with a smaller tolerance δ (bottom row).

We conclude by testing the last co-evolution strategy, namely the gradient descent-like technique (3.26) (indicated from now on as GD co-evolution), against the the ε-finite co-evolution and the ε-free co-evolution. Figure 3.16 shows the evolution of the growth rate for three QL simulations (all performed with a tolerance $\delta = 0.1$ and $\varepsilon = 0.01$) over global time (left) and compares the number of solver iterations required to re-establish the marginally-stable condi-

tion with the three different techniques. The number of iterations for the GD co-evolution is comparable to the one for the ε-free co-evolution, therefore representing a more efficient choice with respect to the ε-finite co-evolution. This technique has also an other remarkable advantage, that makes it preferable even to the ε-free co-evolution: it updates the mean field only using the eigenfunction resulting from solving the eigenvalue problem, and therefore it does not require any additional information other than the one already present in the QL simulation. This advantage will become crucial in the next chapters (and specifically in § 5) when extending this methodology to higher dimensions.

The entire QL algorithmic structure proposed and tested in this chapter, including both the extension for finite scale separation and for bursting events is shown by the flowchart in figure 3.17, where all the logical and computational steps are summarised.

3.6   Conclusions

Starting from the approach of Michel and Chini [Michel and Chini (2019)] we have developed a numerical procedure that can properly accommodate finite scale separation and bursting events associated with positive fluctuation growth rates.

When a finite scale separation is considered the algorithmic procedure we have derived consists of different algorithms, simulated in different stability conditions, coherently connected to each other. The main difference compared to the infinite scale separation algorithm is the emergence/modification of three regions: the marginally stable region, the stable region and the region in between. While in the case $\varepsilon \to 0$, the marginally stable condition is verified at σ exactly zero, the finite ε case allows for the identification of an extended region comprehensive of positive and negative values of σ (after a certain tolerance is set). In this σ-range the growth/decay of the fluctuations is close enough to zero (according to the tolerance) to compute an amplitude. Similarly the algorithm identifies the region where the growth rate is, this time, negative enough to ensure the decay of the fast modes over slow time and therefore set the fluctuations feedback to zero. This latter region, also present in the infinite scale separation scenario, is now separated from the marginally-stable one by the appearance of a new region where the fluctuation growth rate is neither close enough nor far enough from zero to simulate one of the two QL dynamics. Therefore the co-evolution of the two fields has to be performed here.

This QL methodology has then been further extended to handle bursting scenarios where the scale separation is temporarily lost due to the realisation of positive fluctuations growth rates, requiring again the co-evolution of the coupled system. In this regard three different co-evolution methods were tested: finite-ε DNS (the full non-linear system), ε-free DNS (the re-scaled non-linear system for the bursting regime) and a gradient descent technique. The first two methods explicitly reintroduce the fluctuation non-linearities in the dynamics, which generally are not negligible when fluctuation amplitudes are large and which may be crucial for the saturation of instabilities. The third method exploits information from the eigenvalue

problem by shooting in the direction provided by its linear eigenfunctions. Although all the techniques successfully drive the dynamics to a new marginally-stable manifold, the computational expense of the last two approaches, ε-free DNS and the gradient descent technique, is shown to be one order of magnitude smaller than that of the full DNS. Moreover the gradient descent technique, although crude, has the advantage in many cases (as remarked in § 5) of not requiring further information or arbitrary choices, like the domain size and initial conditions for the fast field, other then the ones already present in the QL approximation.
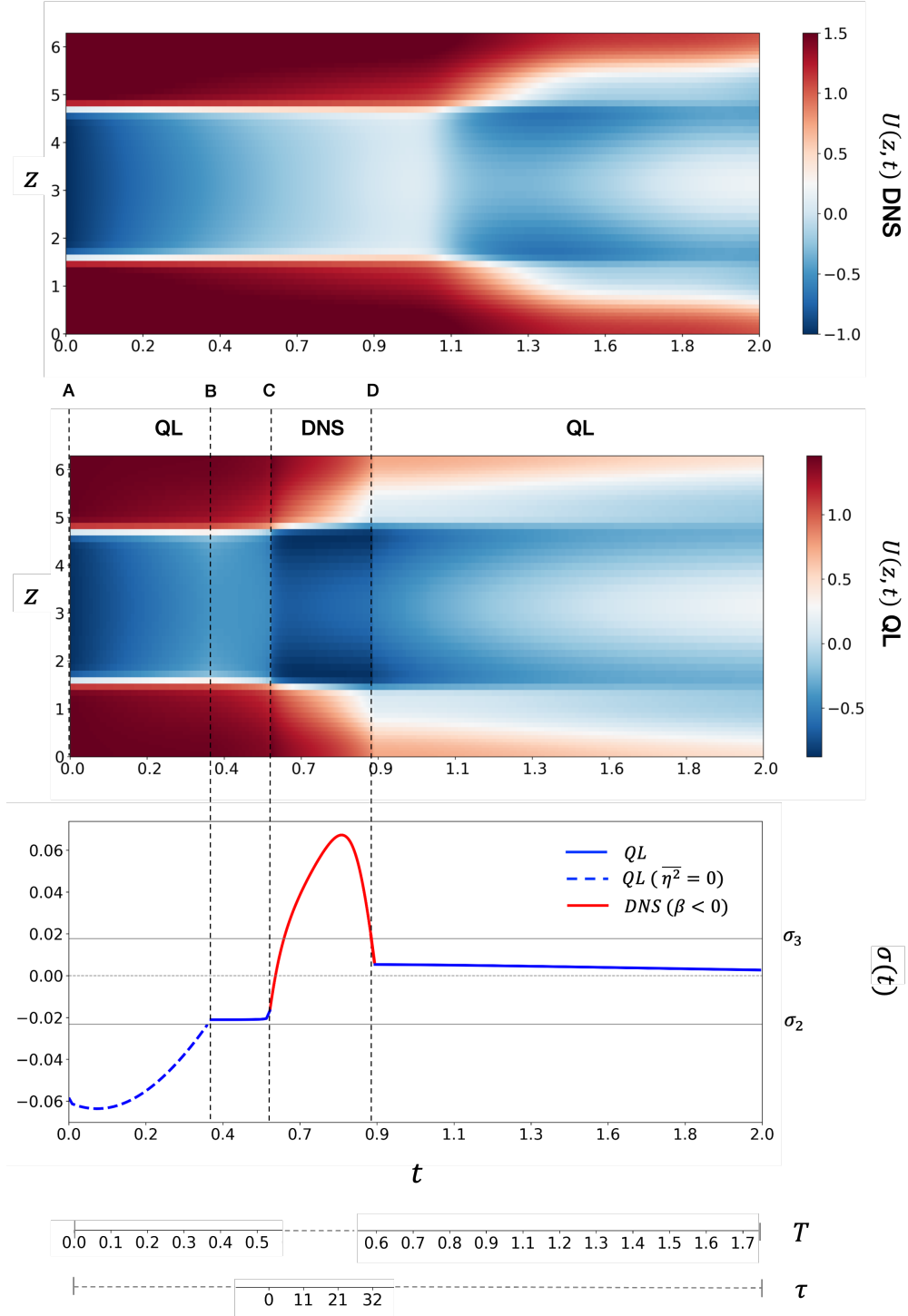
Figure 3.9 – Space-time evolution of the mean field $U(z,t)$ during the bursting event from the DNS simulation (top) and the QL algorithm (center), and corresponding evolution of the linear growth rate σ over global time $t = T + \tau/\varepsilon$ (bottom) from the QL simulation. Capital letters mark the connections between the different algorithms: the QL algorithm with zero fluctuation feedback (3.9) is performed from A to B for growth rates $\sigma < \sigma_2$ (blue dashed line); the QL algorithm in condition of marginal stability (3.10)-(3.11) is executed when $\sigma_2 < \sigma < \sigma_3$ in $B - C$ and in E (solid blue lines); the finite-ε DNS (3.1)-(3.2) is simulated from C to D in the region $\sigma_2 < \sigma < \sigma_3$ with $\beta < 0$ (solid red line).

41
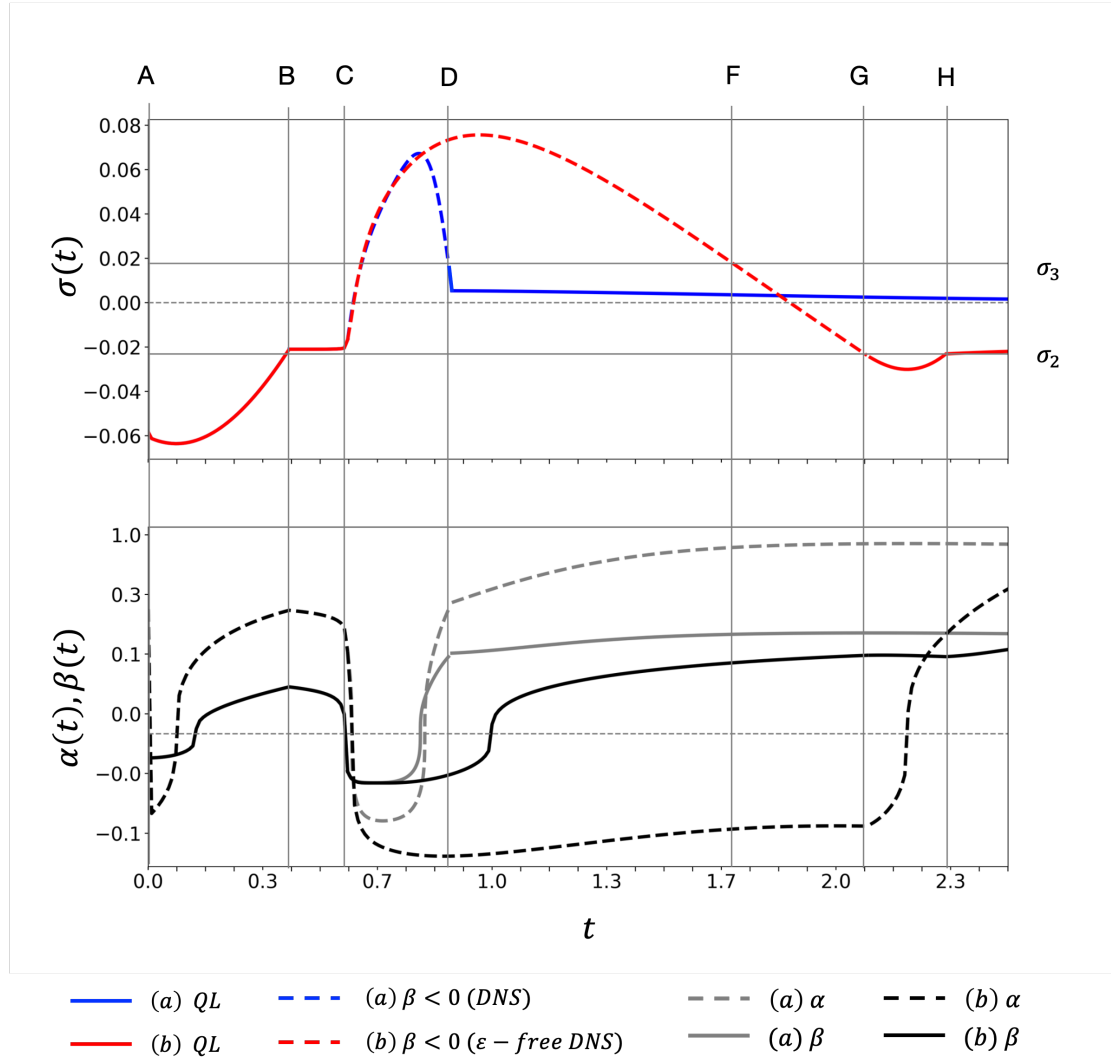
Figure 3.10 – Top: Temporal evolution of the growth rate for two QL simulations (with $\delta = 2 \cdot 10^{-1}$, $T_f = 0.1$, and $\varepsilon = 0.01$) employing different co-evolution techniques during the bursting event: full DNS (3.1)-(3.2) for the simulation (a) (blue line) and ε-free DNS (3.24)-(3.25) for the simulation (b) (red line). Bottom: Temporal evolution of the integral quantities α (dashed line) and β (solid line) corresponding to the QL simulation (a) (grey lines) and to the QL simulation (b) (black lines). Capital letters mark the connections between the different algorithms in time: the QL algorithm with zero fluctuation feedback (3.9) is performed from A to B for growth rates $\sigma < \sigma_2$ in both simulations (blue and red solid lines) and again from G to H for the simulation (b) (red solid line); the QL algorithm in condition of marginal stability (3.10)-(3.11) is executed when $\sigma_2 < \sigma < \sigma_3$ in $B - C$ for both simulations and again in E for the QL simulation (a) (solid blue lines) and in H for the simulation (b) (solid red line); the finite-ε DNS (3.1)-(3.2) is simulated for the case (a) from C to D during the bursting event with $\beta < 0$ (dashed blue line) while the ε-free DNS is used in the case (b) to co-evolve the two fields from C to G (red dashed line).

Figure 3.11 – Temporal evolution of the growth rate for two QL simulations (with $\delta = 10^{-1}$, $T_f = 0.1$ and $\varepsilon = 0.01$) employing different co-evolution techniques during the bursting event: full DNS (3.1)-(3.2) for the simulation (a) (blue line) and ε-free DNS (3.24)-(3.25) for the simulation (b) (red line).
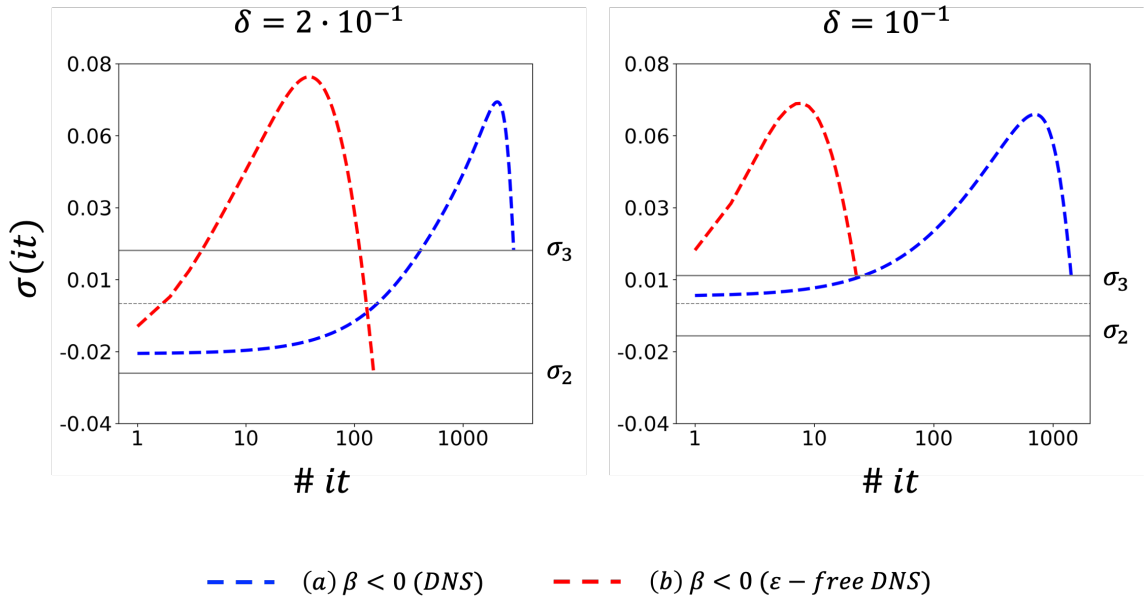
Figure 3.12 – Evolution of the growth rate in solver iteration units during a bursting events ($\beta < 0$) for QL simulations with $\delta = 2{\cdot}10^{-1}$ (left) and $\delta = 10^{-1}$ (right) using different co-evolution techniques: full DNS (3.1)-(3.2) in the case (a) (blue line) and ε-free DNS (3.24)-(3.25) in the case (b) (red line).
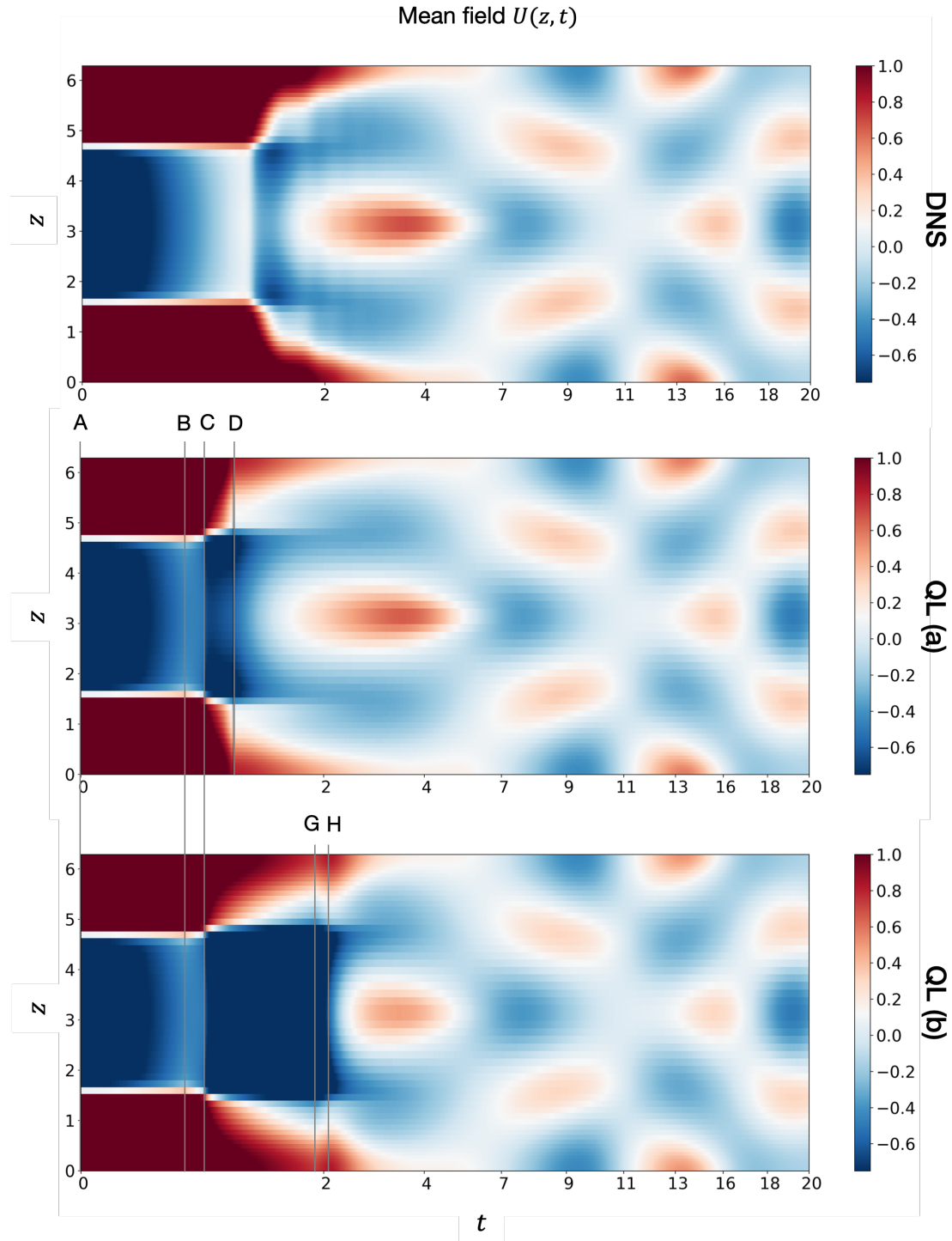
Figure 3.13 – Comparison of the space-time evolution of the slow dynamics resulting from the DNS (3.1)-(3.2)(top), from the QL simulation with finite-ε DNS as a co-evolution technique (center) and from the QL simulation with ε-free DNS (3.24)-(3.25) as a co-evolution technique (bottom). $\varepsilon = 0.01$ in all simulations and the tolerance $\delta = 2 \cdot 10^{-1}$ and $T_f = 0.1$ are fixed for the two QL dynamics.
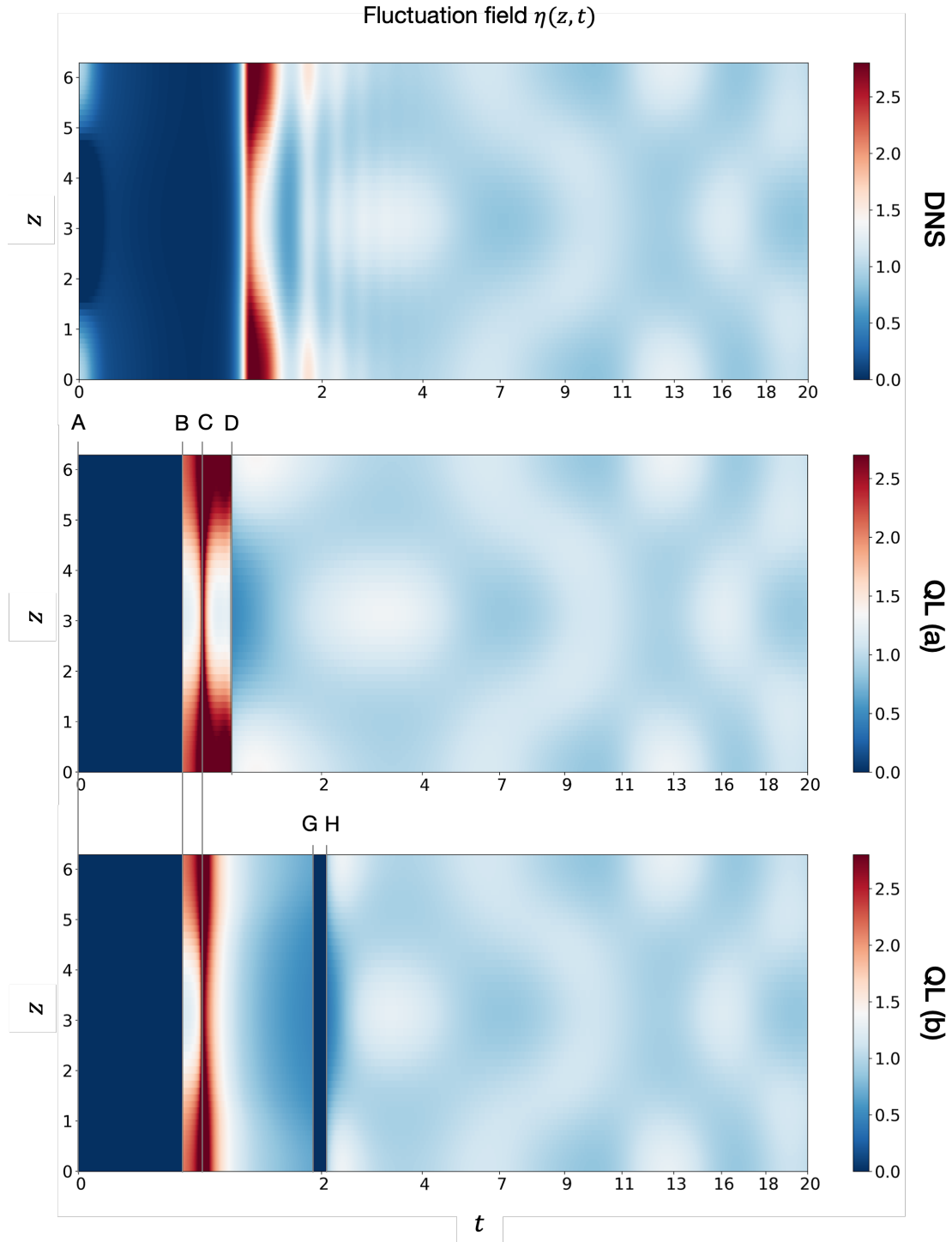
Figure 3.14 – Comparison of the space-time evolution of the fast dynamics resulting from the DNS (3.1)-(3.2)(top), from the QL simulation with finite-ε DNS as a co-evolution technique (center) and from the QL simulation with ε-free DNS (3.24)-(3.25) as a co-evolution technique (bottom). $\varepsilon = 0.01$ in all simulations and the tolerance $\delta = 2 \cdot 10^{-1}$ and $T_f = 0.1$ are fixed for the two QL dynamics.
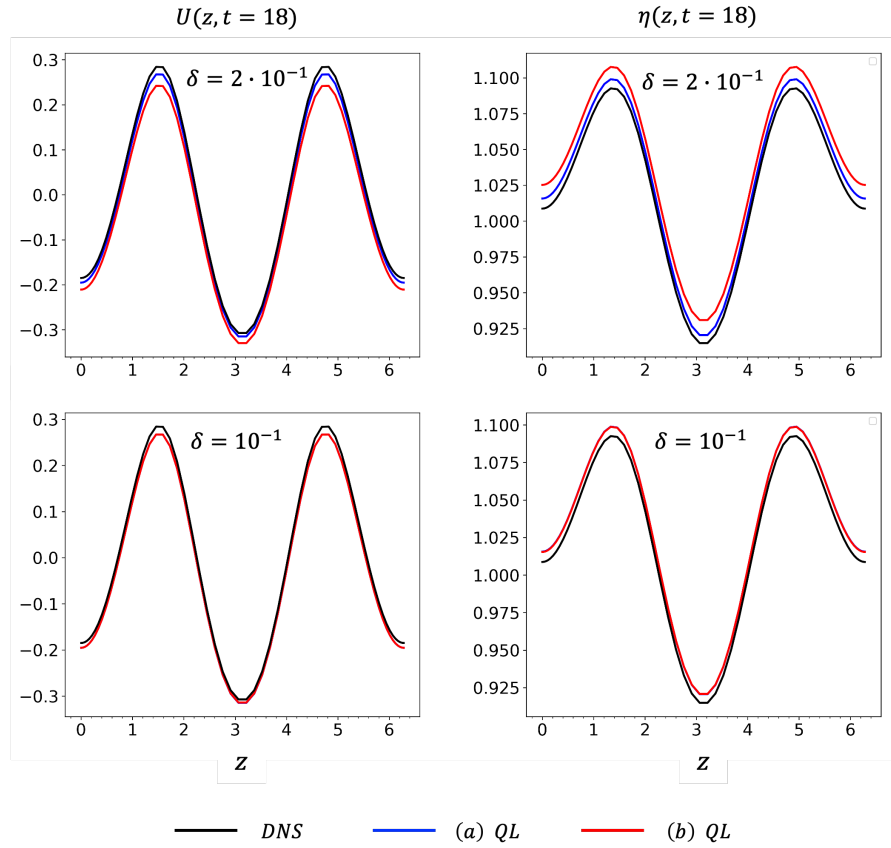
Figure 3.15 – Vertical profiles of the mean field $U(z)$ (left) and the fluctuation field $\eta(z)$ (rigth) at global time $t = 18$ from the DNS simulation (black curve) and from the QL simulations with $\delta = 2 \cdot 10^{-1}$ (top row) and $\delta = 10^{-1}$ (bottom row) where different co-evolution techniques are used during the bursting event: full DNS (3.1)-(3.2) for the QL simulation (a) (blue line) and ε-free DNS (3.24)-(3.25) for the QL simulation (b) (red line).
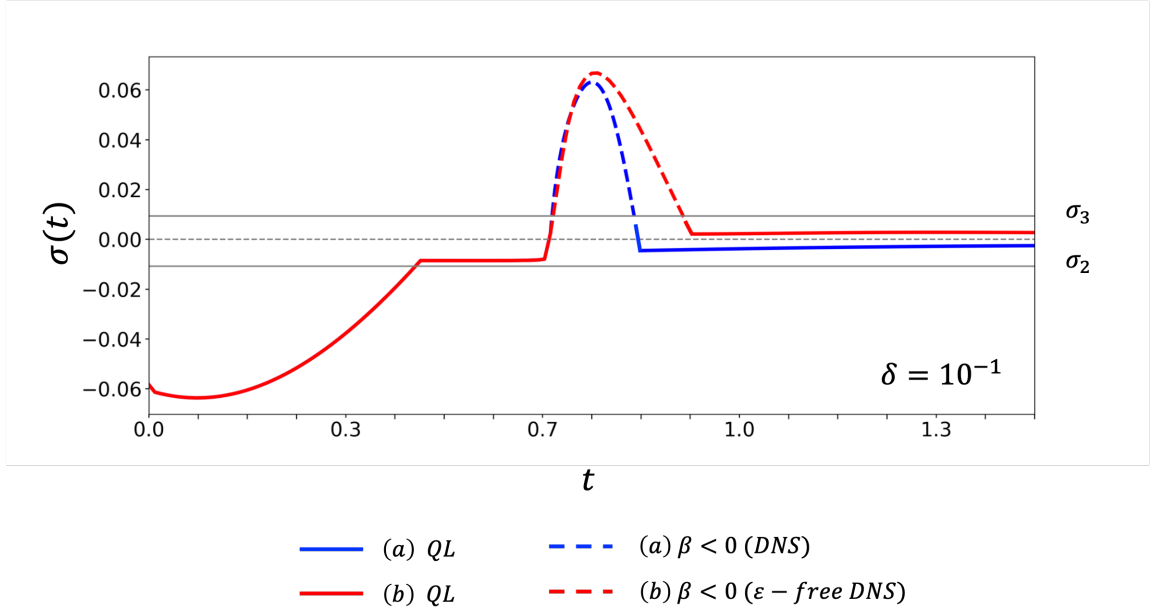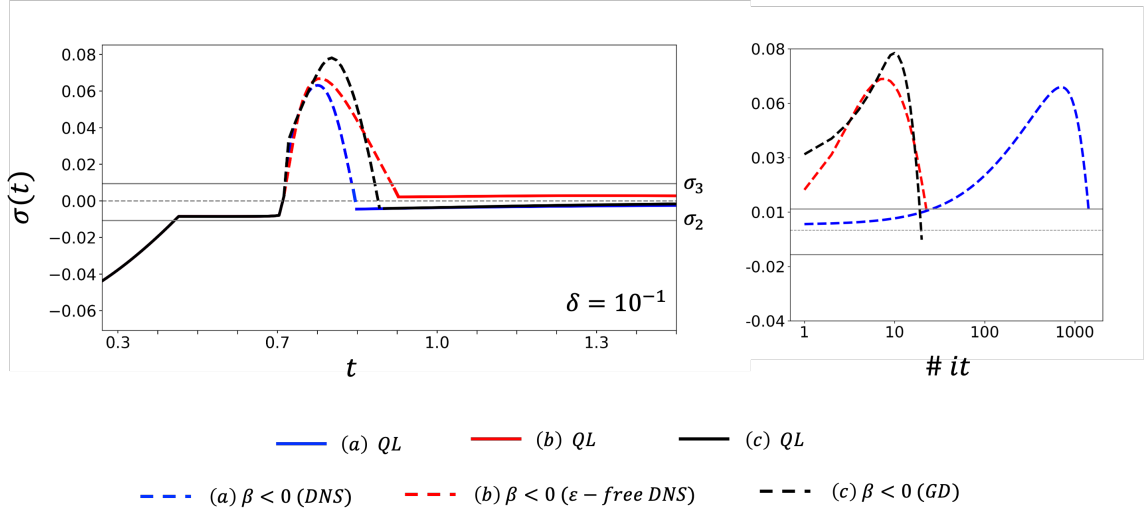
Figure 3.16 – Temporal evolution of the growth rate for three QL simulations (with $\delta = 10^{-1}$, $T_f = 0.1$ and $\varepsilon = 0.01$) employing different co-evolution techniques during the bursting event: full DNS (3.1)-(3.2) for the simulation (a) (blue line), ε-free DNS (3.24)-(3.25) for the simulation (b) (red line), and gradient descent for the simulation (c) (black line). The plot on the left shows the evolution over global time $t = T + \tau/\varepsilon$, while the right plot shows the evolution during the bursting event in terms of solver iterations.
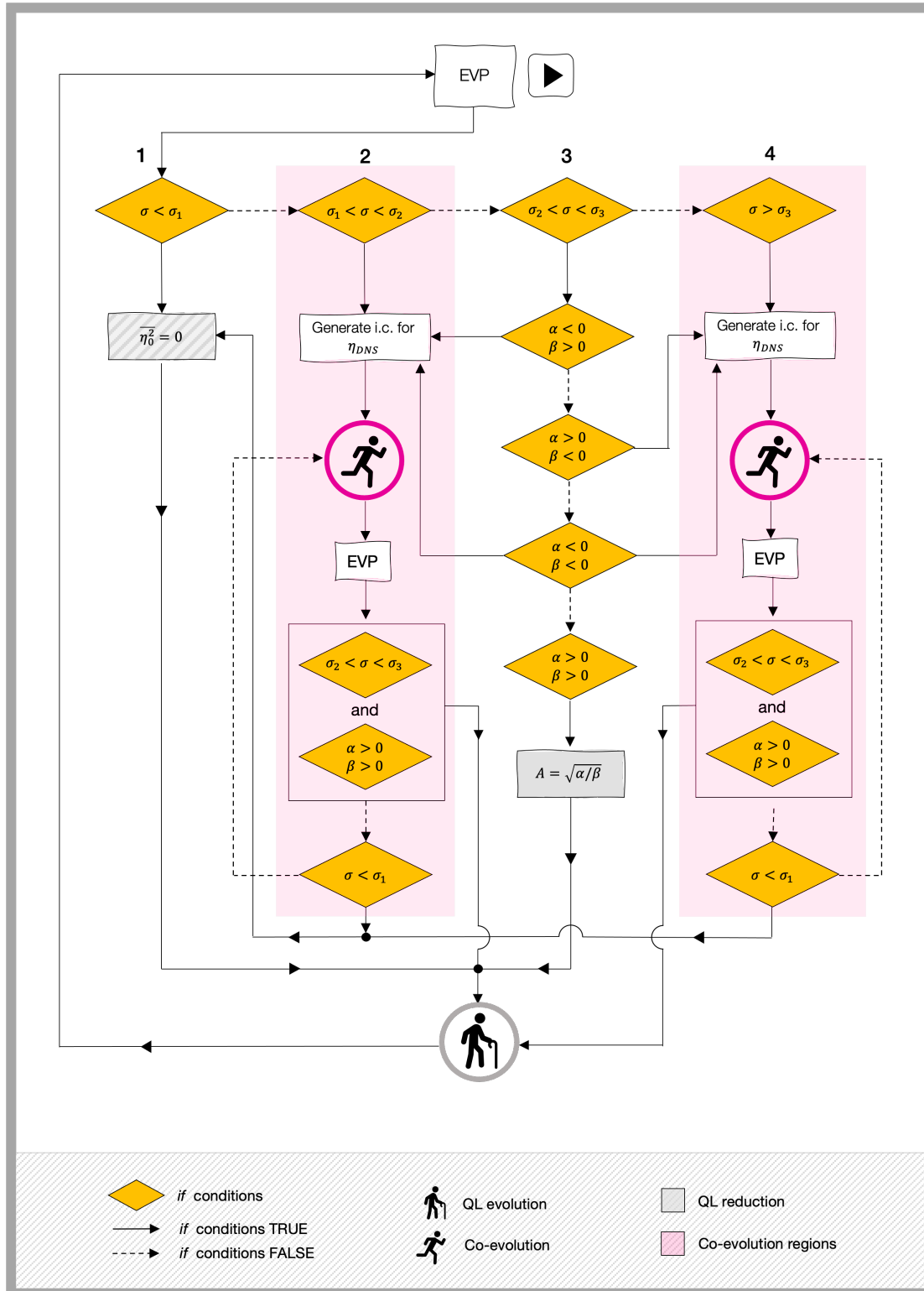
Figure 3.17 – Flowchart of the 1D QL algorithm. Rectangular boxes indicate actions, the white ones for generic actions and the grey ones for actions related to the fluctuation feedback. *if*-statements are represented by yellow diamond-shaped boxes, and their outcome by a continuous arrow-connection when the *if*-condition is meet and with a dashed one otherwise. The loop is started by solving the linear eigenvalue problem for the maximum growth rate σ and the corresponding eigenfunction $\hat{\eta}$. When negative growth rates below σ_1 characterize the state of the system, the slowly-varying amplitude of the fluctuation is set to zero and the mean field is updated on the slow time scale without any feedback term (block 1). Once the destabilising effect of the forcing F brings the system in the stability region $\sigma_1 < \sigma < \sigma_2$ the co-evolution to approach the marginally-stable region is performed simulating the eq. (3.1)-(3.2) (block 2). At the realisation of neutrally-stable growth rates the system enters the block 3, where a fluctuation amplitude is computed in the case $(\alpha > 0 \wedge \beta > 0)$. Any scenario in this region different from $(\alpha > 0 \wedge \beta > 0)$ will cause the termination of the marginally-stable manifold either towards more unstable states (block 4) or towards more stable ones (block 2) causing in any case the co-evolution of the two dynamics. Co-evolutions in block 2 are performed via the full DNS, while co-evolution in block 4 via the re-scaled ε-free DNS. In both cases after a "fast integration"-step the EVP corresponding to the linearised problem is solved and the conditions to exit the co-evolution blocks are checked: the fast integration terminates when the marginally-stable region is approached again with $(\alpha > 0 \wedge \beta > 0)$ or when $\sigma < \sigma_1$, if the previous condition is never verified. In the first case the slaving of the fluctuation dynamics continues, and a zero feedback is enforced in the second case.

4 2D Model Problem - Identification of the Fastest Growing Mode

Chapter summary

A 2-dimensional extension of the QL formalism developed in § 3 for quasi-linear systems that self-tune towards marginally stable states, has been derived. With the final aim of developing a quasi-linear algorithm for the investigation of the strongly stratified flow problem, suited to access extreme parameter regimes, we take one step further in that direction considering

the spatial variability of the fast fluctuations. Such a dependency, appearing in the QL formalism as a wavenumber, introduces the need for an additional evolution equation to identify the wavenumber of the fastest growing mode that then gets slaved to the mean dynamics. Here we illustrate, in the context of a 2-dimensional model problem, the modified QL procedure for the slaving of the fluctuation amplitude and the prediction of the wavenumber of the neutral mode in condition of marginal stability, presenting in the latter case two different but equivalent derivation approaches. An evolution equation for the wavenumber has also been derived for the stable scenario with the purpose of tracking the fastest growing mode.

4.1   Introduction

The evolution of various dynamical systems is characterized by the presence of different temporal and spatial scales. A great example is represented by geophysical and astrophysical flows where often the presence of strong constraints, such as strong rotation, strong stratification or intense magnetic field, gives rise to large anisotropic structures and small scale instabilities [Julien and Knobloch (2007)].

Because of the huge range of spatial and temporal scales to be resolved, accessing these systems via numerical simulations is especially challenging if not impossible when considering the parameter regimes describing the ocean and and the atmosphere dynamics [Bartello and Tobias (2013), Brethouwer et al. (2007)]. Nevertheless in the past several years has been widely proven that by formally taking into account the scale separation, asymptotic techniques leads to reduced systems which are considerably more treatable, from the analytical and the numerical point of view, yet non-linear and capable of capturing the main features of the full dynamics [Julien and Knobloch (2007), Michel and Chini (2019), Malecha et al. (2014), Chini et al. (2022)]. In the case of the strongly stratified flow problem, specifically, the multi-scale analysis for $Fr \to 0$ yields a reduced description where small-scale instabilities evolve linearly about a large-scale hydrostatic field (whose evolution is fully non-linear), they modify it via a feedback term and are advected by it. The resulting problem, described by a coupled system of quasi-linear (QL) PDEs, still gives rise to a rich dynamics thanks to the presence of the two-way coupling between the mean field and the fluctuations, while limiting the range of spatiotemporal scales to be resolved due to the presence of the fluctuation-fluctuation non-linearities in the mean dynamics-only.

Because of its linearity and homogeneity, the evolution of the fast modes allows for modal solutions that are exponentially dependent on the fast timescale ($\psi = A\hat{\psi}\exp\{\sigma\tau\}$), making the integration of such a reduced system on multiple temporal scales non-trivial: fluctuations might blow up on the fast time scale, while the mean field remains frozen, causing the divergence of the feedback term on the latter. Nevertheless a solution to this problems, that leverages on the natural tendency of QL systems of self-tuning towards marginally stable states, has been proposed by Michel and Chini in the context of a one-dimensional model problem [Michel and Chini (2019) and later successfully applied to the stratified flow problem

[Chini et al. (2022)]. The novel idea at the basis of this approach consists in ensuring the convergence of the fluctuation feedback either by slaving the fast dynamics to the slow field, whenever zero growth rates are realized (with the aim of maintaining the marginal stability of the slow dynamics), or setting it to zero otherwise. The zero-feedback scenario naturally results from the exponentially fast decay of the fluctuations on the fast time scale for negative growth rates, and is a necessarily imposed for positive ones, due to the divergence of the fast dynamics. The latter case invalidates the QL reduction requiring the co-evolution of the two fields on the same temporal scale (as discussed in detail in § 3.4).

While the previous chapter has been dedicated to the investigation of the positive growth rate scenario, together with the effect of finite scale separation, here we present a new methodology to efficiently extend the QL algorithm to a two-dimensional case. When considering a strict QL formulation, the two-dimensional version of the reduced dynamics includes the horizontal spatial variability of the fast field, now $\psi = A\hat{\psi} \exp\{\sigma\tau\} \exp\{-ik\chi\}$ (with χ being the characteristic spatial scale of the fast dynamics). This extra spatial dependency, non constant in time, requires an additional (computationally expensive) step in the QL algorithm to first identify the mode/modes that become unstable to then slave it/them to the mean dynamics. In this chapter we illustrate how to cost-effectively address this issue, developing an algorithmic structure that enables the prediction of the wavenumber associated to the fastest growing mode. This will be done making use of a two dimensional model problem, specifically designed to reproduce the main features of the stratified flow problem under investigation, while keeping the overall complexity limited. Following the logical structure of the previous chapter, we will start introducing the fully non-linear governing equations and their reduced version, obtained via multi-scale analysis. We will then re-trace the fundamental steps of the QL procedure for the slaving of the fluctuations (described in [Michel and Chini (2019)]) highlighting the conceptual differences with the one-dimensional case, and present the novel methodology for the prediction of the wavenumber, both in the stable and marginally-stable scenarios. Moreover in condition of marginal stability we will demonstrate how the evolution equation for the wavenumber can be formally obtained from two mathematically different, but equivalent, approaches, confirming the correctness of the result. We finally conclude showing the numerical results of the new QL procedure and its validation against the direct numerical simulations of the fully non-linear system.

4.2 Governing Equations and Multi-Scale Analysis

The slow-evolving field $U(x, z, t)$ and the fast fluctuations $\eta(x, z, t)$ satisfy the following set of equations

$$\frac{\partial U}{\partial t} + U \frac{\partial U}{\partial x} = F(x, z, t) - \nu U - \varepsilon^2 \left(\frac{\partial \eta}{\partial x} \right)^2 + D \left(\frac{\partial^2}{\partial x^2} + \frac{\partial^2}{\partial z^2} \right) U \tag{4.1}$$

$$\varepsilon \frac{\partial \eta}{\partial t} = -\eta - \varepsilon^2 U \frac{\partial^2 \eta}{\partial x^2} - \varepsilon^4 \frac{\partial^4 \eta}{\partial x^4} + \frac{\partial^2 \eta}{\partial z^2} - \varepsilon \eta^3 \tag{4.2}$$

In addition to the one-dimensional case (discussed in § 3), where the dynamics of the mean field was controlled by an external forcing , a linear damping and the cumulative effect of the fast modes, here we introduce a diffusive and an inertial term, like in the Boussinesq equation (1.1). The fluctuation feedback in 4.1, also has been replaced by a flux-type term, suggestive of the eddy flux and buoyancy flux in the real system. As regards the fluctuations the evolution equation is a modified version of the Swift-Hohenberg equation $\partial_t \psi = r\psi - (1 + \nabla^2)^2 \psi + \mathcal{N}(\psi)$ where, instead of a bifurcation parameter r that multiplies the first term on the right-hand side we have the mean field $U(x, z, t)$ that multiplies the second-order horizontal derivative. The reason behind this choice is to provide a playground as near to reality as possible but relatively more controllable and comparable to known cases.

Owing the scale separation due to the small parameter ε, we apply multi-scale analysis, this time introducing a slow-fast time scale and a large-small spatial scale.

$$\begin{aligned} t &\rightarrow (T, \tau) & T &= t \text{ and } \tau = T/\varepsilon \\ x &\rightarrow (X, \chi) & X &= x \text{ and } \chi = X/\varepsilon \end{aligned}$$

$$\begin{aligned} U &= U_0 + \varepsilon U_1 + \varepsilon^2 U_2 + O(\varepsilon^3) \\ \eta &= \eta_0 + \varepsilon \eta_1 + \varepsilon^2 \eta_2 + O(\varepsilon^3) \\ F &= F_0 + \varepsilon F_1 + \varepsilon^2 F_2 + O(\varepsilon^3) \end{aligned} \tag{4.3}$$

Solving the first equation (4.1) order by order in ε, the independence of U of the fast time τ is obtained at order $O(\varepsilon^{-1})$ (being $\partial_\tau U_0 = 0$) and the reduced dynamics at $O(1)$

$$\frac{\partial U_0}{\partial T} + \frac{\partial U_1}{\partial \tau} + U_0 \frac{\partial U_0}{\partial x} + U_0 \frac{\partial U_1}{\partial \chi} + U_1 \frac{\partial U_0}{\partial \chi} = F - \nu U_0 + D \frac{\partial^2 U_0}{\partial z^2} - \left(\frac{\partial \eta_0}{\partial \chi} \right)^2 . \tag{4.4}$$

We then introduce the average over fast time τ and space χ defined for a generic function ψ as

$$\overline{\psi}(x,z,t,\varepsilon) = \lim_{\tau_f, L\chi_f \to \infty} \frac{1}{\tau_f} \frac{1}{L\chi_f} \int_0^{\tau_f} \int_0^{L\chi_f} \psi(\chi,x,z,\tau,t,\varepsilon)\,d\tau\,d\chi \tag{4.5}$$

where $L\chi_f$ and τ_f are the spatial and the temporal scales over which intermediate processes evolve, and can be considered small/fast compared to x and T, yet big/slow with respect to χ and τ.

After fast-averaging (4.4), the final evolution equation for the mean variable $U_0(\chi, x, z, t, \varepsilon)$ reads

$$\frac{\partial U_0}{\partial T} + U_0 \frac{\partial U_0}{\partial x} = F - \nu U_0 + D \frac{\partial^2 U_0}{\partial z^2} - \overline{\left(\frac{\partial \eta_0}{\partial \chi}\right)^2}. \tag{4.6}$$

As for the fluctuation field, the dynamics at the leading order $O(\varepsilon^{-1})$ is given by

$$\frac{\partial \eta_0}{\partial \tau} = -\eta_0 - U_0 \frac{\partial^2 \eta_0}{\partial \chi^2} - \frac{\partial^4 \eta_0}{\partial \chi^4} + \frac{\partial^2 \eta_0}{\partial z^2}. \tag{4.7}$$

Not surprisingly the evolution equation for the fast modes is again linear and homogeneous and the general solution is given by the superposition of modal solutions of the type

$$\eta_0 = A(x,T)\hat{\eta}_0(x,z,T)e^{\sigma(x,T,k)\tau}e^{ik(x,T)\chi} + c.c. \tag{4.8}$$

where $A(x,T)$ is a real amplitude, the real part of $\sigma(x,T,k)$ is the growth rate and $k(x,T)$ the horizontal wave number.

The final reduced dynamics (4.6)-(4.7) results in a coupled system where two temporal and two spatial scales are involved: the slow field U_0 only evolves (fully non-linearly) on the slow time scale T and large space x, and it is modified by the cumulative effect of fluctuations η_0, which conversely linearly evolve only on the fast time τ and small space χ and are advected by the slow field.

It is crucial to notice that, due to the absence of an explicit saturation mechanism in the fast dynamics, now linear, the existence of the flux-type fluctuations feedback in (4.6) in the limit of infinite scale separation $\varepsilon \to 0$, is only possible in condition of marginal stability. Any negative growth rate would cause an exponentially fast damping of the fluctuations on the fast time scale, corresponding to their instantaneous decay on the slow time scale, and conversely any positive growth rate would preclude the convergence of the fluctuation feedback, breaking the posited scale separation. While the first case, $\text{Re}\{\sigma\} < 0$, does not invalidate the QL assumptions, allowing for a filtered dynamics where the slow field evolves without the collective effect of fluctuations, the second case, $\text{Re}\{\sigma\} > 0$, requires the restoration of the non-linear terms in the fast dynamics and the co-evolution of the two fields until a marginally-stable state is approached again.

Dropping the subscript 0 to simplify the notation and substituting the ansatz (4.8) into (4.6)-(4.7), the coupled dynamics is described by an initial value problem for the mean field U and an eigenvalue problem for the fast modes $\hat{\eta}$:

$$\frac{\partial U}{\partial T} + U\frac{\partial U}{\partial x} = F(z,T) - \nu U - 2k^2|A|^2|\hat{\varphi}|^2 + D\frac{\partial^2 U}{\partial z^2}, \tag{4.9}$$

$$\sigma\hat{\eta} = \left(-1 + k^2 U - k^4 + \frac{\partial^2}{\partial z^2}\right)\hat{\eta} \equiv L\hat{\eta}. \tag{4.10}$$

For clarity purposes, we have denoted with $\hat{\eta}$ the eigenfunctions associated with the eigenvalue problem (4.24), in principle defined for any growth rate, and with $\hat{\varphi}$ the neutrally stable fast mode that feeds back on the slow field only in condition of marginal stability. Thus $\hat{\varphi} \equiv \hat{\eta}$ when $\text{Re}\{\sigma\} = 0$.

The backbone of the model, consisting of an initial value problem for the slow variable and an eigenvalue problem for the fast one, reoccurs in this 2D example with the major differences from the 1D model problem being the k-structure of the fluctuations and the dependence of the mean field on slow x. The latter feature, introduced by the convective term in (4.9), allows for the interaction between low Fourier modes, turning the strict mean U in a slowly spatially varying mean (hence the categorization under Generalized Quasi Linear model).

Although of fundamental importance in the real stratified flow system, for purposes of simplifications, the dependence of U on the slow coordinate x (and thus the presence of convective term) will be from now on neglected, postponing its investigation to future work.
The elimination of the slow spatial coordinate x from (4.9)-(4.10) leads to the following strict QL system:

$$\frac{\partial U}{\partial T} = F(z,T) - \nu U - 2k^2|A|^2|\hat{\varphi}|^2 + D\frac{\partial^2 U}{\partial z^2} \tag{4.11}$$

$$\sigma\hat{\eta} = \left(-1 + k^2 U - k^4 + \frac{\partial^2}{\partial z^2}\right)\hat{\eta} \equiv L\hat{\eta} \tag{4.12}$$

where the average over the fast spatial coordinate χ in (4.5) is now interpreted as a strict streamwise average.
We point out that the marginal stability requirement (i.e. $\text{Re}\{\sigma\} = 0$), necessary for the feedback term in (4.23) not to blow up (see § 3.3), has been already taken in to account substituting a zero growth rate while fast averaging over τ and χ.

Similarly to the scenario presented in the previous chapter for the 1D model problem, the

coupling of the system in condition of marginal stability occurs via the modal amplitude $A(T)$ which is *a priori* unknown. The impossibility of deriving an amplitude equation enforcing the solvability of the higher order terms in (4.3), due to the lack of a closure in the system, requires a different constraint to be imposed. Michel and Chini have shown that in such a type of slow-fast quasilinear systems, it is possible to determine the amplitude $A(T)$ leveraging the self-tuning of the slow dynamics towards a marginally stable state [Michel and Chini (2019)]. In other words, when a zero growth rate is attained, the fluctuation dynamics is slaved to the mean field in order to maintain its marginal stability.

Retracing the main logical steps of this approach (illustrated in detail in § 3.3), an expression for the slow evolution of the growth rate, $\mathrm{Re}\{\partial_T \sigma\}$, can be obtained as a first order correction of the time-perturbed eigenvalue problem (4.24). However the presence of the new spatial coordinate χ introduces the dependency of the eigenvalue problem on the wavenumber k, requiring an additional constraint in order to ensure the marginal stability condition in time. Not only the time derivative of the growth rate but also its partial derivative with respect to k must vanish when marginal stability is satisfied. More simply, the tangency condition to the marginal-stability manifold in time has to be satisfied by the fastest growing mode, implying

$$\partial_T \mathrm{Re}\{\sigma\}\bigg|_{k_{max},T} = 0 \quad \wedge \quad \partial_k \mathrm{Re}\{\sigma\}\bigg|_{k_{max},T} = 0 \tag{4.13}$$
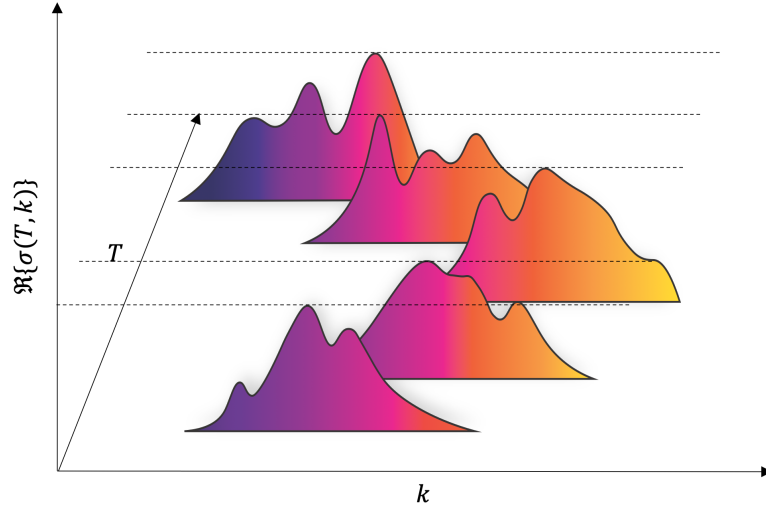
Figure 4.1 – Schematic of the time dependent dispersion relation $\sigma(T,k)$. Black dashed lines represent the growth rate of the of the fastest growing mode at a fixed time T for which $\partial_k \sigma = 0$.

Pragmatically the eigenvalue problem (4.24) must be solved multiple times, i.e. for varying k, to find the mode that first undergoes an instability. Moreover the number of marginally stable modes and the wavenumbers associated with each of them can change in time, requiring for the last step to be repeated, in principle, at each time iteration. Since the eigenvalue problem is the core of the slow-fast QL systems presented in this work, as well as the computational

bottleneck, it is of fundamental importance to develop an algorithmic procedure for the prediction of the wavenumber k in the condition of marginal stability.

4.3 Algorithm for Strict QL Models

In the remainder of this section we present an algorithmic structure for the slaving of the fluctuation amplitude to the mean field in condition of marginal stability as well as a new methodology to predict the wavenumber k associated fastest growing mode, respectively in condition of marginal stability and below it. For the moment the we will limit the complexity to one marginally stable/growing mode.

4.3.1 Slaving of the amplitude and prediction of the wavenumber of the marginally-stable mode

From a geometrical point of view the real part of the time-dependent dispersion relation $\sigma(T,k)$, pictured in figure 4.2, is represented by a three-dimensional landscape that can be described as a continuous parametrised surface in $\mathbb{R}^3$. Defining a continuous mapping function $\Gamma : A \to \mathbb{R}^3$, where $A \subseteq \mathbb{R}^2$, a generic parametrisation of a surface is given by

$$\Gamma(T,k) = (\Gamma_1(T,k), \Gamma_2(T,k), \Gamma_3(T,k)) \tag{4.14}$$

However, being Γ a locally injective map by construction, the specific choice for the parametric equations $\Gamma_1(T,k) = T$, $\Gamma_2(T,k) = k$ can be made and the surface can be described as a graph

$$\Gamma(T,k) = (T,k,\text{Re}\{\sigma(T,k)\}) \tag{4.15}$$

For reasons of simplification, the real and the imaginary part of σ and its derivatives will be denoted, from now on, making use of the subscript r and i respectively:

$$\partial^n \sigma_r = \partial^n \text{Re}\{\sigma\} \quad \text{and} \quad \partial^n \sigma_i = \partial^n \text{Im}\{\sigma\} \tag{4.16}$$

The requirements of marginal stability to be satisfied by the fastest growing mode at each time results in the presence of a ridge (curve in $\mathbb{R}^3$) on the surface Γ, that lies in the horizontal plane $(T,k,\sigma_r = 0)$, and it is characterized by $\nabla \sigma_r = 0$ at each point.

Formally, a parametrised curve γ on a surface Γ is described as a pair of smooth curves μ and γ satisfying $\gamma = \Gamma \circ \mu$. The plane curve μ is said to be the coordinate curve of the pair and in

this case it is the projection of γ onto the bi-dimensional space spanned by T, k

$$\mu(T) = (T, g(T)) \tag{4.17}$$

where $\mu : I \to \mathbb{R}^2$, with $I \subseteq \mathbb{R}$ and $g(T)$ is a smooth function $g : I \to \mathbb{R}$.

The function γ, describing the ridge, is then uniquely determined by the composition $\gamma = \Gamma \circ \mu$

$$\gamma(T) = (T, g(T), \sigma(T, g(T))) = (T, g(T), 0) \tag{4.18}$$

given that the ridge is the intersection between the three-dimensional landscape and the plane at $\sigma_r = 0$.

It follows that, at each time T, the function g provides the k-coordinate $k_M = g(T)$ of the saddle point M on the ridge γ that satisfies

$$
\begin{aligned}
&\sigma_r(T, k_M) = 0, \\
&\partial_k \sigma_r|_{(T, k_M)} = 0, \\
&\partial_T \sigma_r|_{(T, k_M)} = 0 \,.
\end{aligned}
\tag{4.19}
$$
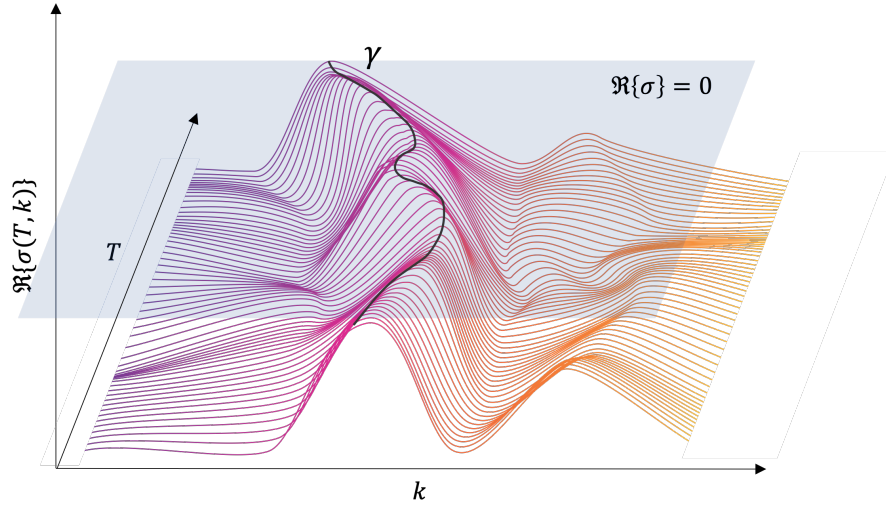
Figure 4.2 – Schematic of the time dependent dispersion relation $\sigma(T, k)$ as a continuous surface in $\mathbb{R}^3$. The black lines represents the curve γ, obtained from the intersection between the surface Γ and the horizontal $k - T$ plane at Re$\{\sigma\} = 0$.

Within this framework the prediction of the wavenumber k in condition of marginal stability translates into deriving an evolution equation for the function $g(T)$ enforcing the propagation in time of the saddle point properties (4.19) along γ.

Indicating with $M = (T_M, k_M)$ a point on the ridge and with $\bar{\delta}$ the tangent vector to the curve γ

$$\bar{\delta} = \gamma' = \left(1, \frac{dg(T)}{dT}\right) \tag{4.20}$$

the Taylor expansion of the growth rate around M along the ridge reads

$$
\begin{aligned}
\sigma_r((T, k)_M + \Delta \bar{\delta}) &\sim \sigma_r(T_M, k_M) + \left(\frac{\partial \sigma_r}{\partial T}\bigg|_M + \frac{\partial \sigma_r}{\partial k}\bigg|_M \frac{dg(T)}{dT}\right)\Delta \\
&+ \frac{1}{2}\left(\frac{\partial^2 \sigma_r}{\partial T^2}\bigg|_M + \frac{\partial^2 \sigma_r}{\partial k^2}\bigg|_M \left(\frac{dg(T)}{dT}\right)^2 + 2\frac{\partial^2 \sigma_r}{\partial T \partial k}\bigg|_M \frac{dg(T)}{dT}\right)\Delta^2 + O(\Delta^3) \\
&= \frac{1}{2}\left(\frac{\partial^2 \sigma_r}{\partial T^2}\bigg|_M + \frac{\partial^2 \sigma_r}{\partial k^2}\bigg|_M \left(\frac{dg(T)}{dT}\right)^2 + 2\frac{\partial^2 \sigma_r}{\partial T \partial k}\bigg|_M \frac{dg(T)}{dT}\right)\Delta^2 + O(\Delta^3)
\end{aligned}
\tag{4.21}
$$

where the marginal stability condition at M and the saddle point conditions (4.19) have been imposed in the last line of (4.21). Requiring then the preservation of marginal stability along γ in (4.21), i.e. $\sigma_r((T, k)_M + \Delta \bar{\delta}) = 0$, or equivalently a zero Gaussian curvature of the surface Γ at the point M, yields an evolution equation for $g(T)$

$$\left(\frac{dg(T)}{dT}\right)^2 + 2\frac{\partial_k(\partial_T \sigma_r)|_M}{\partial_k^2 \sigma_r|_M}\left(\frac{dg(T)}{dT}\right) = -\frac{\partial_T^2 \sigma_r|_M}{\partial_k^2 \sigma_r|_M} \tag{4.22}$$

Consistently with this notation the coupled evolution of the slow and the fast variables, described by (4.23) and (4.24) can be re-written as

$$\frac{\partial U}{\partial T} = F(z, T) - \nu U - 2g(T)^2 |A|^2 |\hat{\varphi}|^2 + D\frac{\partial^2 U}{\partial z^2} \tag{4.23}$$

$$\sigma \hat{\eta} = \left(-1 + k^2 U - k^4 + \frac{\partial^2}{\partial z^2}\right)\hat{\eta} \equiv L\hat{\eta} \tag{4.24}$$

with the main difference being the explicit lack of any k-dependency of the slow dynamics. While the eigenvalue problem for the fast modes is well defined at any point on the surface Γ and therefore for any wavenumber k, the fluctuation feedback on the slow dynamics is given only by the neutrally stable eigenmodes on the ridge γ, for which the wavenumber is defined as a function of time, $g(T)$, yielding

$$\frac{\partial L}{\partial k}\bigg|_M = \left(2kU - 4k^3\right)\bigg|_M = 2g(T)U - 4g(T)^3 \,. \tag{4.25}$$

It follows that the neutral eigenfunctions $\hat{\varphi}$ are only a function of space and time and do not depend on the wavenumber k, $\hat{\varphi} = \hat{\varphi}(z, T)$. We stress the point that while the evaluation of the generic eigenfunction $\hat{\eta}$ at a point M on the ridge is exactly $\hat{\varphi}$

$$\hat{\eta}_M = \hat{\eta}(z, T, k = g(T)) = \hat{\varphi}(z, T) \, , \tag{4.26}$$

their derivatives are different

$$\frac{\partial \hat{\varphi}}{\partial T} = \frac{d\hat{\eta}}{dT} = \frac{\partial \hat{\eta}}{\partial T} + \frac{\partial \hat{\eta}}{\partial k} \frac{dg(T)}{dT} \, . \tag{4.27}$$

The determination of a fluctuation amplitude able to maintain the marginal stability of the slow dynamics in time ($\partial_T \sigma_r|_M = 0$ and $\partial_k \sigma_r|_M = 0$), and the prediction of the corresponding wave number via (4.22), both require to access the first and second derivatives of the growth rate $\sigma_r(k, T)$. In order to construct these derivatives we make use of perturbation analysis. Infinitesimally perturbing the eigenvalue problem (4.24) in k and T such that it can be expanded in series

$$
\begin{aligned}
\sigma(T_M + \Delta T, k_M + \Delta k) \sim{} & \sigma_M + \left.\frac{\partial \sigma}{\partial T}\right|_M \Delta T + \left.\frac{\partial \sigma}{\partial k}\right|_M \Delta k \\
& + \frac{1}{2}\left.\frac{\partial^2 \sigma}{\partial T^2}\right|_M \Delta T^2 + \frac{1}{2}\left.\frac{\partial^2 \sigma}{\partial k^2}\right|_M \Delta k^2 + \left.\frac{\partial^2 \sigma}{\partial k \partial T}\right|_M \Delta T \Delta k
\end{aligned}
\tag{4.28}
$$

$$
\begin{aligned}
L(T_M + \Delta T, k_M + \Delta k) \sim{} & L_M + \left.\frac{\partial L}{\partial T}\right|_M \Delta T + \left.\frac{\partial L}{\partial k}\right|_M \Delta k \\
& + \frac{1}{2}\left.\frac{\partial^2 L}{\partial T^2}\right|_M \Delta T^2 + \frac{1}{2}\left.\frac{\partial^2 L}{\partial k^2}\right|_M \Delta k^2 + \left.\frac{\partial^2 L}{\partial k \partial T}\right|_M \Delta T \Delta k
\end{aligned}
\tag{4.29}
$$

$$
\begin{aligned}
\hat{\eta}(T_M + \Delta T, k_M + \Delta k) \sim{} & \hat{\eta}_M + \left.\frac{\partial \hat{\eta}}{\partial T}\right|_M \Delta T + \left.\frac{\partial \hat{\eta}}{\partial k}\right|_M \Delta k \\
& + \frac{1}{2}\left.\frac{\partial^2 \hat{\eta}}{\partial T^2}\right|_M \Delta T^2 + \frac{1}{2}\left.\frac{\partial^2 \hat{\eta}}{\partial k^2}\right|_M \Delta k^2 + \left.\frac{\partial^2 \hat{\eta}}{\partial k \partial T}\right|_M \Delta T \Delta k
\end{aligned}
\tag{4.30}
$$

and collecting terms order by order the following boundary values problems are obtained

$O(\Delta T)$

$$\mathcal{L}_M \left.\frac{\partial \hat{\eta}}{\partial T}\right|_M = -\left.\frac{\partial L}{\partial T}\right|_M \hat{\eta}_M + \left.\frac{\partial \sigma}{\partial T}\right|_M \hat{\eta}_M \tag{4.31}$$

$O(\Delta k)$

$$\mathcal{L}_M \left.\frac{\partial \hat{\eta}}{\partial k}\right|_M = -\left.\frac{\partial L}{\partial k}\right|_M \hat{\eta}_M + \left.\frac{\partial \sigma}{\partial k}\right|_M \hat{\eta}_M \tag{4.32}$$

$O(\Delta T \Delta k)$

$$\mathscr{L}_M \frac{\partial^2 \hat{\eta}}{\partial k \partial T}\bigg|_M = -\frac{\partial^2 L}{\partial k \partial T}\bigg|_M \hat{\eta}_M - \frac{\partial L}{\partial k}\bigg|_M \frac{\partial \hat{\eta}}{\partial T}\bigg|_M - \frac{\partial L}{\partial T}\bigg|_M \frac{\partial \hat{\eta}}{\partial k}\bigg|_M +$$
$$\frac{\partial \sigma}{\partial T}\bigg|_M \frac{\partial \hat{\eta}}{\partial k}\bigg|_M + \frac{\partial \sigma}{\partial k}\bigg|_M \frac{\partial \hat{\eta}}{\partial T}\bigg|_M + \frac{\partial^2 \sigma}{\partial k \partial T}\bigg|_M \hat{\eta}_M \tag{4.33}$$

$O(\Delta T)^2$

$$\mathscr{L}_M \frac{\partial^2 \hat{\eta}}{\partial T^2}\bigg|_M = -\frac{\partial^2 L}{\partial T^2}\bigg|_M \hat{\eta}_M - 2\frac{\partial L}{\partial T}\bigg|_M \frac{\partial \hat{\eta}}{\partial T}\bigg|_M + 2\frac{\partial \sigma}{\partial T}\bigg|_M \frac{\partial \hat{\eta}}{\partial T}\bigg|_M + \frac{\partial^2 \sigma}{\partial T^2}\bigg|_M \hat{\eta}_M \tag{4.34}$$

$O(\Delta k)^2$

$$\mathscr{L}_M \frac{\partial^2 \hat{\eta}}{\partial k^2}\bigg|_M = -\frac{\partial^2 L}{\partial k^2}\bigg|_M \hat{\eta}_M - 2\frac{\partial L}{\partial k}\bigg|_M \frac{\partial \hat{\eta}}{\partial k}\bigg|_M + 2\frac{\partial \sigma}{\partial k}\bigg|_M \frac{\partial \hat{\eta}}{\partial k}\bigg|_M + \frac{\partial^2 \sigma}{\partial k^2}\bigg|_M \hat{\eta}_M \tag{4.35}$$

where the operator $\mathscr{L}$ is defined as $\mathscr{L} = L - \sigma$.

Because $\mathscr{L}$ is a singular operator by construction, the existence of the solutions of these boundary value problems has to be ensured imposing a solvability condition.
Defining the L^2 inner product for two functions $\psi_1(x)$ and $\psi_2(x)$ as

$$\left\langle \psi_1(z) \big| \psi_2(z) \right\rangle = \int_0^L \psi_1(z)^* \psi_2(z) \, dz \,, \tag{4.36}$$

the Fredholm Alternative theorem states, in the context of singular boundary value problems, that for the generic problem $\mathscr{L}u = f$ (plus boundary conditions) to be solvable the right-hand-side f has to be orthogonal to the null space of the adjoint operator $\mathscr{L}^\dagger$. In other words, denoting with ψ_n and $\psi_n^\dagger$ the eigenvectors of the direct and adjoint operators respectively associated with the the eigenvalues λ_n, the solvability of $\mathscr{L}u = f$ requires

$$\left\langle f \big| \psi_0^\dagger \right\rangle = \left\langle \mathscr{L}u \big| \psi_0^\dagger \right\rangle = \left\langle u \big| \mathscr{L}^\dagger \psi_0^\dagger \right\rangle = 0 \tag{4.37}$$

in which case the direct problem has infinitely many solutions

$$u = C\psi_0 + \sum_{n=1}^{\infty} \frac{\left\langle f \middle| \psi_n^\dagger \right\rangle}{\lambda_n \left\langle \psi_n \middle| \psi_n^\dagger \right\rangle} \psi_n \,. \tag{4.38}$$

By inspection of (4.24) we notice that the linear operator L is again singular and self-adjoint as in the 1-dimensional case, meaning that its eigenvalues are real and the corresponding eigenvectors can be chosen real.

Imposing then the solvability condition (4.37) to the boundary value problem at order $O(\Delta T)$ (4.31)

$$\left\langle \mathscr{L}_M \frac{\partial \hat{\eta}}{\partial T} \bigg|_M \middle| \hat{\eta}_M^\dagger \right\rangle = \left\langle \frac{\partial \hat{\eta}}{\partial T} \bigg|_M \middle| \mathscr{L}_M^\dagger \hat{\eta}_M^\dagger \right\rangle = 0 \tag{4.39}$$

and making use of the self-adjoint nature of the operator $\mathscr{L}$ in this specific problem, we obtain

$$\left\langle \mathscr{L}_M \frac{\partial \hat{\eta}}{\partial T} \bigg|_M \middle| \hat{\eta}_M \right\rangle = -\int_0^{Lz} \left(\frac{\partial L}{\partial T} \bigg|_M \right) |\hat{\eta}_M|^2 dz + \frac{\partial \sigma}{\partial T} \bigg|_M \int_0^{Lz} |\hat{\eta}_M|^2 dz = 0 \tag{4.40}$$

where

$$\frac{\partial L}{\partial T} = k^2 \frac{\partial U}{\partial T} = k^2 \left(F - \nu U + D \frac{\partial^2 U}{\partial z^2} \right) - 2k^2 |A|^2 g^2 |\hat{\varphi}|^2 \tag{4.41}$$

and

$$\frac{\partial L}{\partial T} \bigg|_M = g^2 \left(F - \nu U + D \frac{\partial^2 U}{\partial z^2} \right) - 2|A|^2 g^4 |\hat{\varphi}|^2 \tag{4.42}$$

given that $k_M = g(T)$.

Making the following choice for the normalization of the eigenfunctions

$$\langle \hat{\eta} | \hat{\eta} \rangle = \int_0^{L_z} |\hat{\eta}|^2 dz = 1 \tag{4.43}$$

the solvability condition directly yields an evolution equation for σ on slow time

$$\frac{\partial \sigma}{\partial T} \bigg|_M = g^2 \int_0^{Lz} \left(\frac{\partial U}{\partial T} \right) |\hat{\eta}_M|^2 dz \,. \tag{4.44}$$

Substituting

$$\frac{\partial \sigma}{\partial T} \bigg|_M = g^2 \int_0^{Lz} \left(F - \nu U + D \frac{\partial^2 U}{\partial z^2} \right) |\hat{\eta}_M|^2 dz - 2g^4 |A|^2 \int_0^{Lz} |\hat{\eta}_M|^2 |\hat{\varphi}|^2 dz \,. \tag{4.45}$$

from which an expression for the fluctuation amplitude can be derived imposing the marginal

stability constraint $\partial_T \sigma_r|_M = \partial_T \sigma|_M = 0$ when $\sigma = 0$,

$$|A(T)| = \sqrt{\frac{\alpha}{2g^2\beta}} \tag{4.46}$$

with

$$\alpha = \int_0^{Lz} (F - \nu U - D\partial_z^2 U)|\hat{\varphi}|^2 dz, \tag{4.47}$$

$$\beta = \int_0^{Lz} |\hat{\varphi}|^4 dz. \tag{4.48}$$

Analogously to the 1D model problem presented in the previous chapter, the evolution equation of the growth rate has the form

$$\frac{\partial \sigma}{\partial T} = g^2 \alpha - 2g^4 |A|^2 \beta \tag{4.49}$$

where the sign of the integrals α and β is responsible for the existence of an amplitude A, even when marginal stability is attained, as discussed in § 3.4: negative values of α bring the system towards more stable states ($\partial_T \sigma < 0$), while negative values of β cause bursting events ($\partial_T \sigma > 0$). However, differently from the 1D case, here β is positively definite disallowing for the latter scenario.

The need for the computation of the second derivatives of the growth rate $\partial_T^2 \sigma$ and $\partial_k \partial_T \sigma$ requires to solve for the first order correction of the eigenfunction $\partial_T \hat{\eta}|_M$ as well.
When dealing with a generic singular boundary value problem $\mathcal{L}u = f$, as in this case, this can be done by means of the generalized inverse obtained through applying a QR decomposition, which practically solves

$$\mathcal{L}u_p = f - \left\langle f \middle| \psi_0^\dagger \right\rangle \psi_0^\dagger \tag{4.50}$$

where $\psi_0^\dagger \in ker(\mathcal{L}^\dagger)$ and u_p is a particular solution of $\mathcal{L}u = f$ that minimizes the least squares error

$$\left\| \mathcal{L}u - f \right\|^2. \tag{4.51}$$

The general solution of the system is then defined up to an arbitrary multiple of the null eigenfunction ψ_0 ($\mathcal{L}\psi_0 = 0$)

$$u = C\psi_0 + u_p \tag{4.52}$$

from which a specific solution can be selected imposing the orthogonality of u with respect to

ψ_0, $\langle u|\psi_0\rangle = 0$, yielding

$$C = -\frac{\langle u_p|\psi_0\rangle}{\langle \psi_0|\psi_0\rangle} \ . \tag{4.53}$$

Returning to the boundary value problem (4.31) at order ΔT, we obtain for the first order correction of the eigenfunction

$$\left.\frac{\partial \hat{\eta}}{\partial T}\right|_M = C_1 \hat{\eta}_M + \left.\left(\frac{\partial \hat{\eta}}{\partial T}\right)_p\right|_M \tag{4.54}$$

and for the multiplicative constant C_1

$$C_1 = -\left\langle \left.\left(\frac{\partial \hat{\eta}}{\partial T}\right)_p\right|_M \middle| \hat{\eta}_M \right\rangle \tag{4.55}$$

where the normalisation choice (4.43) has been substituted. The orthogonality between the homogeneous solution η_M and the solution $\partial_T\hat{\eta}|_M$ is, in this case, equivalent to enforcing the preservation of the norm

$$\frac{\partial}{\partial T}\langle \hat{\eta}_M|\hat{\eta}_M\rangle = 2\int_0^{Lz} \left.\frac{\partial \hat{\eta}}{\partial T}\right|_M \hat{\eta}_M dz = 0 \ . \tag{4.56}$$

By applying the same conceptual steps, just exposed for the boundary value problem (4.31), namely

1. determination of the derivative of the growth rate via Fredholm Alternative

2. imposing the saddle-point properties in condition of marginal stability

3. computation of the correction of the eigenfunction via the generalized inverse algorithm and conservation of the norm

to the problem at order $O(\Delta k)$, and only the first step to the boundary value problems at second order (4.33)-(4.35),we obtain the following expressions:

$O(\Delta k)$

$$\left.\frac{\partial \sigma}{\partial k}\right|_M = 2g\int_0^{Lz} U|\hat{\eta}_M|^2 dz - 4g^3 \tag{4.57}$$

which leads, after imposing the marginal stability constraint $\partial_k\sigma|_M = 0$, to the integral relation

$$2g^2 = \int_0^{Lz} U|\hat{\eta}_M|^2 dz \ , \tag{4.58}$$

and solving for $\partial_k \hat{\eta}|_M$

$$\left. \frac{\partial \hat{\eta}}{\partial k} \right|_M = C_2 \hat{\eta}_M + \left. \left(\frac{\partial \hat{\eta}}{\partial k} \right)_p \right|_M \tag{4.59}$$

with

$$C_2 = -\left\langle \left. \left(\frac{\partial \hat{\eta}}{\partial k} \right)_p \right|_M \right| \hat{\eta}_M \right\rangle \tag{4.60}$$

$O(\Delta T \Delta k)$

$$\left. \frac{\partial^2 \sigma}{\partial k \partial T} \right|_M = 2g \int_0^{Lz} U \hat{\eta}_M \left. \frac{\partial \hat{\eta}}{\partial T} \right|_M dz - g^2 \frac{\alpha}{\beta} \int_0^{Lz} \hat{\eta}_M^3 \left. \frac{\partial \hat{\eta}}{\partial k} \right|_M dz + $$
$$+ g^2 \int_0^{Lz} (F - \nu U + D \partial_z^2 U) \hat{\eta}_M \left. \frac{\partial \hat{\eta}}{\partial k} \right|_M dz \tag{4.61}$$

$O(\Delta k)^2$

$$\left. \frac{\partial^2 \sigma}{\partial k^2} \right|_M = -8g^2 + 4g \int_0^{Lz} U \hat{\eta}_M \left. \frac{\partial \hat{\eta}}{\partial k} \right|_M dz \tag{4.62}$$

$O(\Delta T)^2$

$$\left. \frac{\partial^2 \sigma}{\partial T^2} \right|_M = -2g^2 \frac{dg(T)}{dT} \left(\int_0^{Lz} (F - \nu U + D \partial_z^2 U) \hat{\eta}_M \left. \frac{\partial \hat{\eta}}{\partial k} \right|_M dz - \frac{\alpha}{\beta} \int_0^{Lz} \hat{\eta}_M^3 \left. \frac{\partial \hat{\eta}}{\partial k} \right|_M dz \right) \tag{4.63}$$

where α and β are defined in (4.47) and (4.48) respectively, and the corrections of the eigen-function by (4.59) and (4.54).

The conceptual distinction between the eigenfunctions $\hat{\eta}$ and $\hat{\varphi}$ and their dependencies is of fundamental importance for the computation of the latter derivative (4.63). The construction of $\partial_T^2 \sigma|_M$ indeed requires to take the second derivative in time of the operator L on the ridge

$$\mathcal{L}_M \left. \frac{\partial^2 \hat{\eta}}{\partial T^2} \right|_M = - \left. \frac{\partial^2 L}{\partial T^2} \right|_M \hat{\eta}_M - 2 \left. \frac{\partial L}{\partial T} \right|_M \left. \frac{\partial \hat{\eta}}{\partial T} \right|_M + \left. \frac{\partial^2 \sigma}{\partial T^2} \right|_M \hat{\eta}_M \tag{4.64}$$

and consequently the time derivative of the evolution equation of the slow field U

$$\frac{\partial^2 U}{\partial T^2} = \frac{\partial}{\partial T}(F - \nu U + D \frac{\partial^2 U}{\partial z^2}) - 4g \frac{dg}{dT} |A|^2 |\hat{\varphi}|^2 - 4g^2 |A| \frac{dA}{dT} |\hat{\varphi}|^2 - 4g^2 |A|^2 \hat{\varphi} \frac{\partial \hat{\varphi}}{\partial T} \tag{4.65}$$

where the time derivative of the eigenfunction $\hat{\varphi}$ is given by (4.27). Once the derivative $\partial_T \hat{\varphi}$ has been taken correctly, the eigenfunction $\hat{\varphi}$ can be replaced by $\hat{\eta}_M$ yielding the result in (4.63).

Substituting the second derivatives of the growth rate into (4.22), the final evolution equation

for the wavenumber of the neutrally-stable mode reads

$$\frac{dg}{dT} = -\frac{\int_0^{Lz} U\hat{\varphi}\partial_T\hat{\eta}|_M dz}{8g^2 - \int_0^{Lz} U\hat{\varphi}\partial_k\hat{\eta}|_M dz} \ . \tag{4.66}$$

4.3.2 Prediction of k from differential geometry considerations

An alternative approach to derive an evolution equation for the wavenumber of the marginally-stable mode is based on using differential geometry considerations to express curvature properties of the $\sigma(T, k)$-landscape, given by (4.15), along the ridge γ (4.18). In this section we aim to show how the propagation of the saddle point properties along a direction constraints the shape of the parametrised surface Γ along that direction and how an equivalent expression to (**??**) can be derived just from the intrinsic properties of the surface itself.

Considering the parametrised surface (4.15), describing the time-varying dispersion relation $\sigma(T, k)$, re-written here for convenience,

$$(T, k) \rightarrow \Gamma(T, k) = (T, k, \sigma_r(T, k)) \tag{4.67}$$

and its derivatives

$$\Gamma_T' = (\partial_T\Gamma_1, \partial_T\Gamma_2, \partial_T\Gamma_3) = (1, 0, \partial_T\sigma_r) \tag{4.68}$$

$$\Gamma_k' = (\partial_k\Gamma_1, \partial_k\Gamma_2, \partial_k\Gamma_3) = (0, 1, \partial_k\sigma_r) \tag{4.69}$$

at any coordinate point $P = (T, k) \in A$ the tangent space $T_p\Gamma$ to the surface in p is defined as the vectorial space spanned by Γ_T' and Γ_k' evaluated at the point p. The tangent space is then uniquely identified by the normal vector $\mathcal{N}$

$$\mathcal{N} = \frac{\Gamma_T' \times \Gamma_k'}{||\Gamma_T' \times \Gamma_k'||} \tag{4.70}$$

whose derivatives $\mathcal{N}'_T$ and $\mathcal{N}'_k$ lie in the tangent space $T_p\Gamma$ (since $\mathcal{N}$ is normalized $\partial_j|\mathcal{N}|^2 = 2\langle\partial_j\mathcal{N}|\mathcal{N}\rangle = 0$) and carry information about the curvature properties of Γ. However in order to have a formulation that is invariant under re-parametrisation, the curvature of a surface is often described making use of the concept of *shape operator*, rather than via the normal vector $\mathcal{N}$.

Defining the *shape operator*, or *Weingarten mapping*, as the endomorphism mapping elements within the tangent space $T_P\Gamma$ onto the directional derivative of the (normalized) surface normal vector $\mathcal{N}$

$$W = W : T_P\Gamma \rightarrow T_P\Gamma \ , \tag{4.71}$$

$$W(\Gamma'_T) = -\mathscr{N}'_T \quad \text{and} \quad W(\Gamma'_k) = -\mathscr{N}'_k \tag{4.72}$$

its matrix representation with respect to the basis Γ'_T, Γ'_k is given by

$$W = \begin{pmatrix} a & c \\ b & d \end{pmatrix}, \tag{4.73}$$

where $W(\Gamma'_T) = a\Gamma'_T + c\Gamma'_k$ and $W(\Gamma'_k) = b\Gamma'_T + d\Gamma'_k$, and the coefficients are given in terms of first and second partial derivatives of σ_r with respect to k and T, as shown below.

Re-calling the definition of the *first fundamental form* of a parametrisation as the linear map that restricts the inner product canonically induced in $\mathbb{R}^3$ to the tangent space $T_p\Gamma$

$$I_p : T_p\Gamma \to \mathbb{R} \tag{4.74}$$

$$
\begin{aligned}
I_p(u, w) &= I_p(e\Gamma'_T + f\Gamma'_k, g\Gamma'_T + h\Gamma'_k) \\
&= eg\langle\Gamma'_T|\Gamma'_T\rangle + (eh + fg)\langle\Gamma'_T|\Gamma'_k\rangle + fh\langle\Gamma'_k|\Gamma'_k\rangle \\
&= egE + (eh + fg)F + fhG
\end{aligned}
\tag{4.75}
$$

and the definition of the *second fundamental form* as the linear map

$$
\begin{aligned}
II_p(u, w) &= \langle W(u)|w\rangle = \langle W(i\Gamma'_T + l\Gamma'_k)|m\Gamma'_T + n\Gamma'_k\rangle \\
&= mi\langle\Gamma'_T|W(\Gamma'_T)\rangle + ni\langle\Gamma'_k|W(\Gamma'_T)\rangle + ml\langle\Gamma'_T|W(\Gamma'_k)\rangle + nl\langle\Gamma'_k|W(\Gamma'_k)\rangle \\
&= mi\langle\Gamma''_{TT}|\mathscr{N}\rangle + (ni + ml)\langle\Gamma''_{Tk}|\mathscr{N}\rangle + nl\langle\Gamma''_{kk}|\mathscr{N}\rangle \\
&= miL + (ni + ml)M + nlN
\end{aligned}
\tag{4.76}
$$

(here expressed with respect to the basis Γ'_T, Γ'_k), the explicit form of the shape operator W can be constructed from the matrix representations of the these fundamental forms as

$$W = \begin{pmatrix} a & c \\ b & d \end{pmatrix} = \begin{pmatrix} E & F \\ F & G \end{pmatrix}^{-1} \begin{pmatrix} L & M \\ M & N \end{pmatrix}. \tag{4.77}$$

Defining the eigenvectors v_i of the shape operator W as *principal directions* of the tangent space $T_p\Gamma$, and the corresponding eigenvalues λ_i as *principal curvatures* (whose product defines the *Gaussian curvature* of Γ), an expression for the normal curvature, κ_n, of Γ in the direction v_i, follows from (4.76)

$$\kappa_n = II_p(v_i) = v_i W(v_i) = \lambda_i \tag{4.78}$$

which actually corresponds to the normal curvature of all the curves on the surface Γ, with tangent vector v_i in p, and a definition

When considering a specific point $p = M$ on the ridge γ, where all the points are saddle points, the conditions (4.19) enforce zero first derivatives of the growth rate and the tangent plane $T_M\Gamma$ is represented by an horizontal plane spanned by the tangent vectors $\Gamma'_T = (1,0,0)$ and $\Gamma'_k = (0,1,0)$ and with normal $\mathcal{N} = (0,0,1)$, therefore the shape operator W at M simplifies to

$$W = \begin{pmatrix} \partial_T^2 \sigma_r & \partial_T \partial_k \sigma_r \\ \partial_T \partial_k \sigma_r & \partial_k^2 \sigma_r \end{pmatrix} \tag{4.79}$$

Re-writing the tangent vector γ' to the ridge γ in M

$$\gamma' = \left(1, \frac{dg(T)}{dT}, 0 \right) = \Gamma'_T + \frac{dg(T)}{dT}\Gamma'_k \tag{4.80}$$

the propagation the saddle-point properties (4.19) along the curve γ then requires from a geometrical point of view to enforce a zero normal curvature κ_n in the direction of tangent vector γ'

$$W\gamma' = \begin{pmatrix} \partial_T^2 \sigma_r & \partial_T \partial_k \sigma_r \\ \partial_T \partial_k \sigma_r & \partial_k^2 \sigma_r \end{pmatrix} \left(1, \frac{dg(T)}{dT} \right) = (0,0) \tag{4.81}$$

which automatically implies that one of the eigenvalues of the shape operator W vanishes and so will the Gaussian curvature along the curve γ. In other words this is equivalent to state that the operator W is singular and that the tangent vector γ' lies in the nullspace of W.

While enforcing the condition of a zero eigenvalue of W, after the explicit diagonalisation of the operator, yields the following relation between the second derivatives of σ_r

$$\left(\partial_k^2 \sigma_r \right) \left(\partial_T^2 \sigma_r \right) = (\partial_T \partial_k \sigma_r)^2. \tag{4.82}$$

the constraint of zero normal curvature in the direction γ' (4.81) yields the two following conditions

$$\begin{aligned} \partial_T \partial_k \sigma_r \frac{dg(T)}{dT} + \partial_T^2 \sigma_r &= 0, \\ \partial_k^2 \sigma_r \frac{dg(T)}{dT} + \partial_T \partial_k \sigma_r &= 0 \end{aligned} \tag{4.83}$$

which become identical when substituting (4.82) providing a single ordinary differential equation for the evolution of $g(T)$.

$$\partial_k^2 \sigma_r \frac{dg(T)}{dT} + \partial_T \partial_k \sigma_r = 0 \tag{4.84}$$

The linear ordinary equation derived here from differential geometry considerations appears to differ from the formally nonlinear condition (4.22) derived by second-order Taylor expansion along the ridge. However, squaring condition (4.84), dividing by $\partial_k^2 \sigma_r$ and using (4.82) to replace the squared mixed derivative exactly yields (4.22). Consequently, the evolution equations derived by Taylor expansion at quadratic order and by differential geometry arguments are consistent with the former being essentially the square of the later. This reflects the fact that both approaches capture curvature information, either via including the quadratic terms in the Taylor expansion or via the shape operator. Nevertheless, there appear to be possible practical advantages of using the more abstract machinery of differential geometry:

1. The evolution equation for $g(T)$ is linear. In this specific model problem only after computing the expressions for all second derivatives and after simplifications, the $(d_T g(T))^2$ terms in (4.22) drops out and a linear form is recovered.

2. The analytical calculations and numerical evaluations necessary to access all three second derivatives may vastly differ in complexity. Computation of $\partial_T^2 \sigma_r$ is in general significantly more involved than accessing $\partial_k^2 \sigma_r$ and the mixed term $\partial_T \partial_k \sigma_r$ due to the computation of the time-derivative of the fluctuations feedback (induced by $\partial_T^2 U$) which requires the differentiation of the eigenfunction $\hat{\varphi}$ along the ridge and of the amplitude expression (namely of α and β which also involves U and $\hat{\varphi}$). The determination of $\partial_T^2 \sigma$ in condition of marginal stability, already fairly in the case of a 2D model problem, as shown in § 4.3.1, will highly increase in complexity for a system like the stratified flow problem where the linear operator is not self-adjoint and the eigenfunctions can not be chosen real. Here, the relation between second derivatives (4.82) allows for the elimination of $\partial_T^2 \sigma_r$ and thereby for a substantial simplification of the algorithm. Alternatively, the relation can be used to test calculations and accuracy of numerical implementations.

4.3.3 Prediction of the wavenumber of the fastest growing mode below marginal stability

The linear evolution of the fluctuations together with the infinite scale separation make the coupling between the fast and the slow dynamics relevant only when marginal stability is reached. The convergence of the feedback term is indeed not realized for positive growth rates and equals zero for negative ones. The first case lies outside the (asymptotically justified) QL approximation due to the lack of scale separation, and the second one corresponds to an instantaneous decay of the fast modes on the slow time scale leading to the simplified

dynamics

$$\frac{\partial U}{\partial T} = F(z, T) - \nu U + D\frac{\partial^2 U}{\partial z^2} \tag{4.85}$$

$$\sigma\hat{\eta} = \left(-1 + k^2 U - k^4 + \frac{\partial^2}{\partial z^2}\right)\hat{\eta} \equiv L\hat{\eta} \,. \tag{4.86}$$

Considering a scenario where the fluctuations are initially stable, their growth rate σ will gradually increase due to their advection by the mean field (on which an external force is acting), until the marginal stability condition is eventually met by the fastest growing mode and the coupled QL dynamics is recovered. Although the cumulative effect of the fast modes does not affect the slow dynamics it is of fundamental importance to track their evolution in order to detect the mode that first approaches the marginally-stable manifold and gets slaved to the mean field. In the remainder of this section we derive an algorithm for the prediction of the wavenumber of the fastest growing mode below marginal stability under the assumption of infinite scale separation.

Referring again to the time-varying dispersion relation as a three-dimensional surface, we indicate with $Q = (T_Q, k_Q)$ a point on the landscape for which $\sigma_Q < 0$ and the maximum condition in k, $\partial_k \sigma|_Q = 0$, is satisfied. The prediction of the wavenumber k for the fastest stable growing mode then only requires the propagation of the maximum property in time. Expanding in a Taylor series at the first order the derivative of the growth rate $\partial_k \sigma$ around the point Q

$$\frac{\partial \sigma}{\partial k}(T_Q + \Delta T, k_Q + \Delta k) \simeq \left.\frac{\partial \sigma}{\partial k}\right|_Q + \left.\frac{\partial^2 \sigma}{\partial k^2}\right|_Q \Delta k + \left.\frac{\partial^2 \sigma}{\partial T \partial k}\right|_Q \Delta T \tag{4.87}$$

and enforcing the maximum condition in k, an evolution equation for the wavenumber is obtained

$$\frac{\Delta k}{\Delta T} = -\frac{\partial_T(\partial_k \sigma)|_Q}{\partial_k^2 \sigma|_Q}. \tag{4.88}$$

From the geometrical point of view this case substantially differs from the marginally-stable one presented in the previous section. While the maintenance of the marginal stability condition imposes constraints on σ and on both its first derivatives (hence the second-order Taylor expansion of the growth rate) generating the existence of a flat ridge on the landscape, the propagation of the maximum property only constraints the first derivative of the growth rate allowing for a ridge with a non-zero Gaussian curvature.

Nevertheless, similarly to the previous case, the prediction of the wavenumber requires the de-

termination of the second derivatives of the growth rate. The computation of these derivatives can be done either using perturbation analysis and solvability condition at the second order, as detailed in the previous section, or alternatively with the following procedure:

- taking the first derivative of the eigenvalue problem (4.86)

- applying the solvability condition on the parameter dependent boundary value problem, resulting from the previous step, to obtain the first derivative of the growth rate

- differentiating the first derivative of the growth rate and evaluating it at the specific point Q.

with the main difference being the order of differentiation, evaluation and projection onto the null-space of $\mathscr{L}$ (Fredholm alternative).

While both procedures, explicitly leads to the same result for the second derivative with respect to wavenumber k,

$$\frac{\partial^2 \sigma}{\partial k^2}\bigg|_Q = -8k^2 + 4k \int_0^{Lz} U\hat{\eta}_Q \frac{\partial \hat{\eta}}{\partial k}\bigg|_Q dz \, , \tag{4.89}$$

they seemingly do not for the mixed derivative $\partial_k(\partial_T \sigma)|_Q$.

The first methodology, which requires the second order differentiation of the eigenvalue problem (4.86) in k and T evaluated at the point Q and then the application of the solvability condition, gives

$$\frac{\partial^2 \sigma}{\partial k \partial T}\bigg|_Q = 2k \int_0^{Lz} \left(F - vU + D\frac{\partial^2 U}{\partial z^2}\right)|\hat{\eta}_Q|dz + 2k \int_0^{Lz} (U - 2k^2)\hat{\eta}_Q \frac{\partial \hat{\eta}}{\partial T}\bigg|_Q dz +$$
$$+ k^2 \int_0^{Lz} \left(F - vU + D\frac{\partial^2 U}{\partial z^2}\right)\hat{\eta}_Q \frac{\partial \hat{\eta}}{\partial k}\bigg|_Q dz \tag{4.90}$$

while the second approach yields the two following results, depending on whether the first derivative is taken with respect to k or T,

$$\frac{\partial}{\partial k}\left(\frac{\partial \sigma}{\partial T}\right)\bigg|_Q = 2k \int_0^{Lz} \left(F - vU + D\frac{\partial^2 U}{\partial z^2}\right)|\hat{\eta}_Q|dz + 2k^2 \int_0^{Lz} \left(F - vU + D\frac{\partial^2 U}{\partial z^2}\right)\hat{\eta}_Q \frac{\partial \hat{\eta}}{\partial k}\bigg|_Q dz \tag{4.91}$$

and

$$\frac{\partial}{\partial T}\left(\frac{\partial \sigma}{\partial k}\right)\bigg|_Q = 2k \int_0^{Lz} \left(F - vU + D\frac{\partial^2 U}{\partial z^2}\right)|\hat{\eta}_Q|dz + 4k \int_0^{Lz} U\hat{\eta}_Q \frac{\partial \hat{\eta}}{\partial T}\bigg|_Q dz \, . \tag{4.92}$$

Although apparently different, the three expression (4.90)-(4.92) can be proven to be identical confirming the interchangeability of the two approaches. The analytical proof in the case of a self-adjoint operator is provided in § B, and the numerical one can be obtained showing that the following relation among the derivatives of the eigenfunction is satisfied

$$2\int_0^{Lz} U\hat{\eta}_Q \frac{\partial\hat{\eta}}{\partial T}\bigg|_Q dz = k\int_0^{Lz}\left(F - \nu U + D\frac{\partial^2 U}{\partial z^2}\right)\hat{\eta}_Q\frac{\partial\hat{\eta}}{\partial k}\bigg|_Q dz\,. \tag{4.93}$$

Substituting the expressions (4.89) and (4.91) into (4.88) the final evolution equation for the wavenumber of the fastest growing mode reads

$$\frac{\Delta k}{\Delta T} = \frac{2k\int_0^{Lz}(F - \nu U + D\partial_z^2 U)|\hat{\eta}_Q|dz + 2k^2\int_0^{Lz}(F - \nu U + D\partial_z^2 U)\hat{\eta}_Q\partial_k\hat{\eta}|_Q dz}{-8k^2 + 4k\int_0^{Lz} U\hat{\eta}_Q\partial_k\hat{\eta}|_Q dz}\,. \tag{4.94}$$

4.3.4 On the finite scale separation and smoothness of the algorithm

The algorithmic structure presented in this chapter for the slaving of the fluctuations amplitude in condition of marginal stability and for the prediction of the wavenumber associated with the fastest growing mode (both for zero and negative growth rates) assumes the presence of an infinite scale separation between the fluctuations and the mean field dynamics. This fundamental assumption naturally gives rise to a non-smooth algorithm characterized by a discontinuous fluctuation feedback on the slow dynamics for smoothly-varying values of the growth rate: the fast modes do not affect the mean field whenever $\sigma < 0$, and they have a finite amplitude when $\sigma = 0$. As shown in the previous chapter in the case of a 1-dimensional model problem (§3.4.2), a smooth version of the QL algorithm can be derived when taking into account a finite scale separation and allowing for a marginal growth/decay of the fast fluctuations near marginal stability. In such a case, by inspection of the feedback term (), re-written here with a finite yet large $\tau_f = T_f/\varepsilon$,

$$\overline{\left(\frac{\partial\eta}{\partial\chi}\right)^2} = 2k^2|A|^2|\hat{\eta}|^2\frac{\varepsilon}{T_f}\int_0^{T_f/\varepsilon} e^{2\sigma\tau}d\tau = 2k^2|A|^2|\hat{\eta}|^2 f(\sigma) \tag{4.95}$$

it is possible to identify the values of σ for which the function $f(\sigma)$ is negligible (below a certain threshold value δ) or finite (within an interval $1-\delta$ and $1+\delta$) by solving the inequalities (3.28) and (3.29). The resulting values of the growth rate, σ_1, σ_2 and σ_3 (with $\sigma_1 < \sigma_2 < 0 < \sigma_3$), bound the validity regions of the QL reduction for finite scale separation: the mean field U evolves without fluctuation feedback when $\sigma < \sigma_1$, and a fluctuation amplitude is determined when $\sigma_2 < \sigma < \sigma_3$. The remaining connecting region, represented by values of the growth rate $\sigma_1 < \sigma < \sigma_2$ for which none of the QL approximation is suitable, finally requires the fully non-linear co-evolution of the two dynamics on the same temporal scale, described by (4.1)

and (4.2), until the marginally stable region is reached (namely $\sigma_2 < \sigma < \sigma_3$). Similarly it should be treated the case in which positive growth rates $\sigma > \sigma_3$ are realized, here only possible for unstable initial conditions due to the positive definiteness of the term β (4.48), whose sign is responsible for bursting events.

However, although in principle possible, the implementation of a smooth variation of the QL algorithm in the context of this specific model problem would require to address some practical issues arising from the simplification choices made in the derivation of QL algorithm. The elimination of the slow spatial coordinate x, via a stream-wise horizontal average, from (4.9) in order to get a strict QL formulation of the original system leads indeed to a reduced system characterized by a stream-wise invariant mean field and by k-structured-only fluctuations, which is in contrast with the full two-dimensionality of the original system, where both U and η depend on x and z. The implementation of a co-evolution technique within the QL framework will then require either the reintroduction of the convective term in (4.23) (resulting in a GQL formulation) or an ad-hoc modification of the original equations that drops the x-dependent terms in the evolution of the slow variable only. Consequently, here we focus on the infinite scale separation case, only considering scenarios with either stable or marginally stable fluctuations.

4.4 Numerical Implementation and Results

In this section we investigate the dynamics of the reduced system, described by (4.9)-(4.24), and show the effectiveness of the algorithmic structure proposed for the prediction of the wavenumber of the fastest growing mode. This will be done comparing the results from two different versions of the QL algorithm, where the first one performs a rudimentary update of the wavenumber solving the eigenvalue problem multiple times for different k (which it will be referred to as *k-search* algorithm), while the second one predicts it solving the evolution equations (4.66),(4.88) derived in the previous sections (*k-prediction* algorithm). We eventually compare the reduced QL dynamics against the fully non-linear one obtained from the finite-ε direct numerical simulations of (4.1) and (4.2).

4.4.1 Numerical Setup

The implementation of the three different algorithms, the two QL schemes and the DNS, has been carried out with an in-house Python code based on the open-source software *Dedalus* (), which provides a flexible framework for the integration of partial differential equations and for solving various type of eigenvalue and boundary value problems with spectral discretisation in space. All the simulations are performed in a periodic domain of length $L_x \times Lz$ for the DNS and L_z for the QL scheme. We remark that the reduced QL dynamics (4.23)-(4.24), after discarding the convective term in (4.9), is streamwise invariant for the slow field and only allows for a k-structure in the fast modes. In order to capture the variations of the fast modes, the minimum size of the domain length L_x for the DNS is set by the scale separation ε between the slow and the fast dynamics and by the wavenumber of the mode the first becomes unstable, namely $L_x \geq (2\pi/g(T))\varepsilon$. The discretisation is done using Fourier modes in both directions (N_x, N_z) for the DNS and Chebyshev modes (N_z) for the QL model. Although not optimal in the case of a periodic domain, the latter choice has been dictated by the need of solving eigenvalue problems with non-constant coefficient within the *Dedalus* framework, at the moment only possible with a Chebyshev discretisation.

For all the simulations a 4th-order Runge-Kutta scheme has been used for the time-integration with time-step $dt = 10^{-3}$ for the DNS and $dT = 5 \cdot 10^{-3}$ for the QL. Ultimately, for the simulations of the QL dynamics without the k-prediction, a k-resolution for the update of the fastest growing mode has been set to $dk = 5 \cdot 10^{-4}$. The numerical details and parameters are summarized for the different numerical schemes in table 4.1.

	L_x	L_z	N_x	N_z	dt	dk	ε
DNS	2π	2π	128	64	10^{-4}	–	10^{-2}
QL	–	2π	–	64	$5 \cdot 10^{-3}$	$5 \cdot 10^{-4}$	–

Table 4.1 – Numerical parameters used in this study. L_x and L_z being the domain sizes, N_x and N_z the number of collocation points, dt the t-step, dk the accuracy for the update of the wavenumber and ε the scale separation.

The singular eigenvalue problem (4.24) at the basis of the QL algorithm is solved using the *Dedalus* build-in sparse solver, based on the `scipy.sparse.linalg.eig` function which computes a set of eigenvalues close to a given target value ($\sigma = 0$, in this specific case) using Arnoldi iterations.

While the simplified version of the QL scheme, where the wavenumber of the fastest growing mode is updated searching over k, only requires to solve multiple eigenvalue problems for different k, the algorithm for the prediction of k requires an additional numerical procedure to solve the singular boundary value problems (4.32) and (4.31). This has been done extending the *Dedalus* solvers interface to use the *SuiteSparse* QR solver. Regarding the solvability of a singular boundary value problem we would like to stress that, although the generalized inverse method, mentioned in section 4.3.1, automatically imposes the Fredholm alternative solving the least square problem (4.50), this is practically done numerically with respect to an euclidean inner product (matrix product). However we aim at imposing a solvability condition defined via the inner product on the functional space L_2 which differs from the inner product induced by the euclidean inner product of the vector of expansion coefficients passed to the *SPQR* solver. Therefore the Fredholm alternative has to be explicitly imposed to the right-hand-side of the problem before numerically solving it.

A complete overview of the QL algorithm proposed in this work, with and without the prediction of the wavenumber k, is described in figure 4.10.

4.4.2 Simulations of the QL dynamics and prediction of the wavenumber

In this study we focus specifically on the dynamics obtained when a space-and-time varying external force is driving the mean field

$$F(z, T) = 2.5 + 0.5\cos(t)\cos(z) + 0.5\sin(0.6t)\cos(2z) \tag{4.96}$$

and when the diffusive and viscous coefficients are chosen to be unit, $D = 1$ and $v = 1$.

We set an initial condition from which the marginally-stable state can be reached, specifically

$$U(z, T = 0) = 1.9, \qquad \hat{\eta}(z, T = 0) = 0, \qquad F(z, T = 0) = 2.5 + 0.5\cos(z), \tag{4.97}$$

where U has been chosen to be close enough to a condition of marginal stability for the specific choice of the forcing term and of the parameters D and v. In this case the maximum fluctuations growth rate, associated with the mode $k = 0.975$, is initially negative, $\sigma = -0.094$, and the slow field U gets updated without any feedback from the fast modes, accordingly to (4.85). Due to the external forcing F acting on U, the fluctuations get more and more unstable until the marginal-stability condition is satisfied by the mode $k = 1.0012$ at time $T = 0.18$. Starting from this moment the amplitude A of the marginally stable mode is set according to (4.46) producing a restoring force on the slow field that maintains the growth rate at zero. Figures 4.3 and 4.4 show the evolution over (slow) time of the locally maximum growth rate σ

and the evolution of the corresponding wavenumber k, obtained from the elementary *k-search* QL algorithm.

Practically, due to a finite time step dt, the growth rate approaches a finite value slightly larger than zero. However as suggested by Chini *et al.* [Chini et al. (2022)], a dt-independent result can be obtained correcting the fluctuation amplitude (4.46) by means of a damping factor λ, when σ is above a certain tolerance $\tilde{\sigma} = 5 \cdot 10^{-5}$.

Considering the variation of the growth rate between two time steps T_{n+1} and T_n, and enforcing an exponential decay with a factor λ

$$\sigma^{n+1} - \sigma^n = (\tilde{\alpha} - \tilde{\beta}|A|^2)dT = -\frac{\sigma^n}{\lambda} \tag{4.98}$$

(with $\tilde{\alpha} = g^2\alpha$ and $\tilde{\beta} = 2g^4\beta$), the corrected amplitude results

$$|A|^2 = \frac{\tilde{\alpha}}{\tilde{\beta}} + \frac{\sigma}{\lambda\tilde{\beta}dT} \ . \tag{4.99}$$

Due to the absence of a symmetric marginally-stable region in this problem, as a result of the infinite scale separation assumption, the choice of the tolerance $\tilde{\sigma}$ and of the damping factor λ has to be carefully made. The combination of a too low threshold $\tilde{\sigma}$ together with a too small λ would push the growth rate too close to zero with the risk for the realization of slightly negative values, which would instantaneously set the fluctuation feedback to zero, causing artificial discontinuities in the dynamics.

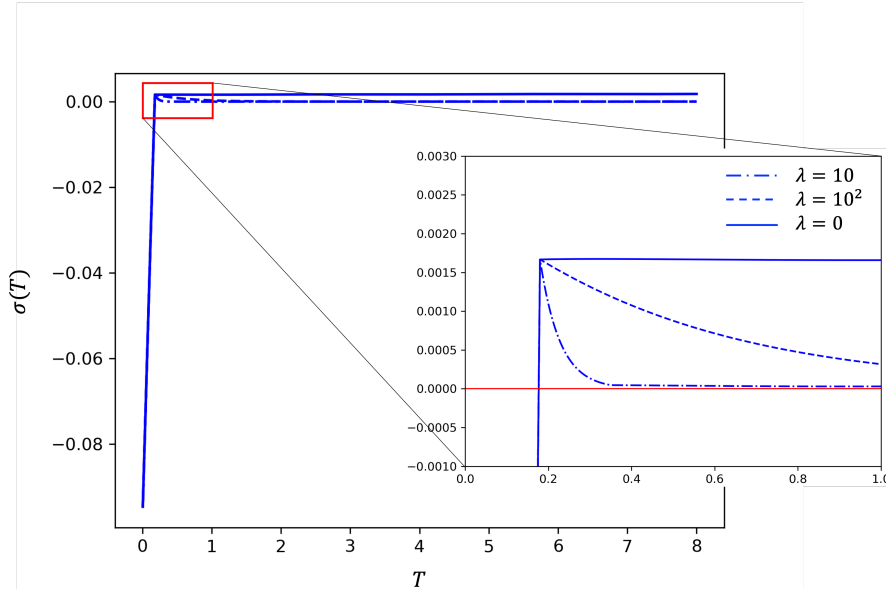Figure 4.3 – Evolution of the growth rate σ over slow time T. The zoom region inset shows the effect of the amplitude correction on the growth rate for 2 different damping factors λ (dashed lines) against the uncorrected one (solid line).
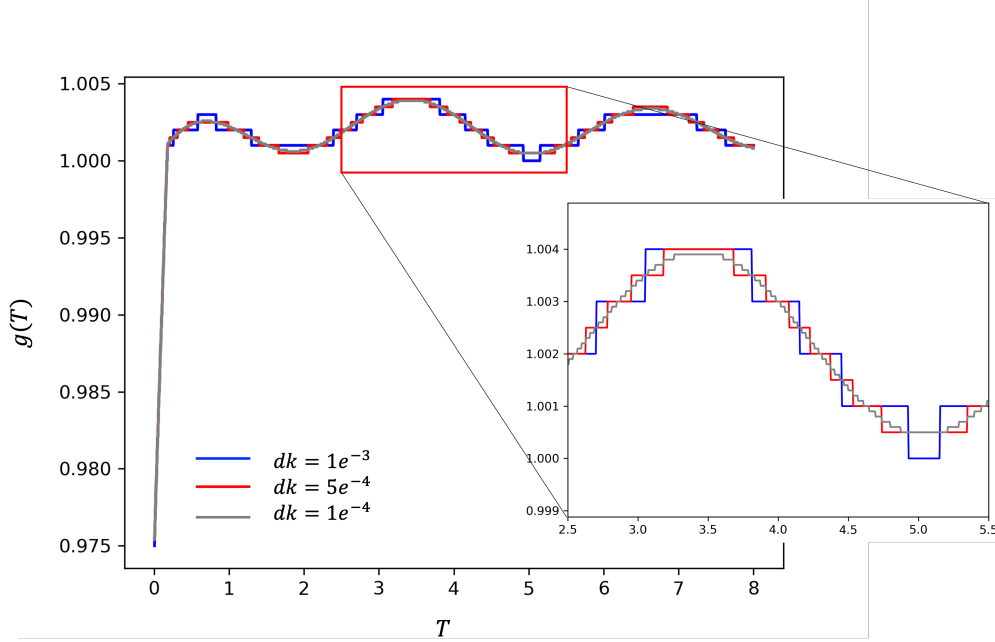
Figure 4.4 – Evolution of the of the wavenumber $g(T)$ associated to the fastest growing mode obtained from the k-search algorithm for different discretisation values dk

The marginally-stable state reached by the system, shown in figure 4.6 , although not an invariant solution of the full system from a dynamical system point of view, can be seen as a non-linear state with a simplified evolution, where the collapse of the fast modes, now slaved to the marginally stable mean field, gives rise to a low-dimensional dynamics.

As evident from figure 4.4 and 4.5, the wavenumber of the marginally-stable mode is, as expected in this model problem, varying in time, oscillating around 1. This requires to solve at each time different eigenvalue problems for different k to identify the peak of the dispersion relation $\sigma(k)$, the more numerous the smaller the dk. Moreover we remark that being the QL dynamics stream-wise invariant, the search has to be performed over a wide range of wavenumbers k (theoretically infinite) highly impacting the wall-clock time of the simulation. This limitation of the *k-search* algorithm becomes of fundamental importance for systems whit a more complex dispersion relation, where different local maxima exist and evolve, and for systems where multiple modes can become marginally-stable at the same time, making the development of the *k-prediction* algorithm a necessity.

The efficacy of the new methodology developed in section 4.3.1 and 4.3.3 for the prediction of the wavenumber in condition of marginal stability and below it, is shown in figure 4.7, where the two QL algorithm are compared. The results presented below are obtained without any amplitude correction (4.99), i.e. in the case $\lambda, \tilde{\sigma} \to \infty$, to highlight the robustness of the *k-prediction* algorithm for non-zero values of the growth rate. The total number of eigenvalue problems solved during the same simulation time, summing up to about 10^5 for the *k-search*
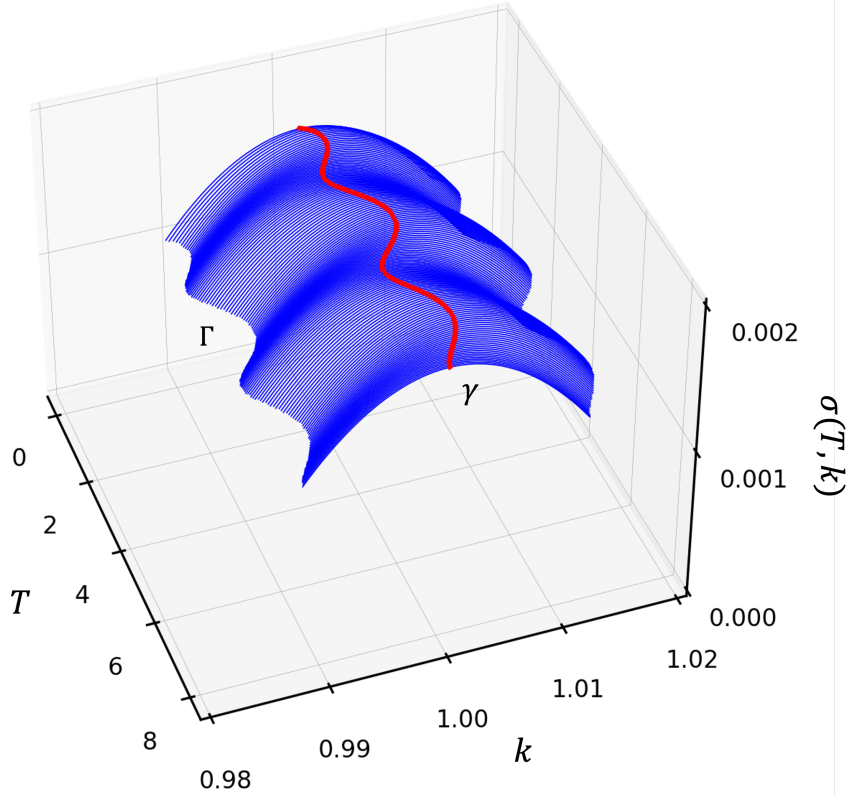
Figure 4.5 – Time-dependent dispersion relation $\sigma(T, k)$ obtained from the *k-search* QL algorithm. The blue surface represents the evolution over slow time of $\sigma(k)$ while the red curve represents the ridge γ given by the evolution in time of the wavenumber of the neutral mode, calculated by (4.66).

algorithm, (about 60 per time iteration when $dk = 10^{-4}$) is lowered by the *k-prediction* procedure down to about $2 \cdot 10^3$. In the latter case one eigenvalue problem is solved at each time iteration for the maximum wavenumber $g(T)$ and only two wide searches over k are performed: the first one at time $T = 0$ to initialise the wavenumber given the initial condition, and the second one when the marginally-stable manifold is approached, to smoothly connect the two different prediction algorithms (4.94) and (4.66), valid for $\sigma < 0$ and $\sigma = 0$ respectively. The evident agreement between the evolution of k (fig. 4.7) and the evolution of the mean field resulting from the two different algorithms is even more remarkable considering the modest variations of the wavenumber in this model problem (about 3%) and the fact that a forward Euler scheme has been used to update k.

4.4.3 Validation of the QL dynamics against direct numerical simulations

In this section we aim to compare the dynamics resulting from the simulation of the fully non-linear system (4.1)-(4.2) for which the final scale separation is set to $\varepsilon = 2 \cdot 10^{-2}$ against
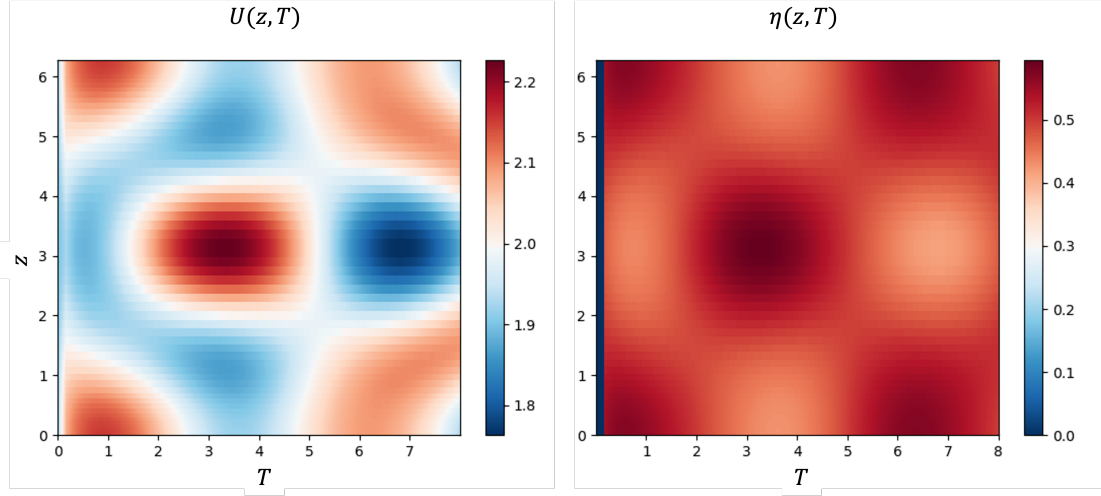
Figure 4.6 – Spece-time evolution of the mean field $U(z,T)$ (left) and fluctuations $\eta(z,T) = A(T)\hat{\eta}(z,T) + c.c$ (right), obtained from the *k-search* QL algorithm.

the QL reduced dynamics presented in the previous section.

As explained in § 4.3.4, the strict QL formulation of the original system is obtained via a stream-wise horizontal averaging procedure yielding an x-independent evolution equation for the mean field $U(z)$ and a χ-varying dynamics for the fluctuations $\eta(z,\chi)$ which results in a varying k within the eigenvalue problem formulation. On the contrary the fully non-linear system spatially evolves in both the vertical and the horizontal directions, making the comparison of the two dynamics non-trivial.

In order to overcome this difficulty, at least for validation and visualisation purposes, a fixed-time comparison between the two systems can be obtained *a posteriori* reducing the domain size L_x in the DNS the full system such that any x-variation of the mean field is suppressed (as proposed by [Chini et al. (2022)]). Practically, once the QL dynamics is known, the wavenumber $g(T^*) = 1.0033$ of the most unstable mode at a specific time $T^* = 3$ (when the system has already approached the marginally-stable manifold) is chosen and a DNS is then performed in a domain $L_x = \varepsilon 2\pi/g(T^*)$, small enough to disallow for x-variations of the mean field but large enough to accommodate the fluctuation structure. Finally the 2-dimensional fields $U_{QL}(x,z,T=T^*)$ and $\eta_{QL}(x,z,T=T^*)$ are re-constructed from the QL simulation via

$$U(z,x,T^*) = U(z,T^*) \tag{4.100}$$

$$\eta(z,x,T^*) = A(T^*)e^{(ig(T^*)x)} + c.c. \tag{4.101}$$

Despite the finite value of ε used for the simulation of the full system and the absence of an amplitude correction in the QL simulation (translating in a $\sigma = 0.001$) the agreement be-
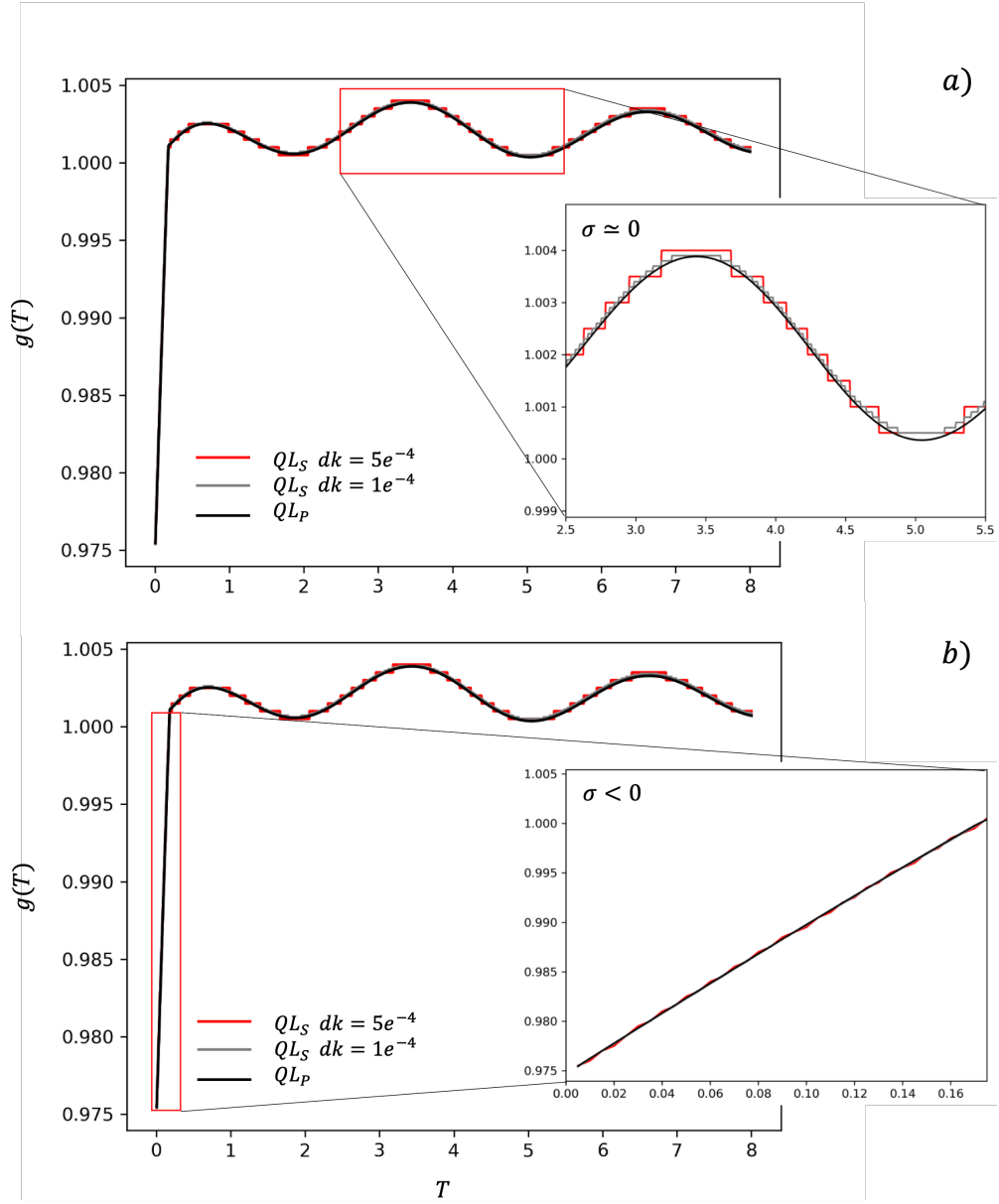
Figure 4.7 – Comparison between the evolution of the wavenumber *k* associated to the fastest growing mode obtained from the *k-search* algorithm (red and grey lines) and the *k-prediction* algorithm (black line). The zoom region inset on the top figure shows the comparison in condition of marginal stability where the wavenumber is updated accordingly to eq. (4.66), while the inset in the bottom figure shows the comparison for negative growth rates, in which case eq. (4.94) has been solved.

tween the results, visible in figure 4.8, confirms the great potential of the QL methodology in capturing the dynamics of systems that self-tune towards marginally stable states. The only difference, noticeable in the comparison of the fast modes (fig. 4.8 bottom row) is due to the translation invariance of the system (4.1)-(4.2) along the *x*-direction that in combination with

periodic boundary conditions allows for the x-shift of the fluctuations. Moreover, we point out that unlike in [Chini et al. (2022)], where a steady state was approached in condition of marginal stability, here, being the system non-autonomous, the marginally-stable dynamics is represented by a non-linear evolution, making the results comparison at fixed time even more noteworthy.

However, while the ε-rescaling of the DNS domain size in the x-direction removes the x-variability of the mean field, it also disallows for any k-variation in the neutrally-stable fluctuations which remains fixed at $g(T^*)$. Figure 4.9 shows an attempt in comparing the temporal evolution of the two systems when the evolution of the wavenumber of the most unstable mode is allowed. In this case the DNS has been run in a x-domain ε^{-1} times larger, $L_x = 2\pi$ with $N_x = 128$ grid points, which practically can accommodate about 50 copies of the marginally-stable mode (being $g(T)$ order $O(1)$) allowing for k-variations of the latter. The x-dependency of the mean field has then been averaged out in order to compare its space-time evolution, in z-only, against the one from the QL simulation.

4.5 Conclusions

With the more ambitious goal of accessing in the future the fully three-dimensional stratified flow dynamics, here we have taken a step forward in that direction increasing the dimensionality of the problem to two-dimensions. This modification introduces the horizontal spatial variability of the dynamics, which appears in the QL formulation as a dependency on the wavenumber of the eigenvalue problem describing the evolution of the fast dynamics. This results in a temporal variation of the dispersion relation $\sigma(T, k)$ and consequently in the temporal variation of the wavenumber associated to the fastest growing mode. The enforcement of the marginal stability constraint now requires to first identify the fastest growing mode and then to determine its amplitude such that marginal stability can be maintained in time. Practically the eigenvalue problem has to be solved for multiple k (and multiple is not *a priori* defined due to the continuous variation of k) at each time iteration, considerably increasing the computational costs of the QL simulation. The solution to this problem has been achieved by deriving an evolution equation for the wavenumber of the marginally-stable mode. In chapter 4 we presented and discussed, making use of a two-dimensional model problem, two alternative (but equivalent) derivations in condition of marginal stability. Within a geometrical description the evolution of the dynamics on the marginally stable manifold is strictly connected to the curvature properties of the $\sigma(T, k)$ landscape. The maintenance of zero growth rates in time, automatically results in a zero Gaussian curvature of this landscape in a specific k-direction, and the evolution of this direction yields at each time the wavenumber associated to the marginally-stable mode. Starting from different considerations, an evolution equation for the wavenumber of the fastest growing mode below marginal stability has also been derived. Although for negative values of the growth rate the fluctuation feedback is set to zero, this algorithm provides a feasible way to track the evolution of the maximum of

QL

DNS

Figure 4.8 – Comparison between the mean field $U(z, x)$ (top) and the fluctuations $\eta(z, x)$ (bottom) obtained from the QL simulation (left) against DNS (right) for fixed time. The QL simulation is performed in a domain $L_z = 2\pi$ with $N_z = 64$ modes and the 2-dimensional fields are re-constructed at time $T* = 3$ with a constant x-dependency for the mean field $U(z, x) = U(z)$ and via $\eta(z, x, T^*) = A(T^*)exp(ig(T^*)x) + c.c.$ for the fluctuations (with $g(T^*) = 1.0033$). As for the DNS the domain in the z-direction is identical to the QL while in the x-direction is set to $L_x = \varepsilon 2\pi / g(T^*)$, with a resolution of $N_x = 4$ modes (with a Fourier transform interpolation).

the dispersion relation, allowing for a more precise detection of the time at which marginal stability is satisfied.
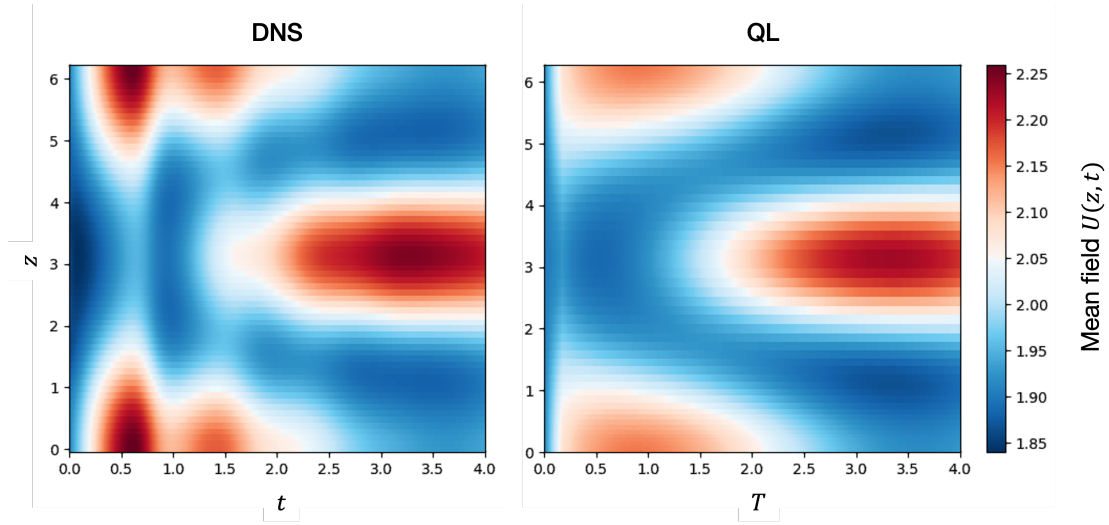
Figure 4.9 – Spatiotemporal evolution of the mean field $U(z$ obtained from the QL simulation (right) against the spatial average of $U(z, x)$ resulting from DNS (left). Both simulations are performed in a domain $L_z = 2\pi$ with $N_z = 64$ modes.
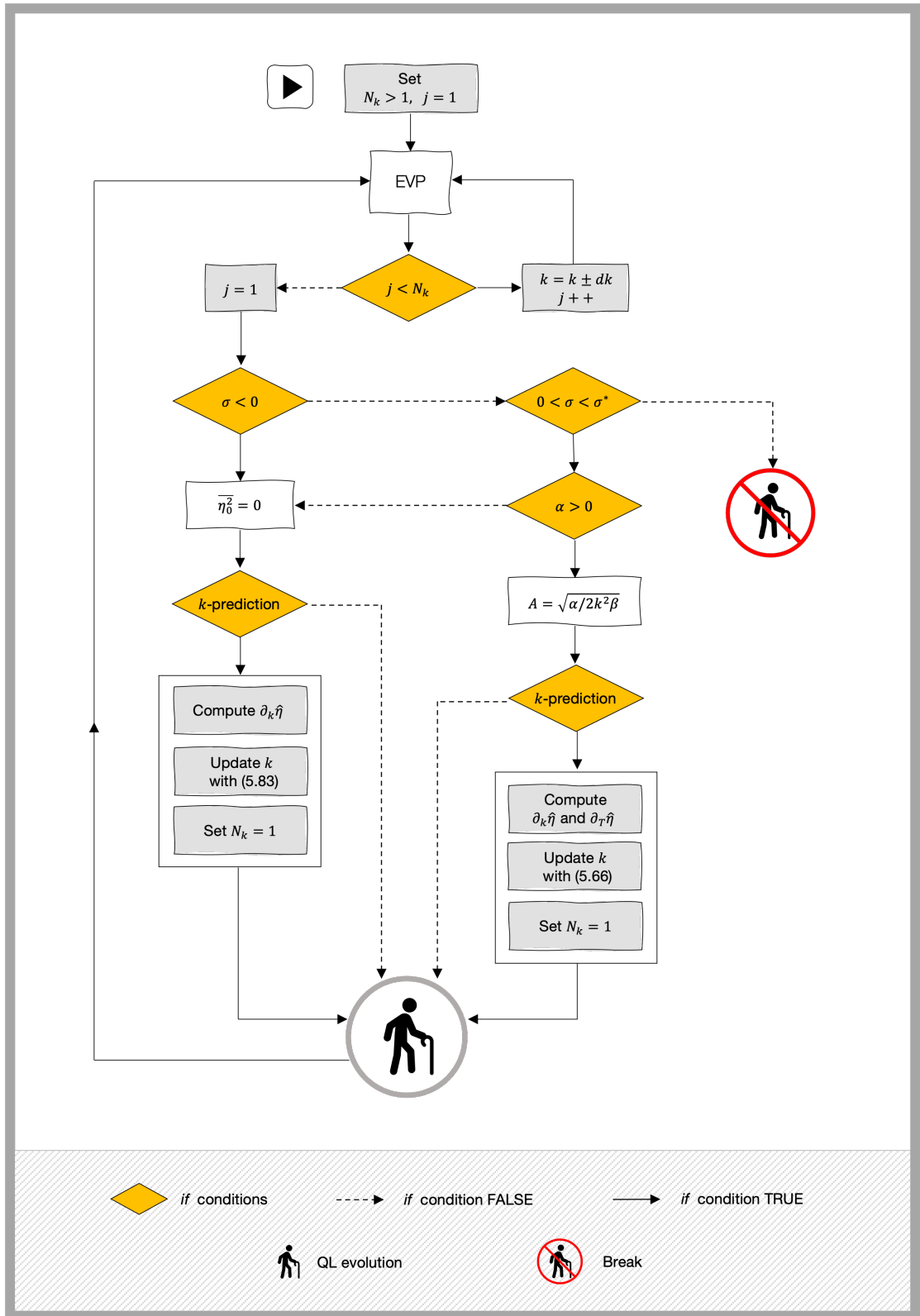
Figure 4.10 – Flowchart of the 2D QL algorithm with and without the prediction of the wavenumber associated to the fastest growing mode.

Rectangular boxes indicate processes, the white ones for generic QL actions and the grey ones for actions related to the update of the wavenumber k. *if*-statements are represented by yellow diamond-shaped boxes, and their outcome by a continuous arrow-connection when the *if*-condition is meet and with a dashed one otherwise.

The simulation starts with an initial wide k-search to identify the fastest growing mode for the chosen initial condition $U(z, T = 0)$. Specifically the eigenvalue problem (4.24) is solved N_k times for varying k with a resolution dk, covering a range of wavenumbers $[k^* - dkN_k/2, k^* + dkN_k/2]$ if the initial guess k^* is greater then $dkN_k/2$ or $[0, k^* - dkN_k/2]$ otherwise. Once the locally maximum growth rate has been singled out (together with the corresponding wavenumber and eigenfunction $\hat{\eta}$) its sign determines which QL reduction is used to compute the fluctuation feedback in (4.23): the feedback is set to 0 when either $\sigma < 0$ or $(0 < \sigma < \sigma^* \wedge \alpha < 0)$, the simulation breaks for $\sigma > \sigma^*$, and an amplitude is computed otherwise. Although when starting from stable initial conditions is not possible for this specific system to leave the marginally-stable manifold due to bursting events (β is positive-definite) the positive threshold σ^* has been introduced to detect initially-unstable states. After the determination of the feedback the QL procedure bifurcates depending on whether the *k-search* or the *k-prediction* algorithm is used. The former case simply proceeds updating the mean field on slow time and re-starting a new search over k to find the σ-pick for the updated U, while the latter case enters the one of the two blocks (depending on the sign of σ) for the computation of the wavenumber k associated to the mode that next will be the most unstable. After the computation of k, via (4.94) or (4.66), which requires to solve one or two boundary value problems for the corrections of the eigenfunction, the *k-prediction* algorithm sets $N_k = 1$, updates U and goes back to the eigenvalue problem which this time will be solved only once for the predicted k.

5 Towards Strongly Stratified Flows

Contents

Chapter summary

This chapter is dedicated to the application to the stratified flow problem of the integration methodology developed for QL slow-fast systems in the previous chapters. After re-deriving and discussing the asymptotically reduced system and its main features, we will re-trace the fundamental steps of the QL procedure that lead to the slaving of the fluctuations dynamics in condition of marginal stability [Chini et al. (2022)]. We will then further proceed presenting the two dimensional extension of the QL algorithm for the identification of the marginally-stable mode when a spatial variability of the fast dynamics is considered. This methodology (discussed in § 4) will be applied to the reduced stratified flow system under two main approximations: independence of the slow mean fields of the horizontal spatial coordinate (strict QL formulation of the problem), and limitation to one single marginally-stable mode. We will then discuss the algorithmic procedure to handle the termination of the marginally-stable manifold and the presence of a finite scale separation (presented in § 3) together with its limitations under the strict QL formulation.

5.1 Introduction

Turbulence is ubiquitous in most of the geophysical flows relevant for the climate of the Earth, particularly in the oceans and the atmosphere. Turbulence involves the interaction of a vast range of spatiotemporal scales, as well as the coexistence of many physical phenomena. In the oceans, where energy is injected at global scales, $O(10^3 - 10^4)km$, and dissipation occurs at the Kolmogorov scale, $O(10)cm$ many different form of turbulence are manifest. At the larger scales the combined effect of rotation and strong density stratification stirs the flow mainly on quasi-horizontal planes coincident with isopycnals. At the so-called microscale, $O(1-100)m$, turbulence is fully 3D and erodes the stable stratification. At this scale, the flow naturally develops an anisotropic layer structure, characterized by a vertical length scale h that is considerably smaller than the horizontal one (L) [Fincham et al. (1996),Herring and Métais (1989), Métais and Herring (1989),Riley et al. (1981),Billant and Chomaz (2001)]. The relative motion of these layers, gives rise to strong shear that can trigger small-scale instabilities, of Kelvin-Helmholtz and Holmboe type, introducing into the system an horizontal characteristic length scale comparable to the layer thickness h. These small isotropic disturbances, although not resolved in numerical regional circulation and global climate models, play a fundamental role in the overall global circulation controlling the vertical mixing of denser water from the deep oceans.

Nevertheless several fundamental questions related to the strongly stratified turbulent regime remain unanswered, (e.g the relative importance of spectrally local and non-local energy transfer and the importance of the initial stratification or the forcing mechanism on mixing [Oglethorpe et al. (2013),Venaille et al. (2017),Tang et al. (2009),Portwood et al. (2016)]) making the parametrisation of the small-scale processes a challenging task. The major obstacle in the investigation of the physical processes is the enormous range of scales that must be resolved in order to capture them. More precisely, the microscale spans from scales L that are small enough not to be affected by the Coriolis force to the Ozmidov scale $L_O = (\epsilon_h/N^3)^{1/2}$, the largest horizontal flow scale *not* influenced by stratification. Denoting by N the Brunt-Väisälä frequency, by $\epsilon_h \sim U^3/L$ the horizontal turbulent energy dissipation rate and by the horizontal Froude number $Fr_h = U/NL$ the inverse measure of the stratification strength, this range of scales is then fixed by the Froude number, as the ratio $L/L_O = O(Fr_h^{-3/2})$. Thus, owing to the strong stratification ($Fr_h < 10^{-3}$) and the considerably high Reynolds number ($Re > 10^9$) required to achieve the strongly stratified turbulence regime, a full 3D direct simulation (DNS) would require a resolution of the order of 10^{18} grid points, far beyond current computational capabilities, as shown in figure 5.1 [Brethouwer et al. (2007),Bartello and Tobias (2013),Zhou and Diamessis (2019)]. The development of new theoretical tools is therefore a prerequisite for further advancements in this subject. A better understanding of strongly stratified turbulence would not only provide a deeper insight on the role of the microscale in the global overturning circulation but it would also facilitate the development of new flow-control techniques.

Scale separation in geophysical flows is very often related to the presence of a strong external
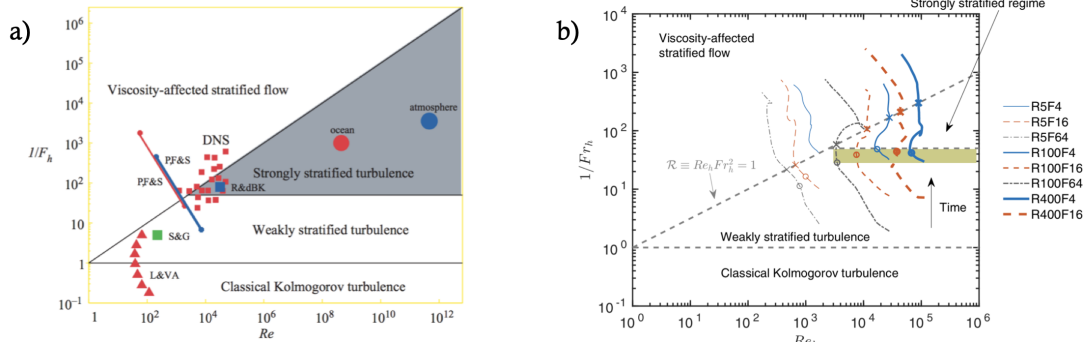
Figure 5.1 – Stratified flow regime diagram as a function of the $Reynolds$ number Re and the $Froude$ number Fr a) from [Brethouwer et al. (2007)] and b) from [Zhou and Diamessis (2019)]. Despite the huge increase of computational power over the past 12 years both diagrams show the gap in parameter space between the parameter regime numerically accessible and the one of interest for geophysical applications.

constraint that is responsible for the coexistence of large-scale anisotropic and small-scale isotropic structures. This translates into the emergence of a dominant balance in the governing equations that can be mathematically exploited to derive simplified equations by means of multi-scale and asymptotic analysis. This approach has been successfully used by Julien and Knobloch to derive *reduced models* when rapid rotation or a strong magnetic field is applied to a flow system [Sprague et al. (2006),Julien and Knobloch (2007)] and by Chini *et al.* for flows subjected to strong stratification [Chini et al. (2022)]. In the latter work, the multi-scale analysis of the Boussinesq equations in the limit of small Fr_h number and large Re reveals two disparate spatiotemporal scales and yields a set of coupled equations for the large anisotropic dynamics and the small-scale disturbances.

The resulting system may be viewed as a generalized quasi-linear model (GQL), in that the evolution of the fast variables is linearised around slowly varying mean fields and the fluctuation-fluctuation interactions are retained only when they feed back onto the mean flow. Although the quasi-linear (QL) approximation has been used in the past to enable the investigation of simplified flow systems [Tobias and Marston (2017)], here it should be emphasized that the quasi-linearity is an intrinsic feature of the asymptotic behaviour of the strongly-stratified dynamical system and not the result of an *ad hoc* approximation. Owing to the linearised evolution of the fluctuations, the first issue concerning slow-fast QL systems is related to the choice of a suitable integration method. Although co-evolution of the mean and fluctuation dynamics on the same fast temporal scale (i.e. the single-time QL algorithm in [Chini et al. (2022)], consisting in a DNS of the simplified system) may ensure accuracy, it does not take computational advantage of the multi-scale nature of the system. On the other hand, the application of the heterogeneous multi-scale algorithm, although more efficient, introduces many arbitrary choices for the initialisation and the duration of the fast-time integration.

Based on the observation that many slow-fast QL systems have the tendency of self-organize

around marginally stable states, Michel & Chini [Michel and Chini (2019)] have recently proposed a new integration strategy that exploits a marginal stability constraint. Due to the linearity of the fluctuations evolution, the fast fields can be expanded in modal solutions and the mode that first realises a zero growth rate get slaved to the mean dynamics to maintain its marginal stability via the feedback coupling. This results in a low dimensional evolution of the two fields on the marginally stable manifold for as long as it exists.

Building up on theirs work, we have developed new extensions to the QL procedure with the final aim of designing an algorithm capable of accessing the extreme parameter regime relevant for stratified flows in ocean and atmosphere. In chapter 3 we have presented a methodology to deal with the termination of the marginally stable manifold and with the presence of a finite scale separation, while in chapter 4 we developed an algorithm to efficiently extend the QL algorithm to more than one spatial dimension. As a natural next step, in this chapter we will discuss the application of these extensions to the strongly stratified flow problem. We will start with a detailed derivation of the reduced set of equations for the system under analysis, showing its key features and its potential for the description of relevant geophysical problems. We will proceed applying the QL integration methodology based on the marginal stability constraint, underlying the main differences with respect to the other problems analysed in this work. Both these two calculations are discussed in Chini et al. (2022) and re-derived here for clarity purposes with the intention of developing a coherent notation and a complete framework. We will then illustrate the mathematical derivation of an evolution equation for the wavenumber associated to the marginally-stable mode which allows to efficiently identify the component of the fast dynamics that needs to be slaved to ensure the evolution of the slow-fast system on the marginally-stable manifold.

5.2   Governing equations and multi-scale analysis

Variations in the density of the fluid are common in most of the geophysical flows. When the vertical density profile is described by a decreasing function of the height , i.e. lighter fluid is placed above heavier fluid, the flow is said to be stably stratified. The main effect of a stable stratification is to constrain the vertical motion of the fluid due to the action of the gravity force. Imagining the simplest scenario, characterized by an incompressible stably stratified fluid in static equilibrium conditions, any small vertical perturbation of the system would cause an oscillatory behaviour about the equilibrium position due to buoyancy and inertia. The oscillation frequency N is set by the vertical density profile and is known as the Brunt-Väisälä frequency (or buoyancy frequency),

$$N = \sqrt{\frac{-g}{\rho_0} \frac{\partial \overline{\overline{\rho}}}{\partial \tilde{z}}} \ . \tag{5.1}$$

Here ρ_0 is a constant density reference value, $\overline{\rho}$ the mean density and together with the fluctuation density $\tilde{\rho}$ they sum up to the total density $\tilde{\rho}_T = \rho_0 + \overline{\tilde{\rho}} + \tilde{\rho}$.

Here the tilde notation $\tilde{(\cdot)}$ indicates dimensional quantities. However, although vertical motion and overturning are inhibited by stable stratification, turbulent dynamics and mixing are still possible when enough energy is provided to the system to overcame the buoyancy barrier. This is the case for many parallel shear flows where the relative motion between layers characterized by different density triggers shear instabilities (like Kelvin-Helmholtz instability) responsible for the mixing of the fluid and the erosion of the density stratification (at least locally).

In a more general case, out of equilibrium, stably stratified flows in which density variations are small compared to the mean background density are well described by the Navier-Stokes equations under Boussinesq approximation [P. et al. (2016),Riley (2021)]. Defining with $\tilde{\boldsymbol{v}} = (\tilde{u}, \tilde{v}, \tilde{w})$ the velocity flow field in the directions $\tilde{\boldsymbol{x}} = (\tilde{x}, \tilde{y}, \tilde{z})$, with $\tilde{\rho}$ the density and with $\tilde{p}$ the pressure, the momentum conservation, the mass conservation and the density equations read

$$\frac{\partial \tilde{\boldsymbol{v}}}{\partial \tilde{t}} + \tilde{\boldsymbol{v}} \cdot \tilde{\nabla} \tilde{\boldsymbol{v}} = -\frac{1}{\rho_0} \tilde{\nabla} \tilde{p} - \frac{\tilde{\rho}}{\rho_0} \boldsymbol{g} + \nu \tilde{\nabla}^2 \tilde{\boldsymbol{v}} \tag{5.2}$$

$$\tilde{\nabla} \cdot \tilde{\boldsymbol{v}} = 0 \tag{5.3}$$

$$\frac{\partial \tilde{\rho}}{\partial \tilde{t}} + \tilde{\boldsymbol{v}} \cdot \tilde{\nabla} \tilde{\rho} + \tilde{w} \frac{d\overline{\tilde{\rho}}}{d\tilde{z}} = \kappa \tilde{\nabla}^2 \tilde{\rho} \tag{5.4}$$

where $\boldsymbol{g}$ is the gravity force $g\boldsymbol{e}_z$ and $\boldsymbol{e}_z$ the vertical versor. In order to match the notation used in Chini et al. (2022) (and by many other authors) and to ease the comparison among results, equations (5.3)-(5.4) can be re-written introducing the buoyancy force $\tilde{\boldsymbol{b}} = -\frac{\tilde{\rho}}{\rho_0} \boldsymbol{g} = \tilde{b}\boldsymbol{e}_z$ yielding

$$\frac{\partial \tilde{\boldsymbol{v}}}{\partial \tilde{t}} + \tilde{\boldsymbol{v}} \cdot \tilde{\nabla} \tilde{\boldsymbol{v}} = -\frac{1}{\rho_0} \tilde{\nabla} \tilde{p} + \tilde{\boldsymbol{b}} + \nu \tilde{\nabla}^2 \tilde{\boldsymbol{v}} \tag{5.5}$$

$$\tilde{\nabla} \cdot \tilde{\boldsymbol{v}} = 0 \tag{5.6}$$

$$\frac{\partial \tilde{b}}{\partial \tilde{t}} + \tilde{\boldsymbol{v}} \cdot \tilde{\nabla} \tilde{b} + \tilde{w} \frac{d\overline{\tilde{b}}}{d\tilde{z}} = \kappa \tilde{\nabla}^2 \tilde{b} \tag{5.7}$$

5.2.1   Anisotropic non-dimensionalisation of the Boussinesq equations

Further approximations of the equations (5.5)-(5.7), and in general the identification of the dominant terms in the different flow regimes can be achieved via non-dimensionalisation.

Strongly stably stratified flows has been shown to spontaneously develop anisotropic struc-
tures, consisting of large horizontal layers with a characteristic length scale that is much larger
than the vertical one (i.e. the layer thickness)[Fincham et al. (1996),Herring and Métais (1989),
Métais and Herring (1989),Billant and Chomaz (2001)]. Therefore it is reasonable, in this
case, to make a distinction between horizontal ($\boldsymbol{x} = (x, y)$) and vertical z directions when
defining characteristic length scales. Indicating now with $\tilde{\boldsymbol{x}} = (\tilde{x}, \tilde{y})$, $\tilde{\boldsymbol{u}} = (\tilde{u}, \tilde{v})$ the dimensional
horizontal velocity and horizontal directions respectively, and with $\tilde{\nabla}_h$ the horizontal gradient
operator, we proceed by introducing the general non-dimensional quantities (without tilde) as

$$\tilde{t} = Tt, \quad \tilde{\boldsymbol{x}} = L\boldsymbol{x}, \quad \tilde{z} = Hz, \quad \tilde{\boldsymbol{u}} = U\boldsymbol{u}, \quad \tilde{w} = Ww$$
$$\tilde{p} = Pp, \quad \tilde{b} = Bb \tag{5.8}$$

Substituting (5.8) into the Boussinesq equations, discriminating between horizontal and
vertical momentum equations yields

$$\frac{U}{T}\frac{\partial \boldsymbol{u}}{\partial t} + \frac{U^2}{L}(\boldsymbol{u} \cdot \nabla_h)\boldsymbol{u} + \frac{UW}{H}w\frac{\partial \boldsymbol{u}}{\partial z} = -\frac{P}{\rho_0 L}\nabla_h p + \nu\left(\frac{U}{L^2}\nabla_h^2\boldsymbol{u} + \frac{U}{H^2}\frac{\partial^2 \boldsymbol{u}}{\partial z^2}\right) \tag{5.9}$$

$$\frac{W}{T}\frac{\partial \boldsymbol{u}}{\partial t} + \frac{UW}{L}(\boldsymbol{u} \cdot \nabla_h)\boldsymbol{u} + \frac{W^2}{H}w\frac{\partial w}{\partial z} = -\frac{P}{\rho_0 H}\nabla_h p + Bb + \nu\left(\frac{W}{L^2}\nabla_h^2 w + \frac{W}{H^2}\frac{\partial^2 w}{\partial z^2}\right) \tag{5.10}$$

$$\frac{U}{L}(\nabla_h \cdot \boldsymbol{u}) + \frac{W}{H}\frac{\partial w}{\partial z} = 0 \tag{5.11}$$

$$\frac{B}{T}\frac{\partial b}{\partial t} + \frac{UB}{L}(\boldsymbol{u} \cdot \nabla_h)b + \frac{WB}{H}\frac{\partial b}{\partial z} = \kappa\left(\frac{B}{L^2}\nabla_h^2 b + \frac{B}{H^2}\frac{\partial^2 b}{\partial z^2}\right). \tag{5.12}$$

Imagining T is the time spent by a fluid element with velocity U to transverse an horizontal
distance L, i.e. $T = L/U$, we can chose H to be the vertical distance spanned in the same
amount of time $H = WT = (WL)/U$. The buoyancy difference resulting from the vertical
displacement of the fluid then scales with

$$B = \left|\frac{d\tilde{\bar{b}}}{d\tilde{z}}\right| H = N^2 \frac{WL}{U}. \tag{5.13}$$

Intuitively, from the hydrostatic balance, a variation in the buoyancy translates into a pressure
variation

$$P = B\rho_0 H = \frac{N^2 WLH\rho_0}{U} = \rho_0 U^2 \tag{5.14}$$

where the pressure scale $P = \rho_0 U^2$ is obtained from the horizontal balance of forces in (5.9).

The previous expression yields both a scale for the buoyancy and a scale for the vertical velocity

$$B = \frac{U^2}{H} \tag{5.15}$$

and

$$W = \frac{U^3}{N^2 L H} \ . \tag{5.16}$$

Defining the Froude number, representing an inverse measure of the stratification as $Fr_h = U/(NL)$ in the horizontal direction and $Fr_v = U/(NH)$ in the vertical direction, the scale for the vertical velocity can be then expressed as follow

$$W = Fr_h^2 U \frac{L}{H} = Fr_v^2 U \frac{H}{L} \ . \tag{5.17}$$

Substituting (5.15), (5.16) and the pressure scale $P = \rho_0 U^2$ into (5.9)-(5.12) the final non-dimensionalised governing equations are

$$\frac{\partial \boldsymbol{u}}{\partial t} + \boldsymbol{u} \cdot \nabla_h \boldsymbol{u} + Fr_v^2 w \frac{\partial \boldsymbol{u}}{\partial z} = -\nabla_h p + \frac{1}{Re} \left(\nabla_h^2 \boldsymbol{u} + \frac{1}{\alpha^2} \frac{\partial^2 \boldsymbol{u}}{\partial z^2} \right) \tag{5.18}$$

$$Fr_h^2 \left(\frac{\partial w}{\partial t} + \boldsymbol{u} \cdot \nabla_h w + Fr_v^2 w \frac{\partial w}{\partial z} \right) = -\frac{\partial p}{\partial z} - b + Fr_h^2 \frac{1}{Re} \left(\nabla_h^2 w + \frac{1}{\alpha^2} \frac{\partial^2 w}{\partial z^2} \right) \tag{5.19}$$

$$\nabla_h \cdot \boldsymbol{u} + Fr_v^2 \frac{\partial w}{\partial z} = 0 \tag{5.20}$$

$$\frac{\partial b}{\partial t} + \boldsymbol{u} \cdot \nabla_h b + Fr_v^2 w \frac{\partial b}{\partial z} + w = \frac{1}{PrRe} \left(\nabla_h^2 b + \frac{1}{\alpha^2} \frac{\partial^2 b}{\partial z^2} \right) \tag{5.21}$$

where the α is the aspect ratio $\alpha = H/L$, $Re = LU/\nu$ is the Reynolds number, a measure of the inertial forces over the viscous ones, and $Pr = \nu/\kappa$ (the ratio between momentum diffusivity and thermal diffusivity).

The set of equations resulting from the anisotropic scaling involves two different Froude numbers, or more specifically a Froude number and the aspect ratio α via $Fr_v = Fr_h \alpha$. The choice of the scaling for α in the limit of strong stratification $Fr_h \ll 1$, is not trivial yet it is crucial to determine the final flow dynamics. If the vertical scale is assumed to remain constant in the limit $Fr_h \to 0$, namely $Fr_v \to 0$, the resulting dynamics becomes vertically decoupled and two-dimensional [Lilly (1983), Riley et al. (1981)]. On the contrary, if H is free

to vary such that $Fr_v = O(1)$ (as proposed by Billant and Chomaz (2001) and later corroborated by Lindborg (2006), Brethouwer et al. (2007), Augier et al. (2012), Maffioli et al. (2016)) the final dynamics is three-dimensional and governed by the hydrostatic primitive equations in the limit $Fr_h \to 0$ and $Re \to \infty$

$$\frac{\partial \boldsymbol{u}}{\partial t} + \boldsymbol{u} \cdot \nabla_h \boldsymbol{u} + \frac{\partial \boldsymbol{u}}{\partial z} = -\nabla_h p \tag{5.22}$$

$$\frac{\partial p}{\partial z} + b = 0 \tag{5.23}$$

$$\nabla_h \cdot \boldsymbol{u} + Fr_v^2 \frac{\partial w}{\partial z} = 0 \tag{5.24}$$

$$\frac{\partial b}{\partial t} + \boldsymbol{u} \cdot \nabla_h b + w \frac{\partial b}{\partial z} + w = 0 \,. \tag{5.25}$$

Equations (5.22)-(5.25) are often used to describe the large-scale flow dynamics in circulation models, but they can not capture the smaller-scale dynamics arising from shear instabilities, whose cumulative effects have be shown to highly impact the hydrostatic flow.

Following Chini *et al.* [Chini et al. (2022)], in the next section we will formally derive the reduced set of equations for the flow dynamics in the limit of strong stratification, making use of asymptotic analysis, leveraging on the small value of the horizontal Froude number, which will be from now on be indicated by Fr (and $Fr_v = Fr_h/\alpha$). The limit $Fr_h \to 0$ will be taken fixing the buoyancy Reynolds number $Re_b = Fr^2 Re$ and the scaling from Billant and Chomaz (2001) for the aspect ratio $\alpha \sim Fr_h$ will be assumed in this case.

5.2.2 Multi-scale analysis of the non-dimensionalised equations

Exploiting the scale separation set by the strong stratification, we can formally introduce two temporal and two spatial scales describing the slow-and-large dynamics $(T, \boldsymbol{x})$, and the fast-and-small one. Formally $(\tau, \boldsymbol{\chi})$, as

$$\begin{aligned} t \to (T, \tau): \qquad & T = t, \quad \tau = (Fr_h)^{-1}T, \quad \partial_t \to \partial_T + (Fr_h)^{-1}\partial_\tau \\ \boldsymbol{x}_h \to (\boldsymbol{x}, \boldsymbol{\chi}): \qquad & \boldsymbol{x} = \boldsymbol{x}_h, \quad \boldsymbol{\chi} = (Fr_h)^{-1}\boldsymbol{x}, \quad \nabla_h \to \nabla_{\boldsymbol{x}} + (Fr_h)^{-1}\nabla_{\boldsymbol{\chi}}. \end{aligned} \tag{5.26}$$

Then, defining the small parameter $\varepsilon = \sqrt{Fr}$, asymptotic expansions of velocity, buoyancy and

pressure fields $\boldsymbol{u}, w, b$ are postulated

$$\boldsymbol{u} \sim \boldsymbol{u}_0 + \varepsilon \boldsymbol{u}_1 + \varepsilon^2 \boldsymbol{u}_2 + O(\varepsilon^3) \tag{5.27}$$

$$b \sim b_0 + \varepsilon b_1 + \varepsilon^2 b_2 + O(\varepsilon^3) \tag{5.28}$$

$$p \sim p_0 + \varepsilon p_1 + \varepsilon^2 p_2 + O(\varepsilon^3) \tag{5.29}$$

$$w \sim \varepsilon^{-1} w_{-1} + w_0 + \varepsilon w + O(\varepsilon^2), \tag{5.30}$$

where the order ε^{-1} in the vertical velocity expansion accounts for the dominant effect of w on the fast scales rather then on the slow ones (where the flow will be shown to be hydrostatic in z) as pointed out in [Brethouwer et al. (2007) and Maffioli et al. (2016)].

Introducing the fast average operator for a generic function ϕ

$$\overline{\phi(z, \boldsymbol{\chi}, \boldsymbol{x}, \tau, T)} = \phi(z, \boldsymbol{x}, T) = \lim_{L_{\chi_f}, \tau_f \to \infty} \frac{1}{L_{\chi_f}} \frac{1}{\tau_f} \int_0^{\tau_f} \int_\Omega \phi(z, \boldsymbol{\chi}, \boldsymbol{x}, \tau, T) d\boldsymbol{\chi} d\tau \tag{5.31}$$

with Ω a periodic domain, and substituting (5.27)-(5.30) into (5.18)-(5.21) the relevant results from multi-scale analysis are summarised below for each equation.

Continuity equation (5.20)

At $O(\varepsilon^{-2})$

$$\nabla_\chi \cdot \boldsymbol{u}_0 = 0 \tag{5.32}$$

from which it follows that $\boldsymbol{u}_0$ does not depend on fast time, $\boldsymbol{u}_0 = \boldsymbol{u}_0(z, x, T, \tau)$.

At $O(\varepsilon^{-1})$

$$\nabla_\chi \cdot \boldsymbol{u}_1 = -\partial_z w_{-1} \tag{5.33}$$

and averaging over fast time and space

$$\partial_z \overline{w}_{-1} = 0 \tag{5.34}$$

therefore implying that $\overline{w}_{-1} = C w'_{-1}$, where the constant C must be set to zero to avoid its linear growth on a periodic domain, yielding $\overline{w} = 0$. As conjectured earlier in the expansion for w, the vertical velocity contribution is negligible on the large-slow spatiotemporal scale and it is expected to be dominant in small-fast one. Subtracting the averaged equation from

(5.33), an equation for the mass conservation of the fluctuations is obtained

$$\nabla_{\chi} \cdot \boldsymbol{u}_1' = -\partial_z w_{-1}'$$

(5.35)

At $O(1)$

$$\nabla_{\boldsymbol{x}} \cdot \boldsymbol{u}_0 + \nabla_{\chi} \cdot \boldsymbol{u}_2 + \partial_z w_0 = 0$$

(5.36)

and averaging over τ and χ yields the continuity equation for the slow fields

$$\nabla_{\boldsymbol{x}} \boldsymbol{u}_0 + \partial_z \overline{w}_0 = 0.$$

(5.37)

Horizontal momentum equation (5.18)

At $O(\varepsilon^{-2})$

$$\partial_\tau \boldsymbol{u}_0 = -\nabla_{\chi} p_0$$

(5.38)

Since $\boldsymbol{u}_0$ is not a function of χ, the boundedness of p_0 over fast space requires to impose that $\boldsymbol{u}_0$ does not depend on τ either. Therefore $\boldsymbol{u}_0 = \boldsymbol{u}_0(z, x, T) = \overline{\boldsymbol{u}}_0$, and $p_0 = p_0(z, x, \tau, T)$.

At $O(\varepsilon^{-1})$

$$\partial_\tau \boldsymbol{u}_1 + (\overline{\boldsymbol{u}}_0 \cdot \nabla_{\chi}) \boldsymbol{u}_1 + w_{-1} \partial_z \boldsymbol{u}_0 = -\nabla_{\chi} p_1,$$

(5.39)

and decomposing all the variables in mean (fast average) and fluctuations an evolution equation for the horizontal fluctuations velocity is found

$$\partial_\tau \boldsymbol{u}_1' + (\overline{\boldsymbol{u}}_0 \cdot \nabla_{\chi}) \boldsymbol{u}_1' + w_{-1}' \partial_z \overline{\boldsymbol{u}}_0 = -\nabla_{\chi} p_1'.$$

(5.40)

At $O(1)$

$$\partial_T \boldsymbol{u}_0 + \partial_\tau \boldsymbol{u}_2 + (\overline{\boldsymbol{u}}_0 \cdot \nabla_{\boldsymbol{x}}) \boldsymbol{u}_0 + (\overline{\boldsymbol{u}}_0 \cdot \nabla_{\chi}) \boldsymbol{u}_2 + (\boldsymbol{u}_1 \cdot \nabla_{\chi}) \boldsymbol{u}_1 + w_{-1} \partial_z \boldsymbol{u}_1 + w_0 \partial_z \boldsymbol{u}_0 = \\ -\nabla_{\boldsymbol{x}} p_0 - \nabla_{\chi} p_2 - \frac{1}{Re} \nabla_{\boldsymbol{x}}^2 \boldsymbol{u}_0$$

(5.41)

decomposing then in mean and fluctuations

$$\partial_\tau \boldsymbol{u}_2' + (\overline{\boldsymbol{u}}_0 \cdot \nabla_{\chi}) \boldsymbol{u}_2' + w_0' \partial_z \overline{\boldsymbol{u}}_0 + \nabla_{\chi} p_2' = \\ -\left(\partial_T \overline{\boldsymbol{u}}_0 + (\overline{\boldsymbol{u}}_0 \cdot \nabla_{\boldsymbol{x}}) \overline{\boldsymbol{u}}_0 + \overline{w}_0 \partial_z \overline{\boldsymbol{u}}_0 + (\boldsymbol{u}_1 \cdot \nabla_{\chi}) \boldsymbol{u}_1' + w_{-1}' \partial_z \boldsymbol{u}_1 + \nabla_{\boldsymbol{x}} p_0 - \frac{1}{Re_b} \partial_z^2 \overline{\boldsymbol{u}}_0 - f_0 \right).$$

(5.42)

and taking the average over fast temporal and spatial scales, the right hand side of the previous

equation gives the horizontal momentum equation for the mean horizontal velocity

$$\partial_T \overline{\boldsymbol{u}}_0 + (\overline{\boldsymbol{u}}_0 \cdot \nabla_{\boldsymbol{x}})\overline{\boldsymbol{u}}_0 + \overline{w}_0 \partial_z \overline{\boldsymbol{u}}_0 = -\partial_z(\overline{w'_{-1}\boldsymbol{u}'_1}) - \nabla_{\boldsymbol{x}} p_0 + \frac{1}{Re_b}\partial_z^2 \overline{\boldsymbol{u}}_0 + f_0, \tag{5.43}$$

where $\nabla_{\boldsymbol{\chi}} \cdot \boldsymbol{u}'_1 = -\partial_z w'_{-1}$ has been substituted.

Vertical momentum equation (5.19)

At $O(\varepsilon^{-2})$

$$-\partial_z p_0 - \frac{1}{Re}\nabla_{\boldsymbol{\chi}}^2 w_0 + b_0 = 0 \tag{5.44}$$

and fast-averaging

$$\partial_z \overline{p}_0 = -\overline{b}_0, \tag{5.45}$$

which confirms the reduction of the vertical momentum equation to the hydrostatic balance obtained from (5.19) in the limit $Fr \to 0$ and $\alpha \sim O(Fr)$.

At $O(\varepsilon^{-1})$

$$\partial_\tau w'_{-1} + (\overline{\boldsymbol{u}}_0 \cdot \nabla_{\boldsymbol{\chi}})w'_{-1} = -\partial_z p_1 + b_1 \tag{5.46}$$

which leads to the evolution equation for the vertical fluctuations, after subtracting from it its average

$$\partial_\tau w'_{-1} + (\overline{\boldsymbol{u}}_0 \cdot \nabla_{\boldsymbol{\chi}})w'_1 = -\partial_z p'_1 + b'_1. \tag{5.47}$$

Buoyancy equation (5.21)

At $O(\varepsilon^{-2})$

$$\partial_\tau b_0 + (\overline{\boldsymbol{u}}_0 \cdot \nabla_{\boldsymbol{\chi}})b_0 = 0 \tag{5.48}$$

from which we can infer that, since p_0 is independent of $\boldsymbol{\chi}$ so is b_0 (from hydrostatic balance), and consequently $b_0 = b_0(z, x, T) = \overline{b}_0$.

At $O(\varepsilon^{-1})$

$$\partial_\tau b'_1 + (\overline{\boldsymbol{u}}_0 \cdot \nabla_{\boldsymbol{\chi}})b'_1 + w'_{-1}\partial_z \overline{b}_0 + w'_{-1} = 0 \tag{5.49}$$

which is the evolution equation for the buoyancy fluctuations.

At $O(1)$

$$\partial_T \overline{b}_0 + (\overline{\boldsymbol{u}}_0 \cdot \nabla_{\boldsymbol{x}})\overline{b}_0 + \overline{w}_0 \partial_z \overline{b}_0 + \overline{w}_0 = -\partial_z \overline{(w'_{-1} b'_1)} + \frac{1}{PrRe_b}\partial_z^2 \overline{b}_0 \qquad (5.50)$$

an evolution equation for the mean buoyancy field is obtained, following the same procedure used to derive (5.43).

Simplifying the notation and dropping the subscripts indicating the asymptotic order, the final system of equation obtained from solving (5.18)-(5.21) order by order in ε eventually yields a coupled system for the mean variables and the fluctuations. respectively,

Mean fields equations

$$\frac{\partial \overline{\boldsymbol{u}}}{\partial T} + (\overline{\boldsymbol{u}} \cdot \nabla_{\boldsymbol{x}})\overline{\boldsymbol{u}} + \overline{w}\frac{\partial \overline{\boldsymbol{u}}}{\partial z} = -\nabla_{\boldsymbol{x}}\overline{p} - \frac{\partial (\overline{w'\boldsymbol{u}'})}{\partial z} + \frac{1}{Re_b}\frac{\partial^2 \overline{\boldsymbol{u}}}{\partial z^2} + \overline{f}, \qquad (5.51)$$

$$0 = -\frac{\partial \overline{p}}{\partial z} + \overline{b}, \qquad (5.52)$$

$$\frac{\partial \overline{b}}{\partial T} + (\overline{\boldsymbol{u}} \cdot \nabla_{\boldsymbol{x}})\overline{b} + \overline{w}\frac{\partial \overline{b}}{\partial z} = -\overline{w} - \frac{\partial (\overline{w'b'})}{\partial z} + \frac{1}{PrRe_b}\frac{\partial^2 \overline{b}}{\partial z^2}, \qquad (5.53)$$

$$\nabla_{\boldsymbol{x}} \cdot \overline{\boldsymbol{u}} + \frac{\partial \overline{w}}{\partial z} = 0. \qquad (5.54)$$

Fluctuation equations

$$\frac{\partial \boldsymbol{u}'}{\partial \tau} + (\overline{\boldsymbol{u}} \cdot \nabla_{\chi})\boldsymbol{u}' + w'\frac{\partial \overline{\boldsymbol{u}}}{\partial z} = -\nabla_{\chi}p', \qquad (5.55)$$

$$\frac{\partial w'}{\partial \tau} + (\overline{\boldsymbol{u}} \cdot \nabla_{\chi})w' = -\frac{\partial p'}{\partial z} + b', \qquad (5.56)$$

$$\frac{\partial b'}{\partial \tau} + (\overline{\boldsymbol{u}} \cdot \nabla_{\chi})b' + w'\frac{\partial \overline{b}}{\partial z} = -w', \qquad (5.57)$$

$$\nabla_{\boldsymbol{x}} \cdot \boldsymbol{u}' + \frac{\partial w'}{\partial z} = 0. \tag{5.58}$$

The mean fields only evolve on the slow-large scales and the fluctuations only on the fast-small ones, uniquely as a consequence of the scale separation between the two dynamics in the limit of strong stratification. Differently from the hydrostatic equations (5.22)-(5.25), the evolution equations for the slowly-varying mean fields obtained from multi-scale analysis are crucially coupled to the fast variables via a Reynolds stress-like feedback (highlighted in red). These terms, of fundamental importance for the understanding of mixing processes in stratified turbulence, are normally included in circulation models via *ad hoc* approximations due to the impossibility of resolving the small-scale dynamics [Gregg et al. (2018)]. The key feature of the reduced system derived by Chini *et al.* [Chini et al. (2022)] lies in the fact that this system is automatically closed, where the cumulative effect of the fast instabilities on the mean fields are determined by the leading order equations (5.55)-(5.58), without the need for any further assumption other than scale separation.

Noticing the linearity of (5.55)-(5.58), the final reduced system (5.51)-(5.58) is classifiable as a GQL system: the non-hydrostatic fluctuations evolve linearly and homogeneously about a slowly-varying (in space and time) mean field, are advected by it (blue terms) and the fluctuations non-linearities only affect the evolution of the latter.

As done for the two-dimensional model problem in § 4, to ease the investigation we will for the moment neglect the convective terms in the mean fields evolution, and focus on the strict QL reduction of the original equations. This is justified by re-interpreting the average over the fast spatial coordinate $\boldsymbol{\chi}$ as a stream-wise average in the horizontal direction $\boldsymbol{x}$.

We further modify the final set of equations by introducing higher-order diffusive terms in the fluctuations evolution (5.55)-(5.58) and consequently the Froude number, as done by Chini et al. (2022), with the purpose of regularizing the dynamics in the event of large vertical gradients.

The final set of equations for the mean fields and the fluctuation fields eventually reads

$$\frac{\partial \overline{\boldsymbol{u}}}{\partial T} = -\frac{\partial (\overline{w' \boldsymbol{u}'})}{\partial z} + \frac{1}{Re_b} \frac{\partial^2 \overline{\boldsymbol{u}}}{\partial z^2} + \overline{f}, \tag{5.59}$$

$$0 = -\frac{\partial^2 \overline{p}}{\partial z^2} + \overline{b}, \tag{5.60}$$

$$\frac{\partial \overline{b}}{\partial T} = -\frac{\partial (\overline{w' b'})}{\partial z} + \frac{1}{Pr Re_b} \frac{\partial^2 \overline{b}}{\partial z^2}, \tag{5.61}$$

$$\nabla_{\boldsymbol{x}} \cdot \overline{\boldsymbol{u}} = 0, \tag{5.62}$$

$$\frac{\partial \boldsymbol{u}'}{\partial \tau} + (\overline{\boldsymbol{u}} \cdot \nabla_\chi) \boldsymbol{u}' + w' \frac{\partial \overline{\boldsymbol{u}}}{\partial z} = -\nabla_\chi p' + \frac{Fr}{Re_b}\left(\nabla_\chi^2 \boldsymbol{u}' + \frac{\partial^2 \boldsymbol{u}'}{\partial z^2}\right), \tag{5.63}$$

$$\frac{\partial w'}{\partial \tau} + (\overline{\boldsymbol{u}} \cdot \nabla_\chi) w' = -\frac{\partial p'}{\partial z} + b' + \frac{Fr}{Re_b}\left(\nabla_\chi^2 w' + \frac{\partial^2 w'}{\partial z^2}\right), \tag{5.64}$$

$$\frac{\partial b'}{\partial \tau} + (\overline{\boldsymbol{u}} \cdot \nabla_\chi) b' + w' \frac{\partial \overline{b}}{\partial z} = -w' \frac{Fr}{PrRe_b}\left(\nabla_\chi^2 b' + \frac{\partial^2 b'}{\partial z^2}\right), \tag{5.65}$$

$$\nabla_x \cdot \boldsymbol{u}' + \frac{\partial w'}{\partial z} = 0. \tag{5.66}$$

5.3   Algorithm for the strict 2D QL formulation

In this section we first discuss the application of the integration methodology, based on the slaving of the fluctuation dynamics (proposed in Chini et al. (2022) and presented in § 3.3, 4.3), to the stratified flow problem and then illustrate its extension to efficiently deal with the spatial horizontal variability of the fast dynamics.

As a further simplification, after the transformation of the GQL-type system into a strict QL one, this will be done limiting the dimensionality of the problem to two dimensions, allowing for a variability of the fields only in z, $\boldsymbol{x} = x$ and $\chi = \chi$. Hence, due to the strict QL formulation, only the fluctuations will have a two dimensional evolution while the mean dynamics will solely vary in the vertical coordinate z.

Within this simplification the fluctuations velocity components can be expressed as the derivatives of the streamfunction ψ'

$$u' = \partial_z \psi', \quad w' = -\partial_\chi \psi' \quad \text{and} \quad \Delta \psi' = (\partial_\chi^2 + \partial_z^2)\psi' \tag{5.67}$$

and equations (5.59)-(5.66) reduce to

$$\frac{\partial \overline{u}}{\partial T} = \frac{\partial}{\partial z}\left(\overline{\frac{\partial \psi'}{\partial z}\frac{\partial \psi'}{\partial \chi}}\right) + \frac{1}{Re_b}\frac{\partial^2 \overline{u}}{\partial z^2} + \overline{f}, \tag{5.68}$$

$$\frac{\partial \overline{b}}{\partial T} = \frac{\partial}{\partial z}\left(\overline{b' \frac{\partial \psi'}{\partial \chi}}\right) + \frac{1}{PrRe_b}\frac{\partial^2 \overline{b}}{\partial z^2}, \tag{5.69}$$

$$\left(\frac{\partial}{\partial \tau} + \overline{u}\frac{\partial}{\partial \chi}\right)\Delta\psi' = \frac{\partial\psi'}{\partial\chi}\frac{\partial^2\overline{u}}{\partial z^2} - \frac{\partial b'}{\partial\chi} + \frac{Fr}{Re_b}\Delta^2\psi', \tag{5.70}$$

$$\left(\frac{\partial}{\partial \tau} + \overline{u}\frac{\partial}{\partial \chi}\right)b' = \left(1 + \frac{\partial\overline{b}}{\partial z}\right)\frac{\partial\psi'}{\partial\chi} + \frac{Fr}{Re_b}\Delta^2 b'. \tag{5.71}$$

Since the mean fields do not depend on the fast spatial coordinate, the linearity and homogeneity of the fluctuations equations allows for modal solutions of the type

$$\psi'(z,\chi,\tau,T) = A(T)\hat{\psi}(z,T)e^{\sigma(T)\tau}e^{ik(T)\chi} + c.c.$$
$$b'(z,\chi,\tau,T) = A(T)\hat{b}(z,T)e^{\sigma(T)\tau}e^{ik(T)\chi} + c.c. \tag{5.72}$$

where $\hat{\psi}(z,T)$ and $\hat{b}(z,T)$ are two vertical structure functions, $A(T)$ is an amplitude, $\text{Re}\{\sigma(T)\}$ the growth rate, and $k(T)$ the associated slowly-varying wavenumber.

From substituting (5.72) into (5.68)-(5.69), it immediately follows that the convergence of the Reynolds-stress and buoyancy flux terms is only guaranteed for non-positive values of the growth rate $\text{Re}\{\sigma\}$. The slow and fast dynamics are decoupled for $\text{Re}\{\sigma\} < 0$, as a result of the exponential decay of the fluctuations over fast time, and a finite feedback is established when $\text{Re}\{\sigma\} = 0$. Because of this observation it is useful to make a distinction between the fluctuations ψ' and b' in the fast evolution equations (5.70)-(5.71) and the fluctuations that feed back on the mean fields *only* in condition of marginal stability. From now on we will denote with φ' the neutrally stable mode corresponding to ψ', similarly with η' the one corresponding to b' and with g the associated wavenumber,

$$\varphi'(z,\chi,\tau,T) = A(T)\hat{\varphi}(z,T)e^{ig(T)\chi} + c.c.$$
$$\eta'(z,\chi,\tau,T) = A(T)\hat{\eta}(z,T)e^{ig(T)\chi} + c.c. \tag{5.73}$$

where $\varphi' \equiv \psi'$, $\eta' \equiv b'$ when $\text{Re}\{\sigma\} = 0$ and $\varphi' = \hat{\eta}' = 0$ when $\text{Re}\{\sigma\} < 0$. The importance of this distinction will became clear in the next section § 5.3.3, when discussing the extension of the QL methodology.

Assuming the realisation of a zero growth rate, the final system of equations reads

$$\frac{\partial\overline{u}}{\partial T} = |A|^2 ig\frac{\partial}{\partial z}\left(\hat{\varphi}\frac{\partial\hat{\varphi}^*}{\partial z} - \hat{\varphi}^*\frac{\partial\hat{\varphi}}{\partial z}\right) + \frac{1}{Re_b}\frac{\partial^2\overline{u}}{\partial z^2} = |A|^2 RS_u + \frac{1}{Re_b}\frac{\partial^2\overline{u}}{\partial z^2} + \overline{f}, \tag{5.74}$$

$$\frac{\partial\overline{b}}{\partial T} = |A|^2 ig\frac{\partial}{\partial z}(\hat{\varphi}\hat{\eta}^* - \hat{\varphi}^*\hat{\eta}) + \frac{1}{PrRe_b}\frac{\partial^2\overline{b}}{\partial z^2} = |A|^2 RS_b + \frac{1}{PrRe_b}\frac{\partial^2\overline{b}}{\partial z^2}, \tag{5.75}$$

$$\sigma\left(\frac{\partial^2}{\partial z^2} - k^2\right)\hat{\psi} = -ik\overline{u}\left(\frac{\partial^2}{\partial z^2} - k^2\right)\hat{\psi} + ik\frac{\partial^2\overline{u}}{\partial z^2}\hat{\psi} - ik\hat{b} + \frac{Fr}{Re_b}\left(\frac{\partial^2}{\partial z^2} - k^2\right)^2\hat{\psi}, \tag{5.76}$$

$$\sigma\hat{b} = -ik\overline{u}\hat{b} + ik\left(1 + \frac{\partial\overline{b}}{\partial z}\right)\hat{\psi} + \frac{Fr}{PrRe_b}\left(\frac{\partial^2}{\partial z^2} - k^2\right)\hat{b} \tag{5.77}$$

where following the notation adopted by Chini et al. (2022), we have compactly indicated the Reynolds stress-like term in (5.74) with RS_u and the buoyancy flux in 5.75 with RS_b. The resulting system is described, as in the other model problems, by an initial value problem for the evolution of the mean fields $(\overline{u}, \overline{b})$ (5.74)-(5.75), and by an eigenvalue problem for the dynamics of the fast fluctuations (5.76)-(5.76), which can be re-written more compactly as

$$\mathcal{L}\hat{\xi} = 0 \tag{5.78}$$

where $\hat{\xi}(z, T)$ is the eigenfunction $\hat{\xi} = (\hat{\psi}, \hat{b}) \in V$ with $V = \{(0, 1) \times \mathbb{R} \to \mathbb{C}^2; (z, T) \to (\hat{\psi}(z, T), \hat{b}(z, T))\}$, and $\mathcal{L}$ is the linear operator defined as

$$\mathcal{L} = \begin{pmatrix} (\sigma + ik\overline{u})(\partial_z^2 - k^2) - ik\partial_z^2\overline{u} - \frac{Fr}{Re_b}(\partial_z^2 - k^2)^2 & ik \\ -ik(1 + \partial_z\overline{b}) & \sigma + ik\overline{u} - \frac{Fr}{PrRe_b}(\partial_z^2 - k^2) \end{pmatrix} \tag{5.79}$$

Defining an inner product between two generic elements of the vector space V, $\hat{u} = (\hat{\psi}_u, \hat{b}_u)$ and $\hat{v} = (\hat{\psi}_v, \hat{b}_v)$ as the sesquilinear form $G: V \times V \to \mathbb{C}$ with

$$\langle u|v \rangle = \int_0^{Lz} uv^* dz = \int_0^{Lz} \hat{\psi}_u\hat{\psi}_v^* + \hat{b}_u\hat{b}_v^* dz \tag{5.80}$$

(namely conjugate-linear in the second argument and linear in the first one), and considering the periodic boundary conditions, we can notice that in this case the operator $\mathcal{L}$ is not self-adjoint with respect to (5.80). The adjoint is

$$\mathcal{L}^\dagger = \begin{pmatrix} (\sigma^* - ik\overline{u})(\partial_z^2 - k^2) - 2ik\partial_z\overline{u}\partial_z - \frac{Fr}{Re_b}(\partial_z^2 - k^2)^2 & ik(1 + \partial_z\overline{b}) \\ -ik & \sigma^* - ik\overline{u} - \frac{Fr}{PrRe_b}(\partial_z^2 - k^2) \end{pmatrix}. \tag{5.81}$$

Consequently the spectrum of $\mathcal{L}$ is complex and its eigenfunctions can not be chosen real, as done in the other model problems presented in this work. We then have to consider general complex-valued eigenfunctions and allow for oscillating eigenvalues with Im$\{\sigma\} \neq 0$. The

inner product (5.80) induces a norm with respect to which we connsider the eigenfunction $\hat{\xi}$ normalized.

5.3.1 Slaving of the fluctuation amplitude

The coupling between the fast and the slow dynamics (5.74)-(5.77) in condition of marginal stability is realised via the collective effect of the fluctuations fields on the respective mean dynamics, for which an amplitude has to be determined. Owing the impossibility of deriving an expression for this amplitude via imposing a solvability condition on the higher-order terms in the expansion (5.30), a different constraint has to be found. Inspired by the numerical and experimental evidences that stably strongly stratified turbulence has the tendency of relaxing towards marginally-stable states [Smyth and Moum (2013), Smyth et al. (2019), Holleman et al. (2016), Salehipour et al. (2018)], Chini et al. (2022) have recently proposed to to exploit this peculiar feature in order to compute a fluctuation amplitude such that the marginally-stable condition of the mean fields is maintained. This constraint mathematically translates into enforcing a zero temporal derivative of the growth rate $\text{Re}\{\sigma\}$ when $\text{Re}\{\sigma\} = 0$, and a zero k-derivative of the same to ensure that the marginally-stable condition is satisfied by the fastest growing mode.

An expression for both these derivatives can be obtained as a first order correction of the perturbed eigenvalue problem (5.78) with respect to slow time T and the wavenumber k.

Assuming the marginally-stable condition is achieved at time T_M by the mode with wavenumber k_M, and expanding the eigenvalue problem (5.78) around a point in the $T - k$ space $M = (T_M, k_M)$

$$L(T_M + \Delta T, k_M + \Delta k) \sim L_M + \frac{\partial L}{\partial T}\bigg|_M \Delta T + \frac{\partial L}{\partial k}\bigg|_M \Delta k \tag{5.82}$$

$$\hat{\xi}(T_M + \Delta T, k_M + \Delta k) \sim \hat{\xi}_M + \frac{\partial \hat{\xi}}{\partial T}\bigg|_M \Delta T + \frac{\partial \hat{\xi}}{\partial k}\bigg|_M \Delta k \tag{5.83}$$

implying

$$\hat{\psi}(T_M + \Delta T, k_M + \Delta k) \sim \hat{\psi}_M + \frac{\partial \hat{\psi}}{\partial T}\bigg|_M \Delta T + \frac{\partial \hat{\psi}}{\partial k}\bigg|_M \Delta k \tag{5.84}$$

$$\hat{b}(T_M + \Delta T, k_M + \Delta k) \sim \hat{b}_M + \frac{\partial \hat{b}}{\partial T}\bigg|_M \Delta T + \frac{\partial \hat{b}}{\partial k}\bigg|_M \Delta k \tag{5.85}$$

yields the following boundary value problems at order $O(\Delta T)$ and $O(\Delta k)$ respectively

$$\mathscr{L}_M \frac{\partial \hat{\xi}}{\partial T}\bigg|_M = -\frac{\partial \mathscr{L}}{\partial T}\bigg|_M \hat{\xi}_M \tag{5.86}$$

$$\mathscr{L}_M \frac{\partial \hat{\xi}}{\partial k}\bigg|_M = -\frac{\partial \mathscr{L}}{\partial k}\bigg|_M \hat{\xi}_M .\tag{5.87}$$

Since $\mathscr{L}$ is a singular operator by construction, $\mathscr{L} = L - \sigma$, the solvability of (5.86)-(5.87) must be enforced, as stated by the Fredholm Alternative theorem (a detailed discussion is provided in section § 3.3 and 4.3.1). Such a condition requires to ensure a zero projection of the right hand side of (5.86)-(5.87) onto the null-space of the adjoint-operator $\mathscr{L}^\dagger$

$$\left\langle \mathscr{L}_M \frac{\partial \hat{\xi}}{\partial T}\bigg|_M \bigg| \hat{\xi}^\dagger \right\rangle = \left\langle \frac{\partial \hat{\xi}}{\partial T}\bigg|_M \bigg| \mathscr{L}_M^\dagger \hat{\xi}^\dagger \right\rangle = 0 \tag{5.88}$$

and

$$\left\langle \mathscr{L}_M \frac{\partial \hat{\xi}}{\partial k}\bigg|_M \bigg| \hat{\xi}^\dagger \right\rangle = \left\langle \frac{\partial \hat{\xi}}{\partial k}\bigg|_M \bigg| \mathscr{L}_M^\dagger \hat{\xi}^\dagger \right\rangle = 0 \tag{5.89}$$

which leads to the following expressions for the first derivatives of σ

$$
\begin{aligned}
\frac{\partial \sigma}{\partial T}&\left[\int_0^{Lz} \hat{\psi}^{\dagger*}\left(\frac{\partial^2}{\partial z^2} - k^2 \right)\hat{\psi} + \hat{b}^{\dagger*}\hat{b}\,dz \right] = \\
&-ik|A|^2 \left\{ \int_0^{Lz} RS_u \left[\hat{\psi}^{\dagger*}\left(\frac{\partial^2}{\partial z^2} - k^2 \right)\hat{\psi} - \hat{\psi}^{\dagger*}\frac{\partial^2\hat{\psi}}{\partial z^2} - \hat{\psi}\frac{\partial^2\hat{\psi}^{\dagger*}}{\partial z^2} - 2\left(\frac{\partial\hat{\psi}}{\partial z} \right)\left(\frac{\partial\hat{\psi}^{\dagger*}}{\partial z} \right) + \hat{b}^{\dagger*}\hat{b} \right]dz+ \\
&+\int_0^{Lz} RS_b \left[\hat{b}^{\dagger*}\frac{\partial\hat{\psi}}{\partial z} + \hat{\psi}\frac{\partial\hat{b}^{\dagger*}}{\partial z} \right]dz \right\}+ \\
&-ik\left\{ \int_0^{Lz} \left(\frac{1}{Re_b}\frac{\partial^2\overline{u}}{\partial z^2} + \overline{f} \right)\left[\hat{\psi}^{\dagger*}\left(\frac{\partial^2}{\partial z^2} - k^2 \right)\hat{\psi} - \hat{\psi}^{\dagger*}\frac{\partial^2\hat{\psi}}{\partial z^2} - \hat{\psi}\frac{\partial^2\hat{\psi}^{\dagger*}}{\partial z^2} - 2\left(\frac{\partial\hat{\psi}}{\partial z} \right)\left(\frac{\partial\hat{\psi}^{\dagger*}}{\partial z} \right) + \hat{b}^{\dagger*}\hat{b} \right]dz+ \\
&+\int_0^{Lz} \left(\frac{1}{PrRe_b}\frac{\partial^2\overline{b}}{\partial z^2} \right)\left[\hat{b}^{\dagger*}\frac{\partial\hat{\psi}}{\partial z} + \hat{\psi}\frac{\partial\hat{b}^{\dagger*}}{\partial z} \right]dz \right\}
\end{aligned}
\tag{5.90}
$$

$$
\begin{aligned}
\frac{\partial \sigma}{\partial k}&\left[\int_0^{Lz} \hat{\psi}^{\dagger*}\left(\frac{\partial^2}{\partial z^2} - k^2 \right)\hat{\psi} + \hat{b}^{\dagger*}\hat{b}\,dz \right] = \\
&-i\int_0^{Lz} \overline{u}\left[\hat{\psi}^{\dagger*}\left(\frac{\partial^2}{\partial z^2} - k^2 \right)\hat{\psi} - \hat{\psi}^{\dagger*}\frac{\partial^2\hat{\psi}}{\partial z^2} - \hat{\psi}\frac{\partial^2\hat{\psi}^{\dagger*}}{\partial z^2} - 2\left(\frac{\partial\hat{\psi}}{\partial z} \right)\left(\frac{\partial\hat{\psi}^{\dagger*}}{\partial z} \right) + \hat{b}^{\dagger*}\hat{b} - 2k^2\hat{\psi}^{\dagger*}\hat{\psi} \right]dz+ \\
&-i\int_0^{Lz} \overline{b}\left(\hat{b}^{\dagger*}\frac{\partial\hat{\psi}}{\partial z} + \hat{\psi}\frac{\partial\hat{b}^{\dagger*}}{\partial z} \right)dz - i\int_0^{Lz} (\hat{\psi}^{\dagger*}\hat{b} - \hat{b}^{\dagger*}\hat{\psi}\,dz + 2ik\,\mathrm{Im}\{\sigma\}\int_0^{Lz} \hat{\psi}^{\dagger*}\hat{\psi}\,dz+ \\
&-2k\frac{Fr}{Re_b}\int_0^{Lz} \left[2\hat{\psi}^{\dagger*}\left(\frac{\partial^2}{\partial z^2} - k^2 \right)\hat{\psi} + \frac{1}{Pr}\hat{b}^{\dagger*}\hat{b} \right]dz .
\end{aligned}
\tag{5.91}
$$

Re-writing expression (5.90) in a more compact form,

$$\frac{\partial \sigma}{\partial T} = \frac{\alpha - |A|^2 \beta}{\gamma} \tag{5.92}$$

and enforcing $\partial_T(\text{Re}\{\sigma\}) = 0$ eventually gives an expression for the amplitude similar to the one obtained for the model problems discussed in § 3 and 4:

$$|A| = \sqrt{\frac{\text{Re}\{\alpha/\gamma\}}{\text{Re}\{\beta/\gamma\}}} \tag{5.93}$$

with

$$\alpha = -ik\left\{ \int_0^{Lz} RS_u \left[\hat{\psi}^{\dagger *}\left(\frac{\partial^2}{\partial z^2} - k^2 \right)\hat{\psi} - \hat{\psi}^{\dagger *}\frac{\partial^2 \hat{\psi}}{\partial z^2} - \hat{\psi}\frac{\partial^2 \hat{\psi}^{\dagger *}}{\partial z^2} - 2\left(\frac{\partial \hat{\psi}}{\partial z} \right)\left(\frac{\partial \hat{\psi}^{\dagger *}}{\partial z} \right) + \hat{b}^{\dagger *}\hat{b} \right] dz + \right.$$
$$\left. + \int_0^{Lz} RS_b \left[\hat{b}^{\dagger *}\frac{\partial \hat{\psi}}{\partial z} + \hat{\psi}\frac{\partial \hat{b}^{\dagger *}}{\partial z} \right] dz \right\} \tag{5.94}$$

$$\beta = ik\left\{ \int_0^{Lz} \left(\frac{1}{Re_b}\frac{\partial^2 \overline{u}}{\partial z^2} + \overline{f} \right)\left[\hat{\psi}^{\dagger *}\left(\frac{\partial^2}{\partial z^2} - k^2 \right)\hat{\psi} - \hat{\psi}^{\dagger *}\frac{\partial^2 \hat{\psi}}{\partial z^2} - \hat{\psi}\frac{\partial^2 \hat{\psi}^{\dagger *}}{\partial z^2} - 2\left(\frac{\partial \hat{\psi}}{\partial z} \right)\left(\frac{\partial \hat{\psi}^{\dagger *}}{\partial z} \right) + \hat{b}^{\dagger *}\hat{b} \right] dz + \right.$$
$$\left. + \int_0^{Lz} \left(\frac{1}{PrRe_b}\frac{\partial^2 \overline{b}}{\partial z^2} \right)\left[\hat{b}^{\dagger *}\frac{\partial \hat{\psi}}{\partial z} + \hat{\psi}\frac{\partial \hat{b}^{\dagger *}}{\partial z} \right] dz \right\} \tag{5.95}$$

$$\gamma = \int_0^{Lz} \left[\hat{\psi}^{\dagger *}\left(\frac{\partial^2}{\partial z^2} - k^2 \right)\hat{\psi} + \hat{b}^{\dagger *}\hat{b} \right] dz \tag{5.96}$$

Similarly can be done with expression (5.91), where enforcing $\partial_k(\text{Re}\{\sigma\}) = 0$ leads to an integral relation between the eigenfunctions, not reported here as not useful for the purpose of this discussion. The full calculation for this section and the next one is detailed in appendix C.

5.3.2 On the termination of the marginally-stable manifold

On the occurrence of bursting events

As visible from (5.92), the maintenance of the marginally-stable condition and consequently the determination of the fluctuation amplitude is conditional upon the signs of the real parts of the ratios between the integrals α/γ and β/γ. Similarly to the 1D model problem presented in § 3, we expect the stratified problem to also exhibit bursting behaviour where the fluctuations grow unbounded causing the response of the slow dynamics on the fast temporal scale. In other words the integral quantity $\text{Re}\{\beta/\gamma\}$ is not sign-definite and its change in sign inevitably

produces a destabilizing effect on the mean fields. This scenario, observed by Chini *et al.*[Chini et al. (2022)] for values of Re_b greater than 10, causes the temporary loss of the scale separation between two dynamics requiring the integration of the two fields on the same temporal scales. In this case not only the QL dynamics loses any asymptotic justification, but it would also not be able to saturate the fluctuation instability due to the lack of any form of fluctuation-fluctuation non-linearity. In chapter § 3 we have presented, in the context of a 1D model problem, different co-evolution techniques to handle the termination of the marginally-stable manifold (not only during a bursting event) and shown their efficacy in re-establishing a new marginally-stable situation. Two of these techniques, the finite-ε DNS and the ε-DNS, are characterised by the reintroduction of the fluctuation-fluctuation non-linearity, while the third one, the gradient descent technique, updates the mean variable in the direction of the linear eigenfunction. However, although in principle all are applicable to the stratified flow problem, the implementation of the DNS-based co-evolution techniques is not possible in this specific case due to the strict QL formulation of the reduced problem. In analogy, this time, with the 2D model problem discussed in § 4, the stream-wise averaging procedure over the horizontal spatial coordinates, aimed at suppressing of the convective term in (5.51)-(5.53), removes any $\boldsymbol{x}$-dependency of the mean dynamics, which in contrast is present in the full dynamics. Therefore the gradient descent technique is the only possible choice, in this specific case, to treat bursting events allowing for a variation of the wavenumber of the neutral mode.

On the finite-scale-separation algorithm

Analogously, the stream-wise invariance of the mean dynamics also prevents from fully implementing the finite-scale-separation algorithm, developed in chapter 3, until the convective terms in the mean fields evolution are re-introduced. While it is still possible to define a marginally-stable region, allowing for a certain (marginal) decay or growth of the fast instabilities about $\text{Re}\{\sigma\} = 0$, the fully-non-linear dynamics in the connecting region between the two validity range of the QL approximation ($\text{Re}\{\sigma_1\} < \text{Re}\{\sigma\} < \text{Re}\{\sigma_2\}$, refer to § 3.4.2) can not be implemented. Since the gradient descent technique updates the mean fields only using the linear eigenfunctions, in stable conditions this technique would lead to the zero solution in both dynamics. Therefore the evolution of the mean fields below marginal stability has to be replaced by the QL evolution with $RS_u = RS_b = 0$. Although in Chini et al. (2022) this does not prevent the dynamics from reaching the same steady state observed in the DNS, it might in different conditions and regimes due to the non-validity of the QL reduction in that range. This caveat is furthermore motivated by the consideration that in this case the QL evolution of the mean fields does not coincides with the fully non-linear one in absence of the fluctuations feedback. In other words, assuming that the QL approximation shares the same relevant state-space structures with the full dynamics, this might no longer be true in the region $\text{Re}\{\sigma_1\} < \text{Re}\{\sigma\} < \text{Re}\{\sigma_2\}$, and simulating a dynamics different from the original one might rule out certain states from the statistically averaged long term dynamics. However this considerations, at this stage only conjectural, are intended to be a warning for future investigations.

5.3.3 Prediction of the wavenumber of the marginally-stable mode

The variability of the fluctuation dynamics over the fast horizontal coordinate χ unfolds in the QL formulation as a k-dependency of the eigenvalue problem (5.78) leading to a time-varying dispersion relation $\sigma(T, k)$. Enforcing the tangency condition to the marginally-stable manifold in presence of zero growth rates then requires at each time T_M to seek for the maximum of $\sigma(T_M, k)$ to identify the wavenumber $k_M = g$ of the fastest growing mode that will then feedback on the mean fields (5.74)-(5.75). As anticipated by our notation, the slow dynamics is only affected by one mode, the one that first undergoes an instability, and therefore it does not depend on k.

Moreover the peak of the dispersion relation $\sigma(T, k)$ in general varies with time, hence $g = g(T)$, implying that the search for the maximum has to be repeated after any update of the mean dynamics, as done in Chini et al. (2022). From the algorithmic point of view this requires to solve the eigenvalue problem multiple times for different k at each time iteration, representing the computational bottleneck of the presented methodology. Furthermore the range of wavenumbers over which the search has to be performed would escalate when considering the possibility of multiple marginally stable modes (not done in this work) or when considering the continuous variability of the wavenumber in such a problem (as a consequence of an infinite domain in the x-direction).

In the light of the previous considerations, in the remaining part of this section we present the crucial extension of the QL methodology for the prediction of the wavenumber in condition of marginal stability.

Re-calling the geometrical description illustrated in figure 4.2 (§ 4.3.1), the real part of the time-varying dispersion relation $\mathrm{Re}\{\sigma(T, k)\}$ can be represented by a three-dimensional surface in $\mathbb{R}^3$ defined with a graph notation as

$$\Gamma(T, k) = (T, k, \mathrm{Re}\{\sigma(T, k)\}) \,. \tag{5.97}$$

Once the marginal stability condition is realized, enforcing its maintenance in time automatically imposes, at each time T_M, a zero normal curvature of this surface in one direction. Such a direction can be identified as the tangent vector to the curve γ at T_M resulting from the intersection of the surface Γ with the plane $(T, k, \mathrm{Re}\{\sigma\} = 0)$. It follows that all points on γ, are saddle points satisfying

$$\mathrm{Re}\{\sigma(T, k)\} = 0, \quad \partial_T(\mathrm{Re}\{\sigma(T, k)\}) = 0 \quad \text{and} \quad \partial_k(\mathrm{Re}\{\sigma(T, k)\}) = 0 \,. \tag{5.98}$$

Appropriately defining γ as a parametrised curve on the surface Γ

$$\begin{aligned}
\gamma(T) = \Gamma(T, k) \circ \mu(T) &= (T, g(T), \mathrm{Re}\{\sigma(T, g(T))\}) \\
&= (T, g(T), 0)
\end{aligned} \tag{5.99}$$

with $\mu : \mathbb{R} \to \mathbb{R}^2$ being the plane parametrised curve $\mu(T) = (T, g(T))$, directly shows that the prediction of the wavenumber k of the fastest growing mode translates into an evolution equation for the function $g(T)$.

For this purpose, following the derivation discussed in § 4.3.1, we expand the growth rate $\text{Re}\{\sigma(T, k)\}$ around a point (T_M, k_M), at which the marginally-stable condition is satisfied, along the direction $\bar{\delta}$ tangent to the curve γ,

$$\sigma_r((T, k)_M + \Delta\bar{\delta}) \sim \sigma_r(T_M, k_M) + \left(\left.\frac{\partial\sigma_r}{\partial T}\right|_M + \left.\frac{\partial\sigma_r}{\partial k}\right|_M \frac{dg(T)}{dT}\right)\Delta$$
$$+ \frac{1}{2}\left(\left.\frac{\partial^2\sigma_r}{\partial T^2}\right|_M + \left.\frac{\partial^2\sigma_r}{\partial k^2}\right|_M \left(\frac{dg(T)}{dT}\right)^2 + 2\left.\frac{\partial^2\sigma_r}{\partial T\partial k}\right|_M \frac{dg(T)}{dT}\right)\Delta^2 + O(\Delta^3) \tag{5.100}$$

with $\bar{\delta} = \gamma' = (1, d_T g(T))$ and $\sigma_r = \text{Re}\{\sigma\}$. Enforcing then the propagation of the saddle-point properties (5.98) along γ, we obtain the evolution equation for $g(T)$ (4.22), re-written here for convenience

$$\left(\frac{dg(T)}{dT}\right)^2 + 2\frac{\partial_k(\partial_T\sigma_r)|_M}{\partial_k^2\sigma_r|_M}\left(\frac{dg(T)}{dT}\right) = -\frac{\partial_T^2\sigma_r|_M}{\partial_k^2\sigma_r|_M} . \tag{5.101}$$

Within this formalism the importance of the distinction between the eigenfunctions $\hat{\psi}, \hat{b}$ and their marginally-stable counterparts $\hat{\varphi}, \hat{\eta}$ is easily understood: while their evaluation on the curve γ is identical, their differentiation is not

$$\frac{d\hat{\varphi}}{dT} = \left.\frac{\partial\hat{\psi}}{\partial T}\right|_M + \left.\frac{\partial\hat{\psi}}{\partial k}\right|_M \frac{dg(T)}{dT} \tag{5.102}$$

and

$$\frac{d\hat{\eta}}{dT} = \left.\frac{\partial\hat{b}}{\partial T}\right|_M + \left.\frac{\partial\hat{b}}{\partial k}\right|_M \frac{dg(T)}{dT} \tag{5.103}$$

where $d_T\hat{\varphi}$ and $d_T\hat{\eta}$ are directional derivatives.

Due to the constraints on the curvature properties of the landscape $\sigma(T, k)$ resulting from the propagation of the saddle point conditions, the evolution equation for the wavenumber of the fastest growing mode requires the computation of the second derivatives of the growth rate. Analogously to what done in the previous section these derivatives can be computed by means of perturbation analysis extending the expansions (5.82)-(5.83) up to the second order

in T and k

$$
\begin{aligned}
L(T_M + \Delta T, k_M + \Delta k) \sim L_M &+ \frac{\partial L}{\partial T}\bigg|_M \Delta T + \frac{\partial L}{\partial k}\bigg|_M \Delta k + \\
&+ \frac{1}{2}\frac{\partial^2 \mathscr{L}}{\partial T^2}\bigg|_M \Delta T^2 + \frac{1}{2}\frac{\partial^2 \mathscr{L}}{\partial k^2}\bigg|_M \Delta k^2 + \frac{\partial^2 \mathscr{L}}{\partial k \partial T}\bigg|_M \Delta T \Delta k
\end{aligned}
\tag{5.104}
$$

$$
\begin{aligned}
\hat{\xi}(T_M + \Delta T, k_M + \Delta k) \sim \hat{\xi}_M &+ \frac{\partial \hat{\xi}}{\partial T}\bigg|_M \Delta T + \frac{\partial \hat{\xi}}{\partial k}\bigg|_M \Delta k \\
&+ \frac{1}{2}\frac{\partial^2 \hat{\xi}}{\partial T^2}\bigg|_M \Delta T^2 + \frac{1}{2}\frac{\partial^2 \hat{\xi}}{\partial k^2}\bigg|_M \Delta k^2 + \frac{\partial^2 \hat{\xi}}{\partial k \partial T}\bigg|_M \Delta T \Delta k
\end{aligned}
\tag{5.105}
$$

$$
\begin{aligned}
\hat{\psi}(T_M + \Delta T, k_M + \Delta k) \sim \hat{\psi}_M &+ \frac{\partial \hat{\psi}}{\partial T}\bigg|_M \Delta T + \frac{\partial \hat{\psi}}{\partial k}\bigg|_M \Delta k \\
&+ \frac{1}{2}\frac{\partial^2 \hat{\psi}}{\partial T^2}\bigg|_M \Delta T^2 + \frac{1}{2}\frac{\partial^2 \hat{\psi}}{\partial k^2}\bigg|_M \Delta k^2 + \frac{\partial^2 \hat{\psi}}{\partial k \partial T}\bigg|_M \Delta T \Delta k
\end{aligned}
\tag{5.106}
$$

$$
\begin{aligned}
\hat{b}(T_M + \Delta T, k_M + \Delta k) \sim \hat{b}_M &+ \frac{\partial \hat{b}}{\partial T}\bigg|_M \Delta T + \frac{\partial \hat{b}}{\partial k}\bigg|_M \Delta k \\
&+ \frac{1}{2}\frac{\partial^2 \hat{b}}{\partial T^2}\bigg|_M \Delta T^2 + \frac{1}{2}\frac{\partial^2 \hat{b}}{\partial k^2}\bigg|_M \Delta k^2 + \frac{\partial^2 \hat{b}}{\partial k \partial T}\bigg|_M \Delta T \Delta k
\end{aligned}
\tag{5.107}
$$

and imposing the solvability condition on the boundary value problems resulting at the second order

$O(\Delta k^2)$

$$
\mathscr{L}_M \frac{\partial^2 \hat{\xi}}{\partial k^2}\bigg|_M = -\frac{\partial^2 \mathscr{L}}{\partial k^2}\bigg|_M \hat{\xi}_M - 2\left(\frac{\partial \mathscr{L}}{\partial k}\right)\bigg|_M \frac{\partial \hat{\xi}}{\partial k}\bigg|_M
\tag{5.108}
$$

$$
0 = \left\langle \mathscr{L}_M \frac{\partial^2 \hat{\xi}}{\partial k^2}\bigg|_M \bigg| \hat{\xi}_M^\dagger \right\rangle = -\int_0^{Lz} \hat{\xi}_M^{\dagger*} \frac{\partial^2 \mathscr{L}}{\partial k^2}\bigg|_M \hat{\xi}_M dz - 2\int_0^{Lz} \hat{\xi}_M^{\dagger*}\left(\frac{\partial \mathscr{L}}{\partial k}\right)\bigg|_M \frac{\partial \hat{\xi}}{\partial k}\bigg|_M dz
\tag{5.109}
$$

$O(\Delta T^2)$

$$
\mathscr{L}_M \frac{\partial^2 \hat{\xi}}{\partial T^2}\bigg|_M = -\frac{\partial^2 \mathscr{L}}{\partial T^2}\bigg|_M \hat{\xi}_M - 2\left(\frac{\partial \mathscr{L}}{\partial T}\right)\bigg|_M \frac{\partial \hat{\xi}}{\partial T}\bigg|_M
\tag{5.110}
$$

$$
0 = \left\langle \mathscr{L}_M \frac{\partial^2 \hat{\xi}}{\partial T^2}\bigg|_M \bigg| \hat{\xi}_M^\dagger \right\rangle = -\int_0^{Lz} \hat{\xi}_M^{\dagger*} \frac{\partial^2 \mathscr{L}}{\partial T^2}\bigg|_M \hat{\xi}_M dz - 2\int_0^{Lz} \hat{\xi}_M^{\dagger*}\left(\frac{\partial \mathscr{L}}{\partial T}\right)\bigg|_M \frac{\partial \hat{\xi}}{\partial T}\bigg|_M dz
\tag{5.111}
$$

$O(\Delta T \Delta k)$

$$\mathscr{L}_M \frac{\partial^2 \hat{\xi}}{\partial T \partial k}\bigg|_M = -\frac{\partial^2 \mathscr{L}}{\partial T \partial k}\bigg|_M \hat{\xi}_M - \left(\frac{\partial \mathscr{L}}{\partial k}\right)\bigg|_M \frac{\partial \hat{\xi}}{\partial T}\bigg|_M - \left(\frac{\partial \mathscr{L}}{\partial T}\right)\bigg|_M \frac{\partial \hat{\xi}}{\partial k}\bigg|_M \tag{5.112}$$

$$0 = \left\langle \mathscr{L}_M \frac{\partial^2 \hat{\xi}}{\partial T \partial k}\bigg|_M \bigg| \hat{\xi}_M^\dagger \right\rangle = -\int_0^{Lz} \hat{\xi}_M^{\dagger *} \frac{\partial^2 \mathscr{L}}{\partial T \partial k}\bigg|_M \hat{\xi}_M \, dz - \int_0^{Lz} \hat{\xi}_M^{\dagger *} \left(\frac{\partial \mathscr{L}}{\partial T}\right)\bigg|_M \frac{\partial \hat{\xi}}{\partial k}\bigg|_M \, dz +$$
$$-\int_0^{Lz} \hat{\xi}_M^{\dagger *} \left(\frac{\partial \mathscr{L}}{\partial k}\right)\bigg|_M \frac{\partial \hat{\xi}}{\partial T}\bigg|_M \, dz \tag{5.113}$$

As clear from (5.109), (5.111) and (5.113), the enforcement of the Fredholm alternative on the second-order BVPs requires the knowledge of the first-order corrections of the eigenfunctions $\partial_k \hat{\xi}|_M$ and $\partial_T \hat{\xi}|_M$ which can be obtained by explicitly solving (5.86) and (5.87).

Because of the singular nature of the operator $\mathscr{L}$ the solution of (5.86)-(5.87) can be pursued via applying a QR decomposition on $\mathscr{L}$ to obtain its pseudo-inverse $\widetilde{\mathscr{L}^{-1}}$ and practically solving

$$\frac{\partial \hat{\xi}}{\partial T}^p\bigg|_M = -\widetilde{\mathscr{L}_M^{-1}} \left(\frac{\partial \mathscr{L}}{\partial T}\bigg|_M \hat{\xi}_M - \left\langle \frac{\partial \mathscr{L}}{\partial T}\bigg|_M \hat{\xi}_M \bigg| \hat{\xi}_M^\dagger \right\rangle \hat{\xi}_M^\dagger \right) \tag{5.114}$$

$$\frac{\partial \hat{\xi}}{\partial k}^p\bigg|_M = -\widetilde{\mathscr{L}_M^{-1}} \left(\frac{\partial \mathscr{L}}{\partial k}\bigg|_M \hat{\xi}_M - \left\langle \frac{\partial \mathscr{L}}{\partial k}\bigg|_M \hat{\xi}_M \bigg| \hat{\xi}_M^\dagger \right\rangle \hat{\xi}_M^\dagger \right) \tag{5.115}$$

where $\partial_T \hat{\xi}^p$ and $\partial_k \hat{\xi}^p$ are the solutions that minimise the least square errors

$$\left\| \mathscr{L}_M \frac{\partial \hat{\xi}}{\partial T}\bigg|_M - \left(\frac{\partial \mathscr{L}}{\partial T}\bigg|_M \hat{\xi}_M\right) \right\|^2 \quad \text{and} \quad \left\| \mathscr{L}_M \frac{\partial \hat{\xi}}{\partial k}\bigg|_M - \left(\frac{\partial \mathscr{L}}{\partial k}\bigg|_M \hat{\xi}_M\right) \right\|^2 . \tag{5.116}$$

In the remaining of this section we summarise the final expressions for the second-order corrections of the eigenvalue σ, obtained with the procedure explained above, and we refer

the interested reader to appendix C, where the full (and lengthy) calculation is reported.

$$
\frac{\partial^2 \sigma}{\partial k^2} = -\frac{2i}{\gamma} \int_0^{Lz} \overline{u} \left(P_k - 2k^2 \hat{\psi}^{\dagger *} \frac{\partial \hat{\psi}}{\partial k} - 3k \hat{\psi}^{\dagger *} \hat{\psi} \right) dz - \frac{2i}{\gamma} \int_0^{Lz} \overline{b} Q_k dz +
$$
$$
-\frac{2}{\gamma} \frac{Fr}{Re_b} \int_0^{Lz} (R + 2kR_k - 4k^2 \hat{\psi}^{\dagger *} \hat{\psi}) dz - 2i \int_0^{Lz} \Pi_k dz +
$$
$$
+\frac{2i}{\gamma} \operatorname{Im}\left\{ \frac{\partial \sigma}{\partial k} \right\} \int_0^{Lz} \left[2k \hat{\psi}^{\dagger *} \hat{\psi} - \hat{\psi}^{\dagger *} \left(\frac{\partial^2}{\partial z^2} - k^2 \right) \frac{\partial \hat{\psi}}{\partial k} - \hat{b}^{\dagger *} \frac{\partial \hat{b}}{\partial k} \right] dz +
$$
$$
2i \operatorname{Im}\{\sigma\} \int_0^{Lz} \left(\hat{\psi}^{\dagger *} \hat{\psi} + 2k \hat{\psi}^{\dagger *} \frac{\partial \hat{\psi}}{\partial k} \right) dz \tag{5.117}
$$

$$
\frac{\partial^2 \sigma}{\partial T^2} = \frac{\beta}{\gamma \operatorname{Re}\{\beta/\gamma\}} \left[\operatorname{Re}\left\{ -\frac{1}{\gamma} \frac{\partial \alpha}{\partial T} + \frac{1}{\gamma} \frac{\partial \gamma}{\partial T} \alpha \right\} - |A|^2 \operatorname{Re}\left\{ \frac{k^2}{\gamma} \beta_{T1} - \frac{ik}{\gamma} \beta_{T3} \right\} +
$$
$$
+ |A|^2 \operatorname{Re}\left\{ \frac{\beta}{\gamma^2} \frac{\partial \gamma}{\partial T} \right\} - k^2 |A|^2 \frac{dg}{dT} \operatorname{Re}\left\{ \frac{\beta_{T2}}{\gamma^2} \right\} \right] +
$$
$$
+ |A|^2 \frac{k^2}{\gamma} \left(\beta_{T1} + \frac{dg}{dT} \beta_{T2} \right) +
$$
$$
- \frac{ik}{\gamma} |A|^2 \int_0^{Lz} RS_u \left(2P_T + \frac{1}{Re_b} \frac{\partial^2 P}{\partial z^2} \right) dz - \frac{ik}{\gamma} \int_0^{Lz} \left(\frac{1}{Re_b} \frac{\partial^2 \overline{u}}{\partial z^2} + \overline{f} \right) \left(2P_T + \frac{1}{Re_b} \frac{\partial^2 P}{\partial z^2} \right) dz +
$$
$$
- \frac{ik}{\gamma} \int_0^{Lz} \frac{\partial \overline{f}}{\partial T} P dz +
$$
$$
- \frac{ik}{\gamma} |A|^2 \int_0^{Lz} RS_b \left(2Q_T + \frac{1}{PrRe_b} \frac{\partial^2 Q}{\partial z^2} \right) dz - \frac{ik}{\gamma} \int_0^{Lz} \frac{1}{PrRe_b} \frac{\partial^2 \overline{b}}{\partial z^2} + \left(2Q_T + \frac{1}{PrRe_b} \frac{\partial^2 Q}{\partial z^2} \right) dz +
$$
$$
- \frac{2i}{\gamma} \operatorname{Im}\left\{ \frac{\partial \sigma}{\partial T} \right\} \int_0^{Lz} \left[\hat{\psi}^{\dagger *} \left(\frac{\partial^2}{\partial z^2} - k^2 \right) \frac{\partial \hat{\psi}}{\partial T} + \hat{b}^{\dagger *} \frac{\partial \hat{b}}{\partial T} \right] dz \tag{5.118}
$$

$$
\frac{\partial^2 \sigma}{\partial T \partial k} = \frac{1}{\gamma} 2ik^2 \int_0^{Lz} \hat{\psi}^{\dagger *} \overline{u} \hat{\psi} dz - \frac{ik}{\gamma} |A|^2 \int_0^{Lz} (RS_u P_k - RS_b Q_k) dz +
$$
$$
- \frac{ik}{\gamma} \int_0^{Lz} \left[\left(\frac{1}{Re_b} \frac{\partial^2 \overline{u}}{\partial z^2} + \overline{f} \right) P_T - \left(\frac{1}{PrRe_b} \frac{\partial^2 \overline{b}}{\partial z^2} \right) Q_T \right] dz +
$$
$$
- \frac{i}{\gamma} \int_0^{Lz} \overline{u} \left(P_T - 2k^2 \hat{\psi}^{\dagger *} \frac{\partial \hat{\psi}}{\partial T} \right) dz + \frac{i}{\gamma} \int_0^{Lz} \overline{b} Q_T dz - \frac{2k}{\gamma} \frac{Fr}{Re_b} \int_0^{Lz} R_T dz - \frac{i}{\gamma} \int_0^{Lz} \Pi_T dz +
$$
$$
- i \operatorname{Im}\left\{ \frac{\partial \sigma}{\partial T} \right\} \int_0^{Lz} \left[2k \hat{\psi}^{\dagger *} \hat{\psi} + \hat{\psi}^{\dagger *} \left(\frac{\partial^2}{\partial z^2} - k^2 \right) \frac{\partial \hat{\psi}}{\partial k} + \hat{b}^{\dagger *} \frac{\partial \hat{b}}{\partial k} - \frac{1}{k} \hat{\psi}^{\dagger *} \left(\frac{\partial^2}{\partial z^2} - k^2 \right) - \frac{1}{k} \hat{b}^{\dagger *} \hat{b} \right] dz +
$$
$$
- i \operatorname{Im}\left\{ \frac{\partial \sigma}{\partial k} \right\} \int_0^{Lz} \left[\hat{\psi}^{\dagger *} \left(\frac{\partial^2}{\partial z^2} - k^2 \right) \frac{\partial \hat{\psi}}{\partial T} + \hat{b}^{\dagger *} \frac{\partial \hat{b}}{\partial T} \right] dz + 2ik \operatorname{Im}\{\sigma\} \int_0^{Lz} \hat{\psi}^{\dagger *} \frac{\partial \hat{\psi}}{\partial T} dz \tag{5.119}
$$

where the following substitutions have been made

$$P = \hat{\psi}^{\dagger *}\left(\frac{\partial^2}{\partial z^2} - k^2\right)\hat{\psi} - \hat{\psi}^{\dagger *}\frac{\partial^2 \hat{\psi}}{\partial z^2} - \hat{\psi}\frac{\partial^2 \hat{\psi}^{\dagger *}}{\partial z^2} - 2\left(\frac{\partial \hat{\psi}^{\dagger *}}{\partial z}\right)\left(\frac{\partial \hat{\psi}}{\partial z}\right) + \hat{b}^{\dagger *}\hat{b} \tag{5.120}$$

$$P_k = \hat{\psi}^{\dagger *}\left(\frac{\partial^2}{\partial z^2} - k^2\right)\frac{\partial \hat{\psi}}{\partial k} - \hat{\psi}^{\dagger *}\frac{\partial^2}{\partial z^2}\left(\frac{\partial \hat{\psi}}{\partial k}\right) - \left(\frac{\partial \hat{\psi}}{\partial k}\right)\frac{\partial^2 \hat{\psi}^{\dagger *}}{\partial z^2} - 2\left(\frac{\partial \hat{\psi}^{\dagger *}}{\partial z}\right)\left(\frac{\partial}{\partial z}\frac{\partial \hat{\psi}}{\partial k}\right) + \hat{b}^{\dagger *}\frac{\partial \hat{b}}{\partial k} \tag{5.121}$$

$$P_T = \hat{\psi}^{\dagger *}\left(\frac{\partial^2}{\partial z^2} - k^2\right)\frac{\partial \hat{\psi}}{\partial T} - \hat{\psi}^{\dagger *}\frac{\partial^2}{\partial z^2}\left(\frac{\partial \hat{\psi}}{\partial T}\right) - \left(\frac{\partial \hat{\psi}}{\partial T}\right)\frac{\partial^2 \hat{\psi}^{\dagger *}}{\partial z^2} - 2\left(\frac{\partial \hat{\psi}^{\dagger *}}{\partial z}\right)\left(\frac{\partial}{\partial z}\frac{\partial \hat{\psi}}{\partial T}\right) + \hat{b}^{\dagger *}\frac{\partial \hat{b}}{\partial T} \tag{5.122}$$

$$P_T^{\dagger} = \left(\frac{\partial \hat{\psi}^{\dagger *}}{\partial T}\right)\left(\frac{\partial^2}{\partial z^2} - k^2\right)\hat{\psi} - \left(\frac{\partial \hat{\psi}^{\dagger *}}{\partial T}\right)\frac{\partial^2 \hat{\psi}}{\partial z^2} - \hat{\psi}\frac{\partial^2}{\partial z^2}\frac{\partial \hat{\psi}^{\dagger *}}{\partial T} - 2\left(\frac{\partial}{\partial z}\frac{\partial \hat{\psi}^{\dagger *}}{\partial T}\right)\left(\frac{\partial \hat{\psi}}{\partial z}\right) + \left(\frac{\partial \hat{b}^{\dagger *}}{\partial T}\right)\hat{b} \tag{5.123}$$

$$Q = \hat{b}^{\dagger *}\frac{\partial \hat{\psi}}{\partial z} + \hat{\psi}\frac{\partial \hat{b}^{\dagger *}}{\partial z} \tag{5.124} \qquad\qquad Q_k = \hat{b}^{\dagger *}\frac{\partial}{\partial z}\frac{\partial \hat{\psi}}{\partial k} + \hat{\psi}\frac{\partial}{\partial z}\frac{\partial \hat{b}^{\dagger *}}{\partial k} \tag{5.125}$$

$$Q_T = \hat{b}^{\dagger *}\frac{\partial}{\partial z}\frac{\partial \hat{\psi}}{\partial T} + \hat{\psi}\frac{\partial}{\partial z}\frac{\partial \hat{b}^{\dagger *}}{\partial T} \tag{5.126} \qquad\qquad Q_T^{\dagger} = \left(\frac{\partial \hat{b}^{\dagger *}}{\partial T}\right)\frac{\partial \hat{\psi}}{\partial z} + \hat{\psi}\frac{\partial}{\partial z}\frac{\partial \hat{b}^{\dagger *}}{\partial T} \tag{5.127}$$

$$R = 2\hat{\psi}^{\dagger *}\left(\frac{\partial^2}{\partial z^2} - k^2\right)\hat{\psi} + \frac{1}{Pr}\hat{b}^{\dagger *}\hat{b} \tag{5.128} \qquad\qquad \Pi = \hat{\psi}^{\dagger *}\hat{b} - \hat{b}^{\dagger *}\hat{\psi} \tag{5.129}$$

$$R_k = 2\hat{\psi}^{\dagger *}\left(\frac{\partial^2}{\partial z^2} - k^2\right)\frac{\partial \hat{\psi}}{\partial k} + \frac{1}{Pr}\hat{b}^{\dagger *}\frac{\partial \hat{b}}{\partial k} \tag{5.130} \qquad\qquad \Pi_k = \hat{\psi}^{\dagger *}\frac{\partial \hat{b}}{\partial k} - \hat{b}^{\dagger *}\frac{\partial \hat{\psi}}{\partial k} \tag{5.131}$$

$$R_T = 2\hat{\psi}^{\dagger *}\left(\frac{\partial^2}{\partial z^2} - k^2\right)\frac{\partial \hat{\psi}}{\partial T} + \frac{1}{Pr}\hat{b}^{\dagger *}\frac{\partial \hat{b}}{\partial T} \tag{5.132} \qquad\qquad \Pi_T = \hat{\psi}^{\dagger *}\frac{\partial \hat{b}}{\partial T} - \hat{b}^{\dagger *}\frac{\partial \hat{\psi}}{\partial T} \tag{5.133}$$

5.4 Conclusions and outlook

In this chapter we have provided an overview of the integration algorithm for slow-fast systems proposed by Michel and Chini [Michel and Chini (2019)] in the context of the stratified flow problem [Chini et al. (2022)] and analytically derived a methodology to efficiently handle the two-dimensional spatial variability of the fast instabilities. When such a variability is considered, the original QL algorithm requires to identify the mode that first becomes unstable, via solving the eigenvalue problem for the fast dynamics multiple times for varying wavenumber k (at each time iteration). Contrarily the methodology discussed here overcomes this issue deriving an evolution equation for the wavenumber associated to the marginally stable mode, lowering the number of eigenvalue problems to be solved at each time step to one.

Based on the results obtained on the two-dimensional model problem (presented in § 4.4), we are confident that the implementation of this extension will positively impact the simulations of the QL dynamics, substantially lowering their computational costs and therefore opening the way for further developments of the QL methodology. Moreover the implementation of the co-evolution regime via the gradient descent technique will enable the characterisation of bursting events providing some insight on their impact on the flow dynamics.
Because of the modularity of the code structure designed for the simulations of the model problems discussed in this work, the implementation of the two extensions above will be fairly straightforward, and will only require few minor modifications due to the change in the functional space on which the eigenfunctions are defined.

Among many others features that one will need to include to eventually access the extreme parameter regimes of the three-dimensional real problem, we believe that the re-introduction of the convective term in the mean equations and the inclusion of multiple marginally stable modes are probably the most important extensions at the current state of the investigation. The first feature will turn the strict QL formulation into its GQL counterpart, re-introducing the horizontal spatial variability of the mean dynamics, and therefore enabling the implementation of the co-evolution regimes should both bursting events occur or/and the scale separation between the fast and the slow dynamics be finite.

6 Conclusions and Further Work

In the limit of small Froude and large Reynolds numbers, stratified shear flows exhibit a strongly constrained form of turbulent dynamics. Multi-scale analysis of this phenomenon leads to a set of reduced, quasi-linear system of equations where fields evolving on different spatiotemporal scales are coupled [Chini et al. (2022)]. The dynamics of the fast variables, or fluctuations, is linear around the slow-evolving mean flow, with the fluctuations being advected by the mean flow and producing a feedback on it. Because the evolution of the fluctuations is linear the only possible long-term dynamics requires the system to self-adjust around a marginal-stability manifold. Michel and Chini [Michel and Chini (2019), Chini et al. (2022)] recently have shown for a 1D model problem that this scenario can be realized in slow-fast QL systems by appropriately slaving the fluctuations dynamics to the mean field so that zero growth rates are ensured.

6.1 Leaving the marginally stable manifold - Bursting events

The interaction between the slow and the fast fields in stratified flows is not sign-definite, potentially allowing for the fluctuations to intermittently prevent marginal stability from being attained. Based on this observation, we have developed and tested different algorithmic techniques to cope with the realisation of these events.
In chapter 3 we investigated a simplified one-dimensional dynamical system and its corresponding asymptotic QL reduction, specifically addressing the two-way nature of the fluctuation feedback. Inspired by the approach of Michel and Chini [Michel and Chini (2019)] we have developed a numerical procedure that can properly accommodate bursting events associated with positive fluctuation growth rates. The algorithm simulates the QL system, exploiting the multi-scale nature of the problem, when marginal stability is satisfied and simulates/emulates the full non-linear system otherwise. In the first case, the fluctuation amplitude is determined such that zero growth rates can be maintained, while in the second one, the co-evolution of the two fields is performed. The purpose of this co-evolution, triggered by the termination of the marginally stable manifold, is to drive the system to a new marginally-stable manifold

where the coupled evolution can continue. In this regard three different methods were tested: finite-ϵ DNS (the full non-linear system), ϵ-free DNS (the re-scaled system for the bursting regime) and a gradient descent technique. The first two methods explicitly reintroduce the fluctuation non-linearities in the dynamics, which generally are not negligible when fluctuation amplitudes are large and which may be crucial for the saturation of instabilities. The third method exploits information from the eigenvalue problem by evolving in the direction provided by its linear eigenfunctions. The numerical simulation of the the three different dynamics show as a first remarkable result, that in all of the cases the QL dynamics captures and successfully performs the transition between marginally stable manifolds, also observable in the full dynamics. An efficiency comparison between the different co-evolution technique confirms the computational advantages of the ε-free co-evolution and the gradient descent co-evolution over the full DNS. The absence of the scale separation parameter in the first two techniques allows for an integration time-step which is $O(\varepsilon^{-1})$ larger then the one required by the fully non-linear dynamics, resulting in a computational advantage of two orders of magnitude in therms of solver iterations. Moreover the observation that the gradient descent methodology only makes use of the linear eigenfunction, already present in the QL dynamics, might make this technique preferable to the ε-free co-evolution, if not the only possible choice certain cases. This feature is key when considering systems like the two-dimensional stratified flow problem discussed in chapters 5. In this case the elimination of the spatial horizontal variability of the mean fields (strict QL formalism) disables the possibility of connecting any non-linear dynamics to the QL reduction due to the dimensions-mismatch. Therefore the gradient descent technique remains the only one applicable to treat bursting events, should positive growth rates be realised.

6.2 Approaching the marginally stable manifold - Finite scale separation

The second extension of the original QL methodology concerns the presence of a finite scale separation between the fast and slow dynamics. In this case the exponentially-fast growth or decay of the fluctuation fields is quantified with respect to the characteristic time scale T over which the slow mean evolves. Due to the averaging over infinite fast times $\tau_f = T/\varepsilon$, the original algorithm for infinite scale separations only considers two regions (more precisely a region and a point): the fluctuation feedback is finite for Re$\{\sigma\}$ exactly zero and is set to zero for any negative value of σ. Differently, when accounting for finite scale separation, the relevance of the fluctuations effects with a given growth rate is determined with respect to slow temporal scale. Namely, when the growth rate is negative enough to ensure the decay of the fast mode over a time comparable or smaller then T the fluctuation contribution is negligible. Similarly when the growth rate is close is enough to zero, to ensure that only a marginal growth or decay of the fluctuations occurs over a time T, the amplitude is compute and the feedback is finite. By introducing a tolerance to quantitatively define "enough" and

"marginal", the different values of σ that bound the validity range of the QL reduction can be found. Differently from the original algorithm, this considerations lead to an extended marginally-stable range around $\sigma = 0$ (with a size that scales with the chosen tolerance), and to the introduction of an intermediate region connecting the two QL filtered dynamics. Due to the non validity of the QL reduction, in these region the coupled dynamics have to be in principle co-evolved. Although this co-evolution can be interchanged in specific systems with the zero-feedback QL dynamics (as detailed explained in § 3.4.3), this algorithmic structure has the advantage of having smoother behavior around the marginally stable region (above all when very small growth rates are enforced via an amplitude correction) and not less important defines thresholds and tolerances that are physically understandable and controllable.

6.3 Identification of the fastest growing mode in two-dimensional problems

With the more ambitious goal of accessing in the future the fully three-dimensional stratified flow dynamics, here we have taken a step forward in that direction increasing the dimensionality of the problem to two-dimensions. This modification introduces the horizontal spatial variability of the dynamics, which appears in the QL formulation as a dependency on the wavenumber of the eigenvalue problem describing the evolution of the fast dynamics. This results in a temporal variation of the dispersion relation $\sigma(T, k)$ and consequently in the temporal variation of the wavenumber associated to the fastest growing mode. The enforcement of the marginal stability constraint now requires to first identify the fastest growing mode and then to determine its amplitude such that marginal stability can be maintained in time. Practically the eigenvalue problem has to be solved for multiple k (and multiple is not *a priori* defined due to the continuous variation of k) at each time iteration, considerably increasing the computational costs of the QL simulation. The solution to this problem has been achieved by deriving an evolution equation for the wavenumber of the marginally-stable mode. In chapter 4 we presented and discussed, making use of a two-dimensional model problem, two alternative (but equivalent) derivations in condition of marginal stability. Within a geometrical description the evolution of the dynamics on the marginally stable manifold is strictly connected to the curvature properties of the $\sigma(T, k)$ landscape. The maintenance of zero growth rates in time, automatically results in a zero Gaussian curvature of this landscape in a specific k-direction, and the evolution of this direction yields at each time the wavenumber associated to the marginally-stable mode. Starting from different considerations, an evolution equation for the wavenumber of the fastest growing mode below marginal stability has also been derived. Although for negative values of the growth rate the fluctuation feedback is set to zero, this algorithm provides a feasible way to track the evolution of the maximum of the dispersion relation, allowing for a more precise detection of the time at which marginal stability is satisfied.

Both algorithms, in condition of marginal stability and below have been successfully tested, reproducing with extreme precision the results obtained solving multiple eigenvalue problems

for varying k.

6.4   Towards the stratified flow problem - Outlook and future work

The extensions derived in the previous chapters, for the two different model problems, have been eventually discussed and applied to the stratify flow problem. Starting from the results obtained by Chini *et al.* [Chini et al. (2022)], we have derived the evolution equation for the prediction of the wavenumber associated to the marginally stable mode.

The obvious immediate next step will be the implementation of this methodology in the algorithm for the stratified flow problem, to test its efficacy in that case. Not least is the implementation of the gradient descent technique to overcome bursting events, which have actually already been found in Chini et al. (2022). Because of the great results that both these extension have produced in the context of model problems, and the modularity of the code structure developed simulate those cases, we believe that tasks can be carried out in the near future.

Further advances towards the real stratified flow problem will require the re-introduction of the convective term in the mean fields evolution and the possibility for the marginally stable condition to be satisfied by more than one mode at the same time. The implementation of the other co-evolution techniques to treat both, unstable and/or finite scale separation scenarios, will be automatically enable with the GQL model of the stratified flow problem.

A Intermediate-time processes and instability of the fluctuations amplitude

The purpose of this appendix is to provide a formal justification for the conjecture proposed in § 3.4.4, regarding the impossibility of determining the fluctuation amplitude in a scenario where negative values of the integrals α and β are realised. This will be pursued performing a three-time-scale analysis, not only considering slow and fast processes but also intermediate ones, whose evolution and instabilities might impact the slow dynamics, invalidating the scale separation at the basis of the QL methodology. The mathematical proof is first illustrated here for a simplified model problem (specifically the model problem presented by Michel and Chini in section § 3 of [Michel and Chini (2019)]), and then compared to the equivalent but inconclusive derivation for the original model problem discussed in § 3. We remark that the calculation presented in the following section is largely inspired by a fruitful discussion with Prof. Chini and Dr. Michel and their previous calculations on the topic.

A.1 Multi-scale analysis with three time scales for a simplified model problem

The slow-fast dynamics for the mean field $U(z, t)$ and the fluctuation $\eta(z, t)$ is described in this case by the following set of equations

$$\frac{\partial U}{\partial t} = F - \nu U - \eta^2 \tag{A.1}$$

$$\varepsilon \frac{\partial \eta}{\partial t} = U\eta + \frac{\partial^2 \eta}{\partial z^2} - \varepsilon \eta^3 \tag{A.2}$$

where ε is the small parameter setting the scale separation (ideally $\varepsilon \to 0$), $F(z, t)$ is an external forcing and ν the damping coefficient. Differently from the model problem presented in § 3, the evolution equation of the mean field is linear in U as well as the advection term in the evolution equation of the fast modes. Owing to the small parameter ε, we can perform multi-scale analysis to obtain a set of quasi-linear PDEs. In addition to what done in § 3.2,

Appendix A. Intermediate-time processes and instability of the fluctuations amplitude

where only a slow and a fast time where introduced, here we also consider an intermediate time ψ

$$t \rightarrow (T, \psi, \tau): \quad T = t, \quad \psi = \frac{T}{\sqrt{\varepsilon}}, \quad \tau = \frac{\psi}{\sqrt{\varepsilon}} \tag{A.3}$$

yielding the evolution equations

$$\frac{\partial U}{\partial \tau} + \sqrt{\varepsilon} \frac{\partial U}{\partial \psi} + \varepsilon \frac{\partial U}{\partial T} = \varepsilon (F - \nu U - \eta^2) \tag{A.4}$$

$$\frac{\partial \eta}{\partial \tau} + \sqrt{\varepsilon} \frac{\partial \eta}{\partial \psi} + \frac{\partial \eta}{\partial T} = U\eta + \frac{\partial^2 \eta}{\partial z^2} - \varepsilon \eta^3 \tag{A.5}$$

.

Assuming the following asymptotic expansion for the variables U and η

$$U(z, T, \psi, \tau) = U_0 + \sqrt{\varepsilon} U_1 + \varepsilon U_2 + O(\varepsilon^{3/2})$$
$$\eta(z, T, \psi, \tau) = \eta_0 + \sqrt{\varepsilon} \eta_1 + \varepsilon \eta_2 + O(\varepsilon^{3/2}) \tag{A.6}$$

and solving (A.4)-(A.5) order by order the following results are obtained

Order $O(1)$

From the evolution equation of the mean field U (A.4)

$$\frac{\partial U_0}{\partial \tau} = 0 \tag{A.7}$$

confirming that at leading order the slow field does not depend on the fast time τ, $U_0 = U_0(z, T, \psi)$ (as in § 3.2), and from the evolution of the fast dynamics (A.5)

$$-\frac{\partial \eta}{\partial \tau} + U_0 \eta_0 + \frac{\partial^2 \eta_0}{\partial z^2} = 0 \tag{A.8}$$

.

Noticing that in the latter equation, only η_0 depends on τ we can set $\partial_\tau \eta_0 = \sigma \eta_0$ assuming a modal solution of the type

$$\eta_0(z, T, \psi, \tau) = A(T, \psi) \hat{\eta}_0(z, T\psi) e^{\sigma \tau} \tag{A.9}$$

where A is an amplitude, $\hat{\eta}_0$ a vertical structure function and Re$\{\sigma\}$ a growth rate.

Substituting the ansatz (A.9) into eq. (A.8) leads to the linear eigenvalue problem

$$L\hat{\eta}_0 = (U_0 + \partial_z^2)\hat{\eta}_0 = \sigma\hat{\eta}_0 \tag{A.10}$$

which can be perturbed with respect to slow time T and intermediate time ψ to obtain two evolution equations for the growth rate (via enforcing a solvability condition as explained in details in § 3.3)

$$\frac{\partial\sigma}{\partial T} = \int_0^{Lz} |\hat{\eta}_0|^2 \frac{\partial U_0}{\partial T} dz \tag{A.11}$$

$$\frac{\partial\sigma}{\partial\psi} = \int_0^{Lz} |\hat{\eta}_0|^2 \frac{\partial U_0}{\partial\psi} dz \tag{A.12}$$

where the normalization condition $\langle\hat{\eta}_0|\hat{\eta}_0\rangle = 1$, with respect to the inner product (3.13) has been used.

Order $O(\sqrt{\varepsilon})$

From eq. (A.4), given that $U_0 = U_0(z, T, \psi)$, we obtain

$$\frac{\partial U_1}{\partial\tau} + \frac{\partial U_0}{\partial\psi} = 0 \tag{A.13}$$

from which it follows that, in order to ensure the boundedness of U_1 in τ, $\partial_\psi U_0 = 0$ must be set. Therefore $U_0 = U_0(z, T)$ only and $U_1 = U_1(z, T, \psi)$ on slow and intermediate time. Consequently neither does the growth rate σ depend on the intermediate time, on account of A.12, nor the eigenfunction $\hat{\eta}_0$, as a solution of the eigenvalue problem (A.10).

As for the fluctuation field at order $O(\sqrt{\varepsilon})$ eq. (A.5) reads

$$-\frac{\partial\eta_1}{\partial\tau} + U_0\eta_1 + \frac{\partial^2\eta_1}{\partial z^2} = \frac{\partial\eta_0}{\partial\psi} - U_1\eta_0 \tag{A.14}$$

from which we can again conclude $\partial_\tau\eta_1 = \sigma\eta_1$ and

$$\eta_1(z, T, \psi, \tau) = B(T, \psi)\hat{\eta}_1(z, T\psi)e^{\sigma\tau} \tag{A.15}$$

(where B is now the amplitude), due to fact that the right hand side of(A.14) only depends on τ exponentially through η_0.

Appendix A. Intermediate-time processes and instability of the fluctuations amplitude

Substituting the ansatz (A.9) and (A.15) into (A.14), and defining the operator $\mathcal{L} = L - \sigma$, yields to the following singular boundary value problem

$$B(\mathcal{L}\hat{\eta}_1) = -AU_1\hat{\eta}_0 + \hat{\eta}_0\frac{\partial A}{\partial \psi} \tag{A.16}$$

for which the enforcement of the Fredholm alternative, leads to an evolution equation for the amplitude A on the intermediate time ψ

$$\frac{\partial A}{\partial \psi} = A \int_0^{Lz} U_1|\hat{\eta}_0|^2 dz. \tag{A.17}$$

Order $O(\varepsilon)$

At this order from the evolution equation of the slow dynamics (A.4) we obtain

$$\frac{\partial U_2}{\partial \tau} + \frac{\partial U_1}{\partial \psi} + \frac{\partial U_0}{\partial T} = F - \nu U_0 - \eta_0^2. \tag{A.18}$$

Re-calling the definition of the average over fast time-scale τ (3.8), introduced in § 3.2, and applying it to the previous expression

$$\frac{\partial U_1}{\partial \psi} + \frac{\partial U_0}{\partial T} = F - \nu U_0 - \overline{\eta_0^2} \tag{A.19}$$

where the fluctuations-induced feedback defined for the infinite scale separation case as

$$\overline{\eta_0^2} = A^2|\hat{\eta}_0|^2\overline{e^{2\sigma\tau}} = A^2|\hat{\eta}_0|^2 \lim_{\tau_f \to \infty} \frac{1}{\tau_f} \int_0^{\tau_f} e^{\sigma\tau} d\tau \tag{A.20}$$

is a finite only provided that $\sigma = 0$. This will be assumed for the rest of the calculation.

Defining an intermediate-time average $\widetilde{(\cdot)}$ for a generic function φ similarly to what done for the fast-time average

$$\varphi(z, T, \tau) = \varphi\widetilde{(z, T, \psi,}\tau) = \lim_{\psi_f \to \infty} \frac{1}{\psi_f} \int_0^{\psi_f} \varphi d\psi \tag{A.21}$$

and further averaging (A.19) over intermediate time (reminding that $\hat{\eta}_0$ is independent of ψ)

we obtain

$$\frac{\partial U_0}{\partial T} = F - \nu U_0 - \widetilde{A^2}|\hat{\eta}_0|^2 \tag{A.22}$$

which can be substituted in the slow evolution equation of the growth rate (A.11) to obtain an expression for the slowly-varying amplitude slaved to the mean field in condition of marginal stability (enforcing $\partial_T \sigma = 0$)

$$\widetilde{A} = \sqrt{\alpha/\beta} \tag{A.23}$$

with

$$\alpha = \int_0^{Lz} (F - \nu U)|\hat{\eta}_0|^2 dz \quad \text{and} \quad \beta = \int_0^{Lz} |\hat{\eta}_0|^4 dz \tag{A.24}$$

Considering now the difference between (A.19) and (A.22) an evolution equation for the correction U_1 to the mean field can be obtained

$$\frac{\partial U_1}{\partial \psi} = (\widetilde{A^2} - A^2)|\hat{\eta}_0|^2 = \left(\frac{\alpha}{\beta} - A^2\right)|\hat{\eta}_0|^2 \tag{A.25}$$

and used in the evolution equation of the amplitude (A.17). We remark that the amplitude here noted as $\widetilde{A}$ is only a function of slow time T, and has the same role that A has in the model problem discussed in § 3 (based on a two time-scale analysis), while the amplitude A, in this context, additionally depends on the intermediate time scale.

Noticing that the evolution equation (A.17) is derived for A, while the evolution equation for U_1 contains A^2, to ease the calculation we will consider the following variation of (A.17)

$$\begin{aligned}
\frac{1}{2}\frac{\partial^2 \ln(A^2)}{\partial \psi^2} &= \frac{\partial^2 \ln(A)}{\partial \psi^2} = \frac{\partial}{\partial \psi}\left(\frac{1}{A}\frac{\partial A}{\partial \psi}\right) \\
&= \frac{\partial}{\partial \psi}\left(\int_0^{Lz} U_1|\hat{\eta}_0|^2 dz\right) = \int_0^{Lz} \frac{\partial U_1}{\partial \psi}|\hat{\eta}_0|^2 dz
\end{aligned} \tag{A.26}$$

obtained by dividing (A.17) by A and taking the derivative w.r.t. ψ. Substituting the evolution equation for U_1 (A.25) leads to

$$\frac{1}{2}\frac{\partial^2 \ln(A^2)}{\partial \psi^2} = \left(\frac{\alpha}{\beta} - A^2\right)\underbrace{\int_0^{Lz} |\hat{\eta}_0|^4 dz}_{\beta} = \alpha - \beta(A^2) \tag{A.27}$$

which can be re-written as

$$A^2 \frac{\partial^2 A^2}{\partial \psi^2} - \left(p d A^2 \psi \right) = (A^2)^2 (\alpha - A^2 \beta) \,. \tag{A.28}$$

Making the ansatz $A^2 = \frac{\alpha}{\beta} e^{\vartheta(\psi)}$ the previous expression provides an evolution equation for the variable $\vartheta(\psi)$

$$\frac{d^2 \vartheta}{d\psi^2} = 2\alpha(1 - e^{\vartheta}) \tag{A.29}$$

and after multiplying both sides by ϑ and integrating by parts, eventually yields the following ODE

$$\frac{1}{2} \frac{d\vartheta}{d\psi} + 2\alpha(e^{\vartheta} - \vartheta) = C \,. \tag{A.30}$$

It is straightforward to notice from (A.30), that the behaviour of the amplitude on the intermediate time scale is controlled by the integral α (A.24), whose negative sign would cause an unbounded growth of the fluctuations. Although in this specific model problem the integral β is positive definite (A.24), the result derived here would provide a mathematical explanation for the supposedly unstable scenario characterized by $\alpha < 0$ and $\beta < 0$ in problems where β can realise negative values (as conjectured in § 3.4.4).

A.2 Comparison to the original model problem

When introducing the intermediate time scale ψ in the multi-scale analysis of the original model problem (3.1)-(3.2) presented in § 3 we obtain the following set of equations

$$\frac{\partial U}{\partial \tau} + \sqrt{\varepsilon} \frac{\partial U}{\partial \psi} + \varepsilon \frac{\partial U}{\partial T} = \varepsilon(F - \nu U - \eta^2 e^{-U^2}) \tag{A.31}$$

$$\frac{\partial \eta}{\partial \tau} + \sqrt{\varepsilon} \frac{\partial \eta}{\partial \psi} + \frac{\partial \eta}{\partial T} = U\eta e^{-U^2} + \frac{\partial^2 \eta}{\partial z^2} - \varepsilon \eta^3 \tag{A.32}$$

with the main difference from (A.4)-(A.5) being the exponential dependency of the two equations from U^2. Positing the same expansion for the variables U and η (A.6) the asymptotic

expansion of the exponential term

$$
\begin{aligned}
e^{-U^2} &\sim 1 - U^2 - \frac{1}{2}U^4 + O(U^6) \\
&= 1 - (U_0 + \sqrt{\varepsilon}U_1 + \varepsilon U_2)^2 - \frac{1}{2}(U_0 + \sqrt{\varepsilon}U_1 + \varepsilon U_2)^4 + O(U^6)
\end{aligned}
\tag{A.33}
$$

introduces an additional term (highlighted in red) in the evolution equation for the fluctuations at order $O(\sqrt{\varepsilon})$)

$$
-\frac{\partial \eta_1}{\partial \tau} + \eta_1 U_0 e^{-U_0^2} = \frac{\partial \eta_0}{\partial \psi} - \eta_0 U_1 e^{-U_0^2} - \eta_0 U_0 e^{-U_0 U_1}
\tag{A.34}
$$

and consequently in the evolution equation of the amplitude

$$
\frac{\partial A}{\partial \psi} = A\left(\int_0^{Lz} |\hat{\eta}_0|^2 U_1 e^{-U_0^2} dz + \int_0^{Lz} |\hat{\eta}_0|^2 U_0 e^{-U_0 U_1} dz \right)
\tag{A.35}
$$

Further taking the ψ derivative of the previous expression divided by A, as done in (A.26) will now yield

$$
\frac{1}{2}\frac{\partial^2 \ln(A^2)}{\partial \psi^2} = \int_0^{Lz} |\hat{\eta}_0|^2 \frac{\partial U_1}{\partial \psi} e^{-U_0^2} dz - \int_0^{Lz} |\hat{\eta}_0|^2 U_0 \frac{\partial U_1}{\partial \psi} e^{-U_0 U_1} dz.
\tag{A.36}
$$

An evolution equation over intermediate time for the correction U_1 at order ε, is obtained via the same procedure illustrated in the previous section (namely subtracting the the τ-and-ψ-averaged equation for U from the τ-averaged one)

$$
\frac{\partial U_1}{\partial \psi} = (\widetilde{A^2} - A^2)|\hat{\eta}_0|^2 U_0 e^{-U_0^2}
\tag{A.37}
$$

where in this case the integrals α and β defining the slowly-varying amplitude $\widetilde{A} = \sqrt{\alpha/\beta}$ are given by

$$
\alpha = \int_0^{Lz} (F - \nu U)|\hat{\eta}_0|^2 dz \quad \text{and} \quad \beta = \int_0^{Lz} (1 - 2U_0^2)e^{-2U_0^2}|\hat{\eta}_0|^4 dz
\tag{A.38}
$$

identical to those derived in § 3.3, since they results from the solvability condition of the T-perturbed eigenvalue problem at order $O(1)$ (A.11).

As clearly visible the substitution of (A.37) into (A.36) does not lead in this case to any simplifi-

cation, due to the more complex form of β

$$\frac{1}{2}\frac{\partial^2 \ln(A^2)}{\partial \psi^2} = (\widetilde{A^2} - A^2)\Bigg(\underbrace{\int_0^{Lz} |\hat{\eta}_0|^4 U_0 e^{-2U_0^2}\, dz}_{\gamma_1} - \underbrace{\int_0^{Lz} |\eta_0|^4 U_0^2 e^{-U_0^2 - U_0 U_1}\, dz}_{\gamma_2} \Bigg) \tag{A.39}$$

$$= \left(\frac{\alpha}{\beta} - A^2\right)(\gamma_1 - \gamma_2).$$

Consequently we can not draw direct conclusions on the behaviour of the amplitude at intermediate time scales, based on the sign of α (or any other parameter).

B Mixed derivatives of singular eigen-value problems

Considering a vector space $V : [0,1] x\mathbb{R} \to \mathbb{R}$ with inner product $\langle \cdot | \cdot \rangle : V \times V \to \mathbb{R}$, we introduce a generic operator L acting on its elements v, $L(a,b) : V \to V$ dependent on two parameters a and b with $a, b \in \mathbb{R}$. This operator is defined self-adjoint, or symmetric, if $\langle Lv_1 | v_2 \rangle = \langle v_1 | Lv_2 \rangle$, namely if it is identical to its adjoint $L^\dagger$. Denoting with $\hat{\eta}$ the eigenfunction of L (with normalisation $\langle \hat{\eta} | \hat{\eta} \rangle = 1$) associated to the eigenvalue σ the following eigenvalue problem is well defined for any $a, b \in \mathbb{R}$

$$L(a,b)\hat{\eta}(a,b) = \sigma(a,b)\hat{\eta}(a,b) \ . \tag{B.1}$$

The perturbation of this eigenvalue problem with respect to one or both the parameters a and b allows to derive expressions for the corresponding correction of the eigenvalue σ, via ensuring the solvability of the resulting singular boundary value problem, as detailed in § 3.3 and § 4.3. When seeking for the second-order correction of σ with respect to a and b, namely $\partial_a(\partial_b \sigma)$, the order of the two differentiations and the imposition of the solvability condition can be exchanged, yielding apparently different expressions.

Denoting the partial derivatives of L and σ with the more compact notation $\partial_i(\partial_j L) = L_{ij}$ and $\partial_i(\partial_j \sigma) = \sigma_{ij}$, the three different derivations are summarised below.

Differentiation w.r.t a and b followed by solvability condition

Taking the second derivative of (B.1) with respect to both parameters a and b

$$L\hat{\eta}_{ab} = -L_{ab}\hat{\eta} - L_a\eta_b - L_b\eta_a + \sigma\hat{\eta}_{ab} + \sigma_a\eta_b + \sigma_b\eta_a + \sigma_{ab}\hat{\eta} \tag{B.2}$$

and defining the operator $\mathscr{L}$ as $\mathscr{L} = L - \sigma$, singular by definition, yields

$$\mathscr{L}\hat{\eta}_{ab} = -L_{ab}\hat{\eta} - L_a\eta_b - L_b\eta_a + \sigma_a\eta_b + \sigma_b\eta_a + \sigma_{ab}\hat{\eta} \tag{B.3}$$

Appendix B. Mixed derivatives of singular eigenvalue problems

for which the solvability condition (3.18) has to be enforced taking the inner product with $\hat{\eta}$

$$\sigma_{ab} = \langle L_{ab}\hat{\eta}|\hat{\eta}\rangle + \langle L_a\hat{\eta}_b|\hat{\eta}\rangle + \langle L_b\hat{\eta}_a|\hat{\eta}\rangle \tag{B.4}$$

where $\sigma_a\langle\eta_b|\hat{\eta}\rangle = \sigma_b\langle\eta_a|\hat{\eta}\rangle = 0$ due to the preservation of the norm $\langle\hat{\eta}_\phi|\hat{\eta}\rangle = \frac{1}{2}\langle\hat{\eta}|\hat{\eta}\rangle_\phi = 0$.

Differentiation w.r.t a, followed by solvability condition and further differentiation w.r.t b

Taking now the first derivative of (B.1) with respect to the parameter a

$$\mathscr{L}\hat{\eta}_a = -L_a\hat{\eta} + \sigma_a\hat{\eta} \tag{B.5}$$

and projecting the previous expression onto the null-space of $\mathscr{L}$ we obtain

$$\sigma_a = \langle L_a\hat{\eta}|\hat{\eta}\rangle . \tag{B.6}$$

Taking then the derivative with respect to the second parameter b a second expression for the mixed derivative of the eigenvalue is obtained

$$\sigma_{ab} = \langle L_{ab}\hat{\eta} + L_a\hat{\eta}_b|\hat{\eta}\rangle + \langle L_a\hat{\eta}|\hat{\eta}_b\rangle \tag{B.7}$$

which in the case of a self-adjoint operator becomes

$$\sigma_{ab} = \langle L_{ab}\hat{\eta} + 2L_a\hat{\eta}_b|\hat{\eta}\rangle \tag{B.8}$$

owing to $\langle L_a\hat{\eta}|\hat{\eta}_b\rangle = \langle L_a\hat{\eta}_b|\hat{\eta}\rangle$.

Differentiation w.r.t b, followed by solvability condition and further differentiation w.r.t a

Re-taking the same steps as in the previous case switching the order of the differentiation with respect to a and the one with respect to b leads to

$$\mathscr{L}\hat{\eta}_b = -L_b\hat{\eta} + \sigma_b\hat{\eta} \tag{B.9}$$

and

$$\sigma_b = \langle L_b\hat{\eta}|\hat{\eta}\rangle . \tag{B.10}$$

after imposing the Fredholm alternative.

Differentiating then (B.10) w.r.t. b, the third expression for the second mixed derivative of $\sigma(a, b)$ reads

$$\sigma_{ab} = \langle L_{ab}\hat{\eta} + 2L_b\hat{\eta}_a | \hat{\eta} \rangle \tag{B.11}$$

.

The three seemingly different expressions obtained just inverting the order of differentiation and projection onto the null-space of $\mathscr{L}$ can be proven identical demonstrating

$$\langle L_b\hat{\eta}_a | \hat{\eta} \rangle = \langle L_a\hat{\eta}_b | \hat{\eta} \rangle . \tag{B.12}$$

For this purpose we re-write (B.5) and (B.9) as

$$0 = L\hat{\eta}_a - L_a\hat{\eta} + \sigma\hat{\eta}_a + \sigma_a\hat{\eta} \tag{B.13}$$

$$0 = L\hat{\eta}_b - L_b\hat{\eta} + \sigma\hat{\eta}_b + \sigma_b\hat{\eta} \tag{B.14}$$

and we take the inner product of these expression against η_b and η_a respectively, obtaining

$$0 = \langle L\hat{\eta}_a | \hat{\eta}_b \rangle - \langle L_a\hat{\eta} | \hat{\eta}_b \rangle + \sigma\langle \hat{\eta}_a | \hat{\eta}_b \rangle + \sigma_a\langle \hat{\eta} | \hat{\eta}_b \rangle \tag{B.15}$$

$$0 = \langle L\hat{\eta}_b | \hat{\eta}_a \rangle - \langle L_b\hat{\eta} | \hat{\eta}_a \rangle + \sigma\langle \hat{\eta}_b | \hat{\eta}_a \rangle + \sigma_b\langle \hat{\eta} | \hat{\eta}_a \rangle . \tag{B.16}$$

Subtracting (B.16) from (B.16) and recalling that $\langle \hat{\eta}_a | \hat{\eta}_b \rangle = \langle \hat{\eta}_b | \hat{\eta}_a \rangle$ and $\langle \hat{\eta} | \hat{\eta}_a \rangle = \langle \hat{\eta} | \hat{\eta}_b \rangle = 0$ because of the normalisation, yields

$$\langle L_a\hat{\eta} | \hat{\eta}_b \rangle - \langle L_b\hat{\eta} | \hat{\eta}_a \rangle = \langle L\hat{\eta}_a | \hat{\eta}_b \rangle - \langle L\hat{\eta}_b | \hat{\eta}_a \rangle \tag{B.17}$$

from which (B.12) directly follows making use of the self-adjointness of the operator L and the symmetry of the inner product that give $\langle L\hat{\eta}_a | \hat{\eta}_b \rangle = \langle \hat{\eta}_a | L\eta_b \rangle = \langle L\hat{\eta}_b | \hat{\eta}_a \rangle$.

C | QL algorithm for the strongly stratified flow problem - A lengthy calculation

In this appendix we report the full calculation to derive the evolution equation for the wavenumber associated to the marginally stable mode, for the two-dimensional stratified flow problem considered in § 5, and described by the following set of coupled quasi-linear PDEs

$$\frac{\partial \overline{u}}{\partial T} = |A|^2 i g \frac{\partial}{\partial z}\left(\hat{\varphi}\frac{\partial \hat{\varphi}^*}{\partial z} - \hat{\varphi}^* \frac{\partial \hat{\varphi}}{\partial z}\right) + \frac{1}{Re_b}\frac{\partial^2 \overline{u}}{\partial z^2} = |A|^2 RS_u + \frac{1}{Re_b}\frac{\partial^2 \overline{u}}{\partial z^2} + \overline{f}, \tag{C.1}$$

$$\frac{\partial \overline{b}}{\partial T} = |A|^2 i g \frac{\partial}{\partial z}(\hat{\varphi}\hat{\eta}^* - \hat{\varphi}^* \hat{\eta}) + \frac{1}{PrRe_b}\frac{\partial^2 \overline{b}}{\partial z^2} = |A|^2 RS_b + \frac{1}{PrRe_b}\frac{\partial^2 \overline{b}}{\partial z^2}, \tag{C.2}$$

$$\sigma\left(\frac{\partial^2}{\partial z^2} - k^2\right)\hat{\psi} = -ik\overline{u}\left(\frac{\partial^2}{\partial z^2} - k^2\right)\hat{\psi} + ik\frac{\partial^2 \overline{u}}{\partial z^2}\hat{\psi} - ik\hat{b} + \frac{Fr}{Re_b}\left(\frac{\partial^2}{\partial z^2} - k^2\right)^2\hat{\psi}, \tag{C.3}$$

$$\sigma\hat{b} = -ik\overline{u}\hat{b} + ik\left(1 + \frac{\partial \overline{b}}{\partial z}\right)\hat{\psi} + \frac{Fr}{PrRe_b}\left(\frac{\partial^2}{\partial z^2} - k^2\right)\hat{b}. \tag{C.4}$$

GEOMETRICAL DESCRIPTION
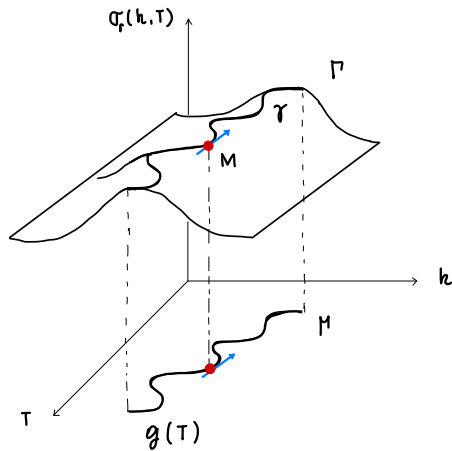
surface $\quad \Gamma : A \to \mathbb{R}^3 \quad A \subseteq \mathbb{R}^2$

$\Gamma(T,h) : (T,h) \to (T, h, \text{Re}\{\sigma(T,h)\})$ as a graph

Γ injective because $\forall (T,h) \; \exists! \; \sigma_r(T,h)$ by construct

ridge $\quad \gamma : I \to \mathbb{R}^3 \quad I \subseteq \mathbb{R}$

$\gamma = \Gamma \circ M$

$M : I \to \mathbb{R}^2 \quad I \subseteq \mathbb{R}$

$M(T) : T \to (T, g(T))$ as a graph

$M(T)$ is injective when considering only one mode $\to \forall$ mode you can have a different M

Indicating with $\sigma_r = \text{Re}\{\sigma\}$

Taylor expansion of $\sigma_r(T,h)$ along the ridge $\gamma' = \bar{d} = \left(1, \frac{dg(T)}{dT}, 0 \right)$ around a point $M = (T_M, h_M, \sigma=0)$

$$\sigma_r\left((h,T)_M + \Delta \bar{d} \right) \sim \sigma_{rM} + \left\{ \partial_T \sigma_r \big|_M + \partial_h \sigma_r \big|_M \frac{dg}{dT} \right\} \Delta +$$

$$+ \left\{ \frac{1}{2} \partial_h^2 \sigma_r \big|_M \left(\frac{dg}{dT} \right)^2 + \partial_T (\partial_h \sigma_r) \big|_M \frac{dg}{dT} + \frac{1}{2} \partial_T^2 \sigma_r \big|_M \right\} \Delta^2 + O(\Delta^3)$$

enforcing $\quad \partial_k \sigma_r \big|_M = \partial_T \sigma_r \big|_M = 0 \quad$ when $\sigma_r = \sigma_r \big|_M = 0 \quad$ (saddle point condit. for M) and the propagation of those properties along the ridge $\left(\sigma_r((h,T)_M + \Delta \bar{d}) = 0 \right)$ we obtain

$$\boxed{ \left(\frac{dg(T)}{dT} \right)^2 + 2 \; \frac{\partial_k (\partial_T \sigma_r)\big|_M}{\partial_k^2 \sigma_r \big|_M} \left(\frac{dg(T)}{dT} \right) = - \frac{\partial_T^2 \sigma_r \big|_M}{\partial_k^2 \sigma_r \big|_M} }$$

Using perturbation analysis we now need to determine $\partial_k (\partial_T \sigma_r)\big|_M$, $\partial_k^2 \sigma_r \big|_M$ and $\partial_T^2 \sigma_r \big|_M$ to determine $d_T g$

2. DERIVATIVES OF $\mathcal{L}$ AND THEIR EVALUATION

Evaluation at M (point on the ridge) $\longrightarrow$ $\quad \mathcal{R}\{\sigma\} = 0 \quad \mathcal{R}\{\partial_n\sigma\} = 0 \quad \mathcal{R}\{\partial_\tau\sigma\} = 0$

$$\mathcal{L} = \begin{bmatrix} (\sigma + i\bar{u}h)(\partial_t^2 - h^2) - ih\,\partial_t^2\bar{u} - \dfrac{Fr}{Re_b}(\partial_t^2 - h^2)^2 & ih \\[2em] -ih(1 + \partial_t\bar{b}) & \sigma + ih\bar{u} - \dfrac{Fr}{Re_b\,Pr}(\partial_t^2 - h^2) \end{bmatrix} \tag{2.1 a}$$

$$\mathcal{L}\big|_M = \begin{bmatrix} (i\mathcal{J}\{\sigma\} + i\bar{u}h)(\partial_t^2 - h^2) - ih\,\partial_t^2\bar{u} - \dfrac{Fr}{Re_b}(\partial_t^2 - h^2)^2 & ih \\[2em] -ih(1 + \partial_t\bar{b}) & i\mathcal{J}\{\sigma\} + ih\bar{u} - \dfrac{Fr}{Re_b\,Pr}(\partial_t^2 - h^2) \end{bmatrix} \tag{2.1 b}$$

$$\partial_n\mathcal{L} = \begin{bmatrix} (\partial_n\sigma + i\bar{u})(\partial_t^2 - h^2) - 2h(\sigma + i\bar{u}h) - i\partial_t^2\bar{u} + 4h\dfrac{Fr}{Re_b}(\partial_t^2 - h^2) & i \\[2em] -i(1 + \partial_t\bar{b}) & \partial_n\sigma + i\bar{u} + 2h\dfrac{Fr}{Re_b\,Pr} \end{bmatrix} \tag{2.2 a}$$

$$\partial_n\mathcal{L}\big|_M = \begin{bmatrix} (i\mathcal{J}\{\partial_n\sigma\} + i\bar{u})(\partial_t^2 - h^2) - 2hi(\mathcal{J}\{\sigma\} + \bar{u}h) - i\partial_t^2\bar{u} + 4h\dfrac{Fr}{Re_b}(\partial_t^2 - h^2) & i \\[2em] -i(1 + \partial_t\bar{b}) & i\mathcal{J}\{\partial_n\sigma\} + i\bar{u} + 2h\dfrac{Fr}{Re_b\,Pr} \end{bmatrix} \tag{2.2 b}$$

$$\partial_\tau\mathcal{L} = \begin{bmatrix} (\partial_\tau\sigma + ih\,\partial_\tau\bar{u})(\partial_t^2 - h^2) - ih\,\partial_t^2\partial_\tau\bar{u} & 0 \\[2em] -ih(\partial_t\partial_\tau\bar{b}) & \partial_\tau\sigma + ih\,\partial_\tau\bar{u} \end{bmatrix} \tag{2.3 a}$$

$$\partial_\tau\mathcal{L}\big|_M = \begin{bmatrix} (i\mathcal{J}\{\partial_\tau\sigma\} + ih\,\partial_\tau\bar{u})(\partial_t^2 - h^2) - ih\,\partial_t^2\partial_\tau\bar{u} & 0 \\[2em] -ih(\partial_t\partial_\tau\bar{b}) & i\mathcal{J}\{\partial_\tau\sigma\} + ih\,\partial_\tau\bar{u} \end{bmatrix} \tag{2.3 b}$$

133

$$\partial^2_{h\tau} \mathcal{L} = \begin{bmatrix} (\partial^2_{h\tau}\sigma + i\partial_\tau\bar{u})(\partial^2_t - h^2) - 2h(\partial_\tau\sigma + ih\,\partial_\tau u) - i\partial^2_t\partial_\tau\bar{u} & 0 \\ \\ i(\partial_t\partial_\tau\bar{b}) & \partial^2_{h\tau}\sigma + i\partial_\tau\bar{u} \end{bmatrix} \qquad (2.4a)$$

$$\partial^2_{h\tau} \mathcal{L}\Big|_n = \begin{bmatrix} (\partial^2_{h\tau}\sigma + i\partial_\tau\bar{u})(\partial^2_t - h^2) - 2h(i\mathcal{J}\{\partial_\tau\sigma\} + ih\,\partial_\tau u) - i\partial^2_t\partial_\tau\bar{u} & 0 \\ \\ i(\partial_t\partial_\tau\bar{b}) & \partial^2_{h\tau}\sigma + i\partial_\tau\bar{u} \end{bmatrix} \qquad (2.4b)$$

$$\partial^2_h \mathcal{L} = \begin{bmatrix} \partial^2_h\sigma\,(\partial^2_t - h^2) - 4h(\partial_n\sigma + i\bar{u}) - 2(\sigma + ih\bar{u}) + 4\,\dfrac{Fr}{Re_b}\,(\partial^2_t - 3h^2) & 0 \\ \\ 0 & \partial^2_h\sigma + 2\,\dfrac{Fr}{Re_b\,Pr} \end{bmatrix} \qquad (2.5a)$$

$$\partial^2_h \mathcal{L} = \begin{bmatrix} \partial^2_h\sigma\,(\partial^2_t - h^2) - 4h(i\mathcal{J}\{\partial_n\sigma\} + i\bar{u}) - 2(i\mathcal{J}\{\sigma\} + ih\bar{u}) + 4\,\dfrac{Fr}{Re_b}\,(\partial^2_t - 3h^2) & 0 \\ \\ 0 & \partial^2_h\sigma + 2\,\dfrac{Fr}{Re_b\,Pr} \end{bmatrix} \qquad (2.5b)$$

$$\partial^2_\tau \mathcal{L} = \begin{bmatrix} (\partial^2_\tau\sigma + ih\,\partial^2_\tau\bar{u})(\partial^2_t - h^2) - ih\,\partial^2_t\partial^2_\tau\bar{u} & 0 \\ \\ -ih(\partial_t\partial^2_\tau\bar{b}) & \partial^2_\tau\sigma + ih\,\partial^2_\tau\bar{u} \end{bmatrix} \qquad (2.6a)$$

$$\partial^2_\tau \mathcal{L}\Big|_H = \partial^2_\tau \mathcal{L} \qquad (2.6b)$$

134

PERTURBATION ANALYSIS

$$L \sim L_M + \Delta k \, \partial_k L|_M + \Delta T \, \partial_T L|_M + \tfrac{1}{2} \Delta k^2 \, \partial_k^2 L|_M + \tfrac{1}{2} \Delta T^2 \partial_T^2 L|_M + \Delta T \Delta k \, \partial_k(\partial_T L)|_M$$

$$\sigma \sim \sigma_M + \Delta k \, \partial_k \sigma|_M + \Delta T \, \partial_T \sigma|_M + \tfrac{1}{2} \Delta k^2 \, \partial_k^2 \sigma|_M + \tfrac{1}{2} \Delta T^2 \partial_T^2 \sigma|_M + \Delta T \Delta k \, \partial_k(\partial_T \sigma)|_M$$

$$\hat{\varphi} \sim \hat{\varphi}_M + \Delta k \, \partial_k \hat{\varphi}|_M + \Delta T \, \partial_T \hat{\varphi}|_M + \tfrac{1}{2} \Delta k^2 \, \partial_k^2 \hat{\varphi}|_M + \tfrac{1}{2} \Delta T^2 \partial_T^2 \hat{\varphi}|_M + \Delta T \Delta k \, \partial_k(\partial_T \hat{\varphi})|_M$$

$$\hat{b} \sim \hat{b}_M + \Delta k \, \partial_k \hat{b}|_M + \Delta T \, \partial_T \hat{b}|_M + \tfrac{1}{2} \Delta k^2 \, \partial_k^2 \hat{b}|_M + \tfrac{1}{2} \Delta T^2 \partial_T^2 \hat{b}|_M + \Delta T \Delta k \, \partial_k(\partial_T \hat{b})|_M$$

indicating $\quad \hat{X} = [\hat{\varphi}(z), \hat{b}(z)]$

$$\hat{X} \sim \hat{X}_M + \Delta k \, \partial_k \hat{X}|_M + \Delta T \, \partial_T \hat{X}|_M + \tfrac{1}{2} \Delta k^2 \, \partial_k^2 \hat{X}|_M + \tfrac{1}{2} \Delta T^2 \partial_T^2 \hat{X}|_M + \Delta T \Delta k \, \partial_k(\partial_T \hat{X})|_M$$

3. ORDER $O(\Delta T)$ — DETERMINATION OF THE AMPLITUDE AND $\partial_T \hat{X}$

$$\mathcal{L}_M \, \partial_T \hat{X}|_M = - (\partial_T \mathcal{L})|_M \, \hat{X}_M \tag{3.1}$$

Solvability condition to find an expression for $\partial_T \sigma$

$$\langle \mathcal{L}_M \partial_T \hat{X}|_M \, | \, \hat{X}_M^+ \rangle = \langle \partial_T \hat{X}|_M \, | \, \mathcal{L}_M^+ \hat{X}_M^+ \rangle = 0$$

$$\langle \mathcal{L}_M \partial_T \hat{X}|_M \, | \, \hat{X}_M^+ \rangle = - \int \hat{X}_M^{+*} (\partial_T \mathcal{L})|_M \, \hat{X}_M \, dz = 0 \tag{3.2}$$

where $\partial_T \mathcal{L}|_M$ is given by (2.3b) just retaining $\partial_T \sigma_r$

$$0 = - \partial_T \sigma \int \hat{\varphi}^{+*} (\partial_z^2 - h^2) \hat{\varphi} \, dz - \iota h \int \hat{\varphi}^+ (\partial_T \bar{u})(\partial_z^2 - h^2)\hat{\varphi} \, dz + \iota h \int \hat{\varphi}^{+*} (\partial_z^2 \partial_T \bar{u}) \hat{\varphi} \, dz^{(1)} +$$

$$+ \iota h \int \hat{b}^{+*} (\partial_z \partial_T \bar{b}) \hat{\varphi} \, dz^{(2)} - \partial_T \sigma \int \hat{b}^{+*} \hat{b} \, dz - \iota h \int \hat{b}^{+*} \partial_T \bar{u} \, \hat{b} \, dz$$

Integrate by parts the two integrals (1) and (2)

$$\iota h \int \hat{\varphi}^{+*} (\partial_z^2 \partial_T \bar{u}) \hat{\varphi} \, dz = \iota h \int (\partial_T \bar{u}) \left[\hat{\varphi}^{+*} \partial_z^2 \hat{\varphi} + \hat{\varphi} \, \partial_z^2 \hat{\varphi}^{+*} + 2 (\partial_z \hat{\varphi})(\partial_z \hat{\varphi}^{+*}) \right] dz$$

$$\iota h \int \hat{b}^{+*} (\partial_z \partial_T \bar{b}) \hat{\varphi} \, dz = - \iota h \int (\partial_T \bar{b}) \left[\hat{b}^{+*} \partial_z \hat{\varphi} + \hat{\varphi} \, \partial_z \hat{b}^{+*} \right] dz$$

$$\partial_\tau \sigma \left\{ \int \hat{\varphi}^{\dagger *}(\partial_z^2 - h^2)\hat{\varphi} + \hat{b}^{\dagger *}\hat{b} \; dz \right\} =$$

$$- ih \int (\partial_\tau \bar{u}) \left[\hat{\varphi}^{\dagger *}(\partial_z^2 - h^2)\hat{\varphi} - \hat{\varphi}^{\dagger *}\partial_z^2\hat{\varphi} - \hat{\varphi}\partial_z^2\hat{\varphi}^{\dagger *} - 2(\partial_z\hat{\varphi})(\partial_z\hat{\varphi}^{\dagger *}) + \hat{b}^{\dagger *}\hat{b} \right] dz$$

$$- ih \int (\partial_\tau \bar{b}) \left[\hat{b}^{\dagger *}\partial_z\hat{\varphi} + \hat{\varphi}\partial_z\hat{b}^{\dagger *} \right] dz$$

Substituting now $\partial_\tau \bar{u}$ and $\partial_\tau \bar{b}$ and rearranging to isolate the unknown amplitude $|A|^2$

$$\partial_\tau \sigma \left\{ \int \hat{\varphi}^{\dagger *}(\partial_z^2 - h^2)\hat{\varphi} + \hat{b}^{\dagger *}\hat{b} \; dz \right\} =$$

$$- ih \, |A|^2 \left\{ \int RSu \left[\hat{\varphi}^{\dagger *}(\partial_z^2 - h^2)\hat{\varphi} - \hat{\varphi}^{\dagger *}\partial_z^2\hat{\varphi} - \hat{\varphi}\partial_z^2\hat{\varphi}^{\dagger *} - 2(\partial_z\hat{\varphi})(\partial_z\hat{\varphi}^{\dagger *}) + \hat{b}^{\dagger *}\hat{b} \right] dz + \right.$$

$$\left. + \int RSb \left[\hat{b}^{\dagger *}\partial_z\hat{\varphi} + \hat{\varphi}\partial_z\hat{b}^{\dagger *} \right] dz \right\} \tag{3.3}$$

$$- ih \left\{ \int \left(\frac{\partial_z^2 \bar{u}}{Reb} + l \right) \left[\hat{\varphi}^{\dagger *}(\partial_z^2 - h^2)\hat{\varphi} - \hat{\varphi}^{\dagger *}\partial_z^2\hat{\varphi} - \hat{\varphi}\partial_z^2\hat{\varphi}^{\dagger *} - 2(\partial_z\hat{\varphi})(\partial_z\hat{\varphi}^{\dagger *}) + \hat{b}^{\dagger *}\hat{b} \right] + \right.$$

$$\left. + \int \left(\frac{\partial_z^2 \bar{b}}{Pr \, Reb} \right) \left[\hat{b}^{\dagger *}\partial_z\hat{\varphi} + \hat{\varphi}\partial_z\hat{b}^{\dagger *} \right] dz \right\}$$

Naming brackets and integrals as follow

$$P = \left[\hat{\varphi}^{\dagger *}(\partial_z^2 - h^2)\hat{\varphi} - \hat{\varphi}^{\dagger *}\partial_z^2\hat{\varphi} - \hat{\varphi}\partial_z^2\hat{\varphi}^{\dagger *} - 2(\partial_z\hat{\varphi})(\partial_z\hat{\varphi}^{\dagger *}) + \hat{b}^{\dagger *}\hat{b} \right] \tag{3.4}$$

$$Q = \left[\hat{b}^{\dagger *}\partial_z\hat{\varphi} + \hat{\varphi}\partial_z\hat{b}^{\dagger *} \right] \tag{3.5}$$

$$\alpha = - ih \left\{ \int \left(\frac{\partial_z^2 \bar{u}}{Reb} + l \right) \left[\hat{\varphi}^{\dagger *}(\partial_z^2 - h^2)\hat{\varphi} - \hat{\varphi}^{\dagger *}\partial_z^2\hat{\varphi} - \hat{\varphi}\partial_z^2\hat{\varphi}^{\dagger *} - 2(\partial_z\hat{\varphi})(\partial_z\hat{\varphi}^{\dagger *}) + \hat{b}^{\dagger *}\hat{b} \right] + \right.$$

$$\left. + \int \left(\frac{\partial_z^2 \bar{b}}{Pr \, Reb} \right) \left[\hat{b}^{\dagger *}\partial_z\hat{\varphi} + \hat{\varphi}\partial_z\hat{b}^{\dagger *} \right] dz \right\} \tag{3.6}$$

$$= - ih \left\{ \int \left(\frac{\partial_z^2 \bar{u}}{Reb} + \bar{l} \right) P \; dz + \int \left(\frac{\partial_z^2 \bar{b}}{Pr \, Rb} \right) Q \; dz \right\}$$

$$\beta = - ih \left\{ \int RSu \left[\hat{\varphi}^{\dagger *}(\partial_z^2 - h^2)\hat{\varphi} - \hat{\varphi}^{\dagger *}\partial_z^2\hat{\varphi} - \hat{\varphi}\partial_z^2\hat{\varphi}^{\dagger *} - 2(\partial_z\hat{\varphi})(\partial_z\hat{\varphi}^{\dagger *}) + \hat{b}^{\dagger *}\hat{b} \right] dz + \right.$$

$$\left. + \int RSb \left[\hat{b}^{\dagger *}\partial_z\hat{\varphi} + \hat{\varphi}\partial_z\hat{b}^{\dagger *} \right] dz \right\} \tag{3.7}$$

$$= - ih \left\{ \int RSu \, P \; dz + \int RSb \, Q \; dz \right\}$$

$$\gamma = \int \hat{\varphi}^{\dagger *}(\partial_z^2 - h^2)\hat{\varphi} + \hat{b}^{\dagger *}\hat{b} \; dz \tag{3.8}$$

136

$$\gamma \partial_1 \sigma = - ih |A|^2 \left\{ \int RSu \ P \ dz - \int RS_b \ a \ dz \right\} - ih \left\{ \int \left(\frac{\partial_z^2 \bar{u}}{Re_b} + \bar{b} \right) P \ dz - \int \left(\frac{\partial_z^2 \bar{b}}{Pr \ Re_b} \right) a \ dz \right\} \quad (3.9)$$

$$= |A|^2 \beta + \alpha$$

We obtain $\partial_1 \sigma = \dfrac{\alpha + |A|^2 \beta}{\gamma}$ then imposing $Re\{\partial_1 \sigma\} = 0$ the equation for the amplitude reads

$$\boxed{|A|^2 = - \frac{Re\{\alpha/\gamma\}}{Re\{\beta/\gamma\}}} \quad (3.10)$$

solve for $\partial_1 \hat{X}$ [BVP (3.1)] using SPQR

— $\mathcal{L} \ \partial_1 \hat{X} = - (\partial_1 \mathcal{L}) \hat{X} + $ solvability condition

— select one specific solution $\quad \partial_1 \hat{X} = (\partial_1 \hat{X})_P + C_T \hat{X}$

— determine C_T using preservation of the norm.

4. ORDER $O(\Delta h)$ — DETERMINATION OF $\partial_n \hat{X}$

$$\mathcal{L}_H \ \partial_n \hat{X}|_H = - (\partial_n \mathcal{L})|_H \ \hat{X}_H \quad (4.1)$$

solvability condition to find an expression for $\partial_n \sigma$

$$\langle \mathcal{L}_H \ \partial_n \hat{X}|_H \ | \ \hat{X}_H^\dagger \rangle = \langle \partial_n \hat{X}|_H \ | \ \mathcal{L}_H^\dagger \hat{X}_H^\dagger \rangle = 0$$

$$\langle \mathcal{L}_H \ \partial_n \hat{X}|_H \ | \ \hat{X}_H^\dagger \rangle = - \int \hat{X}^{\dagger*} (\partial_n \mathcal{L})|_H \ \hat{X} \ dz = 0 \quad (4.2)$$

where $\partial_n \mathcal{L}|_H$ is given by (2.2b) just retaining in this case $\partial_n \sigma$

$$0 = - \partial_n \sigma \int \hat{\varphi}^{\dagger*} (\partial_z^2 - h^2) \hat{\varphi} \ dz - i \int \hat{\varphi}^{\dagger*} \bar{u} (\partial_z^2 - h^2) \hat{\varphi} \ dz + 2ih \ \Im\{\sigma\} \int \hat{\varphi}^{\dagger*} \hat{\varphi} \ dz + 2ih^2 \int \hat{\varphi}^{\dagger*} \bar{u} \ \hat{\varphi} \ dz$$

$$+ i \int \hat{\varphi}^{\dagger*} (\partial_z^2 \bar{u}) \hat{\varphi} \ dz \overset{(1)}{\quad} - 4h \ \frac{Fr}{Re_b} \int \hat{\varphi}^{\dagger*} (\partial_z^2 - h^2) \hat{\varphi} \ dz - i \int \hat{\varphi}^{\dagger*} \hat{b} \ dz +$$

$$+ i \int \hat{b}^{\dagger*} \hat{\varphi} \ dz + i \int \hat{b}^{\dagger*} (\partial_z \bar{b}) \hat{\varphi} \ dz \overset{(2)}{\quad} - \partial_n \sigma \int \hat{b}^{\dagger*} \hat{b} \ dz - i \int \hat{b}^{\dagger*} \bar{u} \ \hat{b} \ dz - 2h \ \frac{Fr}{Pr \ Re_b} \int \hat{b}^{\dagger*} \hat{b} \ dz$$

137

$$\partial_n \sigma \left\{ \int \hat{\psi}^{\dagger *} (\partial_z^2 - h^2) \hat{\psi} + \hat{b}^{\dagger *} \hat{b} \right\} =$$

$$-i \int \bar{u} \left[\hat{\psi}^{\dagger *} (\partial_z^2 - h^2) \hat{\psi} - \hat{\psi}^{\dagger *} \partial_z^2 \hat{\psi} - \hat{\psi} \partial_z^2 \hat{\psi}^{\dagger *} - 2(\partial_z \hat{\psi})(\partial_z \hat{\psi}^{\dagger *}) + \hat{b}^{\dagger *} \hat{b} - 2h^2 \hat{\psi}^{\dagger *} \hat{\psi} \right] dz$$

$$-i \int \bar{b} \left[\hat{b}^{\dagger *} \partial_z \hat{\psi} + \hat{\psi} \partial_z \hat{b}^{\dagger *} \right] dz \quad -i \int \left[\hat{\psi}^{\dagger *} \hat{b} - \hat{b}^{\dagger *} \hat{\psi} \right] dz + 2hi \, \Im\{\sigma\} \int \hat{\psi}^{\dagger *} \hat{\psi} \, dz$$

$$- 2h \frac{Fr}{Re_b} \int \left[2 \hat{\psi}^{\dagger *} (\partial_z^2 - h^2) \hat{\psi} + \frac{1}{Pr} \hat{b}^{\dagger *} \hat{b} \right] dz$$

where integrals (1) and (2) have been integrated by parts

Naming the new brakets

$$R = \left[2 \hat{\psi}^{\dagger *} (\partial_z^2 - h^2) \hat{\psi} + \frac{1}{Pr} \hat{b}^{\dagger *} \hat{b} \right] \tag{4.3}$$

$$\pi = \left[\hat{\psi}^{\dagger *} \hat{b} - \hat{b}^{\dagger *} \hat{\psi} \right] \tag{4.4}$$

$$\gamma \, \partial_n \sigma = -i \int \bar{u} \left[P - 2h^2 \hat{\psi}^{\dagger *} \hat{\psi} \right] dz + i \int \bar{b} \, Q \, dz - i \int \pi \, dz - 2h \frac{Fr}{Re_b} \int R \, dz \tag{4.5}$$

$$+ 2ih \, \Im\{\sigma\} \int \hat{\psi}^{\dagger *} \hat{\psi} \, dz$$

Then enforcing $Re\{\partial_n \sigma\} = 0 \longrightarrow$ Differently from the 2D model, here it does not give anything useful. Then don't.

Solve for $\partial_n \hat{X}$ [BVP (4.1)] using SPQR and select a specific solution using the preservation of the norm

$$\partial_n \hat{X} = (\partial_n \hat{X})_P + C_n \hat{X}$$

$$\mathcal{L}_M \, \partial_n^2 \hat{X}|_M = - (\partial_n^2 \mathcal{L})|_M \, \hat{X}_M - 2 (\partial_n \mathcal{L})_M (\partial_n \hat{X})|_M \tag{5.1}$$

solvability condition to find an expression for $\partial_n^2 \sigma$

$$\langle \mathcal{L}_M \, \partial_n^2 \hat{X}|_M \,|\, \hat{X}_M^+ \rangle = \langle \partial_n^2 \hat{X}|_M \,|\, \mathcal{L}_n^+ \hat{X}_M^+ \rangle = 0$$

$$\langle \mathcal{L}_M \, \partial_n^2 \hat{X}_M \,|\, \hat{X}_M^+ \rangle = - \int \hat{X}^{+*} (\partial_n^2 \mathcal{L})|_M \, \hat{X} \, dz - 2 \int \hat{X}^{+*} (\partial_n \mathcal{L})|_M (\partial_n \hat{X})|_M \, dz \tag{5.2}$$

where $\partial_n^2 \mathcal{L}|_M$, $\partial_n \mathcal{L}|_M$ are given by (2.2b),(2.5b) and $\partial_n \hat{X}$ has been determined at order Δh

$$0 = - \partial_n^2 \sigma \int \hat{\varphi}^{+*} (\partial_z^2 - h^2) \hat{\varphi} \, dz + 6ih \int \hat{\varphi}^{+*} \bar{u} \hat{\varphi} \, dz - 4 \frac{Fr}{Re_b} \int \hat{\varphi}^{+*} (\partial_z^2 - h^2) \hat{\varphi} \, dz + 8h^2 \frac{Fr}{Re_b} \int \hat{\varphi}^{+*} \hat{\varphi} \, dz +$$

$$+ 2i \left(\Im\{\sigma\} + 2h\Im\{\partial_n \sigma\} \right) \int \hat{\varphi}^{+*} \hat{\varphi} \, dz +$$

$$- \partial_n^2 \sigma \int \hat{b}^{+*} \hat{b} \, dz - 2 \frac{Fr}{Pr\,Re_b} \int \hat{b}^{+*} \hat{b} \, dz +$$

$$- 2i \int \hat{\varphi}^{+*} \bar{u} (\partial_z^2 - h^2) \partial_n \hat{\varphi} \, dz + 4ih^2 \int \hat{\varphi}^{+*} \bar{u} \, \partial_n \hat{\varphi} \, dz + 2i \int \hat{\varphi}^{+*} (\partial_z^2 \bar{u}) \partial_n \hat{\varphi} \, dz +$$

$$- 8h \frac{Fr}{Rb} \int \hat{\varphi}^{+*} (\partial_z^2 - h^2) \partial_n \hat{\varphi} \, dz +$$

$$- 2i \Im\{\partial_n \sigma\} \int \hat{\varphi}^{+*} (\partial_z^2 - h^2) \partial_n \hat{\varphi} \, dz + 4hi \Im\{\sigma\} \int \hat{\varphi}^{+*} \partial_n \hat{\varphi} \, dz - 2i \int \hat{\varphi}^{+*} \partial_n \hat{b} \, dz$$

$$+ 2i \int \hat{b}^{+*} (\partial_z \bar{b}) \partial_n \hat{\varphi} \, dz + 2i \int \hat{b}^{+*} \partial_n \hat{\varphi} \, dz - 2i \Im\{\partial_n \sigma\} \int \hat{b}^{+*} \partial_n \hat{b} \, dz - 2i \int \hat{b}^{+*} \bar{u} \, \partial_n \hat{b} \, dz +$$

$$- 4h \frac{Fr}{Pr\,Re_b} \int \hat{b}^{+*} \partial_n \hat{b} \, dz$$

$$\partial_n^2 \sigma \left\{ \int \hat{\varphi}^{+*} (\partial_z^2 - h^2) \hat{\varphi} + \hat{b}^{+*} \hat{b} \, dz \right\} =$$

$$6ih \int \hat{\varphi}^{+*} \bar{u} \hat{\varphi} \, dz - 2 \frac{Fr}{Re_b} \int \left(2 \hat{\varphi}^{+*} (\partial_z^2 - h^2) \hat{\varphi} + \frac{1}{Pr} \hat{b}^{+*} \hat{b} \right) dz + 8h^2 \frac{Fr}{Re_b} \int \hat{\varphi}^{+*} \hat{\varphi} \, dz +$$

$$- 2i \int \bar{u} \left[\hat{\varphi}^{+*} (\partial_z^2 - h^2) \partial_n \hat{\varphi} - \hat{\varphi}^{+*} (\partial_z^2 \partial_n \hat{\varphi}) - (\partial_n \hat{\varphi})(\partial_z^2 \hat{\varphi}^{+*}) - 2 (\partial_z \hat{\varphi}^{+*})(\partial_z \partial_n \hat{\varphi}) \right.$$

$$\left. + \hat{b}^{+*} \partial_n \hat{b} - 2h^2 \hat{\varphi}^{+*} \partial_n \hat{\varphi} \right] dz$$

$$- 2i \int \bar{b} \left[\hat{b}^{+*} (\partial_z \partial_n \hat{\varphi}) + (\partial_n \hat{\varphi})(\partial_z \hat{b}^{+*}) \right] dz$$

$$- 4h \frac{Fr}{Re_b} \int \left[2 \hat{\varphi}^{+*} (\partial_z^2 - h^2) \partial_n \hat{\varphi} + \frac{1}{Pr} \hat{b}^{+*} \partial_n \hat{b} \right] dz - 2i \int \hat{\varphi}^{+*} \partial_n \hat{b} - \hat{b}^{+*} \partial_n \hat{\varphi} \, dz$$

$$+ 2i \Im\{\partial_n \sigma\} \int \left[2h \hat{\varphi}^{+*} \hat{\varphi} - \hat{\varphi}^{+*} (\partial_z^2 - h^2) \partial_n \hat{\varphi} - \hat{b}^{+*} \partial_n \hat{b} \right] dz + 2i \Im\{\sigma\} \int \left[\hat{\varphi}^{+*} \hat{\varphi} + 2h \hat{\varphi}^{+*} \partial_n \hat{\varphi} \right] dz$$

Naming the new brakets

$$P_h = \left[\hat{\varphi}^{+*}(\partial_t^2 - h^2) \partial_n \hat{\varphi} - \hat{\varphi}^{+*}(\partial_t^2 \partial_n \hat{\varphi}) - (\partial_n \hat{\varphi})(\partial_t^2 \hat{\varphi}^{+*}) - 2(\partial_t \hat{\varphi}^{+*})(\partial_t \partial_n \hat{\varphi}) + \hat{b}^{+*} \partial_n \hat{b} \right] \tag{5.3}$$

$$Q_h = \left[\hat{b}^{+*}(\partial_t \partial_n \hat{\varphi}) + (\partial_n \hat{\varphi})(\partial_t \hat{b}^{+*}) \right] \tag{5.4}$$

$$R_h = \left[2 \hat{\varphi}^{+*}(\partial_t^2 - h^2) \partial_n \hat{\varphi} + \frac{1}{Pr} \hat{b}^{+*} \partial_n \hat{b} \right] \tag{5.5}$$

$$\pi_h = \hat{\varphi}^{+*} \partial_n \hat{b} - \hat{b}^{+*} \partial_n \hat{\varphi} \ dt \tag{5.6}$$

where P_n, Q_n, R_n are the same as P, Q, R just with $\partial_n \hat{\varphi}$ instead of $\hat{\varphi}$ (the sub h does not indicate h-derivative)

$$
\begin{aligned}
\partial_{h}^2 \sigma = \ & -\frac{2i}{\gamma} \int \bar{u} \left[P_n - 2h^2 \hat{\varphi}^{+*} \partial_n \hat{\varphi} - 3h \hat{\varphi}^{+*} \hat{\varphi} \right] dt \\
& -\frac{2i}{\gamma} \int \bar{b} \ Q_n \ dt + \\
& -\frac{2}{\gamma} \frac{Fr}{Re_b} \int (R + 2h R_h - 4h^2 \hat{\varphi}^{+*} \hat{\varphi}) dt - 2i \int \pi_h \ dt + \\
& +\frac{2i}{\gamma} \Im\{\partial_n \sigma\} \int \left[2h \hat{\varphi}^{+*} \hat{\varphi} - \hat{\varphi}^{+*}(\partial_t^2 - h^2) \partial_n \hat{\varphi} - \hat{b}^{+*} \partial_n \hat{b} \right] dt + \\
& + 2i \Im\{\sigma\} \int \left[\hat{\varphi}^{+*} \hat{\varphi} + 2h \hat{\varphi}^{+*} \partial_n \hat{\varphi} \right] dt
\end{aligned}
\tag{5.7}
$$

6. ORDER $O(\Delta h \Delta \tau)$ — DETERMINATION OF $\partial_{h\tau}^2 \sigma$

$$\mathcal{L}_H \partial_{h\tau}^2 \hat{X}|_H = -(\partial_{h\tau}^2 \mathcal{L})|_H \hat{X}_H - (\partial_\tau \mathcal{L})|_H (\partial_n \hat{X})|_H - (\partial_n \mathcal{L})|_H (\partial_\tau \hat{X})|_H \tag{6.1}$$

Solvability condition to find an expression for $\partial_{h\tau}^2 \sigma$

$$\left\langle \mathcal{L}_H \partial_{h\tau}^2 \hat{X}|_H \mid \hat{X}^+ \right\rangle = \left\langle \partial_{h\tau}^2 \hat{X}|_H \mid \mathcal{L}_H^+ \hat{X}_H^+ \right\rangle = 0$$

$$\left\langle \mathcal{L}_H \partial_{h\tau}^2 \hat{X}|_H \mid \hat{X}^+ \right\rangle = -\int \hat{X}^{+*}(\partial_{h\tau}^2 \mathcal{L})|_H \hat{X} \ dt - \int \hat{X}^{+*}(\partial_\tau \mathcal{L})|_H (\partial_n \hat{X})|_H \ dt + \tag{6.2}$$

$$-\int \hat{X}^{+*}(\partial_n \mathcal{L})|_H (\partial_\tau \hat{X})|_H \ dt = 0$$

where $\partial_n \mathcal{L}|_H$, $\partial_\tau \mathcal{L}|_H$, $\partial_{\tau n} \mathcal{L}|_H$ are given by (2.2b), (2.3b), (2.4b) and $\partial_n \hat{X}|_H$, $\partial_\tau \hat{X}|_H$ have been determined at orders Δh and $\Delta \tau$.

140

$$0 = -\partial^2_{h\tau}\sigma \int \hat{\psi}^{+*}(\partial^2_z - h^2)\hat{\psi}\, dz \;-\; i\int \hat{\psi}^{+*}\partial_\tau \bar{u}(\partial^2_z - h^2)\hat{\psi}\, dz \;+\; 2ih\, \mathcal{J}\{\partial_\tau\sigma\}\int \hat{\psi}^{+*}\hat{\psi}\, dz$$

$$+\; 2ih^2\int \hat{\psi}^{+*}\partial_\tau \bar{u}\,\hat{\psi}\, dz \;+\; i\int \hat{\psi}^{+*}(\partial^2_z \partial_\tau \bar{u})\hat{\psi}\, dz \;-\; i\int \hat{b}^{+*}(\partial_z \partial_\tau \bar{b})\hat{\psi}\, dz \overset{(1)}{}\; -\; \partial^2_{h\tau}\sigma\int \hat{b}^{+*}\hat{b}\, dz \overset{(2)}{}$$

$$-\; i\int \hat{b}^{+*}\partial_\tau \bar{u}\,\hat{b}\, dz \;+$$

$$-\; i\mathcal{J}\{\partial_\tau\sigma\}\int \hat{\psi}^{+*}(\partial^2_z - h^2)\partial_n\hat{\psi}\, dz \;-\; ih\int \hat{\psi}^{+*}\partial_\tau \bar{u}(\partial^2_z - h^2)\partial_n\hat{\psi}\, dz \;+\; ih\int \hat{\psi}^{+*}(\partial^2_z \partial_\tau \bar{u})\partial_n\hat{\psi}\, dz \overset{(3)}{}\;+$$

$$+\; ih\int \hat{b}^{+*}(\partial_z \partial_\tau \bar{b})\partial_n\hat{\psi}\, dz \overset{(4)}{}\;-\; i\mathcal{J}\{\partial_\tau\sigma\}\int \hat{b}^{+*}\partial_n\hat{b}\, dz \;-\; ih\int \hat{b}^{+*}\partial_\tau \bar{u}\,\partial_n\hat{b}\, dz \;+$$

$$-\; i\mathcal{J}\{\partial_n\sigma\}\int \hat{\psi}^{+*}(\partial^2_z - h^2)\partial_\tau\hat{\psi}\, dz \;-\; i\int \hat{\psi}^{+*}\bar{u}(\partial^2_z - h^2)\partial_\tau\hat{\psi}\, dz \;+\; 2ih\,\mathcal{J}\{\sigma\}\int \hat{\psi}^{+*}\partial_\tau\hat{\psi}\, dz \;+$$

$$+\; 2ih^2\int \hat{\psi}^{+*}\bar{u}\,\partial_\tau\hat{\psi}\, dz \;+\; i\int \hat{\psi}^{+*}(\partial^2_z \bar{u})\partial_\tau\hat{\psi}\, dz \;-\; 4h\,\frac{Fr}{Re_b}\int \hat{\psi}^{+*}(\partial^2_z - h^2)\partial_\tau\hat{\psi}\, dz \overset{(5)}{}\;-\; i\int \hat{\psi}^{+*}\partial_\tau\hat{b}\, dz \;+$$

$$+\; i\int \hat{b}^{+*}\partial_\tau\hat{\psi}\, dz \;+\; i\int \hat{b}^{+*}(\partial_z \bar{b})\partial_\tau\hat{\psi}\, dz \overset{(6)}{}\;-\; i\mathcal{J}\{\partial_n\sigma\}\int \hat{b}^{+*}\partial_\tau\hat{b}\, dz \;-\; i\int \hat{b}^{+*}\bar{u}\,\partial_\tau\hat{b}\, dz \;-$$

$$-\; 2h\,\frac{Fr}{Pr\,Re_b}\int \hat{b}^{+*}\partial_\tau\hat{b}\, dz \, .$$

$$\partial^2_{h\tau}\sigma\left\{\int \hat{\psi}^{+*}(\partial^2_z - h^2)\hat{\psi} + \hat{b}^{+*}\hat{b}\, dz\right\} = \overset{\displaystyle \frac{r}{k}\,i\mathcal{J}(\partial_\tau\sigma)\,\cdot}{}$$

$$\boxed{-\; i\int \partial_\tau \bar{u}\left[\hat{\psi}^{+*}(\partial^2_z - h^2)\hat{\psi}\, dz - \hat{\psi}^{+*}\partial^2_z\hat{\psi} - \hat{\psi}\partial^2_z\hat{\psi}^{+*} - 2(\partial_z\hat{\psi})(\partial_z\hat{\psi}^{*}) + \hat{b}^{+*}\hat{b} - 2h^2\hat{\psi}^{+*}\hat{\psi}\right]dz \;+\; i\int \partial_\tau \bar{b}\left[\hat{b}^{+*}\partial_z\hat{\psi} + \hat{\psi}\partial_z\hat{b}^{+*}\right]dz \;+}$$

$$-\; ih\int \partial_\tau \bar{u}\left[\hat{\psi}^{+*}(\partial^2_z - h^2)\partial_n\hat{\psi} - \hat{\psi}^{+*}(\partial^2_z \partial_n\hat{\psi}) - (\partial_n\hat{\psi})(\partial^2_z\hat{\psi}^{+*}) - 2(\partial_z \partial_n\hat{\psi})(\partial_z\hat{\psi}^{+*}) + \hat{b}^{+*}\partial_n\hat{b}\right]dz$$

$$-\; ih\int \partial_\tau \bar{b}\left[\hat{b}^{+*}\partial_z\partial_n\hat{\psi} + (\partial_n\hat{\psi})\partial_z\hat{b}^{+*}\right]dz$$

$$-\; i\int \bar{u}\left[\hat{\psi}^{+*}(\partial^2_z - h^2)\partial_\tau\hat{\psi} - \hat{\psi}^{+*}(\partial^2_z \partial_\tau\hat{\psi}) - (\partial_\tau\hat{\psi})(\partial^2_z\hat{\psi}^{+*}) - 2(\partial_z \partial_\tau\hat{\psi})(\partial_z\hat{\psi}^{+*}) \;+\right.$$
$$\left.+\; \hat{b}^{+*}\partial_\tau\hat{b} - 2h^2\hat{\psi}^{+*}\partial_\tau\hat{\psi}\right]dz$$

$$+\; i\int \bar{b}\left[\hat{b}^{+*}(\partial_z \partial_\tau\hat{\psi}) + (\partial_\tau\hat{\psi})(\partial_z\hat{b}^{+*})\right]dz \;-\; 2h\,\frac{Fr}{Re_b}\int \left(2\hat{\psi}^{+*}(\partial^2_z - h^2)\partial_\tau\hat{\psi} + \frac{1}{Pr}\hat{b}^{+*}\partial_\tau\hat{b}\right)dz$$

$$-\; i\int \left(\hat{\psi}^{+*}\partial_\tau\hat{b} - \hat{b}^{+*}\partial_\tau\hat{\psi}\right)dz$$

$$-\; i\mathcal{J}\{\partial_\tau\sigma\}\int \left[2h\hat{\psi}^{+*}\hat{\psi} + \hat{\psi}^{+*}(\partial^2_z - h^2)\partial_n\hat{\psi} + \hat{b}^{+*}\partial_n\hat{b}\right]dz \;-\; i\mathcal{J}\{\partial_n\sigma\}\int \left[\hat{\psi}^{+*}(\partial^2_z - h^2)\partial_\tau\hat{\psi} + \hat{b}^{+*}\partial_\tau\hat{b}\right]dz$$

$$+\; 2ih\,\mathcal{J}\{\sigma\}\int \hat{\psi}^{+*}\partial_\tau\hat{\psi}\, dz$$

where integrals (1)-(6) have been integrated by parts.

The expression boxed in red

$$-i \int \partial_t \bar{u} \, P \, dz \; + \; i \int \partial_t \bar{b} \, Q \, dz \; =$$

$$-i \, |A|^2 \left\{ \int (RSu \, P - RSb \, Q) \, dz \right\} \; - i \left\{ \int \left(\frac{\partial_z^2 \bar{u}}{Reb} + \breve{I} \right) P - \left(\frac{\partial_z^2 \bar{b}}{Pr \, Reb} \right) Q \; dz \right\} \; = \; \frac{\gamma \partial_\tau \sigma}{h} \rightarrow \frac{\gamma}{h} i \Im\{\partial_\tau \sigma\}$$

$$\text{since} \quad Re\{\partial_\tau \sigma\} = 0$$

As done before, naming the new brackets

$$P_T = \left[\; \hat{\varphi}^{\dagger *} (\partial_z^2 - h^2) \partial_\tau \hat{\varphi} \; - \; \hat{\varphi}^{\dagger *} (\partial_z^2 \partial_\tau \hat{\varphi}) - (\partial_\tau \hat{\varphi})(\partial_z^2 \hat{\varphi}^{\dagger *}) - 2 (\partial_z \partial_\tau \hat{\varphi})(\partial_z \hat{\varphi}^{\dagger *}) + \hat{b}^{\dagger *} \partial_\tau \hat{b} \; \right] \qquad (6.3)$$

$$Q_T = \left[\; \hat{b}^{\dagger *} (\partial_z \partial_\tau \hat{\varphi}) + (\partial_\tau \hat{\varphi})(\partial_z \hat{b}^{\dagger *}) \right] \qquad (6.4)$$

$$\qquad \qquad \qquad \qquad \qquad \qquad (6.5)$$

$$R_T = \left[2 \hat{\varphi}^{\dagger *} (\partial_z^2 - h^2) \partial_\tau \hat{\varphi} \; + \; \frac{1}{Pr} \hat{b}^{\dagger *} \partial_\tau \hat{b} \right]$$

$$\qquad \qquad \qquad \qquad \qquad \qquad (6.6)$$

$$\pi_T = \left[\hat{\varphi}^{\dagger *} \partial_\tau \hat{b} - \hat{b}^{\dagger *} \partial_\tau \hat{\varphi} \right]$$

$$\gamma \partial_{h\tau}^2 \sigma = 2i \, h^2 \int \hat{\varphi}^{\dagger *} \bar{u} \, \hat{\varphi} \, dz \; +$$

$$\qquad - ih \int \partial_\tau \bar{u} \, P_n \, dz \; - \; ih \int \partial_\tau \bar{b} \, Q_n \, dz$$

$$\qquad - i \int \bar{u} \left[P_T - 2h^2 \hat{\varphi}^{\dagger *} \partial_\tau \hat{\varphi} \right] dz \; - \; i \int \bar{b} \, Q_T \, dz \; - \; 2h \frac{Fr}{Reb} \int R_T \, dz \; - i \int \pi_T \, dz$$

$$\qquad - i \Im\{\partial_\tau \sigma\} \int \left[-2h \hat{\varphi}^{\dagger *} \hat{\varphi} + \hat{\varphi}^{\dagger *}(\partial_z^2 - h^2) \partial_n \hat{\varphi} + \hat{b}^{\dagger *} \partial_n \hat{b} \; \boxed{ + h \hat{\varphi}^{\dagger *}(\partial_z^2 - h^2) \hat{\varphi} \; + h \hat{b}^{\dagger *} \hat{b} } \; \right] dz \qquad \frac{h}{\gamma}$$

$$\qquad - i \Im\{\partial_n \sigma\} \int \left[\hat{\varphi}^{\dagger *}(\partial_z^2 - h^2) \partial_\tau \hat{\varphi} + \hat{b}^{\dagger *} \partial_\tau \hat{b} \right] dz \; + \; ih \, \Im\{\sigma\} \int \hat{\varphi}^{\dagger *} \partial_\tau \hat{\varphi} \, dz$$

substituting the evolution equations $\partial_\tau \bar{u}, \partial_\tau \bar{b}$

$$\boxed{\begin{aligned}
\partial_{h\tau}^2 \sigma = \frac{1}{\gamma} \Bigg\{ & 2i \, h^2 \int \hat{\varphi}^{\dagger *} \bar{u} \, \hat{\varphi} \, dz \; + \\
& - ih \, |A|^2 \left\{ \int (RSu \, P_n - RSb \, Q_n) \, dz \right\} - ih \left\{ \int \left(\frac{\partial_z^2 \bar{u}}{Reb} + \breve{I} \right) P_T - \left(\frac{\partial_z^2 \bar{b}}{Pr \, Reb} \right) Q_T \; dz \right\} \\
& - i \int \bar{u} \left[P_T - 2h^2 \hat{\varphi}^{\dagger *} \partial_\tau \hat{\varphi} \right] dz + i \int \bar{b} \, Q_T \, dz - 2h \frac{Fr}{Reb} \int R_T \, dz - i \int \pi_T \, dz \Bigg\} \\
& - i \Im\{\partial_\tau \sigma\} \int \left[2h \hat{\varphi}^{\dagger *} \hat{\varphi} + \hat{\varphi}^{\dagger *}(\partial_z^2 - h^2) \partial_n \hat{\varphi} + \hat{b}^{\dagger *} \partial_n \hat{b} - \frac{1}{h} \hat{\varphi}^{\dagger *}(\partial_z^2 - h^2) \hat{\varphi} - \frac{1}{h} \hat{b}^{\dagger *} \hat{b} \right] dz \\
& - i \Im\{\partial_n \sigma\} \int \left[\hat{\varphi}^{\dagger *}(\partial_z^2 - h^2) \partial_\tau \hat{\varphi} + \hat{b}^{\dagger *} \partial_\tau \hat{b} \right] dz + 2 \, ih \, \Im\{\sigma\} \int \hat{\varphi}^{\dagger *} \partial_\tau \hat{\varphi} \, dz
\end{aligned}} \qquad (6.7)$$

142

$$\mathcal{L}_H \, \partial_T^2 \hat{X}|_H = -(\partial_T^2 \mathcal{L})|_H \, \hat{X}_H - 2(\partial_T \mathcal{L})|_H (\partial_T \hat{X})|_H \tag{7.1}$$

solvability condition to find an expression for $\partial_T^2 \sigma$

$$\langle \mathcal{L}_H \, \partial_T^2 \hat{X}|_H \mid \hat{X}_H^\dagger \rangle = \langle \partial_T^2 \hat{X}|_H \mid \mathcal{L}_H^\dagger \hat{X}_H^\dagger \rangle = 0$$

$$\langle \mathcal{L}_H \, \partial_T^2 \hat{X}|_H \mid \hat{X}_H^\dagger \rangle = -\int \hat{X}^{\dagger *} (\partial_T^2 \mathcal{L})|_H \, \hat{X} \, dz - 2 \int \hat{X}^{\dagger *} (\partial_T \mathcal{L})|_H (\partial_T \hat{X})|_H \, dz \tag{7.2}$$

where $\partial_T \mathcal{L}|_H$, $\partial_T^2 \mathcal{L}|_H$ are given by (2.3b) and (2.6b) and $\partial_T \hat{X}|_H$ has been determined at order ΔT

$$
\begin{aligned}
0 = \ & -\partial_T^2 \sigma \int \hat{\psi}^{\dagger *} (\partial_z^2 - h^2) \hat{\psi} \, dz - ih \int \hat{\psi}^{\dagger *} (\partial_T^2 \bar{u})(\partial_z^2 - h^2) \hat{\psi} \, dz + ih \int \hat{\psi}^{\dagger *} (\partial_z^2 \partial_T^2 \bar{u}) \hat{\psi} \, dz \; {}^{(1)} + \\
& + ih \int \hat{b}^{\dagger *} (\partial_z \partial_T^2 \bar{b}) \hat{\psi} \, dz \; {}^{(2)} - \partial_T^2 \sigma \int \hat{b}^{\dagger *} \hat{b} \, dz - ih \int \hat{b}^{\dagger *} (\partial_T^2 \bar{u}) \hat{b} \, dz + \\
& - 2i \Im\{\partial_T \sigma\} \int \hat{\psi}^{\dagger *} (\partial_z^2 - h^2) \partial_T \hat{\psi} \, dz - 2ih \int \hat{\psi}^{\dagger *} (\partial_T \bar{u})(\partial_z^2 - h^2)(\partial_T \hat{\psi}) \, dz \\
& \hspace{6cm} + 2ih \int \hat{\psi}^{\dagger *} (\partial_z^2 \partial_T \bar{u})(\partial_T \hat{\psi}) \, dz \; {}^{(3)} + \\
& + 2ih \int \hat{b}^{\dagger *} (\partial_z \partial_T \bar{b})(\partial_T \hat{\psi}) \, dz \; {}^{(4)} - 2i \Im\{\partial_T \sigma\} \int \hat{b}^{\dagger *} \partial_T \hat{b} \, dz - 2ih \int \hat{b}^{\dagger *} (\partial_T \bar{u}) \partial_T \hat{b} \, dz
\end{aligned}
$$

Integrating by parts integrals (1)–(4)

$$
\begin{aligned}
\partial_T^2 \sigma \left\{ \int \hat{\psi}^{\dagger *} (\partial_z^2 - h^2) \hat{\psi} + \hat{b}^{\dagger *} \hat{b} \; dz \right\} = \ & \\
& - ih \int \partial_T^2 \bar{u} \left[\hat{\psi}^{\dagger *} (\partial_z^2 - h^2) \hat{\psi} - \hat{\psi}^{\dagger *} \partial_z^2 \hat{\psi} - \hat{\psi} \partial_z^2 \hat{\psi}^{\dagger *} - 2(\partial_z \hat{\psi})(\partial_z \hat{\psi}^{\dagger *}) + \hat{b}^{\dagger *} \hat{b} \right] dz + \\
& - ih \int \partial_T^2 \bar{b} \left[\hat{b}^{\dagger *} \partial_z \hat{\psi} + \hat{\psi} \partial_z \hat{b}^{\dagger *} \right] dz + \\
& - 2ih \int \partial_T \bar{u} \left[\hat{\psi}^{\dagger *} (\partial_z^2 - h^2) \partial_T \hat{\psi} - \hat{\psi}^{\dagger *} (\partial_z^2 \partial_T \hat{\psi}) - (\partial_T \hat{\psi})(\partial_z^2 \hat{\psi}^{\dagger *}) + \right. \\
& \hspace{3cm} \left. - 2(\partial_z \partial_T \hat{\psi})(\partial_z \hat{\psi}^{\dagger *}) + \hat{b}^{\dagger *} \partial_T \hat{b} \right] dz + \\
& - 2ih \int \partial_T \bar{b} \left[\hat{b}^{\dagger *} \partial_z \partial_T \hat{\psi} + \partial_T \hat{\psi} \, \partial_z \hat{b}^{\dagger *} \right] dz + \\
& - 2i \Im\{\partial_T \sigma\} \int \left[\hat{\psi}^{\dagger *} (\partial_z^2 - h^2) \partial_T \hat{\psi} + \hat{b}^{\dagger} \partial_T \hat{b} \right] dz +
\end{aligned}
$$

143

$$\gamma \, \partial_T^2 \sigma = - ih \int (\partial_T^2 \bar{u}) \, P \, dz \; - \; ih \int (\partial_T^2 \bar{b}) \, Q \, dz$$

$$- 2ih \int (\partial_T \bar{u}) \, P_T \, dz \; - \; 2ih \int (\partial_T \bar{b}) \, Q_T \, dz \qquad (7.3)$$

$$- 2i \, \mathcal{J}\{\partial_T \sigma\} \int \left[\hat{\varphi}^{\dagger *} (\partial_z^2 - h^2) \partial_T \hat{\varphi} + \hat{b}^\dagger \partial_T \hat{b} \right] dz$$

given $\partial_T \bar{u} = |A|^2 \, RS_u + \dfrac{\partial_z^2 \bar{u}}{Re_b} + \bar{f}$ and $\partial_T \bar{b} = |A|^2 \, RS_b + \dfrac{\partial_z^2 \bar{b}}{Pr \, Re_b}$ we have to

compute

$$\partial_T^2 \bar{u} = \partial_T (|A|^2) RS_u + |A|^2 \partial_T (RS_u) + \dfrac{\partial_z^2 \partial_T \bar{u}}{Re_b} + \partial_T \bar{f} \qquad (7.4)$$

$$\partial_T^2 \bar{b} = \partial_T (|A|^2) RS_b + |A|^2 \partial_T (RS_b) + \dfrac{\partial_z^2 \partial_T \bar{b}}{Pr \, Re_b} \qquad (7.5)$$

$$\gamma \, \partial_T^2 \sigma = - ih \, \partial_T(|A|^2) \int RS_u \, P \, dz \quad - ih \, |A|^2 \int (\partial_T RS_u) P \, dz \quad - ih \int \left(\dfrac{\partial_z^2 \partial_T \bar{u}}{Re_b} \right) P \, dz \; - \; ih \int \partial_T \bar{f} \, P \, dz$$

$$- ih \, \partial_T(|A|^2) \int RS_b \, Q \, dz \; - \; ih \, |A|^2 \int (\partial_T RS_b) Q \, dz \; - \; ih \int \left(\dfrac{\partial_z^2 \partial_T \bar{b}}{Pr \, Re_b} \right) Q \, dz \qquad (7.6)$$

$$- 2ih \int (\partial_T \bar{u}) \, P_T \, dz \quad - \; 2ih \int (\partial_T \bar{b}) \, Q_T \, dz \; - \; 2i \, \mathcal{J}\{\partial_T \sigma\} \int \left[\hat{\varphi}^{\dagger *} (\partial_z^2 - h^2) \partial_T \hat{\varphi} + \hat{b}^\dagger \partial_T \hat{b} \right] dz$$

The integrals containing $\partial_T^2 \bar{u}$ and $\partial_T^2 \bar{b}$ require to take

- T-derivative of Reynolds Stresses RS_u and RS_b
- T-derivative of the Amplitude (which contains RS inside β)

since both Reynolds stresses and the Amplitude are given by the neutrally stable

eigenmode on the ridge, the T-derivative is a directional derivative :

$$\hat{\varphi} \rightarrow \hat{\phi} \qquad \partial_T \hat{\phi} = d_T \hat{\varphi} = \partial_T \hat{\varphi} + \partial_h \hat{\varphi} \, \dfrac{dq_-}{dT}$$

$$\hat{b} \rightarrow \hat{\eta} \qquad \partial_T \hat{\eta} = d_T \hat{b} = \partial_T \hat{b} + \partial_h \hat{b} \, \dfrac{dq_-}{dT}$$

where $\hat{\phi}$ and $\hat{\eta}$ are not functions of h

144

$$\partial_T(RSu) = ih\,\partial_z\left[\left(\partial_T\hat{\varphi}+\partial_n\hat{\varphi}\,\frac{d\,g(T)}{dT}\right)\partial_z\hat{\varphi}^* + \hat{\varphi}\left(\partial_z\partial_T\hat{\varphi}^* + \partial_z\partial_n\hat{\varphi}^*\,\frac{dg}{dT}\right)\right.+$$

$$\left.-\left(\partial_T\hat{\varphi}^*+\partial_n\hat{\varphi}^*\,\frac{dg}{dT}\right)\partial_z\hat{\varphi} - \hat{\varphi}^*\left(\partial_z\partial_T\hat{\varphi}+\partial_z\partial_n\hat{\varphi}\,\frac{dg}{dT}\right)\right]$$

Substituting back $\hat{\varphi}\to\hat{\varphi}$ (since $\hat{\varphi}=\hat{\varphi}|_H$)

$$\partial_T(RSu) = ih\left[(\partial_z\partial_T\hat{\varphi})\partial_z\hat{\varphi}^* + (\partial_T\hat{\varphi})\partial_z^2\hat{\varphi}^* + (\partial_z\partial_n\hat{\varphi})\partial_z\hat{\varphi}^*\,d_Tg + (\partial_n\hat{\varphi})(\partial_z^2\hat{\varphi}^*)\,d_Tg \right.+$$

$$+\ (\partial_z\hat{\varphi})(\partial_z\partial_T\hat{\varphi}^*) + \hat{\varphi}(\partial_z^2\partial_T\hat{\varphi}^*) + \partial_z\hat{\varphi}(\partial_z\partial_n\hat{\varphi}^*\,d_Tg) + \hat{\varphi}(\partial_z^2\partial_n\hat{\varphi}^*)\,d_Tg\ +$$

$$-\ (\partial_z\partial_T\hat{\varphi}^*)(\partial_z\hat{\varphi}) - (\partial_T\hat{\varphi}^*)(\partial_z^2\hat{\varphi}) - (\partial_z\partial_n\hat{\varphi}^*)(\partial_z\hat{\varphi})\,d_Tg - (\partial_n\hat{\varphi}^*)(\partial_z^2\hat{\varphi})\,d_Tg\ +$$

$$\left.-\ (\partial_z\hat{\varphi}^*)(\partial_z\partial_T\hat{\varphi}) - \hat{\varphi}^*(\partial_z^2\partial_T\hat{\varphi}) - (\partial_z\hat{\varphi}^*)(\partial_z^2\partial_n\hat{\varphi})\,d_Tg - \hat{\varphi}^*(\partial_z^2\partial_T\hat{\varphi})\,d_Tg\right]$$

$$RSut1$$

$$\partial_T(RSu) = ih\left\{(\partial_T\hat{\varphi})\partial_z^2\hat{\varphi}^* - (\partial_T\hat{\varphi}^*)\partial_z^2\hat{\varphi} + \hat{\varphi}(\partial_z^2\partial_T\hat{\varphi}^*) - \hat{\varphi}^*(\partial_z^2\partial_T\hat{\varphi})\right\}\ +$$

$$+ih\,\frac{dg}{dT}\left\{(\partial_n\hat{\varphi})(\partial_z^2\hat{\varphi}^*) - (\partial_n\hat{\varphi}^*)(\partial_z^2\hat{\varphi}) + \hat{\varphi}(\partial_z^2\partial_n\hat{\varphi}^*) - \hat{\varphi}^*(\partial_z^2\partial_n\hat{\varphi})\right\}$$

$$RSut2$$

$$RSut1 = \left[(\partial_T\hat{\varphi})\partial_z^2\hat{\varphi}^* - (\partial_T\hat{\varphi}^*)\partial_z^2\hat{\varphi} + \hat{\varphi}(\partial_z^2\partial_T\hat{\varphi}^*) - \hat{\varphi}^*(\partial_z^2\partial_T\hat{\varphi})\right] \tag{7.7}$$

$$RSut2 = \left[(\partial_n\hat{\varphi})(\partial_z^2\hat{\varphi}^*) - (\partial_n\hat{\varphi}^*)(\partial_z^2\hat{\varphi}) + \hat{\varphi}(\partial_z^2\partial_n\hat{\varphi}^*) - \hat{\varphi}^*(\partial_z^2\partial_n\hat{\varphi})\right] \tag{7.8}$$

$$\boxed{\partial_T(RSu) = ih\,RSut1 + ih\,\frac{dg}{dt}\,RSut2} \tag{7.9}$$

Analogously for RSb

$$\partial_T(RSb) = ih\,\partial_z\left[\left(\partial_T\hat{\varphi}+\partial_n\hat{\varphi}\,\frac{dg}{dT}\right)\hat{\eta}^* + \hat{\varphi}\left(\partial_T\hat{b}^* + \partial_n\hat{b}^*\,\frac{dg}{dT}\right)\right.+$$

$$\left.-\left(\partial_T\hat{\varphi}^*+\partial_n\hat{\varphi}^*\,\frac{dg}{dT}\right)\hat{\eta} - \hat{\varphi}^*\left(\partial_T\hat{b}+\partial_n\hat{b}\,\frac{dg}{dT}\right)\right]$$

Substituting back $\hat{\varphi}\to\hat{\varphi}$ and $\hat{\eta}\to\hat{b}$ and taking the z-derivative

$$\partial_T (RS_b) = i\hbar \left[\; (\partial_t \partial_T \hat{\varphi}) \hat{b}^* + (\partial_T \hat{\varphi})(\partial_t \hat{b}^*) + (\partial_t \partial_n \hat{\varphi}) \hat{b}^* \, d_T q + (\partial_n \hat{\varphi})(\partial_t \hat{b}^*) \, d_T q \; + \right.$$

$$+ (\partial_t \hat{\varphi})(\partial_T \hat{b}^*) + \hat{\varphi}(\partial_t \partial_T \hat{b}^*) + (\partial_t \hat{\varphi})(\partial_n \hat{b}^*) d_T q + \hat{\varphi} (\partial_t \partial_n \hat{b}^*) d_T q \; +$$

$$- (\partial_t \partial_T \hat{\varphi}^*) \hat{b} - (\partial_T \hat{\varphi}^*)(\partial_t \hat{b}) - (\partial_t \partial_n \hat{\varphi}^*) \hat{b} \, d_T q - (\partial_n \hat{\varphi}^*)(\partial_t \hat{b}) d_T q \; +$$

$$\left. - (\partial_t \hat{\varphi}^*)(\partial_T \hat{b}) - \hat{\varphi}^*(\partial_t \partial_T \hat{b}) - (\partial_t \hat{\varphi}^*)(\partial_n \hat{b}) d_T q - \hat{\varphi}^*(\partial_t \partial_n \hat{b}) d_T q \right]$$

$$\overbrace{}^{RS_{bt}\,1}$$

$$\partial_T (RS_b) = i\hbar \left\{ (\partial_t \partial_T \hat{\varphi}) \hat{b}^* - (\partial_t \partial_T \hat{\varphi}^*) \hat{b} + (\partial_T \hat{\varphi})(\partial_t \hat{b}^*) - (\partial_T \hat{\varphi}^*)(\partial_t \hat{b}) + (\partial_t \hat{\varphi})(\partial_T \hat{b}^*) + \right.$$

$$\left. - (\partial_t \hat{\varphi}^*)(\partial_T \hat{b}) + \hat{\varphi}(\partial_t \partial_T \hat{b}^*) - \hat{\varphi}^*(\partial_t \partial_T \hat{b}) \right\} \; +$$

$$+ i\hbar \frac{dq}{dT} \left\{ (\partial_t \partial_n \hat{\varphi}) \hat{b}^* - (\partial_t \partial_n \hat{\varphi}^*) \hat{b} + (\partial_n \hat{\varphi})(\partial_t \hat{b}^*) - (\partial_n \hat{\varphi}^*)(\partial_t \hat{b}) + \right.$$

$$\left. + (\partial_t \hat{\varphi})(\partial_n \hat{b}^*) - (\partial_t \hat{\varphi}^*)(\partial_n \hat{b}) + \hat{\varphi}(\partial_t \partial_n \hat{b}^*) - \hat{\varphi}^*(\partial_t \partial_n \hat{b}) \right\}$$

$$\underbrace{}_{RS_{bt}\,2}$$

$$RS_{bt}\,1 = \left[(\partial_t \partial_T \hat{\varphi}) \hat{b}^* - (\partial_t \partial_T \hat{\varphi}^*) \hat{b} + (\partial_T \hat{\varphi})(\partial_t \hat{b}^*) - (\partial_T \hat{\varphi}^*)(\partial_t \hat{b}) + (\partial_t \hat{\varphi})(\partial_T \hat{b}^*) + \right. \tag{7.10}$$

$$\left. - (\partial_t \hat{\varphi}^*)(\partial_T \hat{b}) + \hat{\varphi}(\partial_t \partial_T \hat{b}^*) - \hat{\varphi}^*(\partial_t \partial_T \hat{b}) \right]$$

$$RS_{bt}\,2 = \left[(\partial_t \partial_n \hat{\varphi}) \hat{b}^* - (\partial_t \partial_n \hat{\varphi}^*) \hat{b} + (\partial_n \hat{\varphi})(\partial_t \hat{b}^*) - (\partial_n \hat{\varphi}^*)(\partial_t \hat{b}) + \right. \tag{7.11}$$

$$\left. + (\partial_t \hat{\varphi})(\partial_n \hat{b}^*) - (\partial_t \hat{\varphi}^*)(\partial_n \hat{b}) + \hat{\varphi}(\partial_t \partial_n \hat{b}^*) - \hat{\varphi}^*(\partial_t \partial_n \hat{b}) \right]$$

$$\boxed{\partial_T (RS_b) = i\hbar \, RS_{bt}1 + i\hbar \frac{dq}{dT} RS_{bt}2} \tag{7.12}$$

146

Imposing $\text{Re}\{\partial_T \sigma\} = 0$ at $O(\Delta T)$ we found $|A|^2 = -\dfrac{\text{Re}\{\alpha/\gamma\}}{\text{Re}\{\beta/\gamma\}}$ where

$$\alpha = -ih \left\{ \int \left(\frac{\partial_z^2 \bar{u}}{Re_b} + \bar{1} \right) P \, dz + \int \left(\frac{\partial_z^2 \bar{b}}{Pr \, Re_b} \right) Q \, dz \right\}$$

$$= -ih \left\{ \int \left(\frac{\partial_z^2 \bar{u}}{Re_b} + 1 \right) \left[\hat{\psi}^{\dagger *}(\partial_z^2 - h^2)\hat{\psi} - \hat{\psi}^{\dagger *}\partial_z^2\hat{\psi} - \hat{\psi}\partial_z^2\hat{\psi}^{\dagger *} - 2(\partial_z\hat{\psi})(\partial_z\hat{\psi}^{\dagger *}) + \hat{b}^{\dagger *}\hat{b} \right] \right.$$

$$\left. + \int \left(\frac{\partial_z^2 \bar{b}}{Pr \, Re_b} \right) \left[\hat{b}^{\dagger *}\partial_z\hat{\psi} + \hat{\psi}\partial_z\hat{b}^{\dagger *} \right] dz \right\}$$

$$\beta = -ih \left\{ \int Rs_u P \, dz + \int RS_b Q \, dz \right\}$$

$$= -ih \left\{ \int RS_u \left[\hat{\psi}^{\dagger *}(\partial_z^2 - h^2)\hat{\psi} - \hat{\psi}^{\dagger *}\partial_z^2\hat{\psi} - \hat{\psi}\partial_z^2\hat{\psi}^{\dagger *} - 2(\partial_z\hat{\psi})(\partial_z\hat{\psi}^{\dagger *}) + \hat{b}^{\dagger *}\hat{b} \right] dz \right.$$

$$\left. + \int RS_b \left[\hat{b}^{\dagger *}\partial_z\hat{\psi} + \hat{\psi}\partial_z\hat{b}^{\dagger *} \right] dz \right\}$$

$$\gamma = \int \hat{\psi}^{\dagger *}(\partial_z^2 - h^2)\hat{\psi} + \hat{b}^{\dagger *}\hat{b} \, dz$$

$$P = \left[\hat{\psi}^{\dagger *}(\partial_z^2 - h^2)\hat{\psi} - \hat{\psi}^{\dagger *}\partial_z^2\hat{\psi} - \hat{\psi}\partial_z^2\hat{\psi}^{\dagger *} - 2(\partial_z\hat{\psi})(\partial_z\hat{\psi}^{\dagger *}) + \hat{b}^{\dagger *}\hat{b} \right]$$

$$Q = \left[\hat{b}^{\dagger *}\partial_z\hat{\psi} + \hat{\psi}\partial_z\hat{b}^{\dagger *} \right]$$

$$\partial_T(|A|^2) = -\frac{\text{Re}\{\beta/\gamma\} \, \partial_T \text{Re}\{\alpha/\gamma\} - \text{Re}\{\alpha/\gamma\} \, \partial_T \text{Re}\{\beta/\gamma\}}{\text{Re}\{\beta/\gamma\}^2}$$

$$\text{Re}\{\partial_T(\,)\} = \partial_T(\text{Re}\{\,\})$$

$$\partial_T(|A|^2) = -\frac{\text{Re}\{\beta/\gamma\} \, \text{Re}\{\partial_T(\alpha/\gamma)\} - \text{Re}\{\alpha/\gamma\} \, \text{Re}\{\partial_T(\beta/\gamma)\}}{\text{Re}\{\beta/\gamma\}^2}$$

$$= -\underbrace{\frac{\text{Re}\{\partial_T(\alpha/\gamma)\}}{\text{Re}\{\beta/\gamma\}}}_{\boxed{At1}} + \underbrace{\frac{\text{Re}\{\alpha/\gamma\} \, \text{Re}\{\partial_T(\beta/\gamma)\}}{\text{Re}\{\beta/\gamma\}^2}}_{\boxed{At2}} \qquad (7.13)$$

COMPUTE TERM $\boxed{At1}$

$\boxed{At1} = -\dfrac{Re\{\partial_\tau(\alpha/\gamma)\}}{Re\{\beta/\gamma\}} = \dfrac{1}{Re\{\beta/\gamma\}} Re\left\{-\dfrac{\partial_\tau\alpha}{\gamma} + \dfrac{\alpha\partial_\tau\gamma}{\gamma^2}\right\}$ where

$$\partial_\tau\gamma = \int \partial_\tau\hat{\varphi}^{\dagger*}(\partial_z^2-h^2)\hat{\varphi} + \hat{\varphi}^{\dagger*}(\partial_z^2-h^2)\partial_\tau\hat{\varphi} + \partial_\tau\hat{b}^{\dagger*}\hat{b} + \hat{b}^{\dagger*}\partial_\tau\hat{b}]\,dz \qquad (7.14)$$

$$Re\{\beta/\gamma\} = -Re\left\{\dfrac{ih}{\gamma}\int RS_u\,P\,dz + \dfrac{ih}{\gamma}\int RS_b\,Q\,dz\right\} = \qquad (7.15)$$

$$\partial_\tau\alpha = -ih\left\{\int\left(\dfrac{\partial_z^2\partial_\tau\bar{u}}{Re_b} + \partial_\tau\bar{f}\right)\left[\hat{\varphi}^{\dagger*}(\partial_z^2-h^2)\hat{\varphi} - \hat{\varphi}^{\dagger*}\partial_z^2\hat{\varphi} - \hat{\varphi}\partial_z^2\hat{\varphi}^{\dagger*} - 2(\partial_z\hat{\varphi})(\partial_z\hat{\varphi}^{\dagger*}) + \hat{b}^{\dagger*}\hat{b}\right]dz\right.$$

$$+ \int\left(\dfrac{\partial_z^2\partial_\tau\bar{b}}{Pr\,Re_b}\right)\left[\hat{b}^{\dagger*}\partial_z\hat{\varphi} + \hat{\varphi}\partial_z\hat{b}^{\dagger*}\right]dz +$$

$$\int\left(\dfrac{\partial_z^2\bar{u}}{Re_b} + \bar{f}\right)\left[\partial_\tau\hat{\varphi}^{\dagger*}(\partial_z^2-h^2)\hat{\varphi} + \hat{\varphi}^{\dagger*}(\partial_z^2-h^2)\partial_\tau\hat{\varphi} - \partial_\tau\hat{\varphi}^{\dagger*}\partial_z^2\hat{\varphi} - \hat{\varphi}^{\dagger*}\partial_z^2\partial_\tau\hat{\varphi} - \partial_z^2\partial_\tau\hat{\varphi}^{\dagger*}\hat{\varphi} +\right.$$

$$\left. - \partial_z^2\hat{\varphi}^{\dagger*}\partial_\tau\hat{\varphi} - 2(\partial_z\partial_\tau\hat{\varphi})(\partial_z\hat{\varphi}^{\dagger*}) - 2(\partial_z\hat{\varphi})(\partial_z\partial_\tau\hat{\varphi}^{\dagger*}) + \partial_\tau\hat{b}^{\dagger*}\hat{b} + \hat{b}^{\dagger*}\partial_\tau\hat{b}\right]dz +$$

$$+ \int\left(\dfrac{\partial_z^2\bar{b}}{Pr\,Re_b}\right)\left[\partial_\tau\hat{b}^{\dagger*}\partial_z\hat{\varphi} + \hat{b}^{\dagger*}\partial_z\partial_\tau\hat{\varphi} + \partial_\tau\hat{\varphi}\partial_z\hat{b}^{\dagger*} + \hat{\varphi}\partial_z\partial_\tau\hat{b}^{\dagger*}\right]dz \left.\right\}$$

$$\partial_\tau\alpha = -ih\left\{\overbrace{\int\left(\dfrac{\partial_z^2\partial_\tau\bar{u}}{Re_b} + \partial_\tau f\right)P\,dz}^{\alpha t1} + \overbrace{\int\left(\dfrac{\partial_z^2\partial_\tau\bar{b}}{Pr\,Re_b}\right)Q\,dz}^{\alpha t2}\right.$$

$$+ \underbrace{\int\left(\dfrac{\partial_z^2\bar{u}}{Re_b} + f\right)[P_\tau + P_\tau^\dagger]\,dz}_{\alpha t3} + \underbrace{\int\left(\dfrac{\partial_z^2\bar{b}}{Pr\,Re_b}\right)[Q_\tau + Q_\tau^\dagger]\,dz}_{\alpha t4} \left.\right\} \qquad (7.15)$$

$$= -ih\,\alpha t1 - ih\,\alpha t2 - ih\,\alpha t3 - ih\,\alpha t4$$

Where $\partial_\tau P = P_\tau + P_\tau^\dagger$ and $\partial_\tau Q = Q_\tau + Q_\tau^\dagger$

$$P_\tau^\dagger = \left[\partial_\tau\hat{\varphi}^{\dagger*}(\partial_z^2-h^2)\hat{\varphi} - \partial_\tau\hat{\varphi}^{\dagger*}\partial_z^2\hat{\varphi} - (\partial_z^2\partial_\tau\hat{\varphi}^{\dagger*})\hat{\varphi} - 2(\partial_z\partial_\tau\hat{\varphi}^{\dagger*})(\partial_z\hat{\varphi}) + (\partial_\tau\hat{b}^{\dagger*})\hat{b}\right] \qquad (7.16)$$

$$Q_\tau^\dagger = \left[\partial_\tau\hat{b}^{\dagger*}\partial_z\hat{\varphi} + (\partial_z\partial_\tau\hat{b}^{\dagger*})\hat{\varphi}\right] \qquad (7.17)$$

similarly to what done for P_τ and Q_τ, $P_\tau^\dagger$ and $Q_\tau^\dagger$ have the same structure but with the time deriv. on the dagger-eigenfunction.

$$\boxed{\text{AT1}} \;=\; \frac{1}{Re\{\beta/\gamma\}} \; Re\left\{ \frac{ih}{\gamma} \int \left(\frac{\partial_z^2 \partial_T \bar{u}}{Re_b} + \partial_T f \right) P \, dz + \frac{ih}{\gamma} \int \left(\frac{\partial_z^2 \partial_T \bar{b}}{Pr\, Re_b} \right) Q \, dz + \right.$$

$$\left. + \frac{ih}{\gamma} \int \left(\frac{\partial_z^2 \bar{u}}{Re_b} + f \right) [P_T + P_T^+] \, dz + \frac{ih}{\gamma} \int \left(\frac{\partial_z^2 \bar{b}}{Pr\, Re_b} \right) [Q_T + Q_T^+] \, dz + \right. \qquad (7.18)$$

$$\left. - \frac{ih}{\gamma^2} \partial_T \gamma \int \left(\frac{\partial_z^2 \bar{u}}{Re_b} + f \right) P \, dz \; - \; \frac{ih}{\gamma^2} \partial_T \gamma \int \left(\frac{\partial_z^2 \bar{b}}{Pr\, Re_b} \right) Q \, dz \right\}$$

In (7.18) we could group term in the 2nd and 3rd lines however the last line is multiplied by $\frac{\partial_T \gamma}{\gamma^2}$ that are integrals (so it would get messy)

Re-writing (7.18) in short (useful later)

$$\boxed{\text{AT1}} \;=\; \frac{1}{Re\{\beta/\gamma\}} \; Re\left\{ \frac{ih}{\gamma} \alpha_{t1} + \frac{ih}{\gamma} \alpha_{t2} + \frac{ih}{\gamma} \alpha_{t3} + \frac{ih}{\gamma} \alpha_{t4} + \frac{ih}{\gamma^2}(\partial_T \gamma)\alpha \right\} \qquad (7.19)$$

COMPUTE TERM $\boxed{\text{At2}}$

$$\boxed{\text{At2}} \;=\; + \frac{Re\{\alpha/\gamma\}\, Re\{\partial_T(\beta/\gamma)\}}{Re\{\beta/\gamma\}^2} \;=\; \frac{Re\{\alpha/\gamma\}}{Re\{\beta/\gamma\}^2} \; Re\left\{ \frac{\partial_T \beta}{\gamma} - \frac{\beta\, \partial_T \gamma}{\gamma^2} \right\} \qquad \text{where}$$

$$Re\{\alpha/\gamma\} \;=\; -Re\left\{ \frac{ih}{\gamma} \int \left(\frac{\partial_z^2 \bar{u}}{Re_b} + f \right) P \, dz + \frac{ih}{\gamma} \int \left(\frac{\partial_z^2 \bar{b}}{Pr\, Re_b} \right) Q \, dz \right\}$$

$Re\{\beta/\gamma\}$ is given by (7.19), $\partial_T \gamma$ by (7.13)

$$\partial_T \beta \;=\; -ih \left\{ \int (\partial_T RSu) P \, dz + \int (\partial_T RSb) Q \, dz + \int RSu \, [P_T + P_T^+] \, dz + \int RSb \, [Q_T + Q_T^+] \, dz \right\}$$

substituting

$$\partial_T (RSu) = ih \; RSut1 + ih \, \frac{dq}{dt} \; RSut2$$

$$\partial_T (RSb) = ih \; RSbt1 + ih \, \frac{dq}{dT} \; RSbt2$$

$$\partial_T \beta = \overbrace{+ h^2 \int \left[(RSut1)P + (RSbt1).Q \right] d\zeta}^{\beta t1} + \overbrace{h^2 \frac{dg}{dT} \int \left[(RSut2)P + (RSbt2)Q \right] d\zeta}^{\beta t2}$$

$$\underbrace{- ih \left\{ \int RSu \left[P_T + P_T^\dagger \right] d\zeta + \int RSb \left[Q_T + Q_T^\dagger \right] d\zeta \right\}}_{\beta t3}$$

(7.19)

$$\partial_T \beta = h^2 \beta t1 + h^2 \frac{dg}{dT} \beta t2 - ih \beta t3$$

$$\boxed{AT2} = \frac{Re\{\alpha/\gamma\}}{Re\{\beta/\gamma\}^2} Re \left\{ \frac{h^2}{\gamma} \beta t1 - \frac{ih}{\gamma} \beta t3 \right\} + h^2 \frac{dg}{dT} \frac{Re\{\alpha/\gamma\}}{Re\{\beta/\gamma\}} Re \left\{ \frac{\beta t2}{\gamma} \right\}$$

$$- \frac{Re\{\alpha/\gamma\}}{Re\{\beta/\gamma\}^2} Re \left\{ \frac{1}{\gamma^2} \partial_T \gamma \beta \right\}$$

$$\partial_T (|A|^2) = - \frac{Re\{\partial_T(\alpha/\gamma)\}}{Re\{\beta/\gamma\}} + \frac{Re\{\alpha/\gamma\} Re\{\partial_T(\beta/\gamma)\}}{Re\{\beta/\gamma\}^2} = \boxed{AT1} + \boxed{AT2} =$$

$$\partial_T |A|^2 = \frac{1}{Re\{\beta/\gamma\}} Re \left\{ \frac{ih}{\gamma} \alpha t1 - \frac{ih}{\gamma} \alpha t2 + \frac{ih}{\gamma} \alpha t3 - \frac{ih}{\gamma} \alpha t4 + \frac{1}{\gamma^2}(\partial_T \gamma)\alpha \right\} +$$

$$\frac{Re\{\alpha/\gamma\}}{Re\{\beta/\gamma\}^2} Re \left\{ \frac{h^2}{\gamma} \beta t1 - \frac{ih}{\gamma} \beta t3 \right\} + h^2 \frac{dg}{dT} \frac{Re\{\alpha/\gamma\}}{Re\{\beta/\gamma\}} Re \left\{ \frac{\beta t2}{\gamma} \right\} +$$

$$- \frac{Re\{\alpha/\gamma\}}{Re\{\beta/\gamma\}^2} Re \left\{ \frac{1}{\gamma^2} \partial_T \gamma \beta \right\}$$

$$\partial_T |A|^2 = \frac{1}{Re\{\beta/\gamma\}} Re \left\{ \frac{ih}{\gamma} \alpha t1 + \frac{ih}{\gamma} \alpha t2 + \frac{ih}{\gamma} \alpha t3 + \frac{ih}{\gamma} \alpha t4 + \frac{1}{\gamma^2}(\partial_T \gamma)\alpha \right\} +$$

$$- \frac{|A|^2}{Re\{\beta/\gamma\}} Re \left\{ \frac{h^2}{\gamma} \beta t1 - \frac{ih}{\gamma} \beta t3 \right\} - h^2 \frac{dg}{dT} \frac{|A|^2}{Re\{\beta/\gamma\}} Re \left\{ \frac{\beta t2}{\gamma} \right\} +$$

$$+ \frac{|A|^2}{Re\{\beta/\gamma\}} Re \left\{ \frac{1}{\gamma^2} \partial_T \gamma \beta \right\}$$

where we have substit. $|A|^2 = - \frac{Re\{\alpha/\gamma\}}{Re\{\beta/\gamma\}}$

$$\gamma \partial_T^2 \sigma = \overbrace{-ih\, \partial_T(|A|^2)\int RSu\, P\, dz}^{S_1} \quad \overbrace{-ih|A|^2 \int (\partial_T RSu)P\, dz}^{S_2} \quad \overbrace{-ih\int\left(\frac{\partial_z^2\partial_T\bar{u}}{Re_b}\right)P\, dz \quad -ih\int \partial_T\bar{f}\, P\, dz}^{S_3}$$

$$\underbrace{-ih\,\partial_T(|A|^2)\int RSb\, Q\, dz}_{S_4} \quad \underbrace{-ih\,|A|^2\int(\partial_T RSb)Q\, dz}_{S_5} \quad \underbrace{-ih\int\left(\frac{\partial_z^2\partial_T\bar{b}}{Pr\, Re_b}\right)Q\, dz}_{S_6}$$

$$-2ih\int(\partial_T\bar{u})P_T\, dz \quad -2ih\int(\partial_T\bar{b})Q_T\, dz - 2i\,\Im\{\partial_T\sigma\}\int\left[\hat{\phi}^{\dagger *}(\partial_z^2-h^2)\partial_T\hat{\phi} + \hat{b}^\dagger\partial_T\hat{b}\right]dz$$

$S_1 + S_4 = (\partial_T|A|^2)\,\beta$

$S_2 = h^2|A|^2\int(RSut1)P\, dz + h^2|A|^2\frac{dq_c}{dT}\int(RSut2)P\, dz$

$S_5 = +h^2|A|^2\int(RSbt1)Q\, dz + h^2|A|^2\frac{dq_c}{dt}\int(RSbt2)Q\, dz$

$S_2 + S_5 = h^2|A|^2\,\beta t1 + h^2|A|^2\frac{dq_c}{dT}\beta t2$

$S_3 = -ih\,\alpha t2 \qquad S_6 = ih\,\alpha t2 \longrightarrow$ These 2 integrals need to be integrated by parts and grouped with the terms in the last line

$$-ih\int\left(\frac{\partial_z^2\partial_T\bar{u}}{Re_b}\right)P\, dz = -\frac{ih}{Re_b}\int(\partial_T\bar{u})\partial_z^2 P\, dz$$

$$ih\int\left(\frac{\partial_z^2\partial_T\bar{b}}{Pr\, Re_b}\right)Q\, dz = \frac{ih}{Pr\, Re_b}\int(\partial_T\bar{b})\partial_z^2 Q\, dz$$

where $\partial_z^2 P$ and $\partial_z^2 Q$ are quite horrific 👀

$$\gamma \partial_T^2 \sigma = (\partial_T|A|^2)\,\beta + h^2|A|^2\,\beta t1 + \frac{dq_c}{dT}h^2|A|^2\,\beta t2 +$$

$$- ih\int(\partial_T\bar{u})\left[2P_T + \frac{\partial_z^2 P}{Re_b}\right]dz + ih\int(\partial_T\bar{b})\left[2Q_T + \frac{\partial_z^2 Q}{Pr\, Re_b}\right]dz - ih\int\partial_T\bar{f}\cdot P\, dz +$$

$$- 2i\,\Im\{\partial_T\sigma\}\int\left[\hat{\phi}^{\dagger *}(\partial_z^2-h^2)\partial_T\hat{\phi} + \hat{b}^\dagger\partial_T\hat{b}\right]dz$$

$$= (\partial_T|A|^2)\,\beta + h^2|A|^2\,\beta t1 + \frac{dq_c}{dT}h^2|A|^2\,\beta t2 +$$

$$- ih|A|^2\int(RSu)\left[2P_T + \frac{\partial_z^2 P}{Re_b}\right]dz - ih\int\left(\frac{\partial_z^2\bar{u}}{Re_b} + f\right)\left[2P_T + \frac{\partial_z^2 P}{Re_b}\right]dz - ih\int\partial_T\bar{f}\cdot P\, dz +$$

$$- ih|A|^2\int(RSb)\left[2Q_T + \frac{\partial_z^2 Q}{Pr\, Re_b}\right]dz - ih\int\left(\frac{\partial_z^2\bar{b}}{Pr\, Re_b}\right)\left[2Q_T + \frac{\partial_z^2 Q}{Pr\, Re_b}\right]dz +$$

$$- 2i\,\Im\{\partial_T\sigma\}\int\left[\hat{\phi}^{\dagger *}(\partial_z^2-h^2)\partial_T\hat{\phi} + \hat{b}^\dagger\partial_T\hat{b}\right]dz$$

151

Substituting now the expression for $\partial_T |A|^2$.

$$\gamma \, \partial_T^2 \sigma = \frac{\beta}{\mathrm{Re}\{\beta/\gamma\}} \, \mathrm{Re}\left\{ -\frac{\partial_T \alpha}{\gamma} + \frac{\partial_T \gamma}{\gamma} \alpha \right\} - |A|^2 \frac{\beta}{\mathrm{Re}\{\beta/\gamma\}} \, \mathrm{Re}\left\{ \frac{h^2}{\gamma} \beta t_1 - \frac{i h}{\gamma} \beta t_3 \right\}$$

$$+ |A|^2 \frac{\beta}{\mathrm{Re}\{\beta/\gamma\}} \, \mathrm{Re}\left\{ \frac{1}{\gamma^2} \partial_T \gamma \, \beta \right\} - h^2 |A|^2 \frac{d q_r}{dT} \frac{\beta}{\mathrm{Re}\{\beta/\gamma\}} \, \mathrm{Re}\left\{ \frac{\beta t_2}{\gamma^2} \right\}$$

$$+ h^2 |A|^2 \beta t_1 + \frac{d q_r}{dT} h^2 |A|^2 \beta t_2 +$$

$$- i h |A|^2 \int (RSu) \left[2 P_T + \frac{\partial_z^2 P}{\mathrm{Re}_b} \right] dz - i h \int \left(\frac{\partial_z^2 \bar{u}}{\mathrm{Re}_b} + f \right) \left[2 P_T + \frac{\partial_z^2 P}{\mathrm{Re}_b} \right] dz - i h \int \partial_T \hat{f} \cdot P \, dz +$$

$$- i h |A|^2 \int (R S_b) \left[2 a_T + \frac{\partial_z^2 a}{\mathrm{Pr} \, \mathrm{Re}_b} \right] dz - i h \int \left(\frac{\partial_z^2 \bar{b}}{\mathrm{Pr} \, \mathrm{Re}_b} \right) \left[2 a_T + \frac{\partial_z^2 a}{\mathrm{Pr} \, \mathrm{Re}_b} \right] dz +$$

$$- 2 i \, \Im\{\partial_T \sigma\} \int \left[\hat{\varphi}^{\dagger *} (\partial_z^2 - h^2) \partial_T \hat{\varphi} + \hat{b}^\dagger \partial_T \hat{b} \right] dz$$

152

D Polymer-induced drag reduction and viscoelastic invariant solutions

Contents

Initially the core of this thesis was represented by the investigation of viscoelastic turbulent flows and specifically on the generalisation of the numerical tools for the dynamical system analysis of such a flow. Due to a subsequent shift of the focus towards the QL project and the intention to keep this thesis focused, we summarise our achievements regarding viscoelastic invariant solutions in this appendix.

D.1 Phenomenology of polymers-induced turbulent drag reduction

The addition of a tiny amount of flexible long chain polymers to a Newtontian fluid is known to produce a significant reduction, up to 80 %, of friction losses in the turbulent regime of pipe flow. As a result the pressure drop necessary to sustain a certain flow rate decreases and so does the shear rate at the wall.

The elastic behavior of polymers, due to their chemical structure, strongly modifies the stress-strain (rate) relation turning the fluid viscoelastic. The polymer-induced viscoelasticity is measured by the Weissenberg number, defined as the product between the polymer relaxation time and the strength of the stretching exerted by the flow. Once the transition to turbulence

is triggered, the elongation of polymers becomes substantial and the structural change in the nature of stresses gives rise to a non-trivial interaction between polymers and turbulent fluid motion.

Experimental observations (based on PIV and LDV techniques), and numerical simulations have shown that the feedback produced by polymer molecules on the flow strongly affects the statistical properties of the turbulent regime, the linear stability of the laminar state as well as the transition to turbulence and its self-sustaining mechanism [Nadolink and Haigh (1995)]. One of the most characterizing features of this phenomenon is the existence of an upper limit for the amount of drag reduction that can be achieved. This limit, also known as maximum drag reduction asymptote (MDR) or Virk law, is observed to be universal with respect to the specific properties of the solution [Virk (1975); Virk et al. (1970)].

Polymer drag reduction, first observed in 1948 by the chemist Toms Toms (1948), has received a lot of attention in the last decades. Has found uses in many industrial applications related to fluid propulsion, like district heating and cooling systems and fossil fuel transport systems[Burger et al. (1982)]. In spite of the fact that several theories have been formulated and much progress has been achieved on both numerical and experimental sides, the mechanistic underpinning of drag reduction and its universality in the MDR regime still remain not fully understood.

We believe that much progresses in the overall understanding of this phenomenon could be achieved by means of a dynamical systems approach. Direct numerical simulations combined with nonlinear solvers can be used to explore the properties and the structure of the state space that underlies this complex dynamics.
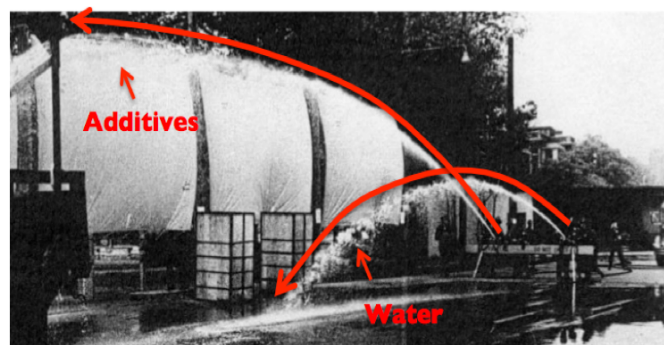

Figure D.1 – The effect of polymers in two fire hoses driven by the same pressure force. Drag reduction induced by polymer results in a higher throughput and greatly increased range.

D.2   Dynamical systems approach to turbulence

In the last 20 years, starting from the Nagata solution of the Navier-Stokes equations [Nagata (1990)], the dynamical systems approach to turbulence gave a deep insight in understanding intermediate Reynolds number phenomena, establishing a link between chaos theory and

turbulence. Thanks to the growth of computational power it has become possible to study turbulent flows as finite high-dimensional systems in their state space, represented by all the possible velocity fields satisfying the discretised primitive equations and the boundary conditions. The long time behaviour of the system is thought to be controlled by the set of solutions that are invariant under the dynamics. These so-called exact invariant solutions include in the simplest form equilibria, but also periodic orbits, and more complex chaotic attractors. These solutions are unstable yet dynamically connected with their entangled stable and unstable manifolds organising the state space. A single flow realization can thus be thought of as a walk in the state space among these invariant solutions modulated by their stability, i.e. the higher the stability of a solution, the longer is the time spent by the trajectory near it [Eckhardt et al. (2007); Gibson et al. (2008)]. This framework promises that statistical properties of turbulent motion can be explained as the average of the physical properties characterizing exact solutions weighted by their relevance in the state space dynamics.

Given the remarkable results obtained by this approach for Newtonian turbulence, where many of this solutions have already been found, we believe the approach will shed some light on the open questions of polymer drag reduction, directly accessing the core elements of the dynamics.

The observation that viscoelastic turbulent flows are characterised by a much less three-dimensional dynamics compared to the Newtonian case, indicates a clear change in the state-space structures and/or in their stability properties. Whether this represents a shift of the dynamics towards a specific set of solutions already existing in the Newtonian dynamics [Xi and Graham (2012)] or a deeper change in their physical properties it nowadays is not clear. Choueiri *et al.* [Choueiri et al. (2018)] have recently shown the possible connection between the universal behavior observed in highly-viscoelastic regimes (MDR) and elasto-inertial turbulence, previously attributed to a polymer-induced change in the stability of the Newtonian solutions [Xi and Graham (2010)]. Elucidating the mechanism underlying polymers drag reduction using dynamical system concepts relies on the capability of computing and characterizing viscoelastic invariant solutions. Only very recently the first viscoelastic invariant solution has been found [Page et al. (2020)].

D.3 Governing equations and numerical tools

The investigation of polymer-induced drag reduction requires direct numerical simulations (DNS) of dilute incompressible viscoelastic flows, fully solving the governing equations. Since polymers modify the linear relation between stresses and rate of deformation, typical of a Newtonian fluid, an additional constitutive equation for the elastic contribution of polymers has to be included. The choice of a mathematical description, as well as its numerical implementation, is a crucial step in simulations of complex fluids where the change in the nature of the equations can trigger mathematical and numerical instabilities [Xi (2009); **?**]. For viscoelas-

tic fluids a good trade-off between numerical feasibility and physical accuracy is represented by the hydrodynamic FENE-P (Finitely Extensible Nonlinear Elastic-Peterlin) model. Based on the assumption that polymers can be modeled as a couple of beads connected by a non-linear entropic spring, the evolution of the end-to-end vector **R** for a single molecule is described by the Langevin equation [Rubinstein and Colby (2003); Doi and Edwards (1986)]. By means of a stochastic integration, the corresponding hydro-dynamical model of FENE-P can be derived, obtaining the evolution equation, at the macroscopic level, for the polymer conformation tensor α given by the average second moment of **R** (eq. D.3), from which the polymeric contribution to the stress tensor $\mathbb{T}^P$ is computed (eq. D.2).

$$\frac{\partial \boldsymbol{u}}{\partial t} + (\boldsymbol{u} \cdot \nabla) \boldsymbol{u} = -\nabla p + \frac{\beta}{Re} \Delta \boldsymbol{u} + \frac{2(1-\beta)}{ReWi} (\nabla \cdot \mathbb{T}^P) \tag{D.1}$$

$$\mathbb{T}^P = \frac{b+5}{b} \left\{ \frac{\alpha}{1 - tr(\alpha)/b} - \left(1 - \frac{2}{b+2}\right)\delta \right\} \tag{D.2}$$

$$\frac{\boldsymbol{\alpha}}{1 - tr(\boldsymbol{\alpha})/b} + \frac{Wi}{2} \left\{ \frac{\partial \boldsymbol{\alpha}}{\partial t} + \boldsymbol{u} \cdot \nabla \boldsymbol{\alpha} - (\nabla \boldsymbol{u})^T \boldsymbol{\alpha} - \boldsymbol{\alpha} \cdot \nabla \boldsymbol{u} \right\} = \left(\frac{b}{b+2}\right)\delta \tag{D.3}$$

Indicating with $\mu_p + \mu_s$ the total zero-shear rate viscosity (where μ_s and μ_p are the solvent and the polymer contribution respectively) and with U and L the characteristic velocity and spatial scale of the flow, here $Re = \rho U L/(\mu_p + \mu_s)$ is the *Reinolds* number, representing the ratio between inertial and viscous forces; $Wi = \tau U/L$ is the *Weissenberg* number indicating the polymer-induced elasticity of the flow as the ratio of the polymer relaxation timescale τ to the flow timescale (shear rate); β is the viscosity ratio $\beta = \mu_s/(\mu_s + \mu_p)$ and b is the maximum extensibility of the polymer dumbbells.

For applying of dynamical systems concepts to verify our hypothesis, first invariant solutions for the above system need to be determined. We define invariant solutions as those flow fields that satisfy

$$\boldsymbol{G}(\boldsymbol{x}(t), t) = \sigma \boldsymbol{f}^T(\boldsymbol{x}(t)) - \boldsymbol{x}(t) = 0 \tag{D.4}$$

where $\boldsymbol{x}(t) = (\boldsymbol{u}(t), \boldsymbol{\alpha}(t))$ is the state-space vector, $\boldsymbol{f}^T$ the time evolution operator determined by the governing equations and boundary conditions and σ is a symmetry operator.
The saddle-type nature of these solutions, which results in the presence of both stable and unstable directions in the state space, does not allow to find them from a natural long term evolution of the system, and thus iterative methods to solve eq. (D.4) are needed. Because of the high dimensionality of the problem, suitable solvers are matrix-free approximations of Newton-Raphson iterations, where the expensive calculation of the entire Jacobian is replaced by the evaluation of its action on a vector v.

The numerical tools necessary to tackle the computational aspects of this project are now provided by our custom developed version of the *Channelflow 2.0* package (www.channelflow.ch [Gibson (2009)]) for which we have implemented a viscoelastic extension.

Channelflow is a pseudo-spectral code, written in C++ and designed to performs direct numerical simulations of incompressible flows in a channel geometry with two periodic directions and no-slip boundary conditions at the physical walls. The Navier-Stokes equations are integrated using a semi-implicit finite differences scheme in time (Adam Bashfort/backward differentiation scheme for the non-linear and the linear terms respectively) and spatially discretised via Fourier and Chebyshev polynomials in the periodic and wall-normal directions respectively. The code provides different DNS algorithms for time forward integration, interfaced with a highly efficient Newton-Krylov solver to handle root-finding and linear algebra problems in high dimensional systems. Thanks to the highly MPI-based parallelisation implemented by our group and the recent extension to viscoelastic fluids, our code has now all the fundamental features to tackle highly resolved viscoelastic simulations.

D.4 Summary of results - Code validation and viscoelastic invariant solutions

The strong computational component at the base of this project makes the implementation of the FENE-P equations a prerequisite for further investigation of the viscoelastic flow problem and the successful achievement of the aforementioned objectives. In this section we first present a qualitative validation of the code, showing its capability of capturing the main features of turbulent drag-reduction. Then the successful computation of two families of invariant solutions in two different systems is shown: a travelling wave in plane-Poiseuille flow and a snaking solution in Couette flow. The aim of this section is not to draw scientific conclusions on the topic , but rather to show the validity of the numerical tools and their potential for future research.

D.4.1 DNS of viscoelastic channelflow: phenomenology of drag reduction

Though turbulence has a chaotic nature to the point where a statistical methods are necessary to describe it, some physical quantities show a very specific behavior close to any solid boundaries in the system. When velocities are scaled with the friction velocity $u_\tau = \sqrt[2]{\tau_w/\rho}$ and distances with the local viscous length $\delta = \nu/u_\tau$ (with $\tau_w = \partial u/\partial y|_{y=0}$ the time and area averaged shear stress at the wall, ρ the density and ν the kinematic viscosity of the flow), the mean stream-wise velocity profile $U^+(y^+)$ expressed in this so-called "inner units" is known to obey the *law of the wall*. It is linear in the viscous sub-layer, nearest to the wall where viscous dissipation takes place, and logarithmic further away from it, where inertial forces dominate

Appendix D. Polymer-induced drag reduction and viscoelastic invariant solutions

[Pope (2000)].

$$U^+ = y^+ \qquad \text{if } y^+ < 5 \qquad (D.5)$$

$$U^+ = \frac{1}{\kappa}\ln(y^+) + C \qquad \text{if } y^+ > 30 \qquad (D.6)$$

For a Newtonian fluid equation (D.6) is known as *von Karman log-law* for which $\kappa \simeq 0.4$ and $C = 5.5$. Experimental observations for viscoelastic flows revealed the existence of an analogous logarithmic dependence with higher slope and intercept ($k \simeq 0.08$ and $C \simeq -17$) that sets the upper limit of drag reduction achievable for a certain flow rate Virk (1975). Data from different setups with different polymer concentrations, species, and pipe sizes, all collapse on this asymptote, highlighting its nearly-universal character. Figure D.2 shows the mean velocity
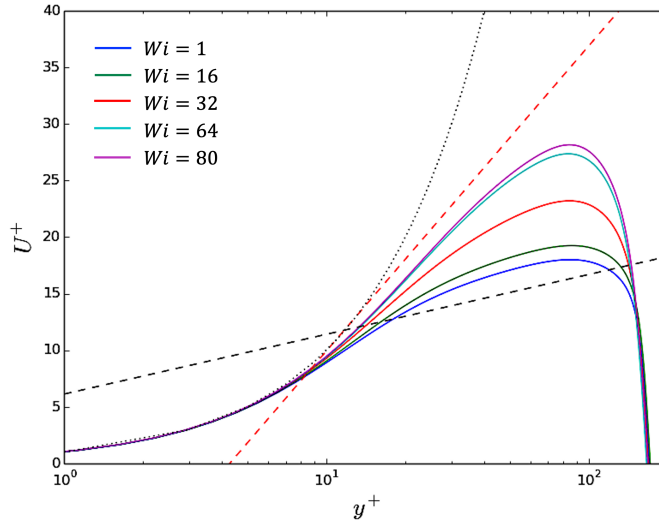

Figure D.2 – Mean velocity profiles in inner units from DNS at $Re_\tau = 84.85$, $Wi = 1 - 80$. Polymer-induced drag reduction, increasing viscoelasticity, corresponds to an higher slope in the mean velocity profile and thus to an higher throughput if a fixed pressure gradient is imposed (Plane-Poiseuille).

profiles obtained from DNS at fixed Reynolds number $Re = 3600$ ($Re_\tau = 84.5$) and increasing Weissenberg number from 1 to 80. The simulations were performed for a plane Poiseuille system (i.e. no-slip boundary conditions in the wall normal direction and periodic conditions in the span-wise and stream-wise directions) at constant pressure gradient. At the onset of drag reduction, for low Wi, the presence of polymers mainly affects the buffer layer, region connecting the viscous and the log-law layers, where the mean velocity profile results shifted upward with respect to the Newtonian case but still keeping the same slope in the log-law region. As viscoelasticity is increased the effects start pervading the inertial layer, causing a departure of the velocity profile from the Von-Karman law towards the MDR asymptote. Variations in the mean velocity U_+ with the distance from the wall are controlled by the shear

stress balance that in the more general case includes viscous, turbulent and polymer shear stresses (eq.D.7).

$$\langle \tau_{xy}^+ \rangle = \beta \frac{dU^+}{dy^+} + \langle -u'^+ v'^+ \rangle + \frac{1-\beta}{Wi} \langle \mathbb{T}_{xy}^P \rangle \qquad \text{(D.7)}$$

Thus, because a fixed pressure gradient is imposed, a decrease in the total shear stress necessarily leads to a higher throughput. Close to the wall, in the viscous sub-layer, turbulent stresses are negligible and all the curves are shown to collapse onto the Newtonian slope, for which the mean wall shear stress is determined by the constant-pressure-drop constraint via $\langle \tau_{xy}^+ \rangle|_w = h\Delta P/\Delta x$ (h being the channel half height). Though viscoelastic stress is in principle not vanishing at the wall, effects of polymers are mostly felt in the buffer and log-low regions, making their contribution negligible close to the wall (up to small corrections to the mean velocity due to shear-thinning effects). This ultimate stage is identified when the convergence of the mean velocity profile with increasing Weissenberg number is reached and only the dependence on Re_τ remains. In the present study a state that shares similar statistic properties it is observed at $Wi \simeq 80$ slightly below the Virk law. Modifications in the mean velocity profiles, due to the reduction of wall friction, reflect a deeper change in the structure of the flow. The most evident consequence of the interaction between polymers and turbulence is a substantial weakening of the coherent structures that characterize and sustain the turbulent regime near the wall. This is well captured by snapshots from our simulations, where velocity and vortical structures, respectively, are compared for a Newtonian and a viscoelastic flow. As clearly visible in figure D.3, stream-wise velocity streaks in the xz plane, wavy and irregular in the Newtonian case, become more elongated and almost stream-wise invariant once polymers are introduced. At the same time vortical motion (shown by vorticity contours in fig. D.3), responsible for the momentum transport in the span-wise and wall-normal directions, is substantially reduced. The suppression of turbulent fluctuations, accompanied by redistribution of stresses and changes in the near-wall dynamics are without doubt the main cause of friction reduction, even though the mechanistic coupling with polymers behavior is still not fully explained.

D.4.2   Viscoelastic invariant solutions

Many invariant solutions have already been computed, both periodic and localized in space, for different Newtonian systems [Kawahara et al. (2012)]: [Gibson et al. (2009); Schneider et al. (2010a,b)] in Couette flows, [Waleffe (2003)] in Poiseuille flow. Nevertheless very few, and only from recent studies, are available for viscoelastic flows. After the development of the necessary numerical tools we have tested them probing the state space of different viscoelastic systems in small computational domains and two family of invariant solutions have been found: a family of travelling waves (TW) in the viscoelastic plane-Poiseuille flow (PPF) and a family of spatially-localised solutions (including equilibria, traveling waves and connecting states) in the viscoelastic plane-Couette flow (PPC).

Appendix D. Polymer-induced drag reduction and viscoelastic invariant solutions
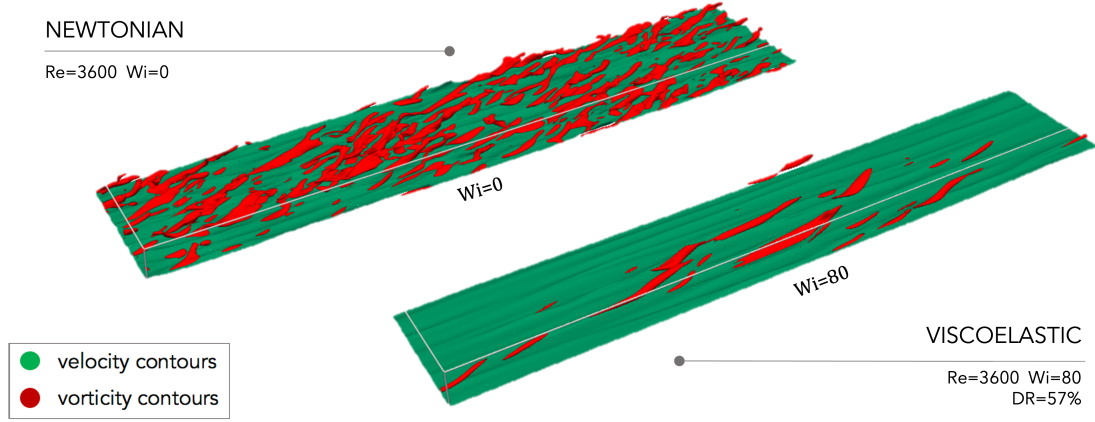

Figure D.3 – Isosurfaces of vorticity at $\Omega = 0.9$ (in red) and isosurfaces of stream-wise velocity at $v_x = 0.3$ (in green) are shown in the bottom half of the pressure-driven channel for a flowfield from DNS at $Re = 3600$ and $Wi = 0,80$

From Newtonian to viscoelastic - Homotopy continuation

Though the dynamics of the system is constrained by restricting the domain size and symmetry subspace, the dimensionality of the problem is still so high that finding invariant solutions requires to provide the Newton method with a reasonably close initial guess. While a Newtonian solution only require an initial guess for the three velocity component, a viscoelastic solution also needs one for the six component of the polymer conformation tensor. In both systems (PPC, and PPF) the initial guess for the velocity fields was provided by existing Newtonian invariant solutions, while the one for the polymer conformation tensor was generated via homotopy continuation as follow:

1. Short viscoelastic DNS (N time iterations) at $Wi = 1$ of the Newtionian invariant solution initialised with a zero polymer conformation tensor α. The purpose of this step is to generate an initial field for α.

2. Short viscoelastic DNS (N time iterations) at $Wi = 1$ of the Newtonian solution and the α-tensor generated from the previous step at iteration N.

3. Repetition of the second step with an iterative update of the initial condition for the conformation tensor, replaced each time with the one obtained from the previous simulation at time N.

4. Viscoelastic Newton search on the Newtonian velocity solution and the final conformation tensor obtained at point 3.

This iterative methodology allows to generate an initial guess for the conformation tensor with a small viscoelasticity degree that matches the Newtonian solution. The resulting solution $(\boldsymbol{u}, \boldsymbol{\alpha})$ can then be used to find invariant solutions in different viscoelastic regimes via

160

continuation in Wi and/or Re.

Viscoelastic solution in PPF

Because of the spatial homogeneity in the spanwise and streamwise directions and the symmetries of the system, solutions in plane-Poiseuille flow are traveling waves, i.e. relative equilibria moving at a constant velocity. Following the homotopy procedure explained above, in this case we have computed the vicoleastic counterpart of one of the Newtonian solution found by Gibson in PPF at $Re = 2300$ [Gibson and Brand (2014)]. We then were able to continue this solution to unexpectedly high viscoelastic regimes ($Wi \simeq 120$) obtaining a family of viscoelastic solutions not available to this date. In figure D.4, the bifurcation diagram for the continuation in Weissenberg(top) is shown together with the velocity contours of the two solutions (bottom) in the Newtonian case (left) and at $Wi = 100$ (right).

In this specific case the physical structure of the velocity component of the solution seems to be unaffected by the presence of polymers. All the symmetries present in the original solution, namely reflections about y and z mid-planes and spatial phase-shifts, are conserved during the homotopy process as well as the characteristic sizes of velocity and vortical structures. However it obviously differ from the original solution for the presence of the polymer conformation tensor α, whose components are shown in figure D.5.

Viscoelastic snaking in PCF

Due to the shortage of available viscoelastic solutions in literature (precisely none before [Page et al. (2020)]) we validated our code computing the well established snaking solutions in PCF adding a small degree of viscoelasticity.
This specific family of solutions, first computed in PCF by Scheider, Marinc and Heckhardt [Schneider et al. (2010b)], consists of two spanwise-localised equilibria and two spanwise localised traveling waves that expand under parametric continuation, adding structures at both fronts as a consequence of recursive saddle-node bifurcations. The two equilibria are related to each other by a reflection symmetry σ_z ($[u, v, w](x, y, z) \rightarrow [u, v, -w](x, y, -z)$), which is a discrete symmetry of the travelling waves, and vice versa the two travelling waves are connected by the rotational symmetry $\sigma_x y$ ($[u, v, w](x, y, z) \rightarrow [-u, -v, w](-x, -y, z)$) which in turn is a discrete symmetry of the equilibrium solutions. The two types of solutions are then connected two each other by non-symmetric rung states, arising from pitchfork bifurcations. All together form the so called snakes-and-ladders structure. Different studies pointed out the strong relation of this structure to the discrete symmetries of the system, a modification of which causes either an alteration or a destruction of the homoclinic snaking [Burke et al. (2009); Knobloch (2015); Azimi and Schneider (2020)]. Since there is no evident symmetry-breaking in the viscoelastic system, compared to the Newtonian one, the homoclinic snaking is expected to be structurally stable and still observable in presence of polymers. The confirmation of this statement is shown in figure D.6 where the bifurcation diagram of the viscoelastic snaking is
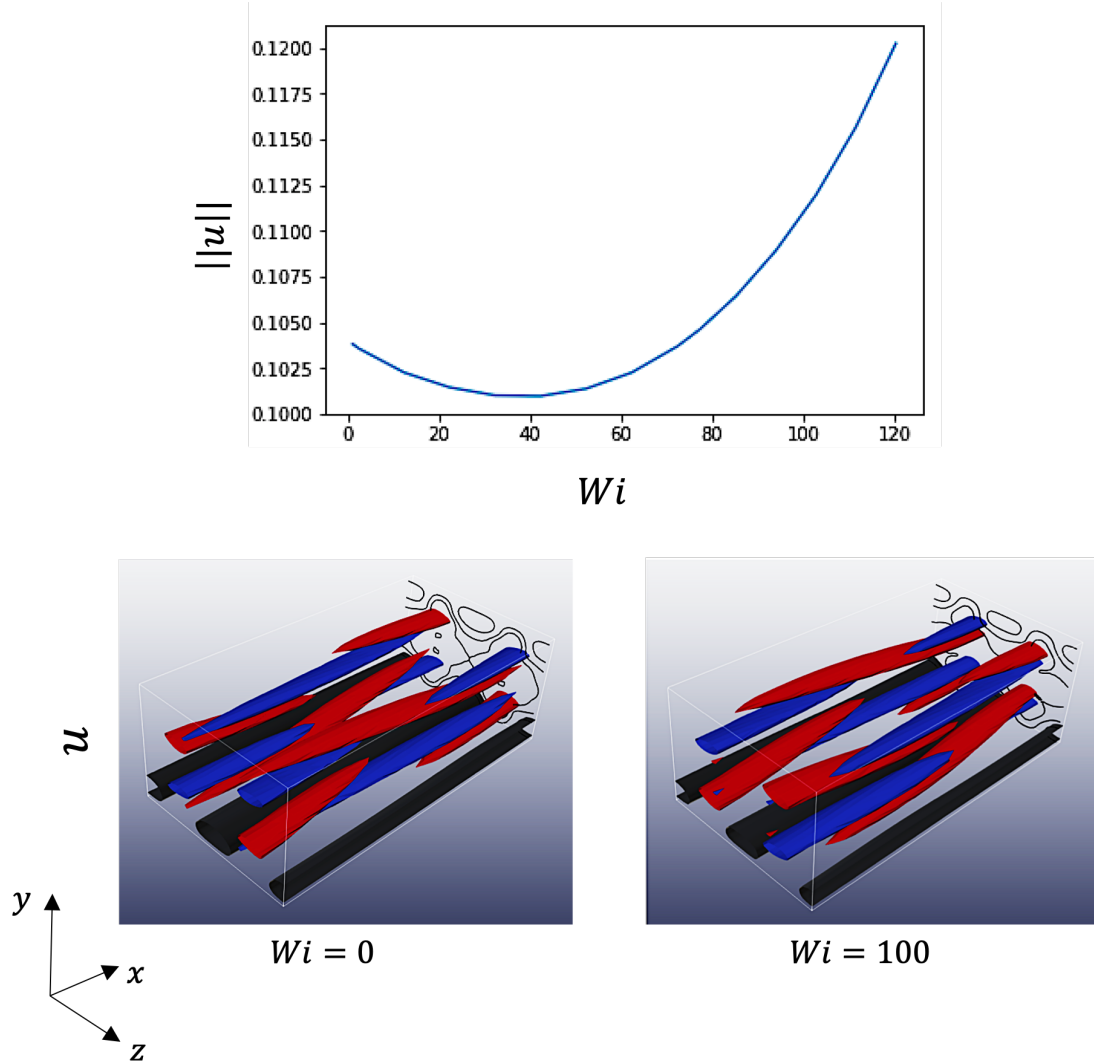
Figure D.4 – (Top)Bifurcation diagram in $Weissenberg$ number from $Wi = 0$ to $Wi = 120$ obtained by homotopy continuation of a spatially periodic travelling wave solution of Newtonian plane Poiseuille flow at $Re = 2300$. (Bottom) Spatially periodic travelling waves of Newtonian (left) and viscoelastic (right) plane Poiseuille system obtained by means of homotopy continuation in Wi number at fixed $Re = 2300$. High speed velocity streaks are represented by black surfaces of streamwise velocity contours at $v_x = 0.02$ in the bottom half part of the channel. Blue and red isosurfaces show the vorticity contours at $\Omega = \pm0.079$.

shown. In this case we have mapped two initial conditions of the Newtonian snaking solutions ($L_x = 3\pi$) [Gibson and Schneider (2016)] for one travelling wave (blue line) and one equilibrium (red line) into the viscoelastic regime at $Wi = 1$ and then continued the solutions in Re. As visible from the flow velocity visualization in fig. D.6 both solutions (plots A-C for the EQ and D-F for the TW), grow structures at their fronts without any alteration of the symmetries observed in the Newtonian case. A similar behaviour is observed for the conformation tensor as shown in figure D.7 (bottom) where its first component α_{xx} for both the equilibrium and
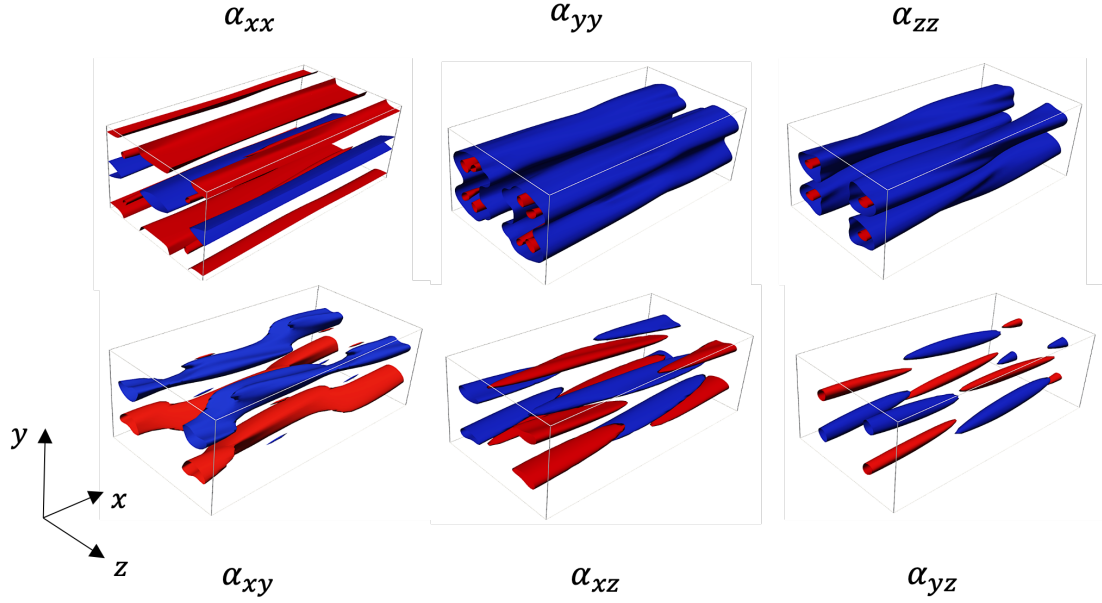
Figure D.5 – Components of the polymer conformation tensor α of the viscoelastic travelling wave shown in figure D.4 at $Wi = 100$ and $Re = 2300$

the travelling wave solutions is plotted along the snaking branches.

D.5 Conclusions

The *Channelflow* package has been successfully extended to investigate viscoelastic shear flows in channel geometry. This includes highly parallelised algorithms for direct numerical simulations as well as an highly efficient Newton-krylow solver for the computation of viscoelastic invariant solutions. The code has been used to compute two new families of invariant solutions in plane-Poiseuille flow and plane-Couette flow, showing its potential for the computation of many others in the future.
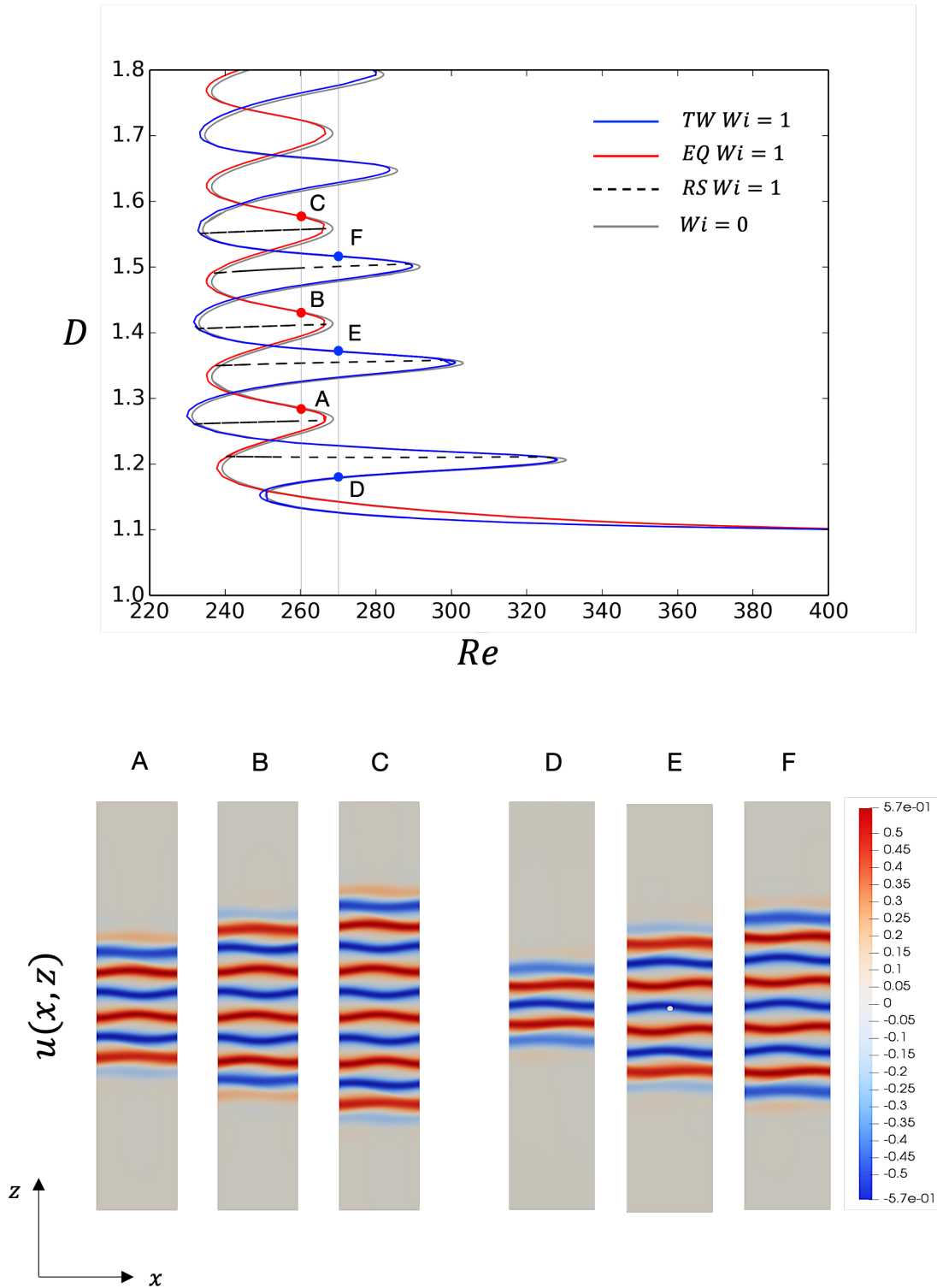
Figure D.6 – Homoclinic snaking in viscoelastic PCF at $Wi = 1$. (Top) Bifurcation diagram of the parametrically continued solutions. The Grey line represent the original Newtonian snaking (for both the TW and EQ), the blue line the viscoelastic TW, the red line the viscoelastic EQ and the black dashed line the viscoelastic rung states. (Bottom) Streamwise velocity component in the xz plane at the center of the channel at different point on the bifurcation diagram: A-C for the equilibrium, and D-F for the travelling wave.
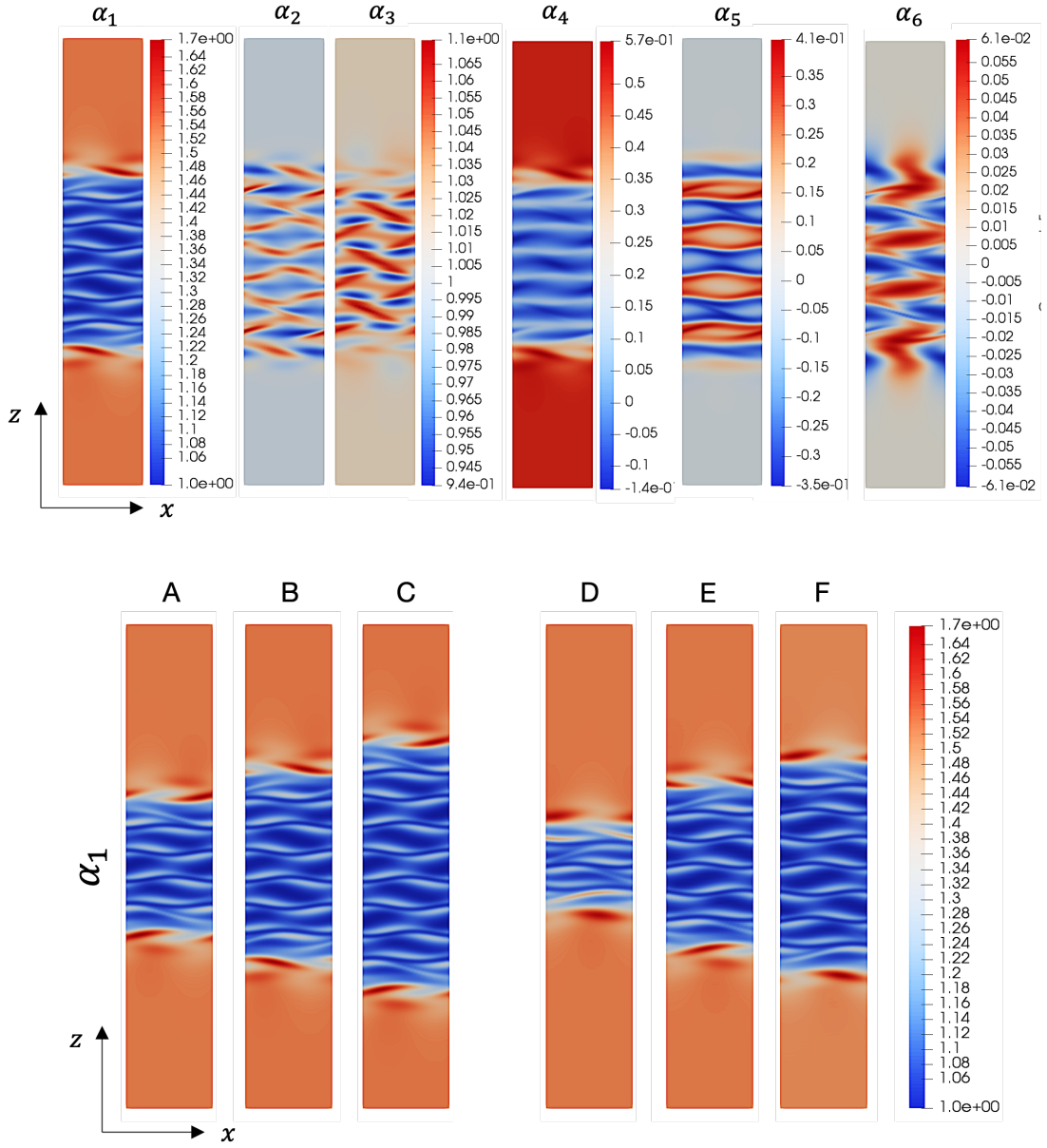
Figure D.7 – Polymer conformation tensor α of the viscoelastic snaking solution in PCF: (Top) the six components of α of the equilibrium at point B in the bifurcation diagram in fig. D.6 and (bottom) first component α_{xx} for the equilibrium and the travelling wave at different points on the snaking: A-C for the EQ, and D-F for the TW. [$\alpha_1 = \alpha_{xx}$, $\alpha_2 = \alpha_{yy}$, $\alpha_3 = \alpha_{zz}$, $\alpha_4 = \alpha_{xy}$, $\alpha_5 = \alpha_{xz}$, $\alpha_6 = \alpha_{yz}$].

Acknowledgements

The work presented in this thesis is the result of five years not only of scientific research but, most importantly, of (highly non-linear) personal developments and growth. I had the great chance of sharing this journey with many extremely valuable people from whom i got inspiration, knowledge and support, and without whom the completion of this chapter of my life would have not been possible.

The major thanks goes to my supervisor, Prof. T. M. Schneider, who gave me, in the first place, the opportunity of doing this PhD and much more. I am thankful for your guidance, for your scientific support and constant trust. I am thankful for of all our scientific discussions, from the calmer to the more heated ones, and for all the hours spent at the blackboard seeking for something we could not see but we knew it was there. I am thankful for your precious confidence boosts, and for believing in me even when I first did not. Thank you for the inexhaustible enthusiasm and creativity you put in everything you do, from research, to teaching, to mentoring and even to yawning. From you, I have learned more than a methodology. I have straightened my scientific backbone and found it connected to deeper rooted personal values. It was an honour to be your student and part of your lab.

Another special thanks goes to Prof. Gregory Chini, and the entire GFD community. I am grateful I had the amazing chance of joining the GFD fellowship during my PhD program, back in the summer of 2019. This experience not only allowed me to connect with incredible people and scientists but re-shaped my way of conceiving research and ultimately this work. I am deeply indebted to Prof. Chini for proposing such a fascinating project, which turned out to be the core of the present thesis, and for letting me work on it till today. Thank you Greg for all our weekly inter-continental Zoom meeting, for all the knowledge you have shared, for trusting the project and my contribution during the past three years. It has been a great pleasure to collaborate with you to and to have you in the jury of my defense.

I would like to take the opportunity to thank the rest of the committee members, Prof. Steve Tobias and Prof. Paolo Ricci for carefully reviewing this thesis, and Prof. J. H. Dil for presiding over the jury. I thank Prof. François Gallaire from LFMI for his numerous useful advises on this work.

Acknowledgements

A huge thanks to all the ECPS members, colleagues and friends, present and past, each one special his own way.

In the first place, thanks to Emilio Lozano, my office mate and close friend. We have started and completed this journey together, counting on each other support and knowing that everything, even the worse day, could be fixed with a tasty meal and a good bottle of (Spanish) wine. I am grateful for all the conversations, meals, holidays and daily adventures we shared in the past five years. I could not have asked for a better person, and friend, to share this part of my life with. I thank Sajjad Azimi for being a great colleague, friend, and a brilliant scientist, from which I learned everything important about code debugging, and grilled chicken. Thanks to Florian Reetz for his support and his constant energy inputs to our lab, and to Simon Schütz for the time spent together. Thanks to Omid Ashtari, who arrived later but immediately got a special place in our group, thanks to his extreme calmness and kindness. Thanks to our postdoc Jeremy Parker, for his British attitude and humor, and for the many good memories we have shared since the time of the GFD program. Thanks to our former postdocs, Mirko Farano and Ayse Yesil, for the many activities and traditions we established during our time together here. Thanks to all the newer ECPS members, which have already brought some fresh air and new ideas (including homemade brioches) to the group. I thank Savyaraj Deshmukh for being the most responsive master student I could have ever got, and now a brilliant colleague. I thank Jean-Clément Ringenbach for our many funny conversations in French, and for helping with the French translation of this abstract. A sincere thanks to Petra Bendel for being my second brain in all the administrative matters and for caring about all of us.

I then would like to extend my thanks to all of my friends, here in Lausanne, in Turin, and all over the word, for their fundamental support.

I thank Matteo for always having wisdom pills (more or less effective) in his pocket to use when needed, and for all the amazing dinners spent talking about abstract and insoluble problems, about the meaning of life, or simply about the food we would have prepared next.

I thank Clara, for being much more than a flatmate. We have started sharing the apartment and we ended up sharing critical and important pieces of our life. Thank you for being "sclero" and a great friend.

A deep acknowledgement to Erica, Francesca and Martina which have put up with me for the past 15 years, and incredibly still do. Thank you very much, your constant backing means a lot to me. Thanks to Ilaria, one of my oldest friend. Time passes, geographical distances do not seem to decrease but still I can always count on you.

Thanks to my university colleagues and friends, Francesca, Richard, Alessio, Ottavia, Maddalena and Francesco, for always being there and inspiring me, no matter which country we are leaving in.

Thanks to Jelle for contributing to an amazing summer at GFD. Thank you for the time together, eating steaks, playing softball, feeding Anuj (whom i thank too) or looking at the Milky way.

A special thanks to François, for his patience and understanding during the past months of intense work that led to the writing of this thesis. Thank you for the countless coffee breaks,

for the long walks in all the possible weather conditions, just because i felt the urge of moving my legs, and for the constant support.

Last but not least, I want to thank my parents and my family for their unconditional love, support and continuous encouragement. My sister, my brother in law and my beautiful nieces. Always close even when far. Words can not express my gratitude for everything you have done and keep doing.

Lausanne, June 25, 2022   Alessia Ferraro

Bibliography

Abdulle, A. and E, W. (2003). Finite difference heterogeneous multi-scale method for homogenization problems. *Journal of Computational Physics*, 191:18–39.

Augier, P., Chomaz, J.-M., and Billant, P. (2012). Spectral analysis of the transition to turbulence from a dipole in stratified fluid. *Journal of Fluid Mechanics*, 713:86–108.

Azimi, S. and Schneider, T. M. (2020). Self-similar invariant solution in the near-wall region of a turbulent boundary layer at asymptotically high reynolds numbers. *Journal of Fluid Mechanics*, 888:A15.

Barry, M. E., Ivey, G. N., Winters, K. B., and Imberger, J. (2001). Measurements of diapycnal diffusivities in stratified fluids. *Journal of Fluid Mechanics*, 442:267–291.

Bartello, P. and Tobias, S. M. (2013). Sensitivity of stratified turbulence to the buoyancy reynolds number. *Journal of Fluid Mechanics*, 725:1–22.

Billant, P. and Chomaz, J.-M. (2001). Self-similarity of strongly stratified inviscid flows. *Physics of Fluids*, 13:1645–1651.

Brethouwer, G., Billant, P., Lindborg, E., and Chomaz, J.-M. (2007). Scaling analysis and simulation of strongly stratified turbulent flows. *Journal of Fluid Mechanics*, 585:343–368.

Burger, E. D., Munk, W., and Wahl, H. (1982). Flow increase in the trans alaska pipeline through use of a polymeric drag-reducing additive. *Society of Petroleum Engineers of AIME*, pages 377–386.

Burke, J., Houghton, S. M., and Knobloch, E. (2009). Swift-hohenberg equation with broken reflection symmetry. *Physical Review E - Statistical, Nonlinear, and Soft Matter Physics*, 80:036202.

Burns, K. J., Vasil, G. M., Oishi, J. S., Lecoanet, D., and Brown, B. P. (2020). Dedalus: A flexible framework for numerical simulations with spectral methods. *Physical Review Research*, 2:023068.

Chini, G. P., Michel, G., Julien, K., Rocha, C. B., and cille P. Caulfield, C. (2022). Exploiting self-organized criticality in strongly stratified turbulence. *Journal of Fluid Mechanics*, 933:A22.

Bibliography

Choueiri, G. H., Lopez, J. M., and Hof, B. (2018). Exceeding the asymptotic limit of polymer drag reduction. *Phys. Rev. Lett.*, 120.

Constantinou, N. C., Lozano-Durán, A., Nikolaidis, M.-A., Farrell, B. F., Ioannou, P. J., and Jiménez, J. (2014). Turbulence in the highly restricted dynamics of a closure at second order: comparison with dns. *Journal of Physics: Conference Series*, 506:012004.

Davis, K. A. and Monismith, S. G. (2011). The modification of bottom boundary layer turbulence and mixing by internal waves shoaling on a barrier reef. *Journal of Physical Oceanography*, 41:2223–2241.

Doi, M. and Edwards, S. (1986). The theory of polymer dynamics.

E, W., Engquist, B., Li, X., Ren, W., and Vanden-Eijnden, E. (2007). The heterogeneous multi-scale method: A review. *Communications in Computational Physics*, 2:367–450.

Eckhardt, B., Schneider, T. M., Hof, B., and Westerweel, J. (2007). Turbulence transition in pipe flow. *Annual Review of Fluid Mechanics*, 39:447–468.

Farrell, B. F., Ioannou, P. J., Jiménez, J., Constantinou, N. C., Lozano-Durán, A., and Nikolaidis, M.-A. (2016). A statistical state dynamics-based study of the structure and mechanism of large-scale motions in plane poiseuille flow. *Journal of Fluid Mechanics*, 809:290–315.

Ferrari, R. (2014). What goes down must come up. *Nature*, 513:179–180.

Fincham, A. M., Maxworthy, T., and Spedding, G. R. (1996). Energy dissipation and vortex structure in freely decaying stratified grid turbulence. *Dynamics of Atmospheres and Oceans*, 23:155–169.

Fitzgerald, J. G. and Farrell, B. F. (2014). Mechanisms of mean flow formation and suppression in two-dimensional rayleigh-bénard convection. *Physics of Fluids*, 26:054104.

Fitzgerald, J. G. and Farrell, B. F. (2018). Statistical state dynamics of vertically sheared horizontal flows in two-dimensional stratified turbulence. *Journal of Fluid Mechanics*, 854:544–590.

Gear, C. W., Li, J., and I., G. K. (2003). The gap-tooth method in particle simulations. *Physics Letters A*, 316:190–195.

Gibson, J. F. (2009). Channelflow users' manual 0.9.18.

Gibson, J. F. and Brand, E. (2014). Spanwise-localized solutions of planar shear flows. *Journal of Fluid Mechanics*, 745:25–61. windowing.

Gibson, J. F., Halcrow, J., and Cvitanović, P. (2008). Visualizing the geometry of state space in plane couette flow. *Journal of Fluid Mechanics*, 611:107–130.

Gibson, J. F., Halcrow, J., and Cvitanović, P. (2009). Equilibrium and traveling-wave solutions of plane couette flow. *Journal of Fluid Mechanics*, 638:243–266.

Gibson, J. F. and Schneider, T. M. (2016). Homoclinic snaking in plane couette flow: bending, skewing and finite-size effects. *Journal of Fluid Mechanics*, 794:530–551.

Grabowski, W. W. (2004). An improved framework for superparameterization. *Journal of the atmospheric sciences*, 61:1940–1952.

Gregg, M., D'Asaro, E., Riley, J., and Kunze, E. (2018). Mixing efficiency in the ocean. *Annual Review of Marine Science*, 10:443–473.

Herring, J. R. and Métais, O. (1989). Numerical experiments in forced stably stratified turbulence. *Journal of Fluid Mechanics*, 202:97–115.

Holleman, R. C., Geyer, W. R., and Ralston, D. K. (2016). Stratified turbulence and mixing efficiency in a salt wedge estuary. *Journal of Physical Oceanography*, 46:1769–1783.

Julien, K. and Knobloch, E. (2007). Reduced models for fluid flows with strong constraints. *Journal of Mathematical Physics*, 48:065405.

Kawahara, G., Uhlmann, M., and van Veen, L. (2012). The significance of simple invariant solutions in turbulent flows. *Annual Review of Fluid Mechanics*, 44:203–225.

Knobloch, E. (2015). Spatial localization in dissipative systems. *Annual Review of Condensed Matter Physics*, 6:325–359.

Lilly, D. K. (1983). Stratified turbulence and the mesoscale variability of the atmosphere. *Journal of the Atmospheric Sciences*, 40:749–761.

Lindborg, E. (2006). The energy cascade in a strongly stratified fluid. *Journal of Fluid Mechanics*, 550:207.

Lindzen, R. S. and Holton, J. R. (1968). A theory of the quasi-biennial oscillation. *Journal of the Atmospheric Sciences*, 25:1095–1107.

Maffioli, A., Brethouwer, G., and Lindborg, E. (2016). Mixing efficiency in stratified turbulence. *Journal of Fluid Mechanics*, 794:R3.

Malecha, Z., Chini, G., and Julien, K. (2014). A multiscale algorithm for simulating spatially-extended langmuir circulation dynamics. *Journal of Computational Physics*, 271:131–150.

Marston, J., Chini, G., and Tobias, S. (2016). Generalized quasilinear approximation: Application to zonal jets. *Physical Review Letters*, 116:214501.

Michel, G. and Chini, G. P. (2019). Multiple scales analysis of slow-fast quasi-linear systems. *Proceedings of the Royal Society A: Mathematical, Physical and Engineering Sciences*, vol. 475.

Métais, O. and Herring, J. R. (1989). Numerical simulations of freely evolving turbulence in stably stratified fluids. *Journal of Fluid Mechanics*, 202:117–148.

Bibliography

Nadolink, R. H. and Haigh, W. W. (1995). No title. *ASME Appl. Mech. Rev*, 48:351.

Nagata, M. (1990). Three-dimensional finite-amplitude solutions in plane couette flow: bifurcation from infinity. *Journal of Fluid Mechanics*, 217:519–527.

Newman, M. E. J. (2011). Complex systems: A survey.

Oglethorpe, R. L. F., Caulfield, C. P., and Woods, A. W. (2013). Spontaneous layering in stratified turbulent taylor–couette flow. *Journal of Fluid Mechanics*, 721:R3.

Osborn, T. R. (1980). Estimates of the local rate of vertical diffusion from dissipation measurements. *Journal of Physical Oceanography*, 10:83–89.

Osborn, T. R. and Cox, C. S. (1972). Oceanic fine structure. *Geophysical Fluid Dynamics*, 3:321–345.

P, K. K., I., M. C., and D., R. D. (2016). *Fluid Mechanics*. sixth edition.

Page, J., Dubief, Y., and Kerswell, R. R. (2020). Exact traveling wave solutions in viscoelastic channel flow. *Physical Review Letters*, 125:154501.

Pope, S. B. (2000). *Turbulent flows*. Cambridge university press.

Portwood, G. D., de Bruyn Kops, S. M., Taylor, J. R., Salehipour, H., and Caulfield, C. P. (2016). Robust identification of dynamically distinct regions in stratified turbulence. *Journal of Fluid Mechanics*, 807:R2.

Riley, J. J. (2021). *Advanced Approaches in Turbulence*.

Riley, J. J. and Lindborg, E. (2008). Stratified turbulence: A possible interpretation of some geophysical turbulence measurements. *Journal of the Atmospheric Sciences*, 65:2416–2424.

Riley, J. J., Metcalfe, R. W., and Weissman, M. A. (1981). Direct numerical simulations of homogeneous turbulence in density-stratified fluids. volume 76, pages 79–112. AIP.

Rubinstein, M. and Colby, R. H. (2003). Polymer physics.

Salehipour, H., Peltier, W. R., and Caulfield, C. P. (2018). Self-organized criticality of turbulence in strongly stratified mixing layers. *Journal of Fluid Mechanics*, 856:228–256.

Schneider, T. M., Gibson, J. F., and Burke, J. (2010a). Snakes and ladders: Localized solutions of plane couette flow. *Physical Review Letters*, 104:104501.

Schneider, T. M., Marinc, D., and Eckhardt, B. (2010b). Localized edge states nucleate turbulence in extended plane couette cells. *Journal of Fluid Mechanics*, 646:441–451.

Shih, L. H., Koseff, J. R., Ivey, G. N., and Ferziger, J. H. (2005). Parameterization of turbulent fluxes and scales using homogeneous sheared stably stratified turbulence simulations. *Journal of Fluid Mechanics*, 525:193–214.

Smyth, W., Nash, J., and Moum, J. (2019). Self-organized criticality in geophysical turbulence. *Sci Rep*, 9.

Smyth, W. D. and Moum, J. N. (2013). Marginal instability and deep cycle turbulence in the eastern equatorial pacific ocean. *Geophysical Research Letters*, 40:6181–6185.

Sprague, M., Julien, K., Knobloch, E., and Werne, J. (2006). Numerical simulation of an asymptotically reduced system for rotationally constrained convection. *Journal of Fluid Mechanics*, 551:141.

Srinivasan, K. and Young, W. R. (2012). Zonostrophic instability. *Journal of the Atmospheric Sciences*, 69:1633–1656.

Tang, W., Caulfield, C. P., and Kerswell, R. R. (2009). A prediction for the optimal stratification for turbulent mixing. *Journal of Fluid Mechanics*, 634:487.

Tobias, S. M., Dagon, K., and Marston, J. B. (2011). Astrophysical fluid dynamics via direct statistical simulation. *The Astrophysical Journal*, 727:127.

Tobias, S. M. and Marston, J. B. (2013). Direct statistical simulation of out-of-equilibrium jets. *Physical Review Letters*, 110:104502.

Tobias, S. M. and Marston, J. B. (2017). Three-dimensional rotating couette flow via the generalised quasilinear approximation. *Journal of Fluid Mechanics*, 810:412–428.

Toms, B. A. (1948). Some observations on the flow of linear polymer solutions through straight tubes at large reynolds numbers. volume 2, pages 135–141.

Venaille, A., Gostiaux, L., and Sommeria, J. (2017). A statistical mechanics approach to mixing in stratified fluids. *Journal of Fluid Mechanics*, 810:554–583.

Virk, P. S. (1975). Drag reduction fundamentals. *AIChE Journal*, 21:625–656.

Virk, P. S., Mickley, H. S., and a. Smith, K. (1970). The ultimate asymptote and mean flow structure in toms' phenomenon. *Journal of Applied Mechanics*, 37:488.

Waleffe, F. (2003). Homotopy of exact coherent structures in plane shear flows. *Physics of Fluids*, 15:1517–1534. lowest Reynolds number for Nagata.

Wunsch, C. and Ferrari, R. (2004). V ertical m ixing , e nergy , and the g eneral c irculation of the o ceans. *Annual Review of Fluid Mechanics*, 36:281–314.

Xi, L. (2009). Nonlinear dynamics and instabilities of viscoelastic fluid flows.

Xi, L. and Graham, M. D. (2010). Active and hibernating turbulence in minimal channel flow of newtonian and polymeric fluids. *Physical Review Letters*, 104:218301.

Xi, L. and Graham, M. D. (2012). Dynamics on the laminar-turbulent boundary and the origin of the maximum drag reduction asymptote. *Physical Review Letters*, 108:028301.

Bibliography

Zhou, Q. and Diamessis, P. J. (2019). Large-scale characteristics of stratified wake turbulence at varying reynolds number. *Physical Review Fluids*, 4:084802.

ALESSIA FERRARO

PERSONAL INFO

+41765374069 📞

alessiaferraro.0@gmail.com ✉

26/03/1991 🎂

EDUCATION

PhD IN PHYSICS:
Physics of Complex Systems

Jan 2017 – Jun 2022
EPFL, Lausanne

EDUCATION DIPLOMA:
Graphic Design

Sep 2019 – Jun 2019
IPAC Design Geneva

MASTER'S DEGREE:
Physics of Complex Systems

Oct 2014 – Oct 2016
University of Turin
Final grade: 110/110 with honors

BACHELOR'S DEGREE:
Physics Engineering

Oct 2010 – Mar 2014
Polytechnic of Turin
Final grade: 104/110

HIGH SCHOOL DIPLOMA:
Liceo Classico

Sep 2005 – Jun 2010
Liceo Classico V. Alfieri (Torino)
Final grade: 91/100

LANGUAGES

Italian (Native)
Englis (Fluent)
French (B2)

RESEARCH EXPERIENCE

PhD STUDENT IN PHYSICS (FLUID DYNAMICS)
January 2017 – June 2022

Emergent Complexity in Physical Systems, EPFL, Lausanne (Switzerland)
Research project 1: Exploiting Marginal Stability in Slow-Fast Quasilinear Dynamical Systems
Research project 2: Turbulent Drag Reduction in Polymers Solutions
Advisor: Prof. Tobias M. Schneider

GEOPHYSICAL FLUID DYNAMICS RESEARCH FELLOWSHIP
June 2019 – Aug 2019

Woods Hole Oceanographic Institution
(Woods Hole, Massachusetts, United States)
Research project: Mathematical formalism and simulations for quasi linear reductions of the stratified flow problem.
Advisors: Prof. G. Chini, Prof. C. Caulfield

MASTER'S THESIS
February 2016 – October 2016

University of Turin
Research project: Area Restricted Search for Foraging in Zooplankton
Advisors: Dr. Filippo de Lillo, Prof. Guido Boffetta

RESEARCH INTERSHIP
April 2013 – July 2013

National Institute of Metrology (INRiM), Turin
Research project: growth and characterisation of superconductive thin-layers of Magnesium diboride (MgB_2).
Advisors: Dr. Eugenio Monticone

TEACHING EXPERIENCE

MASTER THESIS AND SEMESTER PROJECT SUPERVISION

EPFL (2021) – Tutored a Master students at EPFL.

Title of the Master Thesis: "Nonlinear analysis of coarse-grained transport equations underlying global-to-local control in swarm robotics".

Title of the semester project: "Nonlinear analysis of bacterial turbulence".

TEACHING ASSISTANT

EPFL (2018 – 2022)
Turbulence (Mechanical Engineering, Master)
Advisor: Tobias M. Schneider

EPFL (2017 – 2018)
Incompressible Fluid Mechanics (Mechanical Engineering, Bachelor)
Advisor: Tobias M. Schneider

SKILLS

C, C++,
Fortran 77/90
Python, Matlab
MPI
Windows, Linux, Unix
Latex, Microsoft Office
Adobe cc (Ps, Id, Ai)

CONFERENCES

74th Annual Meeting of the APS Division of Fluid Dynamics
Nov 2021 – Phoenix (US)

"Integration of Slow-Fast Quasilinear Models of Turbulent Shear Flows.", A. Ferraro, G. Chini, T.M. Schneider

17th European Turbulence Conference
Sep 2019 – Turin (IT)

"Exploiting Marginal Stability in Slow-Fast Quasilinear Systems"
A. Ferraro, G. Chini, C. Caulfield

12th European Fluid Mechanics Conference
Sep 2018 – Vienna (AT)

"Viscoelastic Invariant Solutions in plane Poiseuille flow"
A. Ferraro, H. Schrobsdorff, T.M. Schneider

ADDITIONAL COURSES

Scientific Programming for Engineers
Prof. Gillaume Anciaux, EPFL, Lausanne, Switzerland

HPC and Parallel Programming (MPI)
J. Latt, V. Keller, CADMOS, Château-d'Oex, Switzerland

Fourier analysis and boundary value problems
Prof. Andrea Rinaldo, EPFL, Lausanne, Switzerland

COMPUTATIONAL ACHIEVEMENTS

RESEARCH PROPOSAL
Production Project CSCS/ETH (Zürich, Switzerland)
(Nov 2018)

"Turbulent drag reduction in polymers solutions"
T.M. Schneider (PI), A. Ferraro, H. Schrobsdorff
Allocation resources 9 million CPU hours

CHANNELFLOW 2.0 Release
(Sep 2018)

Release of the Channelflow 2.0 package for the analysis of incompressible fluid flow in channel geometries. The software, written in C++ and fully parallelized, has been developed by the ECPS lab at the EPFL, based on the previous serial version Channelflow 1.5 created by John Gibson.

178